Circuit QED: Superconducting Qubits Coupled to Microwave Photons

Steven M. Girvin

Yale University
Department of Physics
New Haven, CT 06520
United States of America

OXFORD
UNIVERSITY PRESS

These lectures are based on work done in collaboration with many students, postdocs and colleagues, including particularly my friends and colleagues Michel H. Devoret and Robert J. Schoelkopf.

Preface

These lecture notes discuss the quantum electrodynamics of superconducting circuits. I am grateful for research support provided by Yale University, the National Science Foundation, the Army Research Office, the Laboratory for Physical Sciences and IARPA.

Some useful papers that students may wish to consult in learning this field are:

- Makhlin et al., 'Quantum-state engineering with Josephson-junction devices,' Rev. Mod. Phys. **73**, 357 (2001).
- Blais et al., 'Cavity quantum electrodynamics for superconducting electrical circuits: An architecture for quantum computation,' Phys. Rev. A **69**, 062320 (2004).
- Clerk et al., 'Introduction to quantum noise, measurement and amplification,' Rev. Mod. Phys (2008). (The full version with pedagogical appendices is most conveniently available at http://arxiv.org/abs/arXiv:0810.4729)

Contents

1
Introduction to Quantum Machines

A quantum machine is a device whose degrees of freedom are intrinsically quantum mechanical. Of course, every machine is made of atoms and its microscopic degrees of freedom (the electrons and nuclei) are intrinsically quantum. Atomic physicists have developed remarkable optical techniques to control these microscopic degrees of freedom. In these notes we will take the condensed matter physics perspective: by degrees of freedom we mean collective variables that are sufficiently 'macroscopic' that we can couple to them and control them with externally applied electrical signals or forces. We will extensively study the currents and voltages in superconducting circuits as 'macroscopic' quantum degrees of freedom. Another modern example of growing importance would be the center of mass position of a movable mirror acting as a mechanical oscillator coupled to the radiation pressure of light in an optomechanical system.

While we do not yet fully understand the properties and capabilities of quantum machines, there is great hope (and some mathematical proof) that such devices will have novel capabilities that are impossible to realize on classical hardware. You might think that quantum machines have already been built. For example, the laser and the transistor would seem to rely on quantum physics for their operation. It is clear that the frequency of a laser cannot be computed without the quantum theory that predicts the excitation energies of the atoms in the laser. Similarly the optimal bias voltage of a bipolar transistor depends on the electronic band gap energy of the material from which it is made. Nevertheless, it is only the particular values of the operating *parameters* of these machines that are determined by quantum physics. Once we know the values of these parameters, we see that these are classical machines because their degrees of freedom are purely classical. Indeed the light output from a laser is special because it is exactly like the RF output of the classical oscillator that powers a radio station's antenna. Similarly, the currents and voltages in an ordinary transistor circuit need not be treated as non-commuting quantum operators in order to understand the operation of the circuit. Its degrees of freedom are, for all intents and purposes, classical.

These lectures are devoted to understanding the basic components of quantum machines that can be constructed from superconducting electrical circuits. These circuits can be used to create resonators which store individual microwave photons and to create superconducting quantum bits. Both of these circuit elements are intrinsically quantum mechanical. They have quantized energy levels with spacing much greater than temperature (for low enough temperatures!) and they can be placed into quantum superpositions of different energy states. To properly predict their properties, the

currents and voltages in such circuits must be represented by non-commuting quantum operators.

The beauty of electrical circuits is that they can be constructed in a modular manner combining together a few different building blocks in simple ways. The wires connecting these building blocks have to be capable of carrying quantum signals (Schoelkopf and Girvin, 2008; Devoret and Schoelkopf, 2013), but are still relatively simple and the problem of spatial mode matching that occurs in optical circuits is largely eliminated (becoming simply a question of impedance matching). Furthermore, with modern lithographic techniques, parallel fabrication of complex structures is relatively straightforward lending hope that (someday) it will be possible to scale up to processors with large numbers of qubits.

We will study different qubit designs and their relative merits. We will also learn how to control and read out the quantum states of qubits and cavities, and how to entangle their different quantum degrees of freedom. In recent decades, we have come to understand that superposition and entanglement are features of quantum physics which can be used as resources to make powerful quantum computers to process information in ways that are impossible classically. What else we can do with quantum machines is not yet fully understood. The people who invented the laser had no idea that it would be used to play music, communicate over optical fiber, and perform eye surgery. We expect that similar surprises and unexpected applications will be developed once quantum hardware becomes routine enough to play with.

2
Quantum Electrical Circuits

2.1 Introduction

Quantum electrodynamics is the theory of interaction between electrons (and atoms) with electromagnetic fields. These lecture notes discuss the closely related problem of quantization of electrical circuits (Devoret, 1997; Schoelkopf and Girvin, 2008). Experimental progress over the last decade in creating and controlling quantum coherence in superconducting electrical circuits has been truly remarkable. The quantum electrodynamics of superconducting microwave circuits has been dubbed 'circuit QED' by analogy to cavity QED in quantum optics. These lecture notes will describe the quantum optics approach to microwave circuits with superconducting qubits playing the role of artificial atoms whose properties can be engineered. Despite being large enough to be visible to the naked eye, these artificial atoms have a very simple discrete set of quantized energy levels which are nearly as well understood (Nigg *et al.*, 2012) as those of the prototypical single-electron atom, hydrogen. Furthermore it has proven possible to put these atoms into coherent superpositions of different quantum states so that they can act as quantum bits. Through clever engineering, the coherence times of such superposition states has risen more than four orders of magnitude from nanoseconds for the first superconducting qubit created in 1999 (Nakamura *et al.*, 1999) up to $\sim 30 - 150$ microseconds today (Paik *et al.*, 2011; Rigetti *et al.*, 2012; Chang *et al.*, 2013; Barends *et al.*,). Recent experiments with the fluxonium qubit design (Manucharyan *et al.*, 2009*b*) have achieved T_1 times exceeding 1 millisecond (Geerlings *et al.*, 2013). 'Schoelkopf's Law' for the exponential growth of coherence time is illustrated in Fig. (2.1).

Simple quantum machines have already been built using superconducting circuits which can manipulate and measure the states of individual qubits (Nakamura *et al.*, 1999; Mooij *et al.*, 1999; Vion *et al.*, 2002) as well as individual microwave quanta (Houck *et al.*, 2007; Hofheinz *et al.*, 2008; Hofheinz *et al.*, 2009; Johnson *et al.*, 2010; Mariantoni *et al.*, 2011*a*; Wang *et al.*, 2011), entangle two (Ansmann *et al.*, 2009; Chow *et al.*, 2010) and three qubits (Neeley *et al.*, 2010; DiCarlo *et al.*, 2010), run simple quantum algorithms (DiCarlo *et al.*, 2009; Mariantoni *et al.*, 2011*b*) and perform rudimentary quantum error correction (Reed *et al.*, 2012). Future improved qubit designs, microwave circuit designs, and materials improvements should allow this trend to continue unabated. In addition to being a potentially powerful engineering architecture for building a quantum computer, circuit QED opens up for us a novel new regime to study ultra-strong coupling between 'atoms' and individual microwave photons (Devoret *et al.*, 2007). The concept of the photon is a subtle one, but hopefully these notes

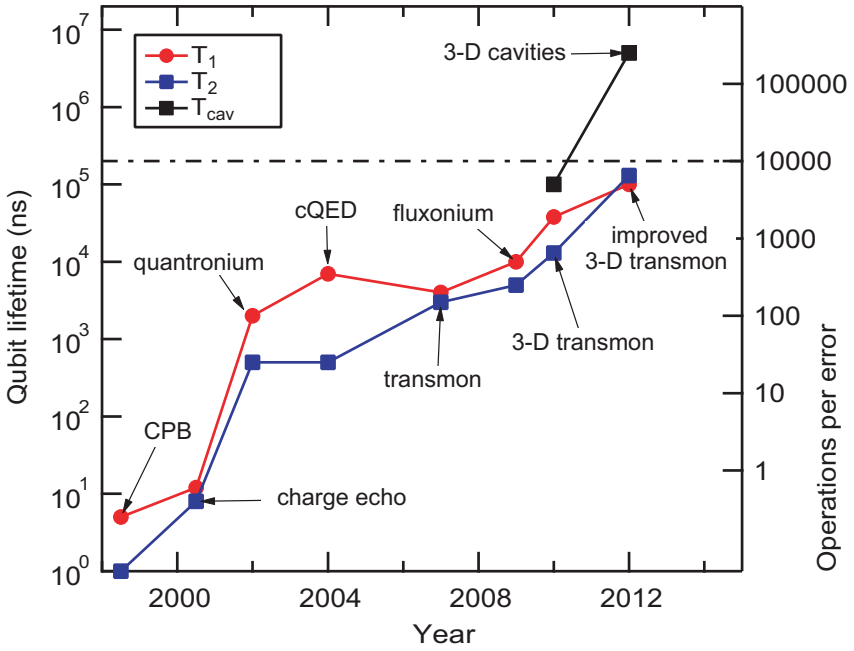

Fig. 2.1 "Schoelkopf's Law" plot illustrating the exponential growth for superconducting (charge-) qubit coherence times. Recent experiments (Geerlings *et al.*, 2013) with the 'fluxonium' qubit design have achieved T_1 times exceeding one millisecond.

will convince the reader that microwaves, despite their name, really are particles. We will accordingly begin our study with a review of the quantization of electromagnetic fields in circuits and cavities.

The quantization of electrical circuits has been thoroughly addressed in the Les Houches lecture notes of my colleague, Michel Devoret (Devoret, 1997), to which I direct the interested reader. The circuit elements that are available to the quantum engineer include those familiar to classical engineers: resistors, capacitors, and inductors. Resistors cause unwanted dissipation and we will attempt to avoid them. See however further discussion in the Appendix (B) of spontaneous emission into transmission lines which act effectively as fixed impedances. Dissipation into a cold resistor can in fact be useful for qubit reset(Reed *et al.*, 2010*b*) to the ground state since reset requires removal of entropy to a cold bath.

In addition to these standard circuit elements, there is one special element in superconducting circuits, the Josephson tunnel junction. We will be learning more about superconductivity and Josephson junctions later, but for now we simply note the following. With capacitors and inductors we can build simple LC harmonic oscillators. If we can eliminate all resistors then the harmonic oscillations will be undamped. The use of superconducting circuits takes us a long way towards this goal of zero dissipation, about which more later. The essential feature of (ordinary) superconductivity is

that electrons of opposite spin pair up and condense into a special ground state with a substantial excitation gap 2Δ needed to break one of the pairs and create an excited state. This pair excitation gap is essential to the ability of current to flow in a superconductor without dissipation.[1] A closely related advantage of the excitation gap is that it dramatically reduces the number of effective degrees of freedom in the circuit, allowing us to construct artificial 'atoms' that behave like simple single-electron atoms even though they are made up of $10^9 - 10^{12}$ aluminum atoms. The extremely powerful force of the Coulomb interactions also plays an essential role in limiting the low energy degrees of freedom in circuits. When the Coulomb interaction is unscreened, the gapless collective motion of currents is lifted up to the plasma frequency which is orders of magnitude higher than any relevant frequency scale for the circuits we will consider. (This effect of the long-range Coulomb force occurs in both normal metals and superconductors.) In the presence of screening due to ground planes or shields, the plasma oscillations are 'acoustic modes' with a linear dispersion and velocity close to the speed of light in vacuum.[2] When quantized, these will be our propagating photons.

2.2 Plasma Oscillations

Because the powerful effect of long-range Coulomb interactions plays a crucial role in simplifying the spectrum of quantum electrical circuits, let us begin our analysis by reviewing the plasma oscillations in a bulk metal. Throughout this work we will use SI units. We will consider infinitesimal density fluctuations δn around the mean electron number density n. In the 'jellium' model the mean charge density is canceled by the ionic background so the net charge density is

$$\rho(\vec{r}) = -e\,\delta n. \tag{2.1}$$

The current flowing (to zeroth order in δn) is

$$\vec{J}(\vec{r},t) = -en\vec{v}(\vec{r},t), \tag{2.2}$$

where the local electron mean velocity field obeys Newton's law

$$\frac{\partial}{\partial t}\vec{v} = \frac{-e}{m}\vec{E}, \tag{2.3}$$

where m is the electron (effective) mass. This in turn yields

$$\frac{\partial}{\partial t}\vec{J} = \frac{ne^2}{m}\vec{E}. \tag{2.4}$$

Taking the divergence of both sides of this equation and applying Gauss's law

[1] There do exist gapless superconductors (e.g. d-wave materials like YBCO) which can carry a dc current without dissipation, but at the microwave frequencies of interest for qubits, the lack of a gap implies significant dissipation.

[2] Flat metallic surfaces and long wires exhibit so-called surface plasmons which are gapless and have approximately linear dispersion relations due to electrodynamic retardation effects. The purpose of the ground shield surrounding the central wire in a coaxial cable is to prevent radiation losses when the cable is bent into a curve.

$$\vec{\nabla} \cdot \vec{E} = \frac{\rho}{\epsilon_0}, \tag{2.5}$$

and the continuity equation

$$\vec{\nabla} \cdot \vec{J} + \frac{\partial}{\partial t}\rho = 0, \tag{2.6}$$

yields

$$\frac{\partial^2}{\partial t^2}\rho = -\omega_{\rm p}^2 \rho \tag{2.7}$$

where the so-called 'plasma frequency' is given by[3]

$$\omega_{\rm p}^2 \equiv \frac{ne^2}{m\epsilon_0}. \tag{2.8}$$

Electromagnetic waves cannot propagate in a plasma at frequencies below the plasma frequency (Jackson, 1999). In the earth's ionosphere, the typical plasma frequency is in the range of 10's of MHz and varies between night and day, thereby affecting short-wave radio reception. In the typical metals we will be concerned with (e.g., aluminum), the valence electron density is sufficiently high that the plasma frequency is in the ultraviolet region of the optical spectrum. Hence aluminum (whose plasma frequency $\omega_{\rm p}/(2\pi) \sim 3.6 \times 10^{15}$Hz corresponds to a photon energy of ~ 15 eV) is highly reflective in the visible. Essentially, the electrons are so dense and so agile that they screen out any electric fields almost perfectly over a very short screening distance. For frequencies far below the plasma frequency, Maxwell's equations yield

$$\vec{\nabla} \times \vec{\nabla} \times \vec{E} \approx -\lambda_{\rm p}^{-2} \vec{E}, \tag{2.9}$$

where the London penetration depth, $\lambda_{\rm L}$, of the electromagnetic fields is

$$\lambda_{\rm L} = \frac{c}{\omega_{\rm p}} = \frac{1}{\sqrt{4\pi n r_{\rm e}}}, \tag{2.10}$$

where the classical radius of the electron is given by

$$r_{\rm e} = \frac{e^2}{4\pi\epsilon_0}\frac{1}{mc^2} \approx 2.818 \times 10^{-15}{\rm m}. \tag{2.11}$$

For Al, Eq. 2.10 yields[4] $\lambda_{\rm L} \sim 14$nm We will be dealing with GHz frequency scales many orders of magnitude below the plasma frequency and centimeter wavelength scales relative to which the penetration depth is effectively zero.

[3]We neglect here the various details of the band structure of Al as well as the possibility that the core electrons in the atoms of the metal contribute a dielectric constant $\epsilon \neq 1$ seen by the valence electrons whose dynamics create the plasma oscillations of the metal.

[4]The measured value of the London penetration depth in Al (at zero frequency) is somewhat larger, $\lambda_{\rm L} \sim 51.5$nm. The difference is presumably due to variation in the core electron dielectric constant with frequency which has been neglected in our model. It should also be noted that in dirty superconductors, the reduction in the superfluid stiffness causes the penetration depth to increase.

Exercise 2.1 Derive Eq. 2.9 in the limit of low frequencies and show that it leads to exponential decay of transverse electromagnetic waves with decay length $\lambda_{\rm p}$.

The above simplified[5] jellium model yields a plasma mode which is completely dispersionless–the mode frequency is independent of wave vector q. The frequency of the bulk collective plasma mode is vastly higher than any microwave frequency that we will be dealing with. From the point of view of quantum mechanics, the amount of energy required to create a bulk plasmon is so large that we can consider these degrees of freedom to be frozen into their quantum mechanical ground state. Hence they can be ignored. The approximations leading to Eq. (2.2) breakdown at short distances due to the granularity of the electron charge. At very large wave vectors approaching the Fermi wave vector, the jellium continuous charge picture breaks down and the plasma oscillation frequency rises and the mode becomes 'Landau-damped' due to the collective charge oscillation mode decaying into single-particle excitations (Pines, 1963). Conversely for extremely small wave vectors, there is a cutoff associated with the finite size of any sample. This we can take into account by considering the capacitance matrix between different lumps of metal in the circuit we are trying to quantize. In certain circumstances, the capacitance matrix is such that there do exist collective charge oscillation modes which are down in the microwave range. These will be the important modes which we will quantize. Here the superconductivity is vital for gapping the single-particle excitations so that the collective charge modes are both simple and extremely weakly damped.

2.3 Quantum LC Oscillator

The circuit element with the simplest dynamics is the LC oscillator illustrated schematically in Fig. (2.2a). Now that we understand that supercurrents can flow essentially without dissipation and that the great strength of the Coulomb interaction lifts density fluctuations up to optical frequencies, we can understand that the LC oscillator has, to a very good approximation, only a single low-energy degree of freedom, namely uniform divergenceless current flow in the wire of the inductor which does not build up charge anywhere except on the plates of the capacitor. This is a very good approximation in the 'lumped element' limit where the physical size of the LC oscillator is much smaller than than the wavelength of electromagnetic waves at the frequency of the oscillator, $\lambda = 2\pi c/\Omega$. [This caveat is associated with the unstated assumption in our discussion of plasma oscillations that we neglected electrodynamic retardation effects. That is, we effectively assumed $c = \infty$.] In terms of the capacitor charge q and the inductor current I the Lagrangian is readily written

$$\mathcal{L} = \frac{1}{2}LI^2 - \frac{1}{2}\frac{q^2}{C}. \tag{2.12}$$

Using charge conservation, $I = +\dot{q}$, this can be cast into the more familiar form

[5] A more careful treatment would have included the change in the Fermi energy as the density oscillates. The resulting Fermi pressure gradients produce a positive quadratic dispersion of the plasma mode with increasing wave vector.

$$\mathcal{L} = \frac{L}{2}\dot{q}^2 - \frac{1}{2C}q^2. \tag{2.13}$$

Remarkably, we have reduced a complex circuit containing an enormous number of electrons to a system with a *single* degree of freedom q with 'mass' L and 'spring constant' $1/C$). This is possible only because all but this one degree of freedom are effectively gapped out by a combination of superconductivity (which gaps out the single-particle excitations) and the long-range Coulomb force (which gaps out the collective plasmon (density fluctuation) degrees of freedom). All that is left is the rigid collective motion of the incompressible electron fluid sloshing back and forth, charging and discharging the capacitor.

Eq. (2.13) yields the Euler-Lagrange equation of motion

$$\ddot{q} = -\Omega^2 q, \tag{2.14}$$

where the natural oscillation frequency is

$$\Omega = \frac{1}{\sqrt{LC}}. \tag{2.15}$$

The momentum conjugate to the charge is the flux through the inductor

$$\Phi = \frac{\delta \mathcal{L}}{\delta \dot{q}} = L\dot{q} = LI. \tag{2.16}$$

Thus the Hamiltonian can be written

$$H = \Phi\dot{q} - \mathcal{L} = \frac{\Phi^2}{2L} + \frac{1}{2C}q^2. \tag{2.17}$$

Hamilton's equations of motion then give the current through the inductor and the voltage at the node connecting the inductor and the capacitor

$$\dot{q} = \frac{\partial H}{\partial \Phi} = \frac{\Phi}{L} = I \tag{2.18}$$

$$\dot{\Phi} = -\frac{\partial H}{\partial q} = -\frac{q}{C} = V. \tag{2.19}$$

In the usual way, the coordinate and its conjugate momentum can be promoted to quantum operators obeying the canonical commutation relation

$$[\hat{\Phi}, \hat{q}] = -i\hbar \tag{2.20}$$

and we can write the Hamiltonian

$$H = \frac{\hbar\Omega}{2}\left\{\hat{a}^\dagger\hat{a} + \hat{a}\hat{a}^\dagger\right\} = \hbar\Omega\left\{\hat{a}^\dagger\hat{a} + \frac{1}{2}\right\}, \tag{2.21}$$

in terms of raising and lowering operators

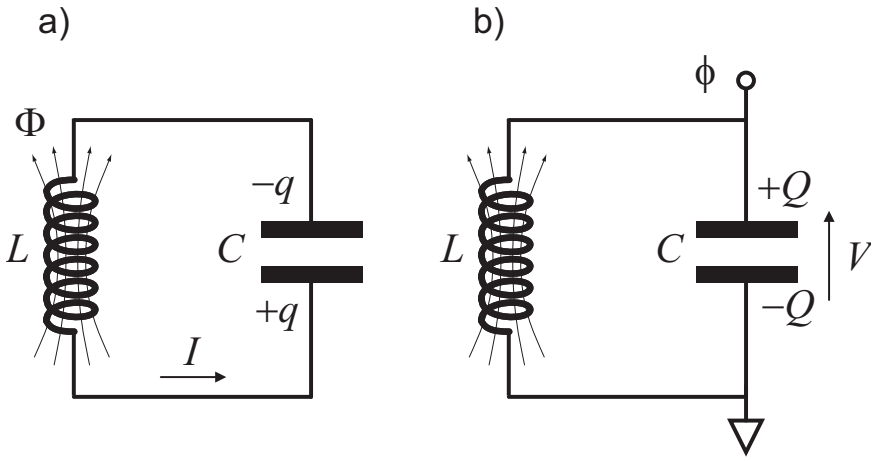

Fig. 2.2 Simple LC electrical oscillator analogous to a mass and spring mechanical oscillator. In panel a) the position coordinate of the mass is taken to be q, the charge accumulated on the capacitor by the current I flowing through the inductor, and the flux Φ through the inductor is the momentum. The sign convention for the charge is such that $\dot{q} = I$ and therefore the inductance L is analogous to the mass. The role of the spring constant is played by $1/C$ and the potential energy of the capacitor is $(q - q_q)^2/2C$, where q_0 is the offset charge of the capacitor (the equivalent of the equilibrium length of the spring). Hamilton's equation for the time rate of change of the momentum is $\dot{\Phi} = -(q - q_0)/C$. In panel b) the position coordinate is now taken to be ϕ, the time integral of the voltage V across the capacitor (i.e., the node flux) and the conjugate momentum is Q, the charge on the capacitor resulting from the electrochemical potential difference between the two plates. The role of the mass is played by C and the spring constant is now $1/L$, with the energy of the inductor given by $(\phi - \phi_0)^2/2L$, where ϕ_0 is the external flux in the loop of the circuit (including the coil of the inductor). Hamilton's equation for the time rate of change of position is $\dot{\phi} = Q/C$. Note the important sign change in the denition of charge: $Q = q_0 - q$, needed to make the Hamilton equations of motion correct in each case. The classical Poisson brackets and the quantum canonical commutation relations between position and momentum are maintained between the two cases: $[\hat{q}, \hat{\Phi}] = [\hat{\phi}, Q] = +i\hbar$.

$$\hat{a} = +i\frac{1}{\sqrt{2L\hbar\Omega}}\hat{\Phi} + \frac{1}{\sqrt{2C\hbar\Omega}}\hat{q} \tag{2.22}$$

$$\hat{a}^\dagger = -i\frac{1}{\sqrt{2L\hbar\Omega}}\hat{\Phi} + \frac{1}{\sqrt{2C\hbar\Omega}}\hat{q} \tag{2.23}$$

which obey the usual relation

$$[\hat{a}, \hat{a}^\dagger] = 1. \tag{2.24}$$

In the above discussion we chose the charge q on the capacitor as the natural coordinate of the harmonic oscillator and found that the inductor flux Φ was the momentum conjugate to this flux. In the picture we interpret the capacitance C as the inverse of the 'spring constant,' and the inductance L as the 'mass.' This seems natural

from our intuitive view of the capacitance as storing the potential energy and the inductor storing the kinetic energy (actually the kinetic energy of the electrons makes only a small contribution (called the 'kinetic inductance') to the total inductance. It is primarily the energy stored in the magnetic field created by the current which dominates the inductance in most situations.)

When dealing with Josephson junctions we will start with this same representation but then find that they act as non-linear inductors and so it will be more convenient to take the node flux (defined below) to be the coordinate rather than the momentum. In order to get used to this alternative representation, we will practice here on the LC oscillator. Following Devoret (Devoret, 1997) let us define the node flux at the point shown in Fig. (2.2b) by

$$\phi(t) = \int^t d\tau V(\tau), \tag{2.25}$$

so that $V(t) = \dot{\phi}$. Then the potential energy stored on the capacitor is

$$U = \frac{1}{2} C \dot{\phi}^2 \tag{2.26}$$

and now looks like the kinetic energy with this choice of coordinate. Similarly, using Faraday's law and the sign convention for the direction of the current defined in Fig. (2.2b) we have

$$V = L\dot{I} = \dot{\phi} \tag{2.27}$$

and thus see that the node flux variable ϕ really is the physical magnetic flux Φ winding through the inductor (ignoring any possible external flux applied through the loop of the circuit or the inductor). Hence the kinetic energy stored in the inductor is

$$T = \frac{1}{2L} \phi^2, \tag{2.28}$$

which now looks like the potential energy. With this choice of coordinate the Lagrangian becomes

$$\mathcal{L} = \frac{1}{2} C \dot{\phi}^2 - \frac{1}{2L} \phi^2, \tag{2.29}$$

and the momentum conjugate to the flux

$$Q = \frac{\delta \mathcal{L}}{\delta \dot{\phi}} = C \dot{\phi} \tag{2.30}$$

is now the charge as defined with the sign convention in Fig. (2.2b). Notice the crucial minus sign relative to the previous result. This is necessary to maintain the sign of the commutation relation when we interchange the momentum and coordinate. To reiterate: when the charge is the coordinate and the flux is the conjugate momentum, the commutation relation is:

$$[\hat{q}, \hat{\Phi}] = +i\hbar, \tag{2.31}$$

whereas when the flux is the coordinate and the charge is the conjugate momentum, the commutation relation is:

$$[\hat{\phi}, \hat{Q}] = +i\hbar. \tag{2.32}$$

Since we have chosen a convention in which $\hat{\Phi} = \hat{\phi}$, we require $\hat{Q} = -\hat{q}$.

Just to be completely explicit, we now repeat the derivation of the Hamiltonian and its quantization for this new choice which we will be using throughout the remainder of these notes. Thus the Hamiltonian can be written

$$H = Q\dot{\phi} - \mathcal{L} = \frac{1}{2C}Q^2 + \frac{\phi^2}{2L}. \tag{2.33}$$

Hamilton's equations of motion are then

$$\dot{\phi} = +\frac{\partial H}{\partial Q} = +\frac{Q}{C} \tag{2.34}$$

$$\dot{Q} = -\frac{\partial H}{\partial \phi} = -\frac{\phi}{L}. \tag{2.35}$$

Again in the usual way, the coordinate and its conjugate momentum can be promoted to quantum operators obeying the canonical commutation relation (but note the important position reversal from Eq. (2.20))

$$[\hat{Q}, \hat{\phi}] = -i\hbar \tag{2.36}$$

and we can write the Hamiltonian

$$H = \frac{\hbar\Omega}{2}\left\{\hat{a}^\dagger\hat{a} + \hat{a}\hat{a}^\dagger\right\} = \hbar\Omega\left\{\hat{a}^\dagger\hat{a} + \frac{1}{2}\right\}, \tag{2.37}$$

in terms of raising and lowering operators

$$\hat{a} = +i\frac{1}{\sqrt{2C\hbar\Omega}}\hat{Q} + \frac{1}{\sqrt{2L\hbar\Omega}}\hat{\phi} \tag{2.38}$$

$$\hat{a}^\dagger = -i\frac{1}{\sqrt{2C\hbar\Omega}}\hat{Q} + \frac{1}{\sqrt{2L\hbar\Omega}}\hat{\phi} \tag{2.39}$$

which obey the usual relation

$$[\hat{a}, \hat{a}^\dagger] = 1. \tag{2.40}$$

The charge and flux operators can be expressed in terms of the raising and lowering operators as

$$\hat{Q} = -iQ_{\rm ZPF}\left(\hat{a} - \hat{a}^\dagger\right) \tag{2.41}$$

$$\hat{\phi} = \Phi_{\rm ZPF}\left(\hat{a} + \hat{a}^\dagger\right), \tag{2.42}$$

where

$$Q_{\rm ZPF} = \sqrt{\frac{C\hbar\Omega}{2}} = \sqrt{\frac{\hbar}{2Z}} \tag{2.43}$$

$$\Phi_{\rm ZPF} = \sqrt{\frac{L\hbar\Omega}{2}} = \sqrt{\frac{\hbar Z}{2}}, \tag{2.44}$$

where Z is the characteristic impedance of the oscillator

$$Z = \sqrt{\frac{L}{C}}. \tag{2.45}$$

Notice that the notation has been chosen such that the quantum ground state uncertainties in charge and flux are given by

$$\langle 0|\hat{Q}^2|0\rangle = Q_{\rm ZPF}^2 \tag{2.46}$$
$$\langle 0|\hat{\phi}^2|0\rangle = \Phi_{\rm ZPF}^2. \tag{2.47}$$

Exercise 2.2 There is a certain arbitrariness in the choice of phase factors that enter in definition of the raising and lowering operators in Eq. (2.42). We have chosen a convention in which the flux is related to the real part of $\hat{a}$ and the charge is related to the imaginary part of $\hat{a}$. Consider the unitary transformation $U = e^{i\theta\hat{n}}$, where $\hat{n} = a^\dagger a$ is the photon number operator. What does this transformation do to the Fock state $|n\rangle$? How do the raising and lowering operators transform under the action of U? What happens to the expressions for charge and flux under the transformation of U when $\theta = \pi/2$?

Using the superconducting resistance quantum

$$R_{\rm Q} \equiv \frac{h}{(2e)^2} \approx 6,453.20\,\text{Ohms}, \tag{2.48}$$

we can define a dimensionless characteristic impedance

$$z \equiv Z/R_{\rm Q}, \tag{2.49}$$

to obtain

$$Q_{\rm ZPF} = (2e)\sqrt{\frac{1}{4\pi z}} \tag{2.50a}$$
$$\Phi_{\rm ZPF} = \Phi_0\sqrt{\frac{z}{4\pi}}, \tag{2.50b}$$

where

$$\Phi_0 \equiv \frac{h}{2e} \tag{2.51}$$

is the superconducting flux quantum. Notice that the usual uncertainty product is obeyed.

$$Q_{\rm ZPF}\Phi_{\rm ZPF} = \frac{\hbar}{2}. \tag{2.52}$$

The voltage is an important physical variable and the voltage operator is given by

$$\begin{aligned}\hat{V} &= \frac{d\hat{\phi}}{dt} = \frac{i}{\hbar}[H,\hat{\phi}] \\ &= \frac{1}{C}\hat{Q} = -i\sqrt{\frac{\hbar\Omega}{2C}}\left(\hat{a}-\hat{a}^\dagger\right) = -iV_{\rm ZPF}\left(\hat{a}-\hat{a}^\dagger\right),\end{aligned} \tag{2.53}$$

where

$$V_{\rm ZPF} = \Omega\Phi_{\rm ZPF} = \Omega\Phi_0\sqrt{\frac{z}{4\pi}}. \tag{2.54}$$

The superconducting flux quantum in convenient units is given by

$$\Phi_0 \approx 2.06783367\,\mu{\rm V/GHz} \tag{2.55}$$

which tells us that the vacuum fluctuations of the voltage across the capacitor in a typical 10 GHz, $Z = 100$ Ohm impedance resonator circuit will be on the scale of $\sim (1/3)\mu$V. Correspondingly the vacuum fluctuations of the current are on the scale of $\sim$ 3nA. It is remarkable that the quantum fluctuations of currents and voltages in these microwave circuits have the same scales as are routinely measured in the audio range with standard laboratory instruments.

How do we interpret the excitation quanta of this harmonic oscillator? We can think of these as excitations of the collective motion of the electrons in the wire, or we can think of them as photons of the electromagnetic field. Because this is a lumped element resonator (as opposed to a cavity or other distributed resonator), the electric field appears between the capacitor plates and the magnetic field appears in a separate place, namely within the coil of the inductor. Nevertheless it is perfectly acceptable to think of these excitations as photons. The coordinate of the oscillator is the flux in the coil (or in the first choice we made, the charge on the capacitor plates which is equivalent to the electric field in the gap between the plates.

One does not normally think about photons in the context of first quantization, but this is also useful for building up intuition and for thinking about things like the full probability distribution of electric field measurement results. The wave function of the vacuum state is a gaussian in the coordinate ϕ as shown in Fig. (2.3)

$$\Psi_0(\phi) = \frac{1}{[2\pi\Phi_{\rm ZPF}^2]^{1/4}} e^{-\frac{1}{4}\frac{\phi^2}{\Phi_{\rm ZPF}^2}}\,. \tag{2.56}$$

If in the vacuum state we make a precise measurement of the flux, the resulting value will be random and have a gaussian probability distribution given by

$$P(\phi) = |\Psi_0(\phi)|^2. \tag{2.57}$$

Hence the most probable value of the flux is zero. On the other hand, in the one-photon state

$$\Psi_1(\phi) = \frac{\phi}{\Phi_{\rm ZPF}}\frac{1}{[2\pi\Phi_{\rm ZPF}^2]^{1/4}} e^{-\frac{1}{4}\frac{\phi^2}{\Phi_{\rm ZPF}^2}} \tag{2.58}$$

zero flux would never be measured because the wave function vanishes at $\phi = 0$. The measured flux is still zero on average. This is true for any (odd) photon Fock state (number eigenstate) from simple parity considerations. On the other hand, if the photon number is uncertain, for example in the coherent superposition state

$$\Psi_+ = \frac{1}{\sqrt{2}}\left(\Psi_0 + \Psi_1\right), \tag{2.59}$$

then the centroid of the probability distribution is displaced away from zero as shown in Fig. (2.3) and the average value of the flux will be non-zero. A similar conclusion

is readily reached within the second quantized formulation of Eq. (2.42) by noticing that the flux and charge operators are purely off-diagonal in the photon number basis.

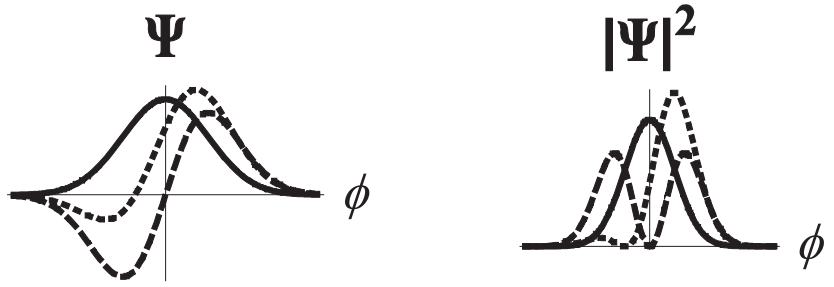

Fig. 2.3 LC oscillator wave function amplitude (left panel) and probability density (right panel) plotted vs. the coordinate ϕ. Solid: ground state, Ψ_0; Long-Dashed: first excited state, Ψ_1; Short-dashed: linear combination of the ground and first excited states, $\frac{1}{\sqrt{2}}(\Psi_0 + \psi_1)$.

Such superpositions of zero and one-photon states cannot be achieved by simply weakly driving the oscillator as this produces a coherent superposition of all photon number states (to be described further below). However they have been achieved experimentally (Houck *et al.*, 2007; Hofheinz *et al.*, 2008; Hofheinz *et al.*, 2009) by applying control pulses to a qubit to put it into a superposition of the ground state $|g\rangle$ and the excited state $|e\rangle$

$$|\psi_{\text{initial}}\rangle = \alpha|g\rangle + \beta|e\rangle. \tag{2.60}$$

Allowing the qubit to spontaneously decay (if it is excited) leaves the qubit in the ground state and the electromagnetic field in a superposition of zero and one photon with coefficients α and β inherited from the qubit

$$|\psi_{\text{final}}\rangle = |g\rangle\left[\alpha|0\rangle + \beta|1\rangle\right]. \tag{2.61}$$

This operation maps a stationary qubit onto a 'flying qubit' (the photon) and is an essential step towards communicating quantum information via photons. In the experiment of Houck et al. (Houck *et al.*, 2007) the photons could be sent into a square law detector to measure the photon number, or into a homodyne detector to measure either quadrature of the electric field (equivalent to measuring $\hat{Q}$ or $\hat{\phi}$ in Eq. (2.42). The experiment directly showed that the one photon Fock state had zero electric field on average and that the phase of the electric field for superposition states was determined by the phase imposed initially upon the qubit superposition state. We tend to think of spontaneous emission as an incoherent process but the above results show that this is not entirely correct. What we really mean by incoherent is that the decay of an atom which starts purely in the excited state yields a photon state which varies randomly from shot to shot and which vanishes only on average.

In the UCSB experiments (Hofheinz *et al.*, 2008; Hofheinz *et al.*, 2009), complex superpositions of resonator Fock states were engineered and then measured via the

their effect on the state of the qubit, rather than by homodyne measurement of the photon state.

2.3.1 Driven LC Oscillators

Before continuing, it is useful to return to the classical circuit analysis and think about how we should include a driving force on the oscillator. Returning to Fig. (2.2), let us consider adding a signal source to the circuit at the node labelled ϕ as shown in Fig. (2.4a). The first question we have to answer is whether we should use a voltage source or a current source. Ideally, the former has zero impedance and the latter has infinite impedance. A voltage source set to zero drive amplitude would short the ϕ node to ground and ruin the oscillator. Conversely, a current source set to zero drive amplitude would have no effect on the oscillator at all since the voltage oscillations would not be damped by the infinite impedance of the current source. Thus we should use a current source which will minimize the damping. [Generically resonators will be driven through a coupling capacitor or antenna structure connected to a $\sim 50\Omega$ transmission lines which will introduce some damping.] For the moment we will assume the drive is classical. (More on the meaning of classical further below.)

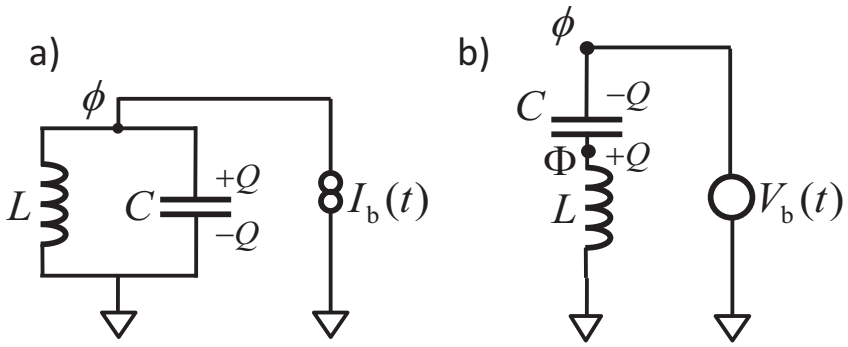

Fig. 2.4 (a) Parallel LC oscillator driven at the node ϕ by a classical external current source with infinite impedance. (b) Series LC oscillator driven at the node ϕ by a classical external voltage source with zero impedance.

Consider the following modification of the Lagrangian in Eq. (2.29)

$$\mathcal{L} = \frac{1}{2}C\dot{\phi}^2 - \frac{1}{2L}\phi^2 + I_b\phi, \tag{2.62}$$

where $I_b(t)$ is the (classical) time-dependent bias current delivered by the source. We can think of the third term as a Lagrange multiplier which enforces current conservation. From the Euler-Lagrange equation of motion

$$-\frac{d}{dt}\frac{\delta\mathcal{L}}{\delta\dot{\phi}} + \frac{\delta\mathcal{L}}{\delta\phi} = 0 \tag{2.63}$$

we obtain

$$\dot{Q} + \frac{\phi}{L} = I_{\rm b}(t), \tag{2.64}$$

which is simply the equation for current conservation at the ϕ node. Converting the Lagrangian to the classical Hamiltonian yields

$$H = \frac{Q^2}{2C} + \frac{\phi^2}{2L} - I_{\rm b}(t)\phi, \tag{2.65}$$

we see that the bias current acts as a force conjugate to the coordinate ϕ. We can view the current conservation equation above as Hamilton's equation of motion giving the time rate of change of the momentum in terms of the sum of the oscillator spring force plus the external force

$$\dot{Q} = -\frac{\phi}{L} + I_{\rm b}(t). \tag{2.66}$$

So far we have only considered the parallel LC resonator. We turn now to the series resonator illustrated in Fig. (2.4b). Clearly there can be no oscillations unless the node ϕ is connected to ground so that current can flow. This means that the series resonator should be driven by a zero impedance voltage source instead of a current source. The Lagrangian for this system is

$$\mathcal{L} = \frac{1}{2}C[\dot{\Phi} - \dot{\phi}]^2 - \frac{\Phi^2}{2L}, \tag{2.67}$$

from which it follows that the Hamiltonian is

$$H = \frac{Q^2}{2C} + \frac{\Phi^2}{2L} + V_{\rm b}(t)Q, \tag{2.68}$$

where $\dot{\phi} = V_{\rm b}(t)$ is fixed by the bias voltage. In this case, the external control parameter is the voltage rather than the drive current and the internal variable being controlled is the charge rather than the flux.

Exercise 2.3 Rederive the Lagrangian and the Hamiltonian for the series resonator shown in Fig. (2.4b) except with the capacitor and inductor interchanged so that the external voltage source is attached to the inductor rather than the capacitor. The physics should be identical to the previous case, but the mathematical expressions will look rather different. Can you find a change of coordinates that maps the problem back to the previous form?

2.3.2 Coherent States

Now that we understand the classically driven quantum harmonic oscillator, we are in a position to study coherent states of oscillation. A simple way to achieve a superposition of different number states in a quantum oscillator is to drive it with a classical external driving force so that the ground state is displaced and mapped to a so-called 'coherent state'

$$\Psi_0(\phi) \longrightarrow \Psi_\Delta(\phi) = \Psi_0(\phi - \Delta)). \tag{2.69}$$

Coherent states are discussed below and in further detail in Appendix E. In addition to having coherent states displaced in position, one can also have them displaced

in momentum. These simply correspond to being in different parts of the classical oscillation cycle. We also discuss below what it means to have a 'classical' drive.

Using the Taylor series expansion to all orders we can write the unitary transformation that displaces the state as

$$\Psi_\Delta(\phi) = e^{-\Delta\frac{\partial}{\partial\phi}}\Psi_0(\phi) \tag{2.70}$$

$$= e^{-\frac{i}{\hbar}\Delta\hat{Q}}\Psi_0(\phi), \tag{2.71}$$

which illustrates the fact that the momentum $\hat{Q}$ is the generator of displacements of its conjugate coordinate ϕ. The unitary displacement operator may be written as

$$U_\alpha = e^{-\frac{i}{\hbar}\Delta\hat{Q}} = e^{-\alpha(\hat{a}-\hat{a}^\dagger)}, \tag{2.72}$$

where the dimensionless displacement parameter is

$$\alpha \equiv \frac{\Delta Q_{\rm ZPF}}{\hbar} = \frac{\Delta}{2\Phi_{\rm ZPF}}. \tag{2.73}$$

Now using the Feynman disentangling theorem (Mahan, 2000) derived in Appendix D, this can be normal ordered

$$U_\alpha = e^{+\alpha\hat{a}^\dagger}e^{-\alpha\hat{a}}e^{-\frac{1}{2}|\alpha|^2}. \tag{2.74}$$

Taking advantage of the fact that $\hat{a}|0\rangle = 0$, we see that in second-quantized notation the coherent state becomes

$$|\alpha\rangle = e^{-\frac{1}{2}|\alpha|^2}\,e^{\alpha\hat{a}^\dagger}|0\rangle \tag{2.75}$$

Exercise 2.4 Since U_α is unitary, it must be that $\langle\alpha|\alpha\rangle = 1$. Verify this by direct calculation from Eq. (2.75).

Coherent states have some very nice properties. For example, because they are special coherent superpositions of all possible photon numbers, they are eigenstates of the photon destruction operator

$$\hat{a}|\alpha\rangle = \alpha|\alpha\rangle. \tag{2.76}$$

You can destroy a photon and still be in the same state! Curiously coherent states are *not* eigenstates of $\hat{a}^\dagger$. It is clear that $\hat{a}^\dagger|\alpha\rangle$ has no amplitude for zero photons and hence is linearly independent of $|\alpha\rangle$ (and therefore not an eigenstate). One can reach the same conclusion by noting that $\hat{a}$ and $\hat{a}^\dagger$ do not commute.

$$[\hat{a},\hat{a}^\dagger]|\alpha\rangle = |\alpha\rangle \neq 0. \tag{2.77}$$

On the other hand, it is true that the mean phonon number is given by

$$\bar{N} = \langle\alpha|\hat{a}^\dagger\hat{a}|\alpha\rangle = |\alpha|^2. \tag{2.78}$$

The phonon number distribution in a coherent state is given by the standard Poisson distribution

$$P_n = |\langle n|\alpha\rangle|^2 = \frac{\bar{N}^n}{n!}e^{-\bar{N}}. \tag{2.79}$$

Exercise 2.5 Derive Eq. (2.76) and Eq. (2.79).

Because $\hat{a}^\dagger$ is a raising operator for the energy, the coherent state has a very simple time evolution even though it is itself not an energy eigenstate. The displacement parameter α becomes complex and its phase increases linearly in time. That is, the real and imaginary parts of α simply vary sinusoidally in time indicating that the displacement alternates between position and momentum:

$$|\alpha(t)\rangle = |e^{-i\Omega t}\alpha(0)\rangle = e^{-\frac{1}{2}|\alpha|^2}\, e^{\alpha e^{-i\Omega t}\hat{a}^\dagger}|0\rangle. \tag{2.80}$$

This corresponds in the classical limit to the circular motion in phase space of the simple harmonic oscillator.

Rather than working with $\hat{\phi}$ and $\hat{Q}$, we will find it convenient to work with the dimensionless quadrature amplitudes

$$\hat{X} \equiv \frac{1}{2}\left[\hat{a} + \hat{a}^\dagger\right] \tag{2.81}$$

$$\hat{Y} \equiv -i\frac{1}{2}\left[\hat{a} - \hat{a}^\dagger\right]. \tag{2.82}$$

These hermitian operators are effectively the real and imaginary parts of the $\hat{a}$. Like $\hat{\phi}$ and $\hat{Q}$, they are canonically conjugate with the following commutator

$$[\hat{X}, \hat{Y}] = +\frac{i}{2} \tag{2.83}$$

and for coherent states obey

$$\langle\alpha|\hat{X}|\alpha\rangle = \text{Real}\,\alpha(t) \tag{2.84}$$

$$\langle\alpha|\hat{Y}|\alpha\rangle = \text{Imag}\,\alpha(t) \tag{2.85}$$

$$\langle\alpha|[\hat{X} - \langle\hat{X}\rangle]^2|\alpha\rangle = \langle 0|[\Delta\hat{X}]^2|0\rangle = \frac{1}{4} \tag{2.86}$$

$$\langle\alpha|[\hat{Y} - \langle\hat{Y}\rangle]^2|\alpha\rangle = \langle 0|[\Delta\hat{Y}]^2|0\rangle = \frac{1}{4}. \tag{2.87}$$

The last two equations show that there are quantum fluctuations in $\hat{X}$ and $\hat{Y}$ (as there must be since they do not commute with each other). The resulting uncertainties in the measured values of these quantities play a central in understanding quantum noise (Clerk *et al.*, 2010). The energy of the oscillator (in units of $\hbar\Omega$) is

$$\hat{\epsilon} = \hat{X}^2 + \hat{Y}^2 = \hat{N} + \frac{1}{2}, \tag{2.88}$$

so the number operator is simply

$$\hat{N} = \hat{X}^2 + \hat{Y}^2 - \frac{1}{2}. \tag{2.89}$$

To understand the fluctuations in photon number, let us consider a coherent state with amplitude $\alpha = \sqrt{\bar{N}}$ which is real. As illustrated in Fig. (2.5), fluctuations in $\hat{X}$

lead to photon number fluctuations (fluctuations in the length of the phasor) while fluctuations in $\hat{Y}$ lead to fluctuations in the phase of the coherent state as measured in homodyne detection (Clerk *et al.*, 2010). As we have seen, the coherent state is nothing more than a displaced vacuum state

$$|\alpha\rangle = U_\alpha|0\rangle. \tag{2.90}$$

Instead of actively displacing the physical system, we can equivalently leave the system alone and displace the coordinate system, transforming all operators according to the usual rule

$$\tilde{a} = U_\alpha^\dagger \hat{a} U_\alpha = \hat{a} + \alpha \tag{2.91}$$

$$\tilde{a}^\dagger = U_\alpha^\dagger \hat{a}^\dagger U_\alpha = \hat{a}^\dagger + \alpha^*. \tag{2.92}$$

Note that the analog of Eq. (2.76) is

$$\tilde{a}|0\rangle = \alpha|0\rangle. \tag{2.93}$$

We commonly refer to α as the classical amplitude of the motion and if $|\alpha| \gg 1$ it dominates over the quantum fluctuations around the classical value of the amplitude. As mentioned earlier, weakly coupling a system to an oscillator mode in a large amplitude coherent state produces what is effectively a classical drive with negligible quantum fluctuations. For example we might apply a force $\hat{F}$ to an oscillator whose coordinate is $\hat{y} = y_{\rm ZPF}(\hat{b} + \hat{b}^\dagger)$ via the coupling

$$\hat{V} = -\hat{F}\hat{y}. \tag{2.94}$$

For the case in which the force is supplied by linear coupling to a second 'drive' oscillator whose position operator is $\hat{x} = x_{\rm ZPF}(\hat{a} + \hat{a}^\dagger)$, the Hamiltonian would have the generic form

$$H = \omega_{\rm R}\hat{b}^\dagger\hat{b} + \omega_{\rm d}\hat{a}^\dagger\hat{a} + g(\hat{a} + \hat{a}^\dagger)(\hat{b} + \hat{b}^\dagger). \tag{2.95}$$

Changing to a frame rotating with the drive oscillator via the unitary transformation

$$\hat{U} = e^{+i\omega_{\rm d} t\hat{a}^\dagger\hat{a}} \tag{2.96}$$

the Hamiltonian becomes

$$H_1 = UHU^\dagger + U[-i\frac{d}{dt}, U^\dagger] = \omega_{\rm R}\hat{b}^\dagger\hat{b} + g\left(e^{-i\omega_{\rm d}t}\hat{a} + e^{-i\omega_{\rm d}t}\hat{a}^\dagger\right)(\hat{b} + \hat{b}^\dagger). \tag{2.97}$$

If the drive oscillator is initially placed in a high amplitude coherent state it is convenient to make the displacement transformation in Eq. (2.92) to obtain the transformed coupling Hamiltonian

$$H_2 = \omega_{\rm R}\hat{b}^\dagger\hat{b} + g\left(e^{-i\omega_{\rm d}t}\alpha + e^{-i\omega_{\rm d}t}\alpha^*\right)(\hat{b} + \hat{b}^\dagger) + H_{\rm Q}. \tag{2.98}$$

We see in the first two terms that the system oscillator is quantum and subject to a classical drive. The last term describes the quantum fluctuations associated with the drive

$$H_{\rm Q} = g\left(e^{-i\omega_{\rm d}t}\hat{a} + e^{-i\omega_{\rm d}t}\hat{a}^\dagger\right)(\hat{b} + \hat{b}^\dagger). \tag{2.99}$$

Because (initially at least) the drive oscillator is now in the ground state (in the new frame), the quantum fluctuations of the drive are small compared to the classical part,

if (in the original frame) the drive amplitude corresponds to a state with many quanta: $\bar{n} = |\alpha|^2 \gg 1$. This will continue to remain true over time provided that that the drive strength $g|\alpha|$ and the detuning $\omega_{\rm d} - \omega_{\rm R}$ are such that the number of quanta transferred from the drive to the system via the action of $H_{\rm Q}$ remains much smaller than $\bar{n}$.

A good example of this physics is provided by a two-port resonator with one weakly coupled port and one strongly coupled port. The damping of the resonator will be controlled by the port strongly coupled to the environment since most photons will escape through that port. If the system is continuously driven at the weakly coupled port, most photons from the drive line will be reflected, so a relatively large coherent drive from a microwave signal generator is required to excite the resonator cavity. This corresponds to the limit described above of small g and large α for which the classical approximation is valid. All we require is that the power in the incoming drive wave be mostly reflected so that it greatly exceeds the power emitted by the driven resonator from its strongly coupled port. In the theory of parametric amplifiers, this is known as the 'stiff pump' limit. No matter what the driven system does, the pump amplitude stays fixed and essentially classical.

Exercise 2.6 Derive Eqs. (2.91-2.92) by differentiating with respect to α and solving the resulting differential equation.

Exercise 2.7 Solve the Heisenberg equation of motion for $\hat{b}$ using the Hamiltoninan in Eq. (2.98) but neglecting the quantum fluctuation term $H_{\rm Q}$. Show that this classical drive applied to an oscillator initially in a coherent state (including possibly the vacuum state) always leaves the system in a coherent state.

Exercise 2.8 Show by direct computation that for the Bose-Einstein number distribution for a thermal photon state

$$\langle\langle [\hat{N} - \bar{N}]^2 \rangle\rangle = \bar{N}(\bar{N} + 1). \tag{2.100}$$

If you are familiar with Wick's theorem, use that to achieve the same result.

Exercise 2.9 $\hat{X}^2$ and $\hat{Y}^2$ are clearly Hermitian operators with non-negative eigenvalues. How then can you explain the fact that

$$\langle 0|\hat{X}^2\hat{Y}^2|0\rangle = -\frac{1}{16} \tag{2.101}$$

is negative? Similarly how can

$$\langle 0|\hat{X}\hat{Y}|0\rangle = \frac{i}{4} \tag{2.102}$$

be complex?

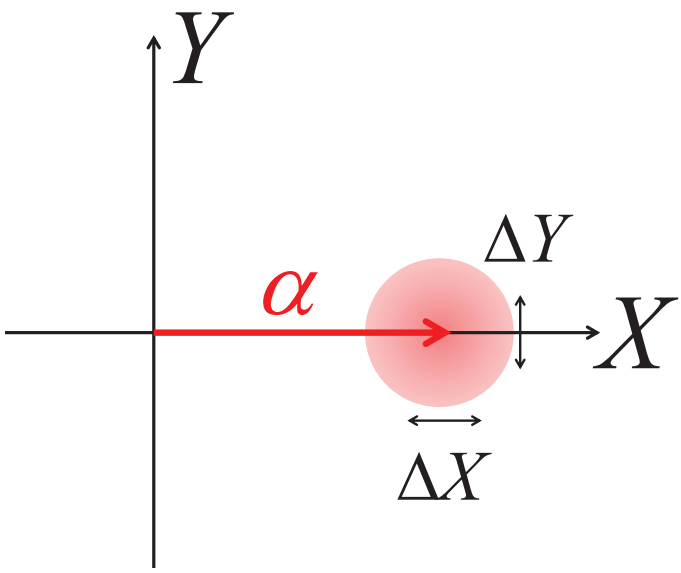

Fig. 2.5 Quantum fluctuations of amplitude and phase quadratures in a coherent state $|\alpha\rangle$.

Writing the X quadrature amplitude as

$$\hat{X} = \alpha + \Delta\hat{X}, \tag{2.103}$$

we see that $\Delta\hat{X}$ has the same statistical properties in the coherent state $|\alpha\rangle$ as $\hat{X}$ does in the vacuum state. The number fluctuations are therefore given by the usual Poisson distribution result derived above

$$\langle\alpha|[\hat{N} - \bar{N}]^2|\alpha\rangle = \langle\alpha|\left[2\alpha\Delta\hat{X} + \Delta\hat{X}^2 + \Delta\hat{Y}^2 - \frac{1}{2}\right]^2|\alpha\rangle = \bar{N}. \tag{2.104}$$

Essentially the above results mean that a coherent laser or microwave beam is as classical as possible. The fluctuations come only from the fact that the photon detection events are discrete and the photons are sprinkled randomly throughout the beam in an uncorrelated manner. A thermal beam has larger fluctuations because the photons tend to bunch together (Clerk *et al.*, 2010).

Fluctuations in the quadrature orthogonal to α cause uncertainty in a measurement of the phase of the coherent state. For the case of α real and in the limit $|\alpha| \gg 1$, we have[6]

$$\Delta\hat{\theta} \approx \frac{\Delta\hat{Y}}{\alpha} \tag{2.105}$$

and

$$\langle\alpha|(\Delta\hat{\theta})^2|\alpha\rangle = \frac{1}{4\bar{N}}. \tag{2.106}$$

[6]The 'phase' operator defined here does not have the angular periodicity of a phase and is only valid for small angles.

Thus we arrive at the fundamental number-phase uncertainty relation

$$\langle\alpha|(\Delta\hat{\theta})^2|\alpha\rangle^{1/2}\langle\alpha|(\Delta\hat{N})^2|\alpha\rangle^{1/2} \geq \frac{1}{2}. \tag{2.107}$$

Coherent states are minimum uncertainty gaussian states which satisfy this relation as an equality. Other non-gaussian states satisfy this relation only as an inequality.

From the equation of motion of the free oscillator we see that the quadrature amplitudes obey

$$\hat{X}(t) = \cos(\Omega t)\hat{X}(0) + \sin(\Omega t)\hat{Y}(0) \tag{2.108}$$
$$\hat{Y}(t) = \cos(\Omega t)\hat{Y}(0) - \sin(\Omega t)\hat{X}(0) \tag{2.109}$$

In Appendix B we study photons traveling in transmission lines and we again find that the traveling modes are also harmonic oscillators. The above results provide the first hint that the $\sin\Omega t$ and $\cos\Omega t$ quadratures of a quantum electrical signal are canonically conjugate and hence cannot be simultaneously measured with perfect accuracy. Equivalently even the vacuum contains noise which will appear in any measurement in which one attempts to measure both quadratures of the signal. Eq. (2.87) tells us that this uncertainty gives a vacuum 'noise energy' (noise power per unit measurement bandwidth) of half a photon (Clerk *et al.*, 2010).

Exercise 2.10 Think through the above statement about noise energy at the classical level. Consider a noise source which is white (i.e., with constant spectral density S) over some large interval. Passing this noise through a filter which transmits a small bandwidth B centered on frequency ω will yield a power of $P = SB$. The wider the bandpass the more power. Thus we see that the spectral density is power per unit bandwidth which has units of energy. For a quantum thermal source feeding a photomultiplier (which measures $\hat{a}^\dagger\hat{a}$), this is $S = \hbar\omega\bar{N}$ and we say that 'the noise energy is $\bar{N}$ photons.' A photomultiplier feed by vacuum noise has zero output. However listening to the vacuum noise power through a phase preserving amplifier or (equivalently) using a heterodyne detector which measures the power in the quadrature amplitudes $\langle\hat{X}^2 + \hat{Y}^2\rangle = \frac{1}{2}$ yields a noise energy of half a photon (Clerk *et al.*, 2010).

2.4 Coupled LC Resonators

Having thoroughly analyzed the simple LC oscillator, it is a useful exercise to consider how to quantize a pair of LC oscillators connected by a coupling capacitor as shown in Fig. (2.6). This will teach us how to handle slightly more complex circuits and will set the stage for understanding the coupling of a qubit to a microwave resonator.

Choosing the fluxes Φ_1 and Φ_2 as the coordinates of the two oscillators, the Lagrangian can be written

$$\mathcal{L} = \frac{1}{2}C_1\dot{\Phi}_1^2 + \frac{1}{2}C_2\dot{\Phi}_2^2 + \frac{1}{2}C_0[\dot{\Phi}_1 - \dot{\Phi}_2]^2 - \frac{1}{2L_1}\Phi_1^2 - \frac{1}{2L_2}\Phi_2^2 \tag{2.110}$$

It is convenient to use a matrix notation

$$\mathcal{L}\frac{1}{2}\dot{\Phi}C\dot{\Phi} - \frac{1}{2}\Phi L^{-1}\Phi, \tag{2.111}$$

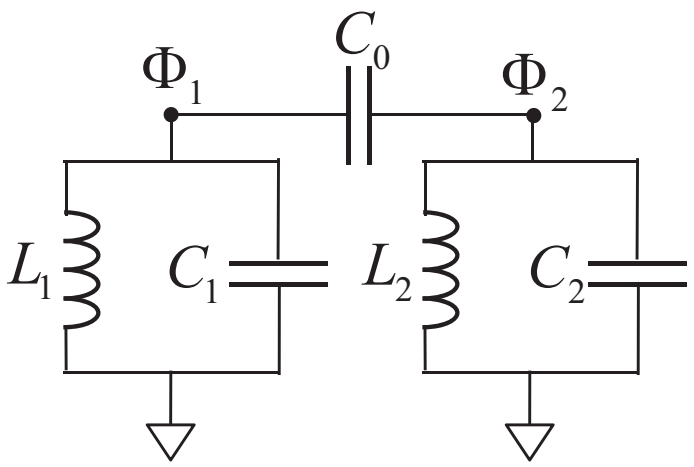

Fig. 2.6 A pair of LC oscillators connected by coupling capacitor C_0.

where the capacitance matrix is

$$C \equiv \begin{pmatrix} C_1 + C_0 & -C_0 \\ -C_0 & C_2 + C_0 \end{pmatrix}, \tag{2.112}$$

and the inverse inductance matrix is

$$L^{-1} \equiv \begin{pmatrix} \frac{1}{L_1} & 0 \\ 0 & \frac{1}{L_2} \end{pmatrix}. \tag{2.113}$$

At this point there are two ways to proceed, which are described below.

METHOD I: FIND THE HAMILTONIAN, THEN DIAGONALIZE. In the first method we will use the given coordinates to find the canonical momenta and from there construct the Hamiltonian which will contain a coupling between the two oscillators.

The canonical momenta are given by

$$Q_i \equiv \frac{\delta \mathcal{L}}{\delta \dot{\Phi}_i} = C_{ij} \dot{\Phi}_j, \tag{2.114}$$

where we employ the Einstein summation convention for repeated indices. In terms of the inverse of the capacitance matrix we have

$$\dot{\Phi} = C^{-1} Q. \tag{2.115}$$

The Hamiltonian $H = Q_i \dot{\Phi}_i - \mathcal{L}$ now takes the canonical form

$$H = \frac{1}{2} Q C^{-1} Q + \frac{1}{2} \Phi L^{-1} \Phi. \tag{2.116}$$

The inverse of the capacitance matrix is

$$C^{-1} = \frac{1}{C_1 C_2 + C_0 C_1 + C_0 C_2} \begin{pmatrix} C_2 + C_0 & +C_0 \\ +C_0 & C_1 + C_0 \end{pmatrix}, \tag{2.117}$$

It is useful to define two frequencies and a coupling constant:

$$\omega_j^2 =\equiv \frac{1}{L_j} \left(C^{-1}\right)_{jj}, \tag{2.118}$$

and

$$\beta \equiv \frac{C_0}{\sqrt{(C_1 + c_0)(C_2 + C_0)}}, \tag{2.119}$$

which yields

$$C^{-1} = \begin{pmatrix} L_1 \omega_1^2 & +\beta \sqrt{L_1 L_2} \omega_1 \omega_2 \\ \beta \sqrt{L_1 L_2} \omega_1 \omega_2 & L_2 \omega_2^2 \end{pmatrix}. \tag{2.120}$$

We can now write the Hamiltonian $H = H_0 + V$ in terms of two oscillators with masses L_j and coupled through their momenta

$$H_0 = \frac{1}{2} L_1 \omega_1^2 Q_1^2 + \frac{1}{2L_1} \Phi_1^2 + \frac{1}{2} L_2 \omega_1^2 Q_2^2 + \frac{1}{2L_2} \Phi_2^2 \tag{2.121}$$

$$V = \beta \sqrt{L_1 L_2} \omega_1 \omega_2 Q_1 Q_2. \tag{2.122}$$

We quantize as usual by converting to operators with the canonical commutation relation

$$[\hat{Q}_i, \hat{\Phi}_j] = -i\hbar \delta_{ij}. \tag{2.123}$$

Defining creation and annihilation operators in the usual way we have

$$H_0 = \sum_{j=1}^{2} \hbar \omega_j \left(\hat{a}_j^\dagger \hat{a}_j + \frac{1}{2} \right) \tag{2.124}$$

$$V = -\beta \hbar \sqrt{\omega_1 \omega_2} (\hat{a}_1 - \hat{a}_1^\dagger)(\hat{a}_2 - \hat{a}_2^\dagger), \tag{2.125}$$

which can be diagonalized via a Bogoljubov transformation.

Exercise 2.11 Find the Bogoljubov transformation which diagonalizes $H_0 + V$ defined above.

METHOD II: DIAGONALIZE THE LAGRANGIAN, THEN THE HAMILTONIAN. The first method used the original coordinates and found their canonical momenta and from there constructed the (non-diagonal) Hamiltonian. In the second method, we will find the normal mode coordinates which diagonalize the Lagrangian. In terms of these, the Hamiltonian will be automatically diagonal.

When we try to diagonalize the Lagrangian in Eq. (2.111), we are faced with the problem that the capacitance and inductance matrices do not commute and hence cannot be simultaneously diagonalized by a unitary transformation. We can cure this problem by making a *similarity transformation* which maps L^{-1} to the identity matrix. We simply choose scaled coordinates

$$\psi_j = \frac{1}{\sqrt{L_j}}\Phi_j. \tag{2.126}$$

In terms of these the Lagrangian becomes

$$\mathcal{L} = \frac{1}{2}\dot{\psi}_i A_{ij}\dot{\psi}_j - \frac{1}{2}\psi_i\delta_{ij}\psi_j \tag{2.127}$$

where

$$A \equiv \begin{pmatrix} \frac{1}{\Omega_1^2} & -\frac{\beta}{\Omega_1\Omega_2} \\ -\frac{\beta}{\Omega_1\Omega_2} & \frac{1}{\Omega_2^2} \end{pmatrix}, \tag{2.128}$$

where we define frequencies (different from the previous method)

$$\frac{1}{\Omega_1^2} \equiv L_1(C_1 + C_0) \tag{2.129}$$

$$\frac{1}{\Omega_2^2} \equiv L_2(C_2 + C_0). \tag{2.130}$$

Since A commutes with the identity matrix, we can now proceed as usual to perform a rotation among the coordinates to diagonalize the Lagrangian. Let S be the orthogonal transformation that diagonalizes A. The normal modes and eigenvalues are then given by

$$\tilde{\psi} = S\psi \tag{2.131}$$

$$\tilde{A} = \begin{pmatrix} \frac{1}{\Omega_1^2} & 0 \\ 0 & \frac{1}{\Omega_2^2} \end{pmatrix} = SAS^{\mathrm{T}}. \tag{2.132}$$

Exercise 2.12 Find the normal modes and eigenfrequencies above. Hint: Write $A = \bar{A} + Z\sigma^z + X\sigma^x$ and think of it as a spin problem which has eigenvalues

$$\epsilon_\pm = \bar{A} \pm \sqrt{X^2 + Z^2} \tag{2.133}$$

and eigenfunctions which follow from

$$S = \begin{pmatrix} +\cos\frac{\theta}{2} & +\sin\frac{\theta}{2} \\ -\sin\frac{\theta}{2} & +\cos\frac{\theta}{2} \end{pmatrix}, \tag{2.134}$$

where $\tan\theta = X/Z$.

2.5 Modes of Transmission Lines Resonators

The above lengthy discussion of the simple harmonic oscillator has laid the very important groundwork for our next topic which is the quantum modes of transmission lines. We will start with finite length transmission lines which have discrete electromagnetic resonances, each of which will turn out to be an independent simple harmonic oscillator. Then we will move on to the semi-infinite transmission line and discover that it can act like a dissipative bath even though every one of its electrical elements is non-dissipative.

Our finite length transmission line could be a length of ordinary coaxial cable or its 2D equivalent, the coplanar waveguide (CPW), which consists of a superconducting wire evaporated on an insulating substrate and having superconducting ground planes adjacent to it on the same surface as shown in Fig. (2.7). Such a system exhibits many standing wave resonances and we will soon see that each resonance is an independent harmonic oscillator equivalent to the simple LC oscillator just discussed. The discretized equivalent circuit for the CPW resonator is also shown in Fig. (2.7). In our initial analysis we will neglect the presence of the qubit and neglect the capacitors C_0 at each end which couple the resonator to the external transmission lines. We can thus assume in this first example open-circuit boundary conditions for which the current (but not the voltage) vanishes at the ends of the resonator.

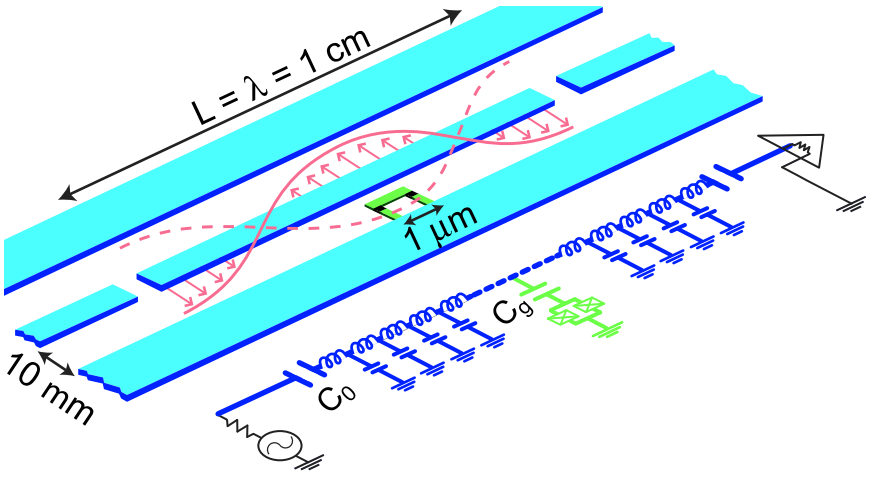

Fig. 2.7 Schematic illustration of a typical coplanar waveguide (CPW) resonator used in circuit QED together with its discretized lumped-element equivalent circuit. The qubit lies between the center pin and the adjacent ground plane and is located at an antinode of the electric field, shown in this case for the full-wave resonance of the CPW. From (Blais *et al.*, 2004).

It is convenient to define a flux variable analogous to that used above but now dependent on position (Devoret, 1997)

$$\Phi(x,t) \equiv \int_{-\infty}^{t} d\tau\, V(x,\tau), \tag{2.135}$$

where $V(x,t) = \partial_t \Phi(x,t)$ is the local voltage on the transmission line at position x and time t. The inductance and capacitance per unit length are ℓ and c respectively. Each segment of the line of length dx has inductance $\ell\, dx$ and the voltage drop along it is $-dx\, \partial_x \partial_t \Phi(x,t)$. The flux through this inductance is thus $-dx\, \partial_x \Phi(x,t)$ and the local value of the current is given by the constitutive equation

$$I(x,t) = -\frac{1}{\ell}\, \partial_x \Phi(x,t). \tag{2.136}$$

The Lagrangian for a system of length L (L is not to be confused with some discrete inductance)

$$\mathcal{L}_g \equiv \int_0^L dx\, \mathcal{L}(x,t) = \int_0^L dx\, \left[\frac{c}{2}(\partial_t \Phi)^2 - \frac{1}{2\ell}\,(\partial_x \Phi)^2\right], \tag{2.137}$$

The Euler-Lagrange equation for this Lagrangian is simply the wave equation

$$v_{\rm p}^2 \partial_x^2 \Phi - \partial_t^2 \Phi = 0. \tag{2.138}$$

The momentum conjugate to $\Phi(x)$ is simply the charge density

$$q(x,t) \equiv \frac{\delta \mathcal{L}_g}{\delta \partial_t \Phi} = c\partial_t \Phi = cV(x,t) \tag{2.139}$$

and so the Hamiltonian is given by

$$H = \int_0^L dx\, \left\{\frac{1}{2c} q^2 + \frac{1}{2\ell}(\partial_x \Phi)^2\right\}. \tag{2.140}$$

Let us next proceed to consider the classical normal mode solutions of Eq. (2.138). If we assume a sinusoidal time-dependence with angular frequency ω,

$$\Phi(x,t) = e^{-i\omega t}\phi(x), \tag{2.141}$$

we arrive at the Schrödinger like eigenvalue problem

$$-\partial_x^2 \phi(x) = k^2 \phi(x), \tag{2.142}$$

where $k = \omega/v_{\rm p}$ and the mode wave velocity is $v_{\rm p} = \frac{1}{\sqrt{\ell c}}$. The open-circuit (zero-current) boundary conditions tell us that the eigenfunctions have vanishing derivative at the boundaries. We choose a particular normalization for eigenfunctions which will keep the equations looking as close to those of the single harmonic oscillator as possible

$$\phi_n(x) = \sqrt{2}\cos(k_n x), \tag{2.143}$$

where $n\,\epsilon\,\{0,1,2,3,\ldots\}$, $k_n = \frac{n\pi}{L}$. Because for these boundary conditions the operator ∂_x^2 is self-adjoint, and because the eigenvalues are non-degenerate, the eigenfunctions have two helpful properties

$$\int_0^L dx\, \phi_n(x)\phi_m(x) = L\delta_{nm} \tag{2.144}$$

$$\int_0^L dx\, [\partial_x \phi_n(x)][\partial_x \phi_m(x)] = Lk_n^2\delta_{nm}. \tag{2.145}$$

From this it follows that the Lagrangian can be diagonalized using these (spatial) normal modes as a basis. Let us parameterize the field $\Phi(x,t)$ by

$$\Phi(x,t) = \sum_{n=0}^{\infty} \xi_n(t)\phi_n(x), \tag{2.146}$$

where the ξ_n are *arbitrary* (i.e. not necessarily sinusoidal) functions of time. Substituting into the Eq. (2.137) and using Eqs. (2.144-2.145)

$$\mathcal{L}_g = \frac{1}{2}Lc\sum_{n=0}^{\infty}[\partial_t\xi_n]^2 - \omega_n^2\xi_n^2 \tag{2.147}$$

we see that each normal mode becomes an independent simple harmonic oscillator. The momentum conjugate to the normal mode amplitude ξ_n is

$$q_n = \frac{\delta\mathcal{L}_g}{\delta\partial_t\xi_n} = Lc\partial_t\xi_n, \tag{2.148}$$

so the Hamiltonian is

$$H = \frac{1}{2}\sum_{n=0}^{\infty}\left\{\frac{1}{Lc}q_n^2 + Lc\omega_n^2\xi_n^2\right\}, \tag{2.149}$$

which we can quantize as before. Before doing so, let us note that the $n = 0$ mode is a 'free particle' rather than a harmonic oscillator because its spring constant vanishes. This mode simply corresponds to a uniform net charge distributed evenly along the transmission line. For a free particle the momentum (in this case charge) is a constant and the coordinate (flux) increases linearly with time. In most situations the total charge is indeed simply a constant of the motion (and typically vanishes) and we can ignore the zero mode altogether. We will assume this is the case henceforth.

We end up with a set of independent normal modes with coordinate ξ_n and conjugate momentum q_n which when quantized can be expressed in terms of mode raising and lowering operators in a manner analogous to Eq. (2.42)

$$\hat{\xi}_n = \sqrt{\frac{\hbar}{2\omega_n Lc}}(\hat{a}_n + \hat{a}_n^\dagger) \tag{2.150}$$

$$\hat{q}_n = -i\sqrt{\frac{\hbar\omega_n Lc}{2}}(\hat{a}_n - \hat{a}_n^\dagger) \tag{2.151}$$

where the ladder operators of the different modes obey

$$[\hat{a}_n, \hat{a}_m^\dagger] = \delta_{nm}. \tag{2.152}$$

Note that, just as in the single mode case in Eq. (2.42), there is a certain arbitrariness in the choice of the phase of the destruction operators (which can be independently varied for each separate mode).

If we are coupling a qubit to a resonator at some particular position x, we need to be able to express the flux and charge density operators at that point in terms of the normal mode operators. Eq. (2.146) is readily extended to the quantum operators

$$\hat{\Phi}(x) = \sum_n^{\infty} \phi_n(x)\hat{\xi}_n, \tag{2.153}$$

as is Eq. (2.139)

$$\hat{q}(x) = \frac{1}{L}\sum_n^{\infty} \phi_n(x)\hat{q}_n. \tag{2.154}$$

Similarly, the analog of Eq. (2.53) for the voltage operator at point x is given by

$$\hat{V}(x) = \frac{1}{c}\hat{q}(x) = \frac{1}{L}\sum_{n=0}^{\infty} \phi_n(x)\hat{q}_n = -i\sum_{n=0}^{\infty}\sqrt{\frac{\hbar\omega_n}{2Lc}}(\hat{a}_n - \hat{a}_n^\dagger)\phi_n(x). \tag{2.155}$$

The total capacitance to ground of the resonator, Lc, enters this expression in a way that is similar to lumped element oscillator expression in Eq. (2.53). (Recall that L is the length of the resonator, not the inductance.)

Notice that the flux and charge density operators obey the following commutation relation

$$[\hat{q}(x), \hat{\Phi}(x')] = -i\hbar\frac{1}{L}\sum_n^{\infty}\phi_n(x)\phi_n(x'). \tag{2.156}$$

Using the completeness relation (and recalling that the factor of L appears because we did not normalize the eigenfunctions to unity) we end up with the standard field theoretic relation

$$[\hat{q}(x'), \hat{\Phi}(x)] = -i\hbar\delta(x - x'). \tag{2.157}$$

Expressing the quantum Hamiltonian in Eq. (2.140) in terms of these operators, we have simply

$$\hat{H} = \int_0^L dx\, \left\{\frac{1}{2c}\hat{q}^2 + \frac{1}{2\ell}(\partial_x\hat{\Phi})^2\right\}. \tag{2.158}$$

As a 'sanity check' let us look at the Hamilton equations of motion. Using commutation relation in Eq. (2.157) and its extension to

$$[\hat{q}(x'), \partial_x\hat{\Phi}(x)] = -i\hbar\partial_x\delta(x - x'). \tag{2.159}$$

we arrive at

$$\partial_t\hat{\Phi}(y) = \frac{i}{\hbar}[\hat{H}, \hat{\Phi}(y)] = \frac{1}{c}\hat{q}(y) \tag{2.160}$$

$$\partial_t\hat{q}(y) = \frac{i}{\hbar}[\hat{H}, \hat{q}(y)] = \frac{1}{\ell}\partial_y^2\hat{\Phi}(y). \tag{2.161}$$

and hence the quantum version of the wave equation in Eq. (2.138)

$$v_{\rm p}^2\partial_x^2\hat{\Phi}(x) - \partial_t^2\hat{\Phi}(x) = 0. \tag{2.162}$$

When we studied coherent states of a single oscillator we found that they were simply the vacuum state displaced in either position (flux) and/or momentum (charge).

For a multi-mode resonator one can coherently displace a linear combination of the of the normal modes. The familiar problem of solving the time evolution of a plucked string is a good classical analog. Suppose that we wish to displace the resonator degrees of freedom so that the local displacement obeys

$$\langle \hat{\Phi}(x) \rangle = \Delta(x), \tag{2.163}$$

where Δ is some specified function. The analog of Eq. (2.72) is simply

$$U_\Delta = e^{-\frac{i}{\hbar}\int_0^L dx\, \Delta(x)\hat{q}(x)}. \tag{2.164}$$

a form which is familiar from the theory of the Luttinger liquid (Kane and Fisher, 1992*b*; Kane and Fisher, 1992*a*). Using Eq. (2.154) this can be understood in terms of coherent displacement of each of the normal modes

$$U_\Delta = e^{-\frac{i}{\hbar}\sum_n \Delta_n \hat{q}_n} = \prod_n e^{-\frac{i}{\hbar}\Delta_n \hat{q}_n}. \tag{2.165}$$

Exercise 2.13 In analogy with Eqs. (2.91-2.92) show that

$$U_\Delta^\dagger \hat{\Phi}(y) U_\Delta = \hat{\Phi}(y) + \Delta(y). \tag{2.166}$$

Hint: It may be useful to scale $\Delta(x)$ by an overall factor θ and differentiate with respect to θ.

2.6 'Black Box' Quantization of Linear Circuits

We have so far studied a single LC oscillator and found that its quantum excitation energy $\hbar\Omega$ is given directly by its classical frequency Ω. We also found in Eq. (2.50) that the characteristic impedance $Z = \sqrt{L/C}$ determines the size of the zero-point fluctuations in flux and charge. The typical circuit that we will study is more complex than a single LC oscillator and might even be a 'black box' whose properties we need to determine. Suppose that we have such a black box and we have access to one port of this structure as shown in Fig. (2.8a). The only thing we know (or assume) is that all the elements inside the black box are linear and purely reactive; i.e., the black box is a network of inductors and capacitors. It might for example be a transmission line resonator such as we studied above. We may ultimately want to connect a qubit or some measurement apparatus to the port of the black box. In order to predict the quantum properties we need to know each of the normal modes of the box and the size of their zero-point fluctuations as seen at the port. Some modes may be localized inside the box and have very little amplitude at the port. Others may be more strongly coupled to the port.

Since the black box is linear, we can probe it by applying a sinusoidal drive and measuring the response. The are two ways to do this. First, one can hook up a current source which forces current

$$I(t) = i[\omega]e^{j\omega t} + i^*[\omega]e^{-j\omega t} \tag{2.167}$$

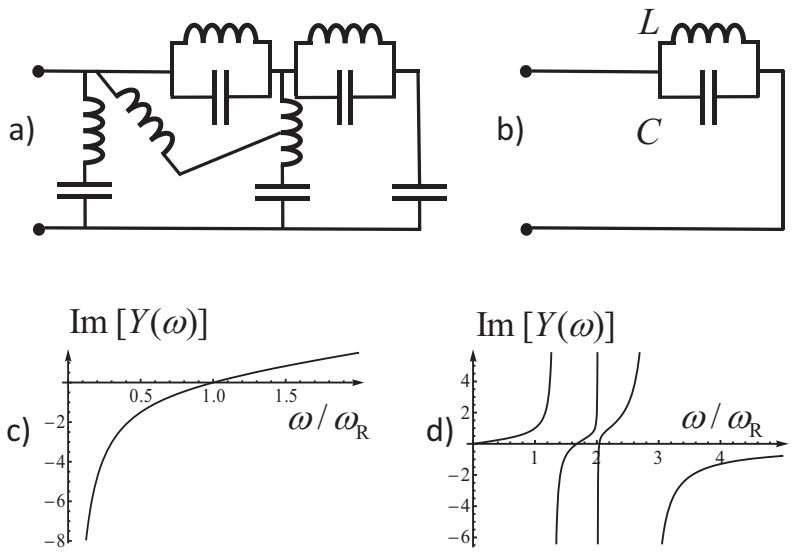

Fig. 2.8 a) One-port black box containing an arbitrary reactive network. b) Lumped element LC resonator. c) Imaginary part of the admittance of the LC resonator in (b) vs. dimensionless frequency showing that the admittance passes through zero with positive slope at the resonance frequency. d) Imaginary part of the admittance of a multi-resonance circuit with a capacitor in the input line similar to (a). Notice that the slope of the admittance at each of the zeros is different, corresponding to different characteristic impedances of the resonances.

through the circuit.[7] The linear response of the circuit is determined by measuring the resulting voltage at the input port

$$V(t) = v[\omega]e^{j\omega t} + v^*[\omega]e^{-j\omega t} \tag{2.168}$$

The linear response coefficient that relates the voltage response to the drive current is known as the impedance

$$v[\omega] = Z[\omega]i[\omega]. \tag{2.169}$$

Because the box contains only reactive elements (assumed finite in number) the impedance is purely imaginary. The poles of $Z[\omega]$ determine the eigenfrequencies of the circuit for which natural oscillations can occur without external input (when the input port is open circuited). Note that this is consistent with the fact that an ideal current

[7] To avoid confusion with the current i we follow the electrical engineering convention of using $j = -\sqrt{-1}$. In addition to avoid confusion between some function of time and its Fourier transform, we will use the convention that Fourier transformed quantities have the frequency argument in square brackets.

source has infinite internal impedance and hence drives the circuit while effectively keeping the input port open-circuited. The circuit presented in Fig. (2.9a) is a natural representation of an arbitrary frequency-dependent impedance[8]. It is important to understand that in general, the circuit elements used in this mathematical representation have no direct correspondence with any of the physical elements in the actual circuit. Note that if there is a pole in the impedance at zero frequency, it corresponds to the 'free-particle' Hamiltonian of a capacitor, $H = \frac{\hat{Q}^2}{2C}$ in series with the input (not shown in Fig. (2.9a).

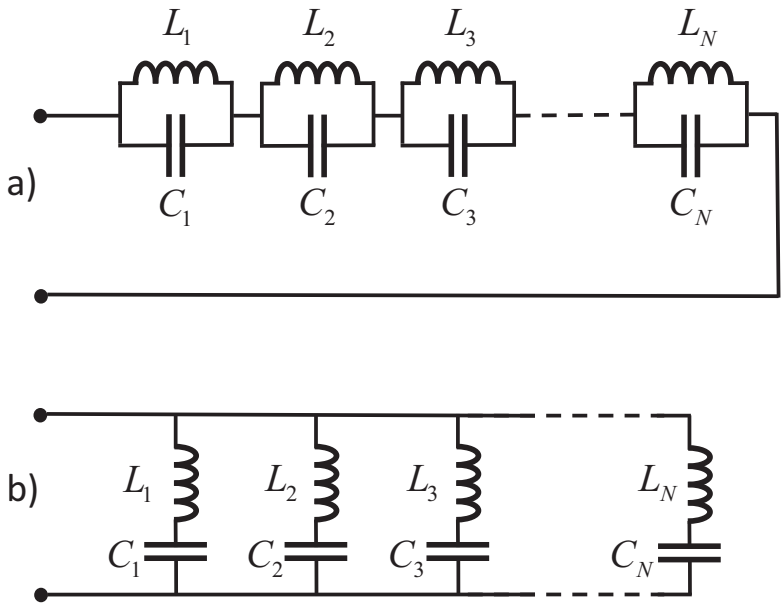

Fig. 2.9 a) Natural representation of an arbitrary impedance (assuming for simplicity that the impedance vanishes at zero frequency). The jth pole of the impedance occurs at the frequency of the jth collective mode $\omega_j = 1/\sqrt{L_j C_j}$ and can be detected by using an infinite-impedance current source to inject RF current into the input port and measuring the resulting RF voltage across across the port. b) Natural representation of an arbitrary admittance (assuming for simplicity that the admittance vanishes at zero frequency). The poles of the admittance determine the natural oscillation frequencies of the circuit when its input is shorted. These can be detected by using a zero-impedance RF voltage source to put a drive voltage across the input port and measuring the resulting RF current that flows into the port.

[8]Note that this particular representation has the property that there is a dc connection through all the inductors to ground. Hence the impedance vanishes at zero frequency. If this is not the case for the physical circuit, then we must include a series capacitor in the input line. This would be necessary for example to represent the impedance of the circuit shown in Fig. (2.8a).

The second way to measure the linear response is to attach a zero-impedance voltage source to the input and measure the resulting current response. The linear response coefficient that relates the current response to the voltage drive is known as the admittance

$$i[\omega] = Y[\omega]v[\omega] \tag{2.170}$$

which is simply the inverse of the impedance

$$Y[\omega] = Z^{-1}[\omega]. \tag{2.171}$$

The circuit presented in Fig. (2.9b) is a natural representation of an arbitrary frequency-dependent admittance. The poles of the admittance determine the natural oscillation frequencies of the circuit when its input port is short-circuited. Again, this is consistent with the excitation of these modes, this time using a zero-impedance voltage source. To reiterate, the poles of the admittance (zeros of the impedance) correspond to effective *s*eries LC resonances which would occur if the input port were short-circuited. These can be important but for the particular case where nothing is hooked up to the external port, these poles do not correspond to active degrees of freedom. An inductor and capacitor in series cannot oscillate on their own at non-zero frequencies unless the circuit is closed at the input port. Finally, we note that according to Foster's theorem (Foster, 1924), the (imaginary) admittance of a reactive circuit always passes through zero with positive slope so therefore each zero must be separated from the next by a pole as shown in Fig. (2.8d).

Physically, poles of response functions are the most natural thing to consider. However in numerical simulations, zeros are sometimes mathematically easier for a computer to handle than poles. Hence it can be convenient to work with the impedance representation in Fig. (2.9a) but numerically ascertain the zero-crossings of the admittance rather than the poles of the impedance.

As an example, suppose that the black box contains a single parallel LC oscillator as shown in Fig. (2.8b). Then the admittance is simply

$$Y[\omega] = j\omega C + \frac{1}{j\omega L} = \frac{+j}{Z_0}\left(\frac{\omega}{\omega_{\rm R}} - \frac{\omega_{\rm R}}{\omega}\right), \tag{2.172}$$

where $Z_0 \equiv \sqrt{\frac{L}{C}}$ is the characteristic impedance of the resonance. Note that this is indeed purely imaginary and further that it passes through zero at the resonance frequency $\Omega = \frac{1}{\sqrt{LC}}$ as shown in Fig. (2.8c). The admittance is zero because the inductor and capacitor have opposite admittances at the resonance frequency. But this is precisely the condition for self-sustaining oscillation where the currents in the inductor and capacitor are opposite to each other and no external input is needed.

It turns out that knowing the admittance (or impedance) of the box port as a function of frequency completely characterizes the classical and the quantum properties of the black box, as long as it contains only linear elements(Manucharyan *et al.*, 2007). We have already seen a hint of this in Eqs. (2.43-2.44) where we learned that the characteristic impedance of a resonance determines the zero-point fluctuations of the charge and flux degrees of freedom. Of course, knowing the frequency of an oscillator

we can immediately write down the quantum Hamiltonian (neglecting the zero-point energy)

$$H_0 = \hbar\Omega\hat{a}^\dagger\hat{a}. \tag{2.173}$$

This is not enough however. If we couple an external circuit to our black box we need to know the matrix elements of the coupling Hamiltonian. For this we need to know how to express the charge and flux in terms of a and $a^\dagger$ and hence must know the characteristic impedance of the resonance. Happily, the slope with which the admittance passes through zero determines the characteristic impedance of the resonance

$$\Omega\left(\frac{\partial Y}{\partial\omega}\right)_\Omega = \frac{2j}{Z_0}, \tag{2.174}$$

so that

$$Z_0 = \frac{2j}{\Omega\left(\frac{\partial Y}{\partial\omega}\right)_\Omega}. \tag{2.175}$$

Using Eqs. (2.43-2.44) we can then find any physical quantity we desire.

To see the generality of this result, consider the example of the lumped element circuit in Fig. (2.10). If $L_1 + L_2 = L$ then this has the same bare resonance frequency Ω but clearly will have a different coupling to the port. Use of Eq. (2.44) yields

$$\Phi^2_{\rm ZPF} = \frac{\hbar\Omega L}{2}\left(\frac{L_1}{L_1+L_2}\right)^2, \tag{2.176}$$

which is just what we expect from the transformer turns ratio.

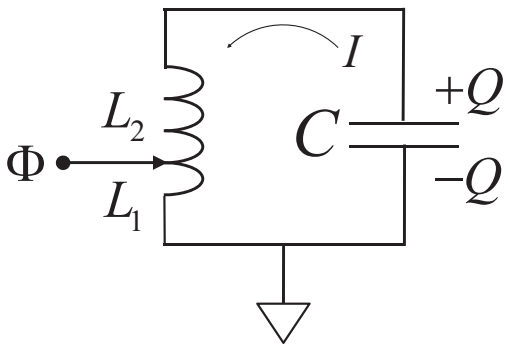

Fig. 2.10 Single port black box containing a simple LC oscillator with the port connected to an inductive divider with $L_1 + L_2 = L$.

Let us suppose for example that we couple to our black box through an inductor $L_{\rm c}$ as shown in Fig. (2.11). The coupling Hamiltonian is

$$H_1 = \frac{1}{2L_c}\left(\hat{\Phi} - \hat{\Phi}_{in}\right)^2. \tag{2.177}$$

The operator $\hat{\Phi}_{in}$ is either a classical control field or is a quantum operator for whatever system we hook up to our black box. Now that we know impedance of the resonance, we know how to express $\hat{\Phi}$ using Eq. (2.44) so that we have

$$H_1 = \frac{1}{2L_c}\left(\Phi_{ZPF}(\hat{a} + \hat{a}^\dagger) - \hat{\Phi}_{in}\right)^2. \tag{2.178}$$

The case of capacitive rather than inductive coupling is more complex as can be seen from the example of two capacitively coupled oscillators shown in Fig. (2.6) which we discussed earlier. We found that it was easy to write down the Lagrangian, but finding the Hamiltonian required inverting the capacitance matrix for the entire system. Hence if we are going to use the flux variable at the input port as the coordinate, it is usually easiest to proceed by treating the coupling capacitor as being inside the black box.

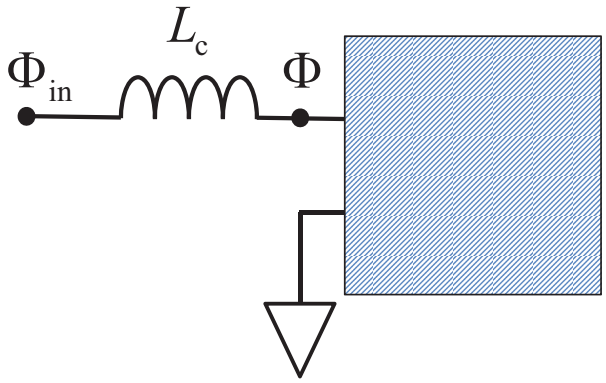

Fig. 2.11 Coupling to a blackbox via an inductor.

The extension of these results to the case of a multi-mode black box Hamiltonian is simply

$$H_0 = \sum_m \Omega_m \hat{a}_m^\dagger \hat{a}_m, \tag{2.179}$$

where the summation is over the different modes and the flux operator at the port of the black box is simply

$$\hat{\Phi} = \sum_m \Phi_{ZPF}^{(m)}\left(\hat{a}_m + \hat{a}_m^\dagger\right). \tag{2.180}$$

This is simply a statement that the voltage across the input port is the sum of the voltages across each of the resonator elements in series as shown in Fig. (2.9a).

This 'black box' formalism will prove useful if it is possible to either measure, or use finite element simulations to compute, the admittance as a function of frequency. So far we have only discussed quantization of linear circuits which are equivalent to coupled simple harmonic oscillators. Qubits are of course not linear circuit elements, but the formalism developed here is especially useful for the study of transmon qubits coupled to resonators since as we will see in Chap. (4), the transmon qubit is essentially a weakly anharmonic oscillator. The generalization of the discussion above to the coupling of a weakly anharmonic oscillator to a linear black box (Manucharyan *et al.*, 2007) is discussed in detail in Appendix C. The reader should familiarize herself with the discussion of the transmon qubit in Chap. (4) before studying Appendix C.

3
Superconductivity

In these notes I will not touch upon the microscopic theory of superconductivity. [For an introduction see the classic text by Tinkham (Tinkham, 1996).] Rather I will present only the minimal phenomenology needed to understand the Josephson effect in small circuits containing tunnel junctions. A useful overview of Josephson tunnel junctions and various qubit circuits may be found in the papers by Devoret and Martinis (Devoret and Martinis, 2004) and Clarke and Wilhelm (Clarke and Wilhelm, 2008).

An ordinary (normal-state) tunnel junction consists of two metallic electrodes separated by a thin oxide barrier which allows electrons to tunnel quantum mechanically from one electrode to the other. Because even in rather small (mesoscopic but not nanoscopic) grains, the size of the grain is much larger than the Ångström scale of a typical Fermi wavelength, the 'particle-in-a-box' quantum level spacing is extremely tiny and the density of states is essentially a continuum as shown in Fig. (3.1a). As a result, the tunneling of electrons is an incoherent process well-described by the irreversible dynamics of Fermi's Golden Rule. Under voltage bias V the chemical potential is higher in one grain than the other by an amount eV. Electrons in this energy interval are able to tunnel from the 'cathode' to 'anode' without blocking due to the Pauli exclusion principle. As a result the tunnel current is linear in the applied voltage (on voltage scales low compared to the tunnel barrier height) and the junction can be characterized as a simple resistor.[1] Because the two electrodes are separated by such a thin barrier they also form a capacitor so the equivalent circuit is that shown in Fig. (3.1b) and the incoherent relaxation of the charge through the junction has the familiar characteristic time scale $\tau = RC$. Obviously this incoherent behavior is not what we seek in a qubit and so we must turn to superconductivity to rescue the situation.

Let us begin our discussion of superconductivity by considering a small isolated metallic electrode of some metallic superconductor. Because the electrode is isolated, the number of electrons in it is fixed and well-defined. For the moment, let us assume that the electron number has even parity. The essential physics of an ordinary superconductor is that effective attractive interaction resulting from virtual phonon-

[1] Strictly speaking this is not correct. There are certain novel many-body effects associated with the quantum fluctuations of the environment to which the tunnel junction is coupled which can produce singularities in the conductance at low temperatures and low bias voltages (Pierre *et al.*, 2001). These environmental fluctuation effects become pronounced as the impedance of the source driving the junction increases and begins to approach the quantum of resistance. See (Devoret *et al.*, 1990; Girvin *et al.*, 1990).

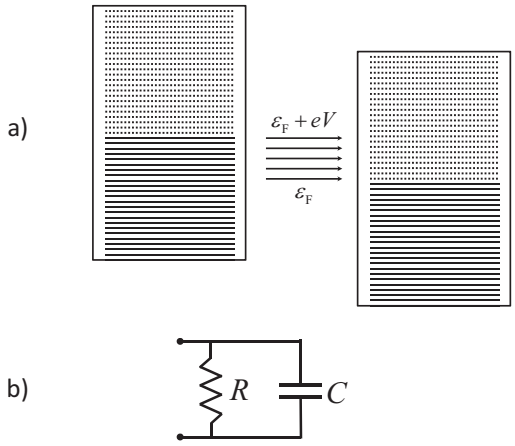

Fig. 3.1 Normal metal tunnel junction with equilibrium Fermi energy ϵ_F and applied voltage bias V. (a) The single-particle spectrum in each electrode is dense and the occupied (empty) states are indicated by solid (dotted) lines. (b) Lumped-element equivalent circuit. N.B. this is an approximate equivalent circuit, only valid when the junction is voltage biased by a zero-impedance source, so that certain many-body Coulomb interaction effects are negligible.

exchange leads to pairing of electrons of opposite spin into so-called Cooper pairs. If the number of electrons in the electrode is even, then the quantum ground state has all of the electrons paired up into a special non-degenerate low-energy ground state. The system has a finite excitation gap, 2Δ, defined by the energy needed to break a Cooper pair into two separate quasiparticles. The scale of this gap is typically several kelvin. As illustrated in Fig. (3.2a), the quasiparticle states form a near continuum above the gap. (Only if the electrode is extremely tiny (on the few nm scale) will the single-particle level spacing be appreciable. We will not consider this limit further.)

Recalling that a temperature of 1.0K corresponds to a frequency of approximately 21 GHz, we will be considering the limit of low temperatures and low frequencies relative to the gap: $k_B T, \hbar\omega \ll 2\Delta$. Hence to a good approximation we can say that the primary effect of superconductivity is the reduce the vast Hilbert space of the electrons in the electrode to a single quantum state, $|N\rangle$, labeled by the number of pairs which is a constant of the motion. This simplification is very important and will explain how we can produce macroscopic circuit elements whose quantum energy level spectrum is as simple as that of a single hydrogen atom. Obviously however we have overshot the mark because a quantum system with only one energy level cannot be used to make a two-level qubit. To repair this error, consider a system with *two* metallic electrodes connected by a tunnel junction as shown in Fig. (3.2b). We will again limit our attention to the quantum ground state of each electrode, assuming the electrons in each are fully paired up. Once again the total number of electron pairs in the system is fixed to some value $N = N_L + N_R$. Unlike the case of the single electrode,

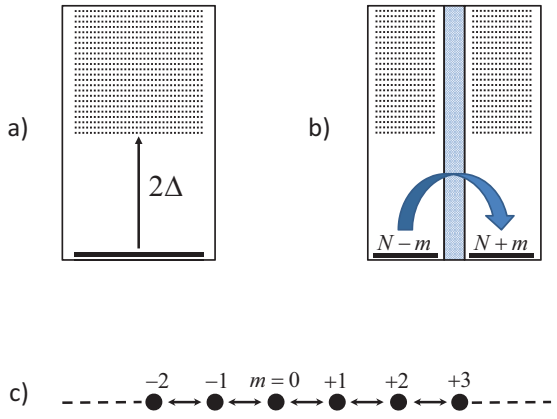

Fig. 3.2 a) Spectrum of a superconducting Cooper pair box (CPB). For the case of an even number of electrons, there is a unique non-degenerate state separated from the excited states by a gap 2Δ. b) A pair of CPB's connected by a tunnel barrier to form a Josephson junction. Ignoring the Coulomb energy, there is a large family of degenerate ground states labeled by an integer m representing the number of Cooper pairs transferred from one condensate to the other. c) 'Tight-binding' lattice along which the junction 'moves' via Josephson tunneling between 'sites' labeled by adjacent values of m.

the total number of pairs no longer uniquely specifies the quantum state. We must specify the number on each electrode. A useful notation for the set of low-energy states is:

$$|m\rangle = |N_{\rm L} - m, N_{\rm R} + m\rangle, \tag{3.1}$$

where m defines the number of pairs that have transferred through the tunnel junction from the left electrode to the right electrode starting from some reference state with pair number $N_{\rm L(R)}$ on the left (right) electrode.

The two electrodes form a small capacitor, but for the moment we will ignore the Coulomb energy that builds up as Cooper pairs are transferred from one electrode to the other. In this case we then have a one-dimensional family of states labeled by the integer m, and which are degenerate in energy[2] Remarkably, it turns out that the tunnel junction permits pairs of electrons to coherently tunnel together from one side to the other. We will discuss the microscopic details further below, but for now consider the phenomenological Hamiltonian

[2]Here we need to point out the crucial difference between the superconducting gap and the gap in a band insulator like silicon. The latter gap is tied to a particular density at which the electrons fill up all the valence band (bonding orbitals) and none of the conduction band. In a superconductor the particular density is not important–the gap follows the Fermi surface as it expands and contracts with density.

$$H_{\mathrm{T}} = -\frac{1}{2}E_{\mathrm{J}} \sum_{m} \left\{ |m\rangle\langle m+1| + |m+1\rangle\langle m| \right\}. \tag{3.2}$$

The parameter E_{J} is called the Josephson coupling energy and is a measure of the ability of Cooper pairs to tunnel through the junction. To rather good accuracy E_{J} is given by the Ambegaokar-Baratoff relation (Ambegaokar and Baratoff, 1963)

$$E_{\mathrm{J}} = \frac{1}{2}\frac{h}{(2e)^2} G_{\mathrm{N}} \Delta, \tag{3.3}$$

where $G_{\mathrm{N}} = 1/R_{\mathrm{N}}$ is the normal state conductance. One can understand this expression by noting that the microscopic tunneling Hamiltonian describes single-electron (not pair) tunneling across the junction. Thus coherent tunneling of a pair of electrons must be second order in the tunneling matrix element t_{LR}. In the intermediate state after the first tunneling, we have an unpaired electron in each island and so there is an energy of order 2Δ appearing in the denominator. Naively, this suggests that the Josephson coupling will scale inversely with the size of the superconducting gap. However we note that after the second electron tunnels, we are left with a pair of holes in one island and an extra pair of electrons in the other. Taking into account the quantum amplitudes for both of these pairs to disappear into the condensate brings in two more factors of Δ (and two factors of the density of states to keep the dimensions correct) which explains why E_{J} is in fact linearly increasing in the superconducting gap. The normal state conductance is computed using Fermi's Golden Rule for the tunneling rate which is of course proportional to the square of the matrix element t_{LR}. Hence we see (qualitatively at least) the origin of Eq. (3.3).

You might wonder why E_{J} is not quartic in the tunneling matrix element since the effective matrix element for the pair tunneling is quadratic and perhaps we should square this as in Fermi's Golden Rule. The answer goes to the heart of the Josephson effect. Our effective Hamiltonian H_{T} connects discrete states (labeled by m) not a discrete state to a continuum. We will find not the irreversible incoherent dynamics of Fermi's Golden Rule (as we did in the normal metal case) but rather coherent tunneling which connects a set of degenerate states $\{|m\rangle\}$. We will in effect be doing degenerate perturbation theory (that is, finding a linear superposition of the degenerate states which diagonalizes H_{T}) and finding energy eigenvalues (and corresponding dynamics) which is first order in E_{J}, not second order.

We see that H_{T} causes m to either increase or decrease by unity corresponding to the tunneling of a pair to the right or the left. We can gain some intuition by noticing that H_{T} is identical to that of a one-dimensional tight-binding lattice model with near-neighbor hopping amplitude E_{J}, as illustrated in Fig. (3.2c). The (unnormalized) eigenfunctions are plane-wave like states labeled by a dimensionless 'wave vector' $\varphi = ka$ where $a = 1$ is the 'lattice constant.'

$$|\varphi\rangle = \sum_{m=-\infty}^{+\infty} e^{+im\varphi} |m\rangle. \tag{3.4}$$

Recalling the cosine dispersion of the one-dimensional tight-binding band with near-neighbor hopping we see that

$$H_{\rm T}|\varphi\rangle = -E_{\rm J}\cos\varphi|\varphi\rangle. \tag{3.5}$$

Imagine a wave packet moving to the right on our tight-binding lattice. This corresponds to a net current of Cooper pairs coherently tunneling through the junction causing the 'position' $\langle m\rangle$ to increase linearly with time. The group velocity of the packet is given by the derivative of the energy with respect to wave vector

$$v_g(\varphi) = \frac{1}{\hbar}\frac{\partial}{\partial\varphi}[-E_{\rm J}\cos\varphi], \tag{3.6}$$

so the net current flowing is given by the celebrated (first) Josephson relation

$$I(\varphi) = 2e\, v_g(\varphi) = \frac{2e}{\hbar}E_{\rm J}\sin\varphi. \tag{3.7}$$

The maximum possible coherent (dissipationless) current occurs at $\varphi = \pi/2$ and is called the critical current

$$I_{\rm c} = \frac{2e}{\hbar}E_{\rm J}. \tag{3.8}$$

If more current than this is forced through the junction, the voltage rises from zero to a high value above the excitation gap and our low-energy effective model is no longer applicable.

As an alternative approach to the derivation of the Josephson relation for the current, let us define the operator $\hat{n}$ to be the number operator for the Cooper pairs transferred across the junction

$$\hat{n} \equiv \sum_m |m\rangle m\langle m|. \tag{3.9}$$

Hamilton's equation of motion gives for the current operator

$$\hat{I} \equiv 2e\frac{d\hat{n}}{dt} = 2e\frac{i}{\hbar}[H_{\rm T},\hat{n}] = -i\frac{e}{\hbar}E_{\rm J}\sum_m\left\{|m\rangle\langle m+1| - |m+1\rangle\langle m|\right\}. \tag{3.10}$$

Next we simply note that the plane wave energy eigenfunctions are also eigenfunctions of the current operator obeying

$$\hat{I}|\varphi\rangle = I_{\rm c}\sin\varphi|\varphi\rangle \tag{3.11}$$

which is of course equivalent to Eq. (3.7).

Exercise 3.1 Derive Eq. (3.11).

Equivalently we note that in the φ representation, the wave function is given by

$$\psi(\varphi) = \langle\varphi|\psi\rangle. \tag{3.12}$$

By using Eq. (3.9) and Eq. (3.4), we see that

$$\hat{n}|\varphi\rangle = -i\frac{d}{d\varphi}|\varphi\rangle. \tag{3.13}$$

Thus it follows that in the φ representation, the number operator is

$$\hat{n} = +i\frac{d}{d\varphi}. \tag{3.14}$$

The confusing sign change comes from considering

$$\langle\varphi|\hat{n}|\psi\rangle = +i\frac{d}{d\varphi}\psi(\varphi). \tag{3.15}$$

From this it follows that

$$\hat{I} = 2e\frac{i}{\hbar}[H_{\mathrm{T}}, \hat{n}] = 2e\frac{i}{\hbar}[-E_{\mathrm{J}}\cos\varphi, +i\frac{d}{d\varphi}] = I_{\mathrm{c}}\sin\varphi. \tag{3.16}$$

We continue for the moment to ignore the Coulomb interaction, but as a first step towards including it, let us think about the situation where an external electric field is applied and maintained in such a way that there is a fixed voltage drop V across the tunnel junction. This adds to the Hamiltonian a term

$$U = -(2e)V\hat{n}. \tag{3.17}$$

Hamilton's equation of motion yields the equally celebrated (second) Josephson relation[3]

$$\hbar\partial_t\varphi = -\frac{\partial H}{\partial\hat{n}} = 2eV, \tag{3.18}$$

relating the time rate of change of the 'momentum' $\hbar\varphi$ to the 'force' $2eV$. Equivalently, the solution of the Schrödinger equation is

$$|\Psi(t)\rangle = e^{+\frac{i}{\hbar}E_{\mathrm{J}}\int_0^t d\tau\,\cos\varphi(\tau)}|\varphi(t)\rangle, \tag{3.19}$$

where

$$\varphi(t) = \varphi(0) + \frac{2e}{\hbar}Vt. \tag{3.20}$$

[3]As we will discuss in Chap. (4), the fact that the time derivative of the phase variable is proportional to the voltage means that φ is directly proportional to the flux variable introduced in Chap. (2).

Exercise 3.2 Verify for yourself that Eq. (3.19) does indeed solve the Schrödinger equation:

$$i\hbar\partial_t|\Psi(t)\rangle = (H_{\rm T} + U)|\Psi(t)\rangle. \tag{3.21}$$

The overall phase factor in front of the wave function is not particularly important, but the time variation of the 'wave vector' $\varphi(t)$ is extremely important because it leads to the ac Josephson effect, namely that dc voltage bias leads to an ac current

$$\langle \hat{I}(t)\rangle = I_{\rm c}\sin(\varphi(0) + \omega t) \tag{3.22}$$

where the ac Josephson frequency is given by

$$\omega = 2\pi\frac{2e}{h}V. \tag{3.23}$$

The inverse flux quantum in frequency units is

$$\frac{2e}{h} \approx 483.597891(12)\text{MHz}/\mu\text{Volt}. \tag{3.24}$$

Since frequency is the easiest physical quantity to measure with high accuracy, the ac Josephson effect finds great practical use in metrology to maintain (but not define) the SI volt.

To summarize our results, we are using here a representation in which the phase $\varphi(t)$ across the Josephson junction is viewed as a (dimensionless) wave vector. The Hamiltonian of the junction with voltage bias V is

$$H = -E_{\rm J}\cos\varphi - 2eV\hat{n}, \tag{3.25}$$

where in the φ representation, the number operator has the form

$$\hat{n} = +i\frac{d}{d\varphi}. \tag{3.26}$$

The pair of Hamilton equations

$$\frac{\partial\hat{n}}{\partial t} = \frac{\partial H}{\partial\hbar\varphi} \tag{3.27}$$

$$\hbar\partial_t\varphi = -\frac{\partial H}{\partial\hat{n}} \tag{3.28}$$

correspond to the pair of Josephson relations found in Eq. (3.7) and Eq. (3.18).

Stepping away from the particular expression of the Hamiltonian in the φ representation, we can write the general abstract representation of the Hamiltonian as

$$H = -E_{\rm J}\widehat{\cos\varphi} - 2eV\hat{n}. \tag{3.29}$$

As noted earlier, for the case of an isolated Josephson junction, the number of Cooper pairs transferred through the junction is a well-defined integer and hence the state $|\varphi\rangle$ and the state $|\varphi + 2\pi\rangle$ are identical. Hence the wave function $\psi(\varphi)$ obeys periodic boundary conditions. Because of this there is no operator $\hat{\varphi}$. Only operators that preserve the periodic boundary conditions (such as $\widehat{\cos\varphi}$ and $\hat{n} = +i\frac{d}{d\varphi}$) exist.

4
Superconducting Qubits

So far we have studied a single isolated Josephson junction which is able to coherently transfer Cooper pairs from one metallic island to another. Our discussion of this simple structure (known as the Cooper pair box) has been incomplete because it has neglected the fact that as current flows through the junction, charge builds up on the islands and the Coulomb energy becomes important. Once we include the Coulomb interaction, we will see that this structure makes an excellent artificial atom which can be used as a superconducting qubit. The first evidence that Josephson tunneling causes the Cooper pair box to exhibit coherent superpositions of different charge states was obtained by Bouchiat *et al.*(Bouchiat *et al.*, 1998). This was followed in 1999 by the pioneering experiment of the NEC group (Nakamura *et al.*, 1999) demonstrating time-domain control of the quantum state of the CPB using very rapid control pulses to modulate the offset charge.

The remarkable recent progress in creating superconducting quantum bits and manipulating their states has been summarized in several reviews (Devoret and Martinis, 2004; Esteve and Vion, 2005; Wendin and Shumeiko, 2006; Wendin and Shumeiko, 2007; Clarke and Wilhelm, 2008; Schoelkopf and Girvin, 2008; You and Nori, 2005; Nori, 2008; Korotkov, 2009). Nearly 30 years ago Leggett discussed the fundamental issues concerning the collective degrees of freedom in superconducting electrical circuits and the fact that they themselves can behave quantum mechanically (Leggett, 1980). As noted earlier, the essential collective variable in a Josephson junction (Devoret and Martinis, 2005) is the phase difference of the superconducting order parameter across the junction. The first experimental observation of the quantization of the energy levels of the phase 'particle' was made by Martinis, Devoret and Clarke in 1985 (Martinis *et al.*, 1985; Clarke *et al.*, 1988).

A number of different qubit designs, illustrated in Fig. (4.1) and Fig. (4.2) have been developed around the Josephson junction including the Cooper pair box (CPB) (Averin *et al.*, 1985; Büttiker, 1987; Lafarge *et al.*, 1993; Bouchiat *et al.*, 1998; Nakamura *et al.*, 1999; Vion *et al.*, 2002; Koch *et al.*, 2007; Schreier *et al.*, 2008) based on charge, the flux qubit (Mooij *et al.*, 1999; van der Wal *et al.*, 2000; Chiorescu *et al.*, 2003), and the phase qubit (Martinis *et al.*, 2002; Berkley *et al.*, 2003). Devoret and coworkers have recently introduced the fluxonium qubit (Manucharyan *et al.*, 2009*b*; Manucharyan *et al.*, 2009*a*) in which the small Josephson junction is shunted by a very high inductance created from a string of larger Josephson junctions. Fig. (4.3) shows an 'evolutionary phylogeny' for these different types of qubits. We will turn now to a discussion of the Hamiltonians of these different types of qubits and subsequently to an analysis of the relative merits in terms of their sensitivity to noise perturbations.

Once we understand the Hamiltonians we will be in a position to classify the qubits according to their location in the 'Mendeleev Table' shown in Fig. (4.4). The lectures by Daniel Esteve will discuss the different methods by which the state of different qubits can be read out.

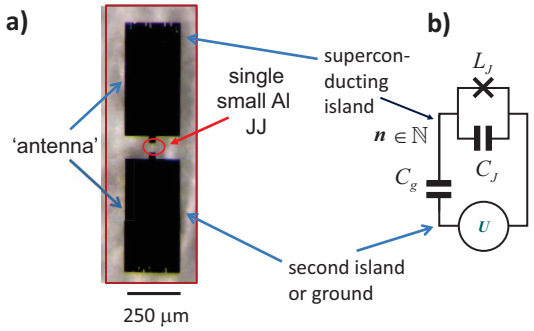

Fig. 4.1 a) Cooper pair box qubit (R. Schoelkopf lab) and b) its equivalent circuit showing a voltage source biasing the box through a coupling ('gate') capacitor c_g. The cross denotes the Josephson junction. The voltage source may represent an intentionally applied bias or be the result of random charges in the insulating substrate supporting the device. The particular device illustrated in (a) is a transmon qubit in a 3D cavity for which there is no dc bias applied (although there may be a random offset voltage due to charges trapped in the substrate).

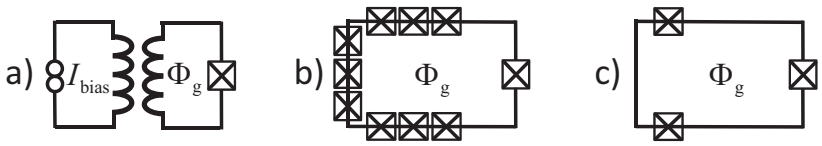

Fig. 4.2 Inductively shunted qubits. a) Phase qubit with a transformer flux bias circuit driven by current $I_{\rm bias}$. Josephson junction is indicated by box with cross. b) Fluxonium qubit. The shunt inductor has been replaced by an array of a large number of Josephson junctions. The array junctions are chosen to have a sufficiently large ratio of Josephson energy $E_{\rm J}$ to charging energy $E_{\rm C}$ that phase slips can be neglected and the array is a good approximation to a very large inductor. Flux bias circuit not shown. c) Flux qubit consisting of a superconducting loop with three Josephson junctions. Flux bias circuit not shown.

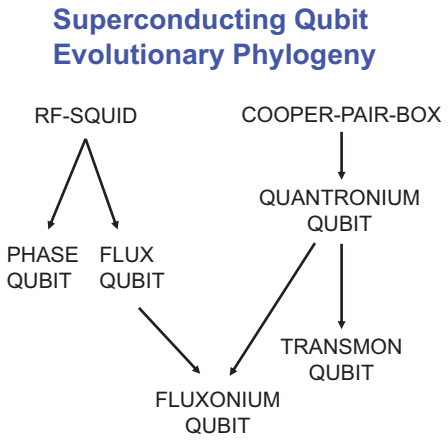

Fig. 4.3 Evolutionary phylogeny of superconducting qubits. (Courtesy M. Devoret.)

4.1 The Cooper Pair Box

The Cooper pair box (CPB) (Devoret, 1997) is topologically distinct from the other designs shown in Fig. (4.2) in that it has no wire closing the loop around the junction. The Hamiltonian will be described below and derived in detail in Appendix A. The number of Cooper pairs transferred through the junction is a well-defined integer as we have already discussed in detail. The integer charge implies the conjugate phase is compact; that is, in the phase representation, the system obeys periodic boundary conditions. As we will see below, this implies that charge-based qubits are sensitive to stray electric field noise, but that this can be overcome by putting the Cooper pair box in the 'transmon' regime where the Josephson tunneling energy dominates over the Coulomb charging energy (Koch *et al.*, 2007; Houck *et al.*, 2009).

Our previous discussion of the Josephson effect has neglected the Coulomb interaction. Let us define the charging energy associated with the transfer of a single electron to be

$$E_{\mathrm{C}} = \frac{e^2}{2C_{\Sigma}}, \tag{4.1}$$

where $C_{\Sigma} = C_{\mathrm{J}} + C_{\mathrm{g}}$ is the total capacitance between the island electrodes. For the equivalent circuit shown in Fig. (4.1) where the CPB is biased by a low impedance voltage source (Devoret, 1997), the total capacitance connecting the island to ground is the sum of the capacitance across the junction plus the gate capacitance: $C_{\Sigma} = C_{\mathrm{J}} + C_{\mathrm{g}}$. The Coulomb energy to transfer a Cooper pair is four times larger than for a single electron, and so the Coulomb energy operator is given by

$$\hat{U} = 4E_{\mathrm{C}}(\hat{n} - n_{\mathrm{g}})^2, \tag{4.2}$$

where

$$n_{\mathrm{g}} \equiv -\frac{C_{\mathrm{g}}V}{2e} \tag{4.3}$$

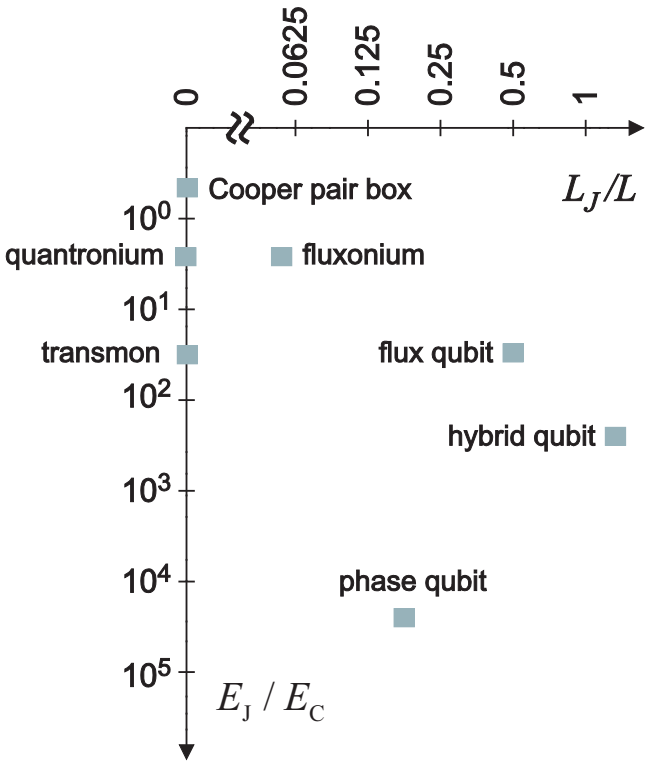

Fig. 4.4 'Periodic Table' of superconducting qubits. E_J is the tunneling Josephson energy, $4E_C$ is the energy cost to charge the junction with one Cooper pair, and $E_L/2$ is the energy cost to 'charge' the shunt inductor with one flux quantum. (Courtesy M. Devoret.)

is called the dimensionless 'gate charge' or 'offset charge' and represents either the effect of an externally applied electric field or some microscopic junction asymmetry which breaks the degeneracy between positive and negative charge transfers (Devoret, 1997). The number operator $\hat{n}$ has integer eigenvalues, while n_g is a continuous variable, which may either intentionally, or randomly and uncontrollably, fluctuate. The effects of such fluctuations on the coherence of the qubit will be discussed in Chapter (5).

As we noted earlier, from Eq. (3.4) we see that φ is a compact variable; that is, the state $|\varphi + 2\pi\rangle$ is identified with the state $|\varphi\rangle$. Hence without loss of generality we may take the wave vector φ to live in the first Brillouin zone $\varphi \epsilon [-\pi, +\pi]$, or equivalently on a circle. In fact, because of this periodic boundary condition, it is convenient to view φ as an angular coordinate living on a circle, rather than as a quasi-momentum as we have been doing until now. In this picture, we reinterpret the expression in Eq. (3.14) as telling us that the number operator $\hat{n}$ is nothing more than (minus) the angular momentum conjugate to the angle φ. Because φ is compact, the conjugate (dimensionless) angular momentum $\hat{n}$ naturally has integer eigenvalues which is just

the property that we require for the operator representing the number of Cooper pairs which have been transferred through the Josephson junction. Except for the $n_{\rm g}$ term (to which we will return shortly) the Hamiltonian becomes that of a quantum rotor in a gravitational field (see Fig. (4.5)

$$H = 4E_{\rm C}\left(\hat{n} - n_{\rm g}\right)^2 - E_{\rm J}\widehat{\cos\varphi}, \tag{4.4}$$

where the charging energy determines the (inverse) moment of inertia, and the Josephson energy is a measure of the torque produced by gravity[1]

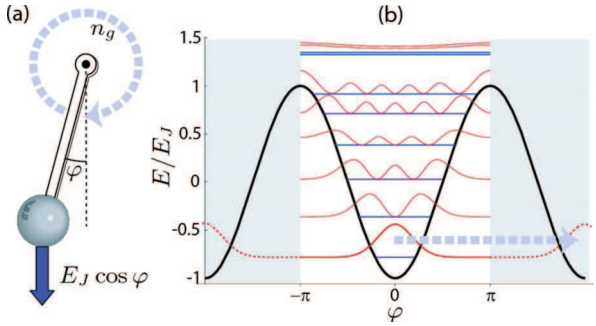

Fig. 4.5 The Cooper pair box Hamiltonian in the phase representation is equivalent to that of a quantum rotor. The offset charge $n_{\rm g}$ is equivalent to an Aharonov-Bohm flux which produces a Berry phase proportional to the winding number of the rotor trajectory. Unlike other qubit circuit topologies, the rotor wave function obeys periodic boundary conditions. From (Koch *et al.*, 2007).

We know that for small amplitude oscillations, the classical quantum rotor is very nearly a simple harmonic oscillator. This can be seen by expanding the cosine to second order (an approximation that is valid in the quantum case in the limit $E_{\rm J} \gg E_{\rm C}$ where the zero-point fluctuations in the phase are small). Up to an irrelevant constant in the energy (and ignoring the offset charge for the moment) we have for the classical Hamiltonian

$$H \approx 4E_{\rm C}n^2 + \frac{1}{2}E_{\rm J}\varphi^2. \tag{4.5}$$

The replacement of the cosine term which is correctly periodic in φ by the quadratic approximation is quite subtle. This is a simple harmonic oscillator only if we extend φ from a compact variable living on a circle to a non-compact variable living on the

[1]This jumping back and forth between representations can easily give beginners a headache. Notice that previously when φ was a momentum and we were studying the pair tunnel Hamiltonian $H_{\rm T}$, we were perfectly happy to have a kinetic energy but no potential energy. This is much like the situation of a particle moving freely in space except here it is hopping on a lattice. Now if we think of φ as a coordinate, we have to think of the Josephson energy as potential energy. Without the Coulomb energy $E_{\rm C}$, our rotor has infinite moment of inertia (and hence no kinetic energy and no dynamics). Only when we add the charging energy do we get a quantum fluctuations in the phase and dynamical oscillations of our qubit. Confusingly this situation is sometimes described by saying that without the charging energy, the phase φ is classical.

real line. For the (quantum) harmonic oscillator, we do not have the requirement that the wave function be periodic in φ. If however E_J/E_C is large enough the wave function will have significant support only near $\varphi = 0$ and hence we are not making a significant mistake by ignoring the requirement of periodic boundary conditions. The boundary condition of vanishing at infinity is close enough because the wave function is extremely small at $\varphi = \pm\pi$ so very nearly obeys the required periodic boundary conditions. Further, the small excursions in φ mean that the Taylor series expansion of the cosine is justified. Under these conditions we obtain a quantum harmonic oscillator with Hamiltonian

$$H \approx 4E_C\hat{n}^2 + \frac{1}{2}E_J\hat{\varphi}^2 \tag{4.6}$$

with $\hat{n}$ now being the ordinary linear (not discrete angular) momentum with continuous spectrum.

It is interesting to try connect the classical Hamiltonian of this Cooper pair box to the classical LC oscillator we studied previously. From the second Josephson relation in Eq. (3.18) we find that the phase angle φ is directly proportional to the flux variable Φ defined in Eq. (2.25) used in the quantization of the LC oscillator.

$$\varphi = \frac{2e}{\hbar}\Phi = 2\pi\frac{\Phi}{\Phi_0}. \tag{4.7}$$

Thus each time the flux variable changes by one flux quantum, the superconducting phase variable winds by 2π. The classical Lagrangian for the Cooper pair box can be written

$$\mathcal{L} = \frac{1}{2}C\dot{\Phi}^2 + E_J\cos\left(2\pi\frac{\Phi}{\Phi_0}\right), \tag{4.8}$$

and the Hamiltonian becomes

$$H = \frac{1}{2C}Q^2 - E_J\cos\left(2\pi\frac{\Phi}{\Phi_0}\right). \tag{4.9}$$

Expanding the cosine term about $\Phi = 0$ to lowest order (and dropping the zeroth order term) we have

$$H \approx \frac{1}{2C}Q^2 + \frac{1}{2L_J}\Phi^2, \tag{4.10}$$

where the (small signal) effective inductance of the Josephson junction is given by

$$L_J = \left(\frac{\hbar}{2e}\right)^2\frac{1}{E_J}. \tag{4.11}$$

In this approximation, the CPB becomes a simple harmonic oscillator with resonant frequency (known as the Josephson plasma frequency) given by

$$\Omega_J \equiv \frac{1}{\sqrt{L_JC}} = \frac{1}{\hbar}\sqrt{8E_JE_C}. \tag{4.12}$$

The Taylor series expansion of the cosine is justified only if we are discussing small amplitude motions. Classically we can always choose to study this limit. Quantum

mechanically, we are forced to deal even in the ground state with zero-point fluctuations in Φ. From Eq. (2.44) we see that (in the harmonic approximation used above)

$$2\pi\frac{\Phi_{\rm ZPF}}{\Phi_0} = \left(2\frac{E_{\rm C}}{E_{\rm J}}\right)^{1/4}, \tag{4.13}$$

so the harmonic approximation is, as suggested above, self-consistent in the limit $E_{\rm J} \gg E_{\rm C}$. In the quantum rotor picture, this corresponds to strong gravity and large mass (moment of inertia).

For general flux Φ, not necessarily small, we can define the differential (inverse) inductance as

$$L^{-1}(\Phi) \equiv \frac{d^2H}{d\Phi^2} = E_{\rm J}\left(\frac{2\pi}{\Phi_0}\right)^2\cos\left(2\pi\frac{\Phi}{\Phi_0}\right), \tag{4.14}$$

we see that the Josephson junction acts as a non-linear inductor. It is this key feature which will make the energy levels of the Cooper pair box anharmonic.

In the quantum case, if the quantum zero-point fluctuations in Φ are small, then the above non-linear inductor picture can be useful, but in general we need to resort to numerical diagonalization of the CPB Hamiltonian. Let us therefore now return to the full Hamiltonian in Eq. (4.4). In the phase basis, the Schrödinger eigenvalue equation is the Matthieu equation whose solutions are formally known in terms of Matthieu functions. Numerical diagonalization is more conveniently performed in the charge (number) basis where the Coulomb term is diagonal and the Josephson term is tri-diagonal: $\langle m \pm 1|\cos\varphi|m\rangle = \frac{1}{2}$. The basis states are labeled by the eigenvalue m of the number operator $\hat{n}$ and the Hilbert space must be truncated at some largest $|m| = m_{\rm max}$. If we are interested only in first N low-lying states, the size of the Hilbert space needed can be estimated from the zero-point fluctuations of the charge in the harmonic limit given in Eq. (2.43)

$$m_{\rm max} \gg \sqrt{N}\frac{Q_{\rm ZPF}}{2e} \sim \sqrt{N}\left(\sqrt{\frac{E_{\rm J}}{32E_{\rm C}}}\right)^{1/4} \tag{4.15}$$

which, conveniently, is usually not very large[2].

The qubit spectrum is periodic in the offset charge $n_{\rm g}$ with unit period as can be seen in Fig. (4.6). Physically this simply means that the integer part of the offset charge can always be canceled out by transferring an integer number of Cooper pairs from one island to the other. To understand this mathematically, recall that the wave functions obey periodic boundary conditions in the angle φ. Thus in the φ representation

$$U_\pm = e^{\pm i\varphi} \tag{4.16}$$

[2]It is useful at this point to note that for a given tunnel barrier thickness, $E_{\rm J}$ scales with junction area but the capacitance $C_{\rm J}$ (which usually dominates over $C_{\rm g}$) and hence the inverse charging energy also scales with junction area. Thus the Josephson plasma frequency is nearly independent of junction area while the impedance of the Josephson plasma oscillator $Z_{\rm J} = \left(\frac{L_{\rm J}}{C_\Sigma}\right)^{1/2} = \frac{1}{\pi}\frac{h}{(2e)^2}\sqrt{\frac{E_{\rm C}}{E_{\rm J}}}$ scales inversely with the area. Hence $m_{\rm max}$ grows with the square root of the area while $\varphi_{\rm ZPF}$ scales inversely with the square root of the junction area.

is a 'legal' unitary transformation which preserves the boundary conditions (and physically transfers one pair through the junction). Recognizing that such a unitary transformation preserves the spectrum of the Hamiltonian and that it shifts the angular momentum (transferred charge) by one unit

$$U_{\pm}\hat{n}U_{\pm}^{\dagger} = \hat{n} \mp 1, \tag{4.17}$$

we see that the spectrum must indeed be invariant under unit translations of $n_{\rm g}$.

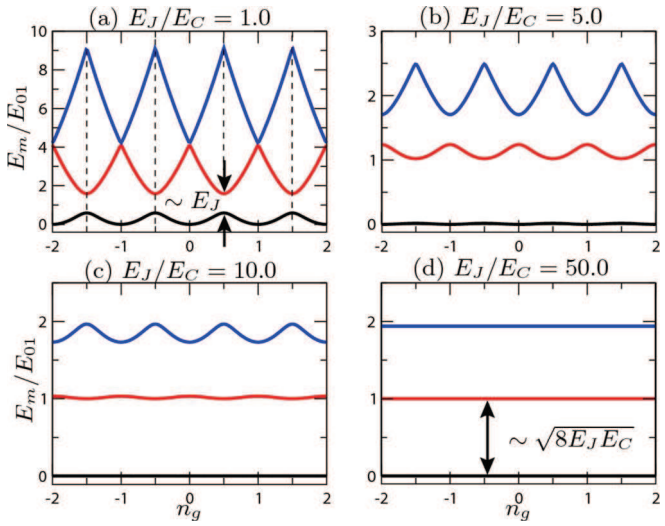

Fig. 4.6 Energy spectrum of the Cooper pair box as a function of offset charge for different values of the dimensionless ratio of Josephson energy to charging energy. The exponential decrease in the charge dispersion is clearly seen. From (Koch *et al.*, 2007).

Since the offset term $n_{\rm g}$ does not appear in the ordinary quantum rotor problem we need to extend our analogy a bit. It turns out that this term can be viewed as resulting from the rotor carrying (fake) charge and undergoing an Aharanov-Bohm phase shift as it circles a line of (fake) magnetic flux which is passing through the axis. To see this, let us recall that for a particle with charge q moving in the presence of a vector potential $\vec{A}$, the canonical momentum is replaced by the mechanical momentum

$$\vec{p} \longrightarrow \vec{p} - q\vec{A}(\vec{r}). \tag{4.18}$$

For our quantum rotor turning on the z axis, we are interested in the angular momentum

$$L_z = (\vec{r} \times \vec{p})_z \longrightarrow (\vec{r} \times \vec{p})_z - q(\vec{r} \times \vec{A})_z. \tag{4.19}$$

If the magnetic field is zero everywhere except for an Aharanov-Bohm tube of flux on the z axis, we can choose the following gauge for the vector potential

$$\vec{A}(\vec{r}) = \Phi_{\rm AB}\frac{1}{2\pi r}\hat{z} \times \hat{r}, \tag{4.20}$$

which has the correct total flux

$$\oint \vec{A} \cdot d\vec{r} = \Phi_{\mathrm{AB}} \tag{4.21}$$

for any loop with winding number +1 around the z axis. The mechanical angular momentum operator thus becomes

$$(\vec{r} \times \vec{p})_z - \frac{q}{2\pi}\Phi_{\mathrm{AB}} = \hbar\left(-i\frac{\partial}{\partial\varphi} - \frac{\Phi_{\mathrm{AB}}}{\Phi_0}\right) \tag{4.22}$$

where Φ_0 is the flux quantum corresponding to charge q (which since it is arbitrary we can choose to be $2e$). By comparison with Eq. (4.4), we see that the real offset charge is equivalent to a fake Aharonov-Bohm flux

$$n_{\mathrm{g}} = \frac{\Phi_{\mathrm{AB}}}{\Phi_0}. \tag{4.23}$$

The fact that the spectrum is periodic in Φ_{AB} is simply a reflection of the fact that a flux tube containing an integer number of flux quanta produces an Aharanov-Bohm phase shift of zero (modulo 2π).

In the 'charge' limit, $E_{\mathrm{C}} \gg E_{\mathrm{J}}$, the states of our rotator and nearly angular momentum (i.e. charge) eigenstates weakly perturbed by the gravitational torque (Josephson coupling). As can be seen in Fig. (4.6a) when the offset charge is half-integer, there are two adjacent charge states which have the same Coulomb energy. This degeneracy is lifted by by the Josephson term. The disadvantage of working in this regime is that E_{C} is large and the excitation energies are extremely strong functions of the offset charge n_{g}. As we will see in Chap. (5) environmental noise in n_{g} will lead to severe qubit decoherence.

In the 'transmon' limit, $E_{\mathrm{J}} \gg E_{\mathrm{C}}$, the states of the quantum rotor are nearly harmonic small-amplitude oscillations near the minimum in gravitational potential energy (i.e. Josephson energy). As can be seen in Fig. (4.6d) the qubit levels are nearly harmonic and very nearly completely insensitive to the value of the offset charge. The reason for this is readily understood within the Aharanov-Bohm analogy of the offset charge. Let us start our discussion with a path integral language. We know that the only way that the system can be aware of the value of the Aharanov-Bohm flux is for the rotor to circle completely around the flux tube in order to acquire the Aharnov-Bohm phase shift. The interference between this path and the path where the rotor does not circle the flux modifies the quantum energy. However in the limit of large E_{J} (strong gravity), the rotor must tunnel through a very high energy barrier in order to wind the phase from $\varphi = 0$ to $\varphi = 2\pi$. The barrier height is proportional to E_{J} and the particle 'mass' is inversely proportional to E_{C}. As a result, the contribution of these processes to the energy is exponentially small.

Let us return now to the language of wave functions for a more quantitative discussion. Mathematically we begin by performing the unitary gauge transformation

$$U = e^{-in_{\mathrm{g}}\varphi}, \tag{4.24}$$

which completely removes the offset charge term from the Hamiltonian

$$U(\hat{n} - n_{\rm g})U^{\dagger} = \hat{n}. \tag{4.25}$$

Notice that the transformed wave function $U\Psi$ no longer obeys periodic boundary conditions:

$$\{U\Psi(\varphi + 2\pi)\} = e^{-i2\pi n_{\rm g}}\{U\Psi(\varphi)\}. \tag{4.26}$$

Thus, while the Hamiltonian becomes independent of $n_{\rm g}$

$$UHU^{\dagger} = H = 4E_{\rm C}(\hat{n})^2 - E_{\rm J}\cos\varphi, \tag{4.27}$$

the change in boundary condition with $n_{\rm g}$ nevertheless changes the energy eigenvalue spectrum. On the other hand, for large $E_{\rm J}/E_{\rm C}$ the wave function is exponentially small at the boundary $\varphi = \pm\pi$, so we do not expect a large change in the spectrum due to this change in boundary condition.

To develop a better intuition for how the change in boundary condition affects the energy eigenvalues, consider the following. Rather than viewing the Hamiltonian as that of a quantum rotor (with compact φ living on the interval $-\pi \leq \varphi \leq +\pi$) let us view this as the Hamiltonian of a phase 'particle' with coordinate (not momentum!) φ moving in the extended cosine potential as shown in Fig. (4.7). Bloch's theorem tells us that the discrete translation symmetry of the potential implies that the wave functions must be of the form

$$\Psi_{mk}(\varphi) = e^{ik\varphi}\psi_m(\varphi), \tag{4.28}$$

where ψ_n obeys periodic boundary conditions $\varphi \longrightarrow \varphi + 2\pi$, m is the band index and (because the 'lattice constant' of the potential is 2π) the wave vector k lives in the first Brillouin zone $-\frac{1}{2} \leq k \leq +\frac{1}{2}$. We now simply invoke the boundary condition in Eq. (4.26) by choosing the Bloch wave vector to be $k = n_{\rm g}$. The use of the extended cosine potential is just a crutch to get us to Eq. (4.28). The Bloch wave solution in the interval $-\pi \leq \varphi \leq +\pi$ solves the quantum rotor problem with compact phase and boundary condition given in Eq. (4.26). Thus we arrive at the important conclusion that the spectrum of the quantum rotor plotted against offset charge in Fig. (4.6) *is nothing more than the band structure of a one-dimensional solid with a cosine potential in which the offset charge defines the Bloch wavevector.* The excited band energies correspond to the excited states of the rotor. The constraint (or 'superselection rule') that the Bloch wavevector is not arbitrary but rather fixed by the offset charge removes the infinite number of extra states that we built into the Hilbert space when we let φ be a non-compact variable.

The band structure picture is useful because in the limit of large $E_{\rm J}$ we can invoke (at least for the low-lying bands) the tight-binding approximation to the band structure in which we envision the phase particle in a bound state within a well being able to hop to the corresponding state in an adjacent well by tunneling through the barrier. We know that for near-neighbor hopping the tight-binding model has a simple cosine dispersion as a function of wave vector (which in this case is offset charge). Hence within this approximation the energy of the mth level has the form (Koch *et al.*, 2007)

$$E_m(n_{\rm g}) \approx \mathcal{E}_m + \epsilon_m\cos(2\pi n_{\rm g}), \tag{4.29}$$

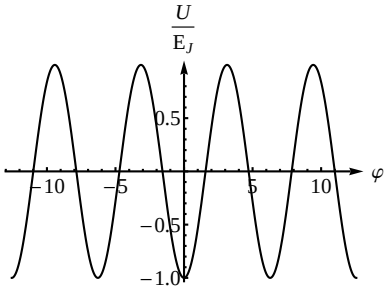

Fig. 4.7 Extended cosine potential $U = -E_{\rm J}\cos(\varphi)$.

where the tight-binding bandwidth $2\epsilon_m$ defines the so-called 'charge dispersion'. Within the WKB approximation for the tight-binding hopping amplitude the charge dispersion for the mth level is given by (Koch *et al.*, 2007)

$$\epsilon_m \sim (-1)^m E_{\rm C}\frac{2^{4m+5}}{m!}\sqrt{\frac{2}{\pi}}\left(\frac{E_{\rm J}}{2E_{\rm C}}\right)^{\frac{m}{2}+\frac{3}{4}} e^{-\sqrt{8E_{\rm J}/E_{\rm C}}}. \tag{4.30}$$

The charge dispersion is a measure of the sensitivity of the energy to the offset charge. We see that going to large $E_{\rm J}/E_{\rm C}$ makes the transmon qubit quite insensitive to (low-frequency) charge noise which dramatically improves the dephasing time. The fact that the 'charge dispersion' is greater for the higher excited states is simply the naturally larger bandwidth of the higher energy states of the band structure. (More energetic particles tunnel through the barrier more readily.)

In the limit of large $E_{\rm J}/E_{\rm C}$ the quantum rotor begins to approach a harmonic oscillator. Fortunately the anharmonicity defined by

$$A \equiv \omega_{12} - \omega_{01} \sim -E_{\rm C} \tag{4.31}$$

goes to zero very slowly as the charging energy is reduced and can be easily kept above 100-200MHz (Koch *et al.*, 2007) which is adequate to prevent smooth nanosecond control pulses from taking the qubit out of the logical subspace (the two lowest levels) (Houck *et al.*, 2009).

We may perturbatively estimate the anharmonicity (in the limit of negligible charge dispersion) from Eq. (4.27) by assuming that the zero-point fluctuations of the phase are small allowing us to expand the cosine potential beyond the second-order considered previously to write

$$H \approx H_0 + V, \tag{4.32}$$

where

$$H_0 = 4E_{\rm C}\hat{n}^2 + \frac{1}{2}E_{\rm J}\hat{\varphi}^2, \tag{4.33}$$

and

$$V = -\frac{1}{24}E_{\rm J}\hat{\varphi}^4. \tag{4.34}$$

Using Eq. (4.13) we find

$$\varphi_{\rm ZPF}^2 = \sqrt{\frac{2E_{\rm C}}{E_{\rm J}}}, \tag{4.35}$$

which as noted earlier in connection with Eq. (4.13) is indeed small for large $E_{\rm J}/E_{\rm C}$, so our assumption is self-consistent in this limit.

Using

$$\hat{\varphi} = \varphi_{\rm ZPF}(\hat{a} + \hat{a}^\dagger), \tag{4.36}$$

and neglecting off-diagonal terms we can write the perturbation in a simple form useful for first order perturbation theory

$$V = -\frac{1}{12}E_{\rm C}(\hat{a} + \hat{a}^\dagger)^4 \approx -\frac{E_{\rm C}}{2}(\hat{a}^\dagger\hat{a}^\dagger\hat{a}\hat{a} + 2\hat{a}^\dagger\hat{a}). \tag{4.37}$$

The second term renormalizes the harmonic oscillator frequency downward slightly

$$\hbar\tilde{\Omega}_{\rm J} = \sqrt{8E_{\rm J}E_{\rm C}} - E_{\rm C} \tag{4.38}$$

and the first introduces an anharmonicity which yields Eq. (4.31).

4.2 Inductively Shunted Qubits

We turn now to the class of superconducting qubits illustrated in Fig. (4.2) which are inductively shunted. In the phase qubit (Martinis *et al.*, 2002; Berkley *et al.*, 2003) the Josephson junction is shunted by a lumped element inductor. In the fluxonium qubit (Manucharyan *et al.*, 2009*b*; Manucharyan *et al.*, 2009*a*), an extremely large value of inductance is required, so large that it is impossible to achieve with a coiled wire. This is due to parasitic capacitance in any coil and is essentially the result of the small value of the fine structure constant[3]. Thus instead of a coil, a long chain of Josephson junctions provides the inductance. The flux qubit (Mooij *et al.*, 1999; van der Wal *et al.*, 2000; Chiorescu *et al.*, 2003) uses only two junctions in this chain and hence it turns out that the shunting inductor is not fully linear.

As stated several times previously, the Cooper pair box is unique in its topology because there is no connection between the two superconducting islands. Thus the only way to change the charge is to tunnel an integer number of Cooper pairs through the Josephson junction. The number of Cooper pairs transferred is represented in the Hamiltonian as an angular momentum operator $\hat{n}$ which is conjugate to a compact phase angle φ. We saw from Eq. (3.4) that the state of the Cooper pair box $|\varphi + 2\pi\rangle$ is not distinct from (and indeed is identical to) $|\varphi\rangle$. This is what we mean when we say that φ is a compact angular variable living on a circle, or equivalently the wave function $\Psi(\varphi)$ obeys periodic boundary conditions. One obvious consequence is that the current flowing through the junction $I = I_{\rm c}\sin(\varphi)$ is (from the first Josephson relation) a periodic function of the phase variable.

[3]The parasitic capacitance in any coil leads to self-resonances. The frequemcy of the lowest of these self-resonances can be very crudely estimated from matching the corresponding free-space wavelength to the total length of wire in the inductor.

On the other hand, we know from the second Josephson relation that the phase variable φ is equivalent to the flux variable Φ which we introduced in quantizing the LC oscillator where we found that the energy stored in the inductor is

$$U = \frac{1}{2L}\Phi^2 = \frac{1}{2}E_{\mathrm{L}}\varphi^2 \tag{4.39}$$

where

$$E_{\mathrm{L}} \equiv \left(\frac{\hbar}{2e}\right)^2 \frac{1}{L} = \left(\frac{\Phi_0}{2\pi}\right)^2 \frac{1}{L}. \tag{4.40}$$

Clearly the energy U stored in the inductor and the current flowing through it

$$I = \frac{dU}{d\Phi} = \frac{\Phi_0}{2\pi L}\varphi \tag{4.41}$$

are *not* periodic in φ. If we shunt our Josephson junction with an external inductor, the change in topology of the circuit has profound consequences on the mathematical description. The state described by φ and $\varphi + 2\pi$ are physically distinct because they differ by how much current is flowing in the inductor. Because charge can move onto the junction capacitor plates continuously through the inductor, the charge variable is no longer integer-valued but rather continuous, as expected from the fact that φ is no longer a compact variable and the system no longer obeys periodic boundary conditions. Rather we expect vanishing boundary conditions because the energy stored in the inductor diverges for large φ: $\Psi(\varphi \longrightarrow \pm\infty) \longrightarrow 0$. Because φ is now an ordinary non-compact coordinate and we will denote this by placing a hat over it when we quantize the system. The Hamiltonian becomes

$$H = 4E_{\mathrm{C}}(\hat{n} - n_{\mathrm{g}})^2 - E_{\mathrm{J}}\cos\hat{\varphi} + \frac{1}{2}E_{\mathrm{L}}\hat{\varphi}^2. \tag{4.42}$$

Because the charge is now a continuous variable we expect on physical grounds that a *static* offset charge n_{g} can be completely screened and should not affect the energy. Mathematically this can be seen by performing the unitary gauge transformation discussed previously in Eq. (4.24). Notice however the important difference that the transformed wave function $U\Psi$ still obeys the same vanishing boundary conditions. Hence unlike the previous case, the spectrum does *not* depend on the static offset charge in any way.

Let us consider the case of a shunt inductor but take the limit $L \longrightarrow \infty$ which means $E_{\mathrm{L}} \longrightarrow 0$. Since the inductor is present, the phase variable is presumably no longer compact and yet it would seem that the inductance term does not change the Hamiltonian. Physically, it seems reasonable to assume that the high frequency oscillations of the qubit would be unaffected by the enormous reactance of the inductor. This is indeed the case and the spectrum is the same as before except that now *all* values of the wave vector k are allowed since the phase is non-compact[4]. Thus there is a continuum of states instead of a single state within each band. The only effect that offset charge has is to shift the k states $k \longrightarrow k + n_{\mathrm{g}}$, but this has no effect on the

[4]That is, the 'superselection rule' discussed previously no longer applies.

spectrum because all values of k are allowed and (in the extended zone scheme) the spectrum is periodic under $k \longrightarrow k+1$. The continuum of states corresponds to the fact that the inductor can have a fixed DC current flowing in it which can taken on any value (below the the critical current of the junction).

Exercise 4.1 In the limit of $L \longrightarrow \infty$ described above, the eigenstates are plane-wave-like Bloch waves. Using the general periodicity properties of Bloch waves, compute the mean charge (which can be non-zero only because of the infinite inductance)

$$\bar{n} = \langle \Psi_{nk} | \hat{n} | \Psi_{nk} \rangle. \tag{4.43}$$

Strictly speaking, the wave vector k is not gauge invariant. What is the correct gauge invariant operator we should have used in this equation?

If the inductive energy $E_{\rm L}$ is non-zero, then Bloch's theorem no longer applies. The quadratic potential in Eq. (4.42) resulting from the inductive energy leads to the curvature illustrated in Fig. (4.8). The interplay between the quadratic term and the Josephson cosine term allows us to create a number of different potential energy well shapes and thus generate different interesting qubit spectra. Before delving into this we need to recognize that there is one more 'control knob' at our disposal, namely externally applied flux which we can view as the inductive analog of the offset charge studied previously. If our inductor is part of a transformer with dc current applied in the other winding then there is a flux offset and the Hamiltonian becomes

$$H = 4E_{\rm C}(\hat{n} - n_{\rm g})^2 - E_{\rm J}\cos\hat{\varphi} + \frac{1}{2}E_{\rm L}(\hat{\varphi} - \varphi_{\rm g})^2. \tag{4.44}$$

It is convenient to translate $\hat{\varphi}$ and $\hat{n}$ using the unitary transformation

$$U = e^{i\varphi_{\rm g}\hat{n}}e^{-in_{\rm g}\hat{\varphi}} \tag{4.45}$$

which yields

$$U\hat{\varphi}U^{\dagger} = \hat{\varphi} + \varphi_{\rm g} \tag{4.46}$$

$$U\hat{n}U^{\dagger} = \hat{n} + n_{\rm g}. \tag{4.47}$$

The Hamiltonian then becomes

$$H = 4E_{\rm C}(\hat{n})^2 - E_{\rm J}\cos(\hat{\varphi} + \varphi_{\rm g}) + \frac{1}{2}E_{\rm L}(\hat{\varphi})^2. \tag{4.48}$$

As with the case of offset charge, we see that the resulting spectrum must be periodic in the offset flux.

The ability of control the three energy scales $E_{\rm J}, E_{\rm C}, E_{\rm L}$ as well as the offset flux $\varphi_{\rm g}$ gives the experimentalist the opportunity to create a rich variety of level structures in the inductance-shunted family of qubits. The phase qubit (Martinis *et al.*, 2002; Berkley *et al.*, 2003) is shunted by a lumped element inductor and typically operates with $E_{\rm J}/E_{\rm C} \sim 10^4$ which makes it very nearly a harmonic oscillator. To increase the anharmonicity it is operated with large flux bias on the inductor which drives a steady

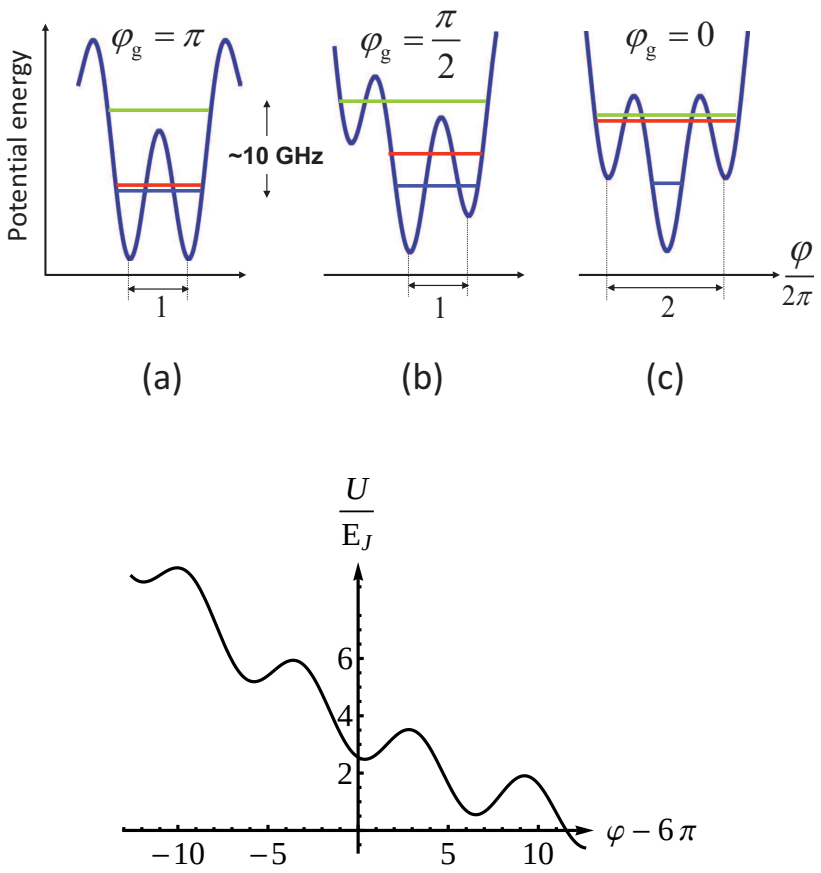

Fig. 4.8 a) Extended cosine potential $U = -E_\mathrm{J}\cos(\varphi + \varphi_\mathrm{g}) + E_\mathrm{L}\varphi^2$, with dimensionless offset flux $\varphi_\mathrm{g} = \pi$. Used in the fluxonium qubit to produce a 'Λ' level configuration; b) Same as (a) but with $\varphi_\mathrm{g} = \pi/2$; c) Same as (a) but with $\varphi_\mathrm{g} = 0$ to produce a 'V' level configuration; (bottom panel) Same as (a) but displaced a distance $\varphi_\mathrm{g} = 6\pi$ to illustrate the current (flux) biased phase qubit. $E_\mathrm{L} = 0.01E_\mathrm{J}$.

state current close to the critical current through the junction. In addition to greatly increasing the anharmonicity, this flux bias also lowers the energy level spacing so the device is typically constructed with large area junctions having a Josephson plasma

frequency $\Omega_J/2\pi = \sqrt{8E_J E_C}/h$ which is very high[5], ~ 50 GHz.

In the fluxonium qubit (Manucharyan *et al.*, 2009*b*; Manucharyan *et al.*, 2009*a*), the large inductance (and correspondingly small E_L) is supplied by the kinetic inductance of a Josephson junction array. It also has the advantage that the anharmonicity can be large. Interestingly, the state-dependent polarizability and the excitation spectrum of this design is such that the qubit state can be measured even when the qubit transition frequency is driven down to very low values of order 0.5 GHz. When the external flux φ_g through the closed loop is zero, the potential energy landscape is that shown in Fig. (4.8c). The ground state wave function has most of its support in the deep well near $\varphi = 0$ and there are two relatively closely spaced excited states with support in the two higher wells. This arrangement of three energy levels is known in atomic physics as a 'V' configuration. When the external flux is $\varphi_g = \pi$, the situation reverses as shown in Fig. (4.8a). There are two low-lying states with a large gap to the next excited state. This arrangement is known in atomic physics as a 'Lambda' configuration. As illustrated in the level scheme of Fig. (4.8b) the fluxonium qubit has the very nice property that its energy spectrum varies smoothly between these two limits and unlike the flux qubit, does not have exponential sensitivity to the external flux (Manucharyan *et al.*, 2009*b*; Manucharyan *et al.*, 2009*a*). A further interesting feature is that, unlike the transmon qubit, the anharmonicity of the level structure can be quite large and it is possible in principle in the 'Λ' configuration to have the low energy level splitting much smaller than the frequency of the readout cavity and yet still achieve strong dispersive coupling to the cavity via virtual transitions to the third energy level. This allows efficient readout with suffering from the Purcell effect enhancement of the qubit decay rate via spontaneous fluorescence into the readout cavity (Manucharyan *et al.*, 2009*b*; Manucharyan *et al.*, 2009*a*).

[5] As noted earlier, if the capacitance is dominated by the junction itself, then $E_J E_C$ is independent of junction area. When external and parasitic capacitance is included, then the plasma frequency rises with junction area.

5

Noise induced Decoherence in Qubit Circuits

The ideal qubit would have a completely stable transition frequency unperturbed by the external environment and yet would have a port open to the outside world through which its state could be controlled and measured. Unfortunately, things are never ideal and it is our job as quantum engineers to design qubits for the real world. Unlike the Cs and Rb atoms used in atomic clocks which are (literally) indistinguishable, each qubit we build is a unique individual. The good news is that we can engineer different classes of Hamiltonians and qubit Hamiltonians with different parameters within the same class. The bad news is that in reality, if we can vary the Hamiltonian parameters, they will tend to vary on their own due to various random sources of noise. This variation of parameters has two effects. First, it can modulate transition frequencies which leads to dephasing of superpositions. Second, if the noise (including as we will see, vacuum noise) is high-frequency, it can cause transitions to occur which change the state of the qubit. A related engineering quandary, which we will explore in more detail below, is the following: a qubit which is completely unperturbed by its environment is also decoupled from our measurement apparatus and hence cannot be read out!

The phenomenological Bloch equation from NMR is a useful starting point to understand the standard parametrization of qubit relaxation rates. In NMR one typically studies the dynamics of a large collection of spin-1/2 (say) nuclei in a sample by coupling a drive/readout coil to the total magnetic moment. In the absence of any perturbations and assuming there are N spins, all having the same Zeeman energy (no 'inhomogeneous broadening'), the Hamiltonian is simply

$$H = \frac{\Omega}{2} \sum_{j=1}^{N} \sigma_j^z. \tag{5.1}$$

The component of the magnetization parallel to the Zeeman field

$$\hat{m}^z \equiv \frac{1}{N} \sum_{j=1}^{N} \sigma_j^z, \tag{5.2}$$

commutes with the Hamiltonian and so is a constant of the motion. The transverse components of the magnetization precess around the magnetic field direction. If we go to a frame rotating at frequency Ω, these transverse components of the magnetization are also constants of the motion (because the Hamiltonian then vanishes).

Inhomogeneous broadening and various fluctuating perturbations will complicate this simple picture and cause the net magnetization to relax to its equilibrium value. This relaxation is characterized in the phenomenological Bloch equations which describe the dynamics of the components of the mean magnetization vector, $m^\mu \equiv \langle \hat{m}^\mu \rangle$, in terms of a longitudinal relaxation time, T_1, and a transverse relaxation time, T_2.

$$\dot{m}^z = -\frac{1}{T_1}(m^z - \bar{m}^z) \tag{5.3}$$

$$\dot{m}^x = -\frac{1}{T_2}m^x \tag{5.4}$$

$$\dot{m}^y = -\frac{1}{T_2}m^y, \tag{5.5}$$

The longitudinal relaxation rate can be shown to be given by the sum of the transition rates from down to up and up to down

$$\frac{1}{T_1} = \Gamma_\uparrow + \Gamma_\downarrow. \tag{5.6}$$

The equilibrium magnetization is given by

$$\bar{m}^z = \frac{\Gamma_\uparrow - \Gamma_\downarrow}{\Gamma_\uparrow + \Gamma_\downarrow}. \tag{5.7}$$

The (ensemble) transverse relaxation rate can be shown to be given by[1]

$$\frac{1}{T_2^*} = \frac{1}{2T_1} + \frac{1}{T_\varphi}. \tag{5.8}$$

The first term represents the fact that if the spin makes a transition from up to down (or vice versa) the coherent superposition of up and down is destroyed. The second term containing $\frac{1}{T_\varphi}$ represents the rate at which the transverse magnetization decays due to random fluctuations in the spin precession rate which cause the different spins to get out of phase with each other and thus destroy the mean transverse polarization.

We will be dealing not with a large ensemble of spins which are simultaneously measured (as in NMR) but rather with an individual spin subject to temporal (rather than spatial) fluctuations which cause the precession rate to vary from measurement to measurement. Since it takes many measurements to determine the average magnetization, we must average the effect of the noise across the ensemble of measurements on the single spin[2]. The mathematics is thus similar to the NMR case but the physical difference in the meaning of the average being taken should be kept in mind.

[1]The notation of the NMR literature is that T_2^* refers to the ensemble transverse relaxation rate which includes dephasing due to spin-lattice interactions, spatial inhomogeneities of the Zeeman field and local chemical shifts of the Zeeman splitting. The relaxation time T_2 is that associated only with the homogeneous broadening of the NMR resonance due to spin-lattice interactions. T_2 can be measured using spin-echo methods to cancel out the inhomogeneous broadening. Strictly speaking, there is no unique phase coherence time. One should specify precisely the experiment used to measure the coherence. Thus it is common to refer to T_2^{Ramsey} and T_2^{echo} in order to be precise. More complex echo sequences (e.g. CPMG) can yield still further measures of coherence.

[2]With a high-fidelity QND measurement of σ^z one can determine that component of the spin in a single measurement. However thermal fluctuations (e.g. the initial state of the spin is fluctuating in

Exercise 5.1 Derive Eqs. (5.6) and (5.7).

We turn now to the microscopic noise which leads to the above phenomenology. Suppose that the qubit Hamiltonian contains a set of n parameters λ_j; $j\epsilon\{1,...,n\}$. Let us take the value of these parameters at the working point to be $\bar{\lambda}_j$; $j\epsilon\{1,...,n\}$, and let the deviation from the nominal working point due to noise in the parameter values be $\eta_j; j\epsilon\{1,...,n\}$. The qubit Hamiltonian can then be expressed in a Taylor series expansion.

$$H[\vec{\lambda}] = H_0 + \sum_{j=1}^{n} \eta_j V_j + \frac{1}{2} \sum_{j,k=1,n} \eta_j \eta_k V_{jk} + \ldots, \tag{5.9}$$

where $H_0 \equiv H[\vec{\bar{\lambda}}]$ and

$$V_j \equiv \left. \frac{\partial H}{\partial \lambda_j} \right|_{[\vec{\bar{\lambda}}]} \tag{5.10}$$

$$V_{jk} \equiv \left. \frac{\partial^2 H}{\partial \lambda_j \partial \lambda_k} \right|_{[\vec{\bar{\lambda}}]}. \tag{5.11}$$

The noise amplitudes η_j could represent classical random variables or quantum operators associated with the bath to which the qubit is coupled.

For simplicity, we will initially work only to first order in the expansion. If V_j commutes with H_0 then it is diagonal in the energy eigenbasis and cannot affect the eigenfunctions, it can only modulate the eigenvalues. Such perturbations can dephase superpositions but cannot cause transitions between levels and hence cannot relax the population. On the other hand if $[V_j, H_0] \neq 0$, then V_j is not diagonal in the energy basis and can cause both dephasing and relaxation.

As a simple example, consider the Hamiltonian of a two-level system

$$H = \frac{\Omega}{2}\sigma^z + \vec{\eta}(t) \cdot \vec{\sigma}. \tag{5.12}$$

Let us first ignore the transverse field fluctuations and focus on the η_z longitudinal term which commutes with H_0. For simplicity we will take η_z to be a classical random variable. The exact time evolution operator in the interaction representation is

$$U(t_1, t_2) = e^{-\frac{i}{2}\theta(t_1,t_2)\sigma^z} \tag{5.13}$$

where the random phase accumulated due to the longitudinal noise is given by

$$\theta(t_1, t_2) = 2 \int_{t_1}^{t_2} d\tau\, \eta_z(\tau). \tag{5.14}$$

thermal equilibrium) and quantum fluctuations (e.g. the spin is actually pointing in the x direction so the measurement result for σ^z is random) imply that one must repeat the experiment many times to determine the quantum/thermal ensemble average magnetization

Assuming η_z has zero mean then θ also has zero mean and variance given by

$$\langle\theta^2\rangle = 4\int_{t_1}^{t_2} d\tau_1 d\tau_2 \,\langle\eta_z(\tau_1)\eta_z(\tau_2)\rangle. \tag{5.15}$$

If we assume that η_z itself is gaussian distributed then θ will be gaussian. Or if η_z is not gaussian but its autocorrelation function appearing in Eq. (5.15) is short-ranged in time compared to $t_2 - t_1$, then (under rather mild assumptions) the central limit theorem applies because θ is the sum of a large number of independent random variables. If θ is gaussian distributed with mean zero, then the cumulant expansion converges at first order and we have the exact result

$$\langle\langle e^{i\theta}\rangle\rangle = e^{-\frac{1}{2}\langle\langle\theta^2\rangle\rangle} \tag{5.16}$$

where $\langle\langle\rangle\rangle$ refers to the statistical ensemble average over the noise. If the autocorrelation time of the noise is short we can write Eq. (5.15) as

$$\langle\langle\theta^2\rangle\rangle \approx 4tS_{\eta_z\eta_z}(0), \tag{5.17}$$

where $S_{\eta_z\eta_z}[\omega]$ is the noise spectral density at frequency ω. The full expressions for the case where the autocorrelation time of the noise is not negligible are given in (Martinis *et al.*, 2003). The important time scale $t_2 - t_1$ in Eq. (5.15) is given self-consistently by T_2^* itself. Noise which is slow on the time scale of T_2^* produces (the analog of) inhomogeneous broadening. Noise which is high-frequency on the scale of T_2^* makes little contribution to the integral in Eq. (5.15). For sufficiently large T_2^*, it is only low frequencies that count here, and it is generally safe to treat η_z classically and ignore that fact that it typically represents a quantum operator describing a bath variable. [This will not be true for the transverse noise fluctuations where the high-frequency spectral density is important.]

Let us define the (pure) dephasing rate $1/T_\varphi$ via

$$\langle\langle e^{i\theta}\rangle\rangle = e^{-\frac{t}{T_\varphi}}, \tag{5.18}$$

from which we see that

$$\frac{1}{T_\varphi} = 2S_{\eta_z\eta_z}(0). \tag{5.19}$$

5.1 Density Matrix Description of Decoherence

It turns out that the important fluctuations of the transverse fields are the ones resonant with the transition frequency of the qubit because this is necessary for energy conservation in the transitions between qubit states. For such high-frequency fluctuations we should more properly use a full quantum theory which involves the quantum density matrix of the qubit. In the presence of quantum or classical noise, we desire the ensemble average over the noise of any given physical observable. Let p_j be the probability that an element of the ensemble is in state $|\psi_j\rangle$ (or equivalently that the

random noise has driven our system to state $|\psi_j\rangle$). The expectation value of observable $\mathcal{O}$ is

$$\langle\langle\mathcal{O}\rangle\rangle = \sum_j p_j \langle\psi_j|\mathcal{O}|\psi_j\rangle = \mathrm{Tr}\,\rho\mathcal{O}, \tag{5.20}$$

where the density matrix is defined by

$$\rho = \sum_j p_j |\psi_j\rangle\langle\psi_j|. \tag{5.21}$$

Clearly the density matrix must satisfy

$$\mathrm{Tr}\,\rho = 1 \tag{5.22}$$

$$\mathrm{Tr}\,\rho^2 \leq 1, \tag{5.23}$$

the latter satisfied as an equality only for a pure state (a state where one of the p_j's is unity and the rest vanish). In fact for a pure state, the density matrix is idempotent

$$\rho^2 = \rho. \tag{5.24}$$

The von Neumann entropy is given by an expression closely analogous to the classical one

$$S = -\mathrm{Tr}\left\{\rho\log\rho\right\} \tag{5.25}$$

Exercise 5.2 Prove Eq. (5.23) and Eq. (5.24).

The density matrix contains all the information we need to compute the expectation value of any observable, or any moment of the distribution of some observable, for example

$$\langle\langle\mathcal{O}^m\rangle\rangle = \mathrm{Tr}\,\rho\mathcal{O}^m \tag{5.26}$$

or even the full probability distribution for the measurement results for the observable

$$P(\lambda) = \mathrm{Tr}\,\left\{\rho\delta(\lambda-\mathcal{O})\right\}. \tag{5.27}$$

Since a two-level qubit or a spin-1/2 particle has only two independent quantum states, the density matrix is 2×2. The most general such matrix which is hermitian and has unit trace can be written

$$\rho = \frac{1}{2}\left(1+\vec{m}\cdot\vec{\sigma}\right), \tag{5.28}$$

where the qubit polarization is given by $\vec{m} = \mathrm{Tr}\rho\vec{\sigma}$, that is

$$m_j = \mathrm{Tr}\,\rho\sigma_j. \tag{5.29}$$

Exercise 5.3 Use Eq. (5.28) to prove Eq. (5.29).

Having now established these statistical results we can proceed to ensemble average the density matrix over the noise to obtain the reduced density matrix where the noise bath degrees of freedom have been integrated out (traced over). In the interaction representation

$$\langle\langle \rho(t_2)\rangle\rangle = \langle\langle U(t_1,t_2)\rho(t_1)U^\dagger(t_1,t_2)\rangle\rangle, \tag{5.30}$$

where we now take ρ to be the full density matrix for system plus bath and the interaction representation of the time evolution operator is given by the time-ordered exponential of the perturbation $\hat{V}(t)$ which couples the system to the bath

$$U(t_1,t_2) = T_\tau \exp\left\{-\frac{i}{\hbar}\int_{t_1}^{t_2} d\tau \hat{V}(\tau)\right\} \tag{5.31}$$

Typically $\hat{V}$ can be expressed as a product (or sum of products) of system operators and bath operators. Notice that we cannot separately average (i.e. trace over the bath) the two time evolution operators appearing in Eq. (5.30) because they are correlated– they depend on the same bath noise. It is convenient to do a perturbative calculation which will be valid for short times $t_2 = t_1 + \Delta t$. We assume the perturbation is weak enough that our perturbative expansion is in fact valid for times longer than the autocorrelation time of the noise, τ_c. In that case we can safely choose a a time step $\Delta t \gg \tau_c$ and the random noise variables in $U(t_1,t_2)$ will be essentially uncorrelated with the past noise variables that led to $\rho(t_1)$. This statistical independence will allow us to make the 'no memory' or Markov approximation (Walls and Milburn, 1994) which will considerably simplify matters Again, we can only justify this for sufficiently weak noise that low-order perturbation theory is still valid for the chosen value of Δt.

By definition we choose $\langle\langle \hat{V}(\tau)\rangle\rangle = 0$ so we must (at least in the Markov approximation) take our expansion to second order (just as we do in Fermi's Golden Rule for transition rates)

$$U(t_1,t_2) \approx 1 - \frac{i}{\hbar}\int_{t_1}^{t_2} d\tau \hat{V}(\tau) - \frac{1}{2\hbar^2}\int_{t_1}^{t_2} d\tau d\tau' T_\tau \hat{V}(\tau)\hat{V}(\tau'). \tag{5.32}$$

The time-ordering operator will prove inconvenient, but we can write

$$T_\tau \hat{V}(\tau)\hat{V}(\tau') = \hat{V}(\tau)\hat{V}(\tau') + \theta(\tau'-\tau)[\hat{V}(\tau'),\hat{V}(\tau)]. \tag{5.33}$$

The commutator term does not necessarily vanish, but it turns out it is possible to lump its effect into the system Hamiltonian where it leads to small corrections to the system energy levels (e.g. the Lamb shift of atomic levels). We presume that this has already been done and so this commutator term drops out. The reader is directed to (Haroche and Raimond, 2006) and (Meystre and III, 1998) for further discussion of these points.

Anticipating being able to drop the terms linear in $\hat{V}$ when we trace out the bath [because they have zero mean and within the Markov approximation no correlations with the prior noise that led to $\rho(t_1)$], we are thus led to

$$\rho(t_2) = \rho(t_1) + \frac{1}{\hbar^2}\int_{t_1}^{t_2} d\tau d\tau' \Big\{ \hat{V}(\tau)\rho(t_1)\hat{V}(\tau') - \frac{1}{2}\hat{V}(\tau)\hat{V}(\tau')\rho(t_1) - \frac{1}{2}\rho(t_1)\hat{V}(\tau)\hat{V}(\tau') \Big\}. \tag{5.34}$$

In order to make further progress we now need to express the perturbation in terms of system and bath variables and trace out the bath variables to obtain an expression for the time evolution of the reduced density matrix describing the system alone. Let us suppose that in the interaction picture, the bath coupling has the form

$$\frac{1}{\hbar}\hat{V}(\tau) = \hat{\eta}_z(\tau)\hat{\sigma}^z(\tau) + \hat{\eta}_x(\tau)\hat{\sigma}^x(\tau) \tag{5.35}$$

$$= \hat{\eta}_z(\tau)\sigma^z + \hat{\eta}_x(\tau)\{e^{i\Omega\tau}\sigma^+ + e^{-i\Omega\tau}\sigma^-\}. \tag{5.36}$$

To keep the discussion simple we will assume that the longitudinal and transverse noises are uncorrelated and can therefore be treated separately in our perturbative treatment. We start with the longitudinal noise and will attempt to reproduce our previous semi-classical result in Eq. (5.19). Introducing the notation

$$\mathrm{Tr}_{\,\mathrm{bath}}\rho(t) \equiv \langle\langle\rho(t)\rangle\rangle, \tag{5.37}$$

we can write

$$\langle\langle\rho(t_1+\Delta t)\rangle\rangle = \langle\langle\rho(t_1)\rangle\rangle + \int_{t_1}^{t_2} d\tau d\tau'\, \mathrm{Tr}_{\,\mathrm{bath}}\Big\{ \hat{\eta}_z(\tau)\sigma^z\rho(t_1)\sigma^z\hat{\eta}_z(\tau') - \frac{1}{2}\hat{\eta}_z(\tau)\hat{\eta}_z(\tau')\sigma^z\sigma^z\rho(t_1) - \frac{1}{2}\rho(t_1)\hat{\eta}_z(\tau)\hat{\eta}_z(\tau')\sigma^z\sigma^z \Big\}. \tag{5.38}$$

Using the cyclic property of the trace in the first term, interchanging the dummy labels τ and τ' in the remaining terms and invoking the Markov approximation we obtain

$$\langle\langle\rho(t_1+\Delta t)\rangle\rangle = \langle\langle\rho(t_1)\rangle\rangle + \int_{t_1}^{t_2} d\tau d\tau'\, \langle\langle\hat{\eta}_z(\tau')\hat{\eta}_z(\tau)\rangle\rangle \Big\{ \sigma^z\langle\langle\rho(t_1)\rangle\rangle\sigma^z - \frac{1}{2}\sigma^z\sigma^z\langle\langle\rho(t_1)\rangle\rangle - \frac{1}{2}\langle\langle\rho(t_1)\rangle\rangle\sigma^z\sigma^z \Big\}. \tag{5.39}$$

Of course $\sigma^z\sigma^z = 1$, but for notational symmetry, we will not use this. Invoking the Markov approximation as in Eq. (5.17) and defining

$$\gamma_\varphi = 2S_{\eta_z\eta_z}(0), \tag{5.40}$$

we have

$$\langle\langle\rho(t_1+\Delta t)\rangle\rangle = \langle\langle\rho(t_1)\rangle\rangle + \Delta t\frac{\gamma_\varphi}{2}D[\sigma^z]\langle\langle\rho(t_1)\rangle\rangle, \tag{5.41}$$

where the 'dissipator' D is called the Lindblad superoperator[3]

[3]A 'superoperator' is an operator on the N^2 dimensional space of ρ if ρ is written as a column vector of length N^2 instead of an $N \times N$ matrix.

$$D[\mathcal{O}]\rho \equiv \mathcal{O}\rho\mathcal{O}^\dagger - \frac{1}{2}\mathcal{O}^\dagger\mathcal{O}\rho - \frac{1}{2}\rho\mathcal{O}^\dagger\mathcal{O}. \tag{5.42}$$

Even though Δt is not supposed to be too small, if we are appropriately cautious about the meaning, we can interpret this difference equation as a differential equation for the time evolution of the reduced density matrix,

$$\frac{d}{dt}\langle\langle\rho(t)\rangle\rangle = \frac{1}{2}\gamma_\varphi D[\sigma^z]\langle\langle\rho(t)\rangle\rangle. \tag{5.43}$$

Let us now try to go from this result to the time evolution of the qubit polarization. Invoking Eq. (5.28) we have

$$\frac{d}{dt}\langle\langle\rho(t)\rangle\rangle = \frac{1}{2}\frac{d\vec{m}}{dt}\cdot\vec{\sigma} = \frac{1}{2}\gamma_\varphi D[\sigma^z]\frac{1}{2}[1+\vec{m}\cdot\sigma]. \tag{5.44}$$

Using the fact that the different Pauli matrices anticommute this can be rewritten

$$\frac{d\vec{m}}{dt}\cdot\vec{\sigma} = -\gamma_\varphi\{m_x\sigma^x + m_y\sigma^y\}. \tag{5.45}$$

From this we immediately obtain

$$\dot{m}^z = 0 \tag{5.46}$$

$$\dot{m}^x = -\frac{1}{T_\varphi}m^x \tag{5.47}$$

$$\dot{m}^y = -\frac{1}{T_\varphi}m^y, \tag{5.48}$$

in agreement with the phenomenological Bloch equations (5.5) with $T_1 = \infty$.

In order to obtain a finite energy relaxation rate, we must allow for noise in the transverse field components. Repeating the derivation above and defining the up and down transition rates (which agree with the derivation of Fermi's Golden Rule in (Clerk *et al.*, 2010)) in terms of the noise spectral densities

$$\Gamma_\downarrow = S_{\eta_x\eta_x}(+\Omega) \tag{5.49}$$

$$\Gamma_\uparrow = S_{\eta_x\eta_x}(-\Omega), \tag{5.50}$$

Eq. (5.43) becomes the standard master equation (Carmichael, 1993) in Lindblad form

$$\frac{d}{dt}\langle\langle\rho(t)\rangle\rangle = \frac{\gamma_\varphi}{2}D[\sigma^z]\langle\langle\rho(t)\rangle\rangle + \Gamma_\uparrow D[\sigma^+]\langle\langle\rho(t)\rangle\rangle + \Gamma_\downarrow D[\sigma^-]\langle\langle\rho(t)\rangle\rangle. \tag{5.51}$$

As discussed extensively in Ref. (Clerk *et al.*, 2010), the bath noise spectral density at frequency $+\Omega$ is a measure of the ability of the bath to absorb energy and thereby de-excite the qubit, while the spectral density at $-\Omega$ gives the ability of the bath to emit energy at that frequency, thereby exciting the qubit. Classically there is no distinction since the noise correlators are real-valued, but quantum mechanically we must distinguish positive and negative frequency because the noise correlators are

complex-valued (which is possible since the noise operators are hermitian but their product is not: they do not commute with each other at different times (Clerk *et al.*, 2010)). Evaluating the above, we arrive at the full Bloch equations in (5.5).

The Bloch equations in NMR refer to the density matrix for a large ensemble of spins. Here we are dealing with the ensemble of many repeated experiments on a single 'spin.' In NMR inhomogeneous line broadening usually comes from different parts of the sample having slightly different spin precession frequencies. Here there is only one spin and inhomogeneous broadening arises from slow temporal (rather than spatial) fluctuations of the qubit splitting over the course of many repeated measurements. Another difference with NMR is that typically in NMR we are in the regime $k_{\rm B}T \gg \hbar\Omega$ and so $\Gamma_\uparrow \approx \Gamma_\downarrow$. With qubits we are (typically) in the opposite regime with high frequency and low temperature where $\Gamma_\downarrow \gg \Gamma_\uparrow$.

Exercise 5.4 Derive Eq. (5.5) in detail from Eq. (5.51).

We emphasize that the Markov approximation is not necessarily valid. For instance the qubit could be looking at the environmental noise filtered by a resonator or cavity, or in the case of dephasing noise at low frequencies the spectrum of the noise may be 1/f rather than white. The former can be handled by adding the filter (as a harmonic oscillator) to the Hamiltonian. The latter complicates the analysis and leads to non-exponential decay (Martinis *et al.*, 2003).

5.1.1 Dephasing and Read Out of Charge Qubits

For generic values of the gate charge, the ground state Ψ_0 and excited state Ψ_1 of a charge qubit differ in their respective static electric 'dipole moments'. Using Eq. (A.18) we see that the state energy depends on bias voltage $V_{\rm B}$ fluctuations via the 'dipole moment'

$$\tilde{p}_j = \langle \Psi_j | \frac{\partial H}{\partial V_{\rm B}} | \Psi_j \rangle \tag{5.52}$$

$$= \beta \langle \Psi_j | \hat{Q}_1 | \Psi_j \rangle, \tag{5.53}$$

where we have ignored the last term in Eq. (A.18) since it is not state-dependent. Nakamura *et al.*(Nakamura *et al.*, 1999) used the dependence of a certain quasi-particle tunneling rate on p_j to differentiate between the ground state ($j = 0$) and the excited state ($j = 1$) and hence readout the state of the qubit. Aassime *et al.*(Aassime *et al.*, 2001) and Lehnert *et al.*(Lehnert *et al.*, 2003) developed an RF single electron transistor readout scheme for charge based qubits.

Unfortunately in the regime where charge based readout works, a stray electric field $\mathcal{E}$ (fluctuation in bias voltage $V_{\rm B}$) causes a first-order perturbation theory shift of the qubit excitation frequency by an amount

$$\delta\omega_{01} = \frac{1}{\hbar}\delta V_{\rm B}(\tilde{p}_1 - \tilde{p}_0). \tag{5.54}$$

This leads to very rapid dephasing of quantum superpositions at rate (Martinis *et al.*, 2003)

$$\frac{1}{T_\varphi} = \frac{1}{2}\left(\frac{\tilde{p}_1 - \tilde{p}_0}{\hbar}\right)^2 S_{V_{\rm B}V_{\rm B}}, \tag{5.55}$$

where $S_{V_{\rm B}V_{\rm B}}$ is the bias voltage spectral density at low frequencies. The total decoherence rate is then given by

$$\frac{1}{T_2^*} = \frac{1}{2T_1} + \frac{1}{T_\varphi}. \tag{5.56}$$

Recognizing this difficulty, Vion et al. (Vion *et al.*, 2002) introduced the notion of operating charge qubits at a 'sweet spot' where the transition frequency is an extremum with respect to the voltage and magnetic field control parameters. Several such extrema (known in atomic physics as 'clock points') are visible (at half-integer gate-charge points) in the Cooper pair box spectrum shown in Fig. (4.6). At these special points, the leading term in the Taylor series expansion presented in Eq. (5.9) vanishes and only the second-order effects of the noise contribute to the dephasing. The qubit coherence time is therefore dramatically increased (Vion *et al.*, 2002). Measurements by the Devoret group have demonstrated that these coherence lifetimes are indeed consistent with the expected second-order effects of the noise determined by the curvature of the spectrum at the extremum (Metcalfe *et al.*, 2007).

We now arrive at an interesting quandary. By tuning the qubit to the sweet spot, the environment is no longer able to detect which state the qubit is in, based on coupling to its electric dipole moment. This is why the coherence time is so dramatically enhanced. But, if the environment cannot measure the state of the qubit by looking at the dipole moment, neither can we! The Saclay group recognized this and developed the concept of reading out the qubit by measuring the state dependent susceptibility (inductance of the quantronium qubit). Rather than going into the details of this, it is easier in the context of the present discussion to instead think about the closely related state-dependent susceptibility method based on capacitance developed by the Yale group (Blais *et al.*, 2004; Wallraff *et al.*, 2004) and which will be explained in detail in Chapter 6. Because the offset charge is essentially equivalent to an applied voltage, and the potential energy of a capacitor is $\frac{1}{2}CV^2$, the second derivative of the transition energy with respect to $n_{\rm g}$ which can be derived from Eq. (4.4) (and illustrated in Fig. (4.6)) is essentially the difference in quantum capacitance (Widom *et al.*, 1984; Averin *et al.*, 1985; Likharev and Zorin, 1985; Averin and Bruder, 2003; Duty *et al.*, 2005; Sillanpää *et al.*, 2005) presented to an external probing field when the qubit is in the ground and excited states. Essentially this effect was used by the Yale group in developing the dispersive readout (Blais *et al.*, 2004; Wallraff *et al.*, 2004) based on (6.13). Working with a low frequency probe, precisely this effect was measured in (Duty *et al.*, 2005; Sillanpää *et al.*, 2005). The difference is that the high-frequency dispersive probe depends on the matrix elements related to the quantum capacitance, but as is clear from (6.13), it also depends on the detuning of the qubit and resonator frequencies. The importance of this difference will become clear below.

The invention of the transmon qubit brings us to our next major quandary. As noted in Fig. (4.6), by going to large $E_{\rm J}/E_{\rm C}$ one can dramatically reduce the curvature of the spectrum at the extrema and eventually make the transition frequency exponentially close to constant independent of the gate charge (Koch *et al.*, 2007;

Houck *et al.*, 2009). Operation in this transmon regime leads to even longer lifetimes and long-term qubit frequency stability (Houck *et al.*, 2009; Paik *et al.*, 2011). If the energy eigenvalues are essentially independent of the offset charge then neither we nor the environment can read the state of the qubit using either the dipole moment or the susceptibility (quantum capacitance) since neither is dependent on the quantum state. While this explains the even longer coherence times of the transmon, we are left to wonder how it is that the dispersive readout still works even though quantum capacitance is zero in both states. Recall that if the qubit were actually a perfect harmonic oscillator, the transition frequencies would not respond at all to changes in offset charge (displacement of the origin of the oscillator). It is obvious from classical considerations that the susceptibility would be a constant (given by the inverse of the spring constant) independent of the state. The oscillator is highly polarizable and responds strongly to slow variations in offset charge by being displaced, but this displacement to a new equilibrium position has no effect on the excitation spectrum. As noted above, the transmon comes exponentially close to this ideal behavior and yet, the dispersive readout still works. This is because, while the charge dispersion falls off exponentially, the transmon retains its anharmonicity. As can be seen from (6.13), the cavity pull due to the virtual polarization of the qubit is strongly dependent on the detuning between the qubit and cavity. For the case of the multi-level transmon, the expression for the cavity pull has to be re-derived, but the essential point is that the detuning for the $0 \rightarrow 1$ transition is not the same as that for the $1 \rightarrow 2$ transition and so the cavity pull is state dependent, provided that the cavity frequency is reasonably close to the qubit. For a very low frequency cavity, we are back in the regime measuring the quantum capacitance where the effect on the cavity is small.

The fluxonium qubit (Manucharyan *et al.*, 2009*b*; Manucharyan *et al.*, 2009*a*) can be operated in a regime which maintains very large anharmonicity even while suppressing the effects of offset charge noise. The fluxonium energy level structure therefore gives the advantage over the transmon that the qubit transition frequency can be far removed from the cavity readout frequency which prevents Purcell enhancement of the excited state decay rate.

6

Introduction to Cavity and Circuit QED

Quantum electrodynamics (QED) studies atoms and electrons coupled to the quantum fluctuations of the electromagnetic field. Cavity QED (cQED) engineers those quantum fluctuations of the vacuum by surrounding the atoms with a resonant cavity which supports only discrete modes of the electromagnetic field. By adjusting the frequencies (and damping) of those resonant modes with respect to the transition frequency of the atoms, one can dramatically alter the coupling of the atoms to their quantum environment (and conversely alter the photon modes via their coupling to the atoms). Because the cavity traps photons, they interact with the atoms repeatedly and one can enter a regime of strong coupling in which the natural excitations of the system are coherent superpositions of atom and photon excitations known as polaritons.

There is a long history of cavity QED studies in the AMO community for both alkali atoms in optical cavities (Mabuchi and Doherty, 2002; Walls and Milburn, 1994; Thompson *et al.*, 1992; Boca *et al.*, 2004; Schuster *et al.*, 2008) and Rydberg atoms in microwave cavities (Nogues *et al.*, 1999; Guerlin *et al.*, 2007; Gleyzes *et al.*, 2007; Deleglise *et al.*, 2008; Raimond *et al.*, 2001; Haroche and Raimond, 2006). In the optical case one typically monitors the effect of the atoms on the photons transmitted through (or reflected from) the cavity. It is not possible to measure the state of the atoms after they have fallen through the cavity because the spontaneous emission lifetime is on the order of nanoseconds at optical frequencies. In the microwave experiments pioneered by the Paris group it is difficult to directly measure the microwave photons but relatively easy to measure the state of the Rydberg atoms with very high fidelity after they exit the cavity since they have a lifetime of approximately 30 ms and can be probed with state-selective ionization.

'Circuit QED' uses superconducting qubits as artificial atoms coupled to microwave resonators (Blais *et al.*, 2004; Wallraff *et al.*, 2004; Chiorescu *et al.*, 2004; Devoret *et al.*, 2007; Schoelkopf and Girvin, 2008) as illustrated schematically[1] in Fig. (6.1). Measuring the amplitude and phase of microwaves transmitted through (or reflected from) the resonator realizes the equivalent of optical cavity QED at microwave frequencies. It is interesting to note that (typically) there is just a single microwave signal channel running to and from the cavity. Application of microwaves near the cavity frequency

[1] There exists a dual geometry in which the Josephson junction qubit is placed in line with the center pin of the resonator and couples directly to the microwave currents flowing in the resonator (Devoret *et al.*, 2007; Bourassa *et al.*, 2009). In this dual geometry the fine structure constant is replaced by its *inverse* and the problem is engineering the circuit to *reduce* the coupling to manageable levels.

excites the cavity and performs a measurement of the state of the qubit. On the other hand application of microwaves at the qubit transition frequency (assumed to be strongly detuned from the cavity frequency) does not strongly excite the cavity and, most importantly, does *not* perform a measurement. Rather such microwaves resonant with the qubit can be used to perform single qubit rotations. Thus we have a very convenient 'frequency multiplexing' in which a single wire carries out different operations depending on the frequency of the microwaves applied to it.

In recent years there were many theoretical proposals for coupling qubits to either three-dimensional cavities or lumped element resonators and for protocols for analyzing microwave photon states (Shnirman *et al.*, 1997; Makhlin *et al.*, 2001; Buisson and Hekking, 2001; Marquardt and Bruder, 2001; Al-Saidi and Stroud, 2001; Plastina and Falci, 2003; Blais *et al.*, 2003; Yang *et al.*, 2003; You and Nori, 2003; Menzel *et al.*, 2010; Koch and Le Hur, 2009; Koch *et al.*, 2010; Nunnenkamp *et al.*, 2011; Viehmann *et al.*, 2011) (and others too numerous to list) and there has been a flurry of experiments on circuit QED (Wallraff *et al.*, 2004; Chiorescu *et al.*, 2004; Schuster *et al.*, 2005; Wallraff *et al.*, 2005; Schuster *et al.*, 2007*b*; Johansson *et al.*, 2006; Siddiqi *et al.*, 2006; Boulant *et al.*, 2007; Schuster *et al.*, 2007*a*; Wallraff *et al.*, 2007; Sillanpää *et al.*, 2007; Houck *et al.*, 2007; Leek *et al.*, 2007; Majer *et al.*, 2007; Astafiev *et al.*, 2007; Metcalfe *et al.*, 2007; Deppe *et al.*, 2008; Fink *et al.*, 2008; Hofheinz *et al.*, 2008; Wang *et al.*, 2008; Schreier *et al.*, 2008; Houck *et al.*, 2008; Fragner *et al.*, 2008; Grajcar *et al.*, 2008; Sandberg *et al.*, 2008; Il'ichev *et al.*, 2009; Bishop *et al.*, 2009*a*; Chow *et al.*, 2009; Hofheinz *et al.*, 2009; DiCarlo *et al.*, 2009; Fink *et al.*, 2009; Baur *et al.*, 2009; Leek *et al.*, 2009; Leek *et al.*, 2010; Bianchetti *et al.*, 2010; Niemczyk *et al.*, 2010; Johnson *et al.*, 2010; DiCarlo *et al.*, 2010; Neeley *et al.*, 2010; Mariantoni *et al.*, 2011*a*; da Silva *et al.*, 2010; Fink *et al.*, 2010; Astafiev *et al.*, 2010; Hoffman *et al.*, 2011*b*; Gambetta *et al.*, 2011*a*; Srinivasan *et al.*, 2011*a*; Wilson *et al.*, 2011; Bylander *et al.*, 2011; Ong *et al.*, 2011; Vijay *et al.*, 2011; Bozyigit *et al.*, 2011; Eichler *et al.*, 2011*b*; Eichler *et al.*, 2011*a*; Lang *et al.*, 2011; Hoi *et al.*, 2011; Paik *et al.*, 2011; Kim *et al.*, 2011; Mariantoni *et al.*, 2011*b*; Dewes *et al.*, 2012; Baur *et al.*, 2012; Eichler *et al.*, 2012; Murch *et al.*, 2012; Johnson *et al.*, 2012; Houck *et al.*, 2012; Underwood *et al.*, 2012; Yin *et al.*, 2013; Sete *et al.*, 2013; Kirchmair *et al.*, 2013; Vlastakis *et al.*, 2013; Hoi *et al.*, 2012; Hoi *et al.*, 2013; Hatridge *et al.*, 2013; Woolley *et al.*, 2013; Córcoles *et al.*, 2013; Murch *et al.*, 2013; Shanks *et al.*, 2013).

In optical cQED, one uses a Fabry-Pérot cavity which (because optical wavelengths are so small) is typically very large compared to a wavelength of light at the frequencies associated with atomic spectra. The frequency of one of the longitudinal modes trapped by the cavity can be adjusted to be close to the transition frequency of the atoms that are dropped into (or nowadays trapped within) the cavity. While the coupling to this one special mode can be significantly modified by the cavity, the spontaneous emission rate of the atom into modes not trapped by the cavity is scarcely affected. The mirrors are relatively far apart and the atom sees a lot of 'free space'. Hence its spontaneous emission time $\gamma^{-1} \sim 1$ns remains largely unaffected. The strong-coupling limit where the atom coherently exchanges energy with the one special longitudinal mode more rapidly than it decays into the continuum of other modes requires considerable effort to achieve (Thompson *et al.*, 1992; Boca *et al.*, 2004; Schuster *et al.*, 2008).

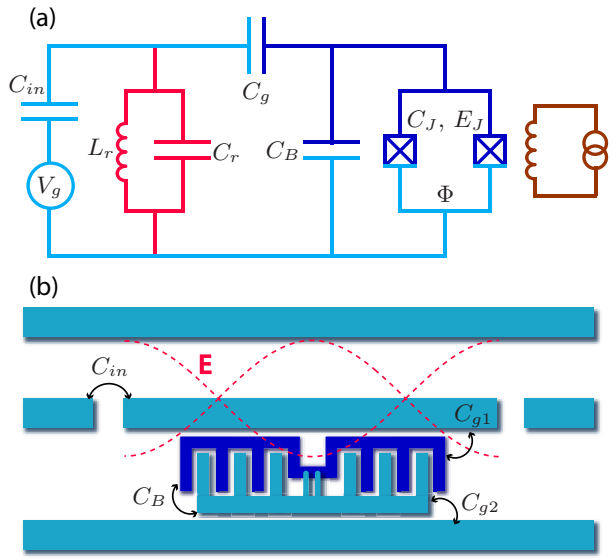

Fig. 6.1 Circuit QED: Schematic illustration (not to scale) of a transmon qubit embedded in a coplanar waveguide resonator. Panel (a) shows the lumped element circuit equivalent to the distributed circuit shown in panel (b). From (Koch *et al.*, 2007).

In circuit QED, extremely strong coupling is trivial to obtain (the atoms can always be made with antennae as large as needed to achieve strong coupling). In fact, it requires care to obtain weak coupling and the main reason that the cavity is useful is to protect the qubit from the environment by filtering out the vacuum noise which causes spontaneous emission. This physics of using a cavity to modify the coupling to the environment is that of the Purcell effect (Purcell, 1946), first observed[2] for a superconducting qubit by (Houck *et al.*, 2008). Here a qubit placed inside a cavity can have its decay rate suppressed if it is far detuned from the cavity resonance or enhanced if the qubit transition frequency is close to a (broad) cavity resonance. The former is useful for protecting quantum superpositions. The latter is useful for providing rapid qubit reset to the ground state. It has also been successfully used to generate single microwave photons on demand and enhance the fidelity of coherent quantum information transfer from a superconducting qubit to a 'flying' photon qubit (Houck *et al.*, 2007). One can view the Purcell effect as the resonator performing an impedance transformation on the external dissipation presented by the environment to the qubit (Houck *et al.*, 2008). The UCSB group (Neeley *et al.*, 2008; Yin *et al.*, 2013; Sete *et al.*, 2013) has used a tunable transformer coupling to quantitatively explore the role of environmental coupling in a phase qubit circuit over a wide range of coupling strengths and to sculpt the shape of the temporal mode of the photon spontaneously emitted

[2]In an early pioneering paper, the Saclay group (Turlot *et al.*, 1989) studied a related dissipation time-delay effect through the variation of the macroscopic quantum tunneling rate of a Josephson junction coupled to a transmission line feeding a microwave absorber whose position along the transmission line could be varied *in situ*.

by an excited qubit. The Houck group has utilized a different approach to control the spontaneous emission wave form. They rapidly vary the effective dipole moment of the qubit on time scales short compared to the spontaneous emission time(Srinivasan *et al.*, 2013). The ETH group has taken still another approach (Pechal *et al.*, 2013).

The coupling between the electric field in the cavity and the dipole moment of a (single) atom at position $\vec{R}$ is given by[3]

$$U = -\vec{p}\cdot\vec{E}(\vec{R}). \tag{6.1}$$

As we have seen, each discrete mode of a resonator is an independent harmonic oscillator. We will assume for now that only a single mode (the one closest in frequency to the atom transition) is important. (Of course it is important to remember that this is not always a good approximation.) The electric field in the cavity (or voltage in a circuit) can be written in terms of the mode polarization direction $\hat{\epsilon}$ and the mode zero point fluctuation amplitude $E_{\rm ZPF}$ (computed at position $\vec{R}$) and the photon operators as[4]

$$\vec{E} = \hat{\epsilon}E_{\rm ZPF}(\hat{a} + \hat{a}^\dagger). \tag{6.2}$$

We assume that the atom can be approximated as a two-level system. The dipole moment operator connects the ground and excited states of the atom and so the interaction Hamiltonian in Eq. (6.1) becomes

$$H_1 = \hbar g(\hat{a} + \hat{a}^\dagger)\sigma^x, \tag{6.3}$$

where σ^x flips the two-level system between states and the 'vacuum Rabi coupling' g is given by the dipole matrix element connecting the ground and excited states of the atom

$$\hbar g = -\langle\psi_1|\vec{p}\cdot\hat{\epsilon}|\psi_0\rangle E_{\rm ZPF} \tag{6.4}$$

where we again emphasize that $E_{\rm ZPF}$ is the vacuum fluctuation amplitude of the cavity mode at $\vec{R}$, the position of the atom. In atomic cQED the atoms move around and the coupling is strongest at the antinodes of the mode and vanishes at the nodes. In circuit QED we have the advantage of being able to place the artificial atoms at any desired fixed location within the cavity.

Eq. (6.3) can be rewritten as

$$H_1 = \hbar g(\hat{a}\sigma^+ + \hat{a}^\dagger\sigma^-) + \hbar g(\hat{a}\sigma^- + \hat{a}^\dagger\sigma^+), \tag{6.5}$$

where

[3]This can be equivalently written in terms of the electromagnetic vector potential and the electron momentum $\sim \vec{P}\cdot\vec{A}$. We neglect the $\vec{A}\cdot\vec{A}$ term which leads to transitions in which the photon is not absorbed or emitted but rather scattered to a new state (Raman scattering) by the electron. See (Nataf and Ciuti, 2010; Viehmann *et al.*, 2011; Ciuti and Nataf, 2011; Viehmann *et al.*, 2012) for additional discussion on this topic.

[4]We make a certain gauge choice here and could have used $\vec{E} = -i\hat{\epsilon}E_{\rm ZPF}(\hat{a} - \hat{a}^\dagger)$ to be closer to the choice made in discussing the voltage of the LC oscillator in Eq. (2.53). Note that one-dimensional coplanar waveguide resonators for microwaves do not have a polarization degree of freedom. Three dimensional microwave cavities and optical cavities of course do.

$$\sigma^{\pm} = \frac{1}{2}(\sigma^x \pm i\sigma^y) \tag{6.6}$$

are the raising and lowering operators for the qubit energy. If the cavity mode is close in frequency to the atom transition frequency, the first term is important because it nearly conserves the total energy. The second term only mixes states that are far away from each other, or equivalently, it is rapidly rotating in the interaction picture. Dropping this term is called the rotating wave approximation (RWA). This is often an excellent approximation but is not necessarily valid if the coupling is very strong or if the detuning of the atom from the cavity is large so that no one cavity mode is singled out.

In this simplest approximation of a two-level atom coupled to a single cavity mode (within the rotating wave approximation), the system is described by the Jaynes-Cummings Hamiltonian

$$H = H_0 + V, \tag{6.7}$$

where

$$H_0 = \hbar\omega_{\rm c}\hat{a}^\dagger\hat{a} + \frac{\hbar\omega_{01}}{2}\sigma^z \tag{6.8}$$

where the single cavity mode is described as a simple harmonic oscillator of angular frequency $\omega_{\rm c}$, the two-level atom is represented as a simple spin-1/2 with excitation frequency ω_{01},

$$V = \hbar g(\hat{a}\sigma^+ + \hat{a}^\dagger\sigma_-) \tag{6.9}$$

and the 'vacuum Rabi coupling', g, represents the dipole matrix element for the process in which the atom absorbs or emits a photon. For the case of a superconducting qubit coupled to an LC resonator, this Hamiltonian is derived in detail in Appendix A).

The external driving and damping terms, not written explicitly here, which help control the electromagnetic state of the cavity, are treated using the input-output formalism of quantum optics (Clerk *et al.*, 2010) described in Appendix B. The extension of this Hamiltonian to the case of multiple qubits is known as the Tavis-Cummings model (Tavis and Cummings, 1968). If we had not made the RWA, we would have the so-called Rabi Hamiltonian which in a certain sense is also integrable(Braak, 2011).

The full Hamiltonian with which we must deal

$$H = \hbar\omega_{\rm c}\hat{a}^\dagger\hat{a} + \frac{\hbar\omega_{01}}{2}\sigma^z + \hbar g(\hat{a}\sigma^+ + \hat{a}^\dagger\sigma_-) + H_{\rm drive} + H_{\rm damping}, \tag{6.10}$$

includes environmental terms which produce the spontaneous emission of energy from the atom at some rate γ. In addition in order to excite the atoms with an external drive one must open a port into the cavity which then allows spontaneous emission of energy from the cavity at some rate κ (or for a two-sided cavity at rates $\kappa_{\rm L}$ and $\kappa_{\rm R}$).

Let us begin our analysis by considering the spectrum of H_0 where the atom and photon are not yet coupled. In Fig. (6.2) we show two ladders of photon states, one for the qubit being in the ground state ($|g\rangle = |\uparrow\rangle$) and the other for the qubit being in the excited state ($|e\rangle = |\downarrow\rangle$). (There is no uniform convention on whether the ground

state should be labeled by spin up or down.) In Fig. (6.2a) we see the case where the detuning between the qubit frequency and the cavity frequency

$$\Delta \equiv \omega_{01} - \omega_c, \tag{6.11}$$

vanishes and in Fig. (6.2b) we see the case where Δ is positive. The detuning is considered strong if $\Delta \gg g$.

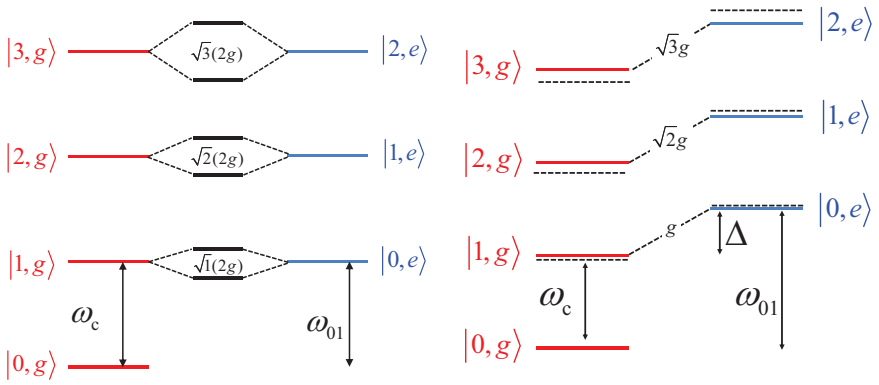

Fig. 6.2 Jaynes-Cummings ladder or 'dressed-atom' level structure. (left panel) Degenerate case $\omega_{01} = \omega_c$. The degenerate levels mix and split by an amount proportional to the vacuum Rabi splitting g. (right panel) Dispersive case $\omega_{01} = \omega_c + \Delta$. For $\Delta > 0$ the level repulsion causes the cavity frequency to decrease when the qubit is in the ground state and increase when the qubit is in the excited state.

First we consider the case $\Delta = 0$ where the states $|n+1, g\rangle$ and $|n, e\rangle$ are degenerate. As shown in Fig. (6.2a) this degeneracy is lifted by the dipole coupling matrix element resulting in an energy splitting $2g$ for the lowest pair and $2g\sqrt{n+1}$ for the higher levels. The splitting $2g$ of the lowest pair of excitations is called the vacuum Rabi splitting (Thompson *et al.*, 1992; Raimond *et al.*, 2001; Wallraff *et al.*, 2004; Boca *et al.*, 2004; Johansson *et al.*, 2006; Schuster *et al.*, 2008). The energy eigenstates of $H_0 + V$ are coherent superpositions

$$|\Psi_\pm\rangle = \frac{1}{\sqrt{2}}\left(|n+1, g\rangle \pm |n, e\rangle\right) \tag{6.12}$$

('bonding-anti-bonding' combinations) of photon excitation and qubit excitation known in the condensed matter and AMO literature as polaritons. The coupling available in circuit QED is now so strong that splittings of ~ 150 MHz corresponding to ~ 300 qubit line widths are easily achieved (Fink *et al.*, 2008; Bishop *et al.*, 2009*a*). The higher lying excited states form a strongly anharmonic ladder which can be explored by either strong driving or use of two excitation tones (Deppe *et al.*, 2008; Fink *et al.*, 2008; Bishop *et al.*, 2009*a*).

In the so-called dispersive regime where the qubit is far detuned from the cavity ($|\omega_{01} - \omega_c| \gg g$), we will see below that diagonalization of the Hamiltonian to lowest order in g leads to a second-order dispersive coupling

$$V_{\text{dispersive}} = \hbar \frac{g^2}{\Delta} \left[\hat{a}^\dagger \hat{a} + \frac{1}{2} \right] \sigma^z. \tag{6.13}$$

This coupling is QND (quantum non-demolition) with respect to both photon number and qubit polarization since it commutes with both. The dispersive coupling can be interpreted either as a shift in the cavity frequency which depends on the state of the qubit, or as the 'ac-Stark' or 'light' shift [plus the Lamb shift (Blais *et al.*, 2004; Schuster *et al.*, 2005; Fragner *et al.*, 2008)] of the qubit frequency proportional to the number of photons in the cavity. The qubit-state-dependent shift of the cavity frequency leads to changes in the amplitude and phase of photons reflected from or transmitted through the cavity and is the basis of the QND readout of the qubit state in circuit QED (Blais *et al.*, 2004; Wallraff *et al.*, 2004). The mean value of the light shift can be used to rapidly tune qubit transition frequencies (Schuster *et al.*, 2005; Schuster *et al.*, 2007*b*; Gambetta *et al.*, 2006; Majer *et al.*, 2007). The fluctuating part of the light shift can be viewed as the quantum back-action (Clerk *et al.*, 2010) of the qubit measurement. As required by the principles of quantum measurement (Clerk *et al.*, 2010), the photon shot noise (Bertet *et al.*, 2005) in the cavity gradually dephases the qubit superposition as information is gained about σ^z. This back-action effect leads to a broadening of the spectroscopic line width of the qubit (Schuster *et al.*, 2005; Schuster *et al.*, 2007*b*; Ithier *et al.*, 2005; Lupascu *et al.*, 2005; Boissonneault *et al.*, 2008; Boissonneault *et al.*, 2009). In the so-called 'strong-dispersive' regime (Schuster *et al.*, 2007*a*), the coupling is so large that the light shift per photon exceeds both the cavity line width κ and the atom line width γ: $\frac{g^2}{\Delta} > \kappa, \gamma$. In this regime the qubit spectrum breaks up into a series of separately resolved peaks representing the distribution of photon numbers within the driven cavity (Schuster *et al.*, 2007*a*). This 'photon number' detector was used to distinguish thermal and coherent states in the cavity and could be used to measure number-squeezed states and other non-classical states (Schuster *et al.*, 2007*a*). Most recently (Paik *et al.*, 2011) have observed light shifts several orders of magnitude larger than the qubit line width. This strong-coupling physics was first beautifully observed in the time domain by the Paris group (Nogues *et al.*, 1999; Guerlin *et al.*, 2007; Gleyzes *et al.*, 2007; Deleglise *et al.*, 2008).

To derive Eq. (6.13) we need to find a unitary transformation

$$U = e^{\hat{\eta}};\ U^\dagger = e^{\hat{\eta}^\dagger} = e^{-\hat{\eta}}, \tag{6.14}$$

which removes the off-diagonal term in Eq. (6.9) which is first-order in g. Using the Baker-Campbell-Hausdorff expansion we have

$$\tilde{H} = UHU^\dagger = H + [\hat{\eta}, H] + \frac{1}{2}[\hat{\eta}, [\hat{\eta}, H]] + \ldots \tag{6.15}$$

In perturbation theory we write $H = H_0 + V$ where V is the off-diagonal term linear in g and we expect $\hat{\eta}$ to therefore be of order g. Expanding to second order in g we have

$$\tilde{H} \approx H_0 + V + [\hat{\eta}, H_0] + [\hat{\eta}, V] + \frac{1}{2}[\hat{\eta}, [\hat{\eta}, H_0]]. \tag{6.16}$$

We need to choose $\hat{\eta}$ to satisfy

$$[\hat{\eta}, H_0] = -V \tag{6.17}$$

in order to remove the lowest-order off-diagonal term. We are then left with only the second-order terms which conveniently combine to

$$\tilde{H} = H_0 + \frac{1}{2}[\hat{\eta}, V]. \tag{6.18}$$

It is straightforward to verify that the solution to Eq. (6.17) is

$$\hat{\eta} = \frac{g}{\Delta}(\hat{a}\sigma^+ - \hat{a}^\dagger\sigma^-). \tag{6.19}$$

Clearly the expansion in g is valid only for large enough detuning so that $g/\Delta \ll 1$. (On the other hand if Δ becomes too large the RWA fails so caution is required.) Computing the second-order term (and dropping an irrelevant constant) we arrive at the dispersive Hamiltonian

$$\tilde{H} = H_0 + \chi\left(\hat{a}^\dagger\hat{a} + \frac{1}{2}\right)\sigma^z, \tag{6.20}$$

where

$$\chi \equiv \hbar\frac{g^2}{\Delta}. \tag{6.21}$$

For the case of a closed cavity (no damping and no drive) we can do better than this dispersive approximation. Without drive or damping, the Hamiltonian in Eq. (6.7) has the special property (due to the rotating wave approximation) that it commutes with the excitation number

$$[H_0 + V, \hat{N}_{\rm ex}] = 0, \tag{6.22}$$

with

$$\hat{N}_{\rm ex} \equiv \hat{a}^\dagger\hat{a} + \frac{1+\sigma^z}{2} \tag{6.23}$$

being the sum of the cavity excitation number and the qubit excitation number. This extra symmetry means that the Hamiltonian is block diagonal. The only state to which $|n,\uparrow\rangle$ is coupled by V is $|n+1,\downarrow\rangle$. Hence the largest block we have to diagonalize is 2×2. The ground state $|0,\downarrow\rangle$ is (in the RWA) not connected to any other state by V and hence is an eigenstate on its own. For the higher pairs of states containing a total of $n+1$ excitations we can write

$$\Psi^{(n+1)} = \alpha|n,\uparrow\rangle + \beta|n+1,\downarrow\rangle, \tag{6.24}$$

for which the $2x2$ eigenvalue problem becomes

$$H_{2\times 2}^{(n+1)}\begin{pmatrix}\alpha\\ \beta\end{pmatrix} = E_\pm^{(n)}\begin{pmatrix}\alpha\\ \beta\end{pmatrix} \tag{6.25}$$

where

$$H_{2\times2}^{(n+1)} = \hbar \begin{pmatrix} n\omega_c + \frac{1}{2}\omega_{01} & g\sqrt{n+1} \\ g\sqrt{n+1} & (n+1)\omega_c - \frac{1}{2}\omega_{01} \end{pmatrix} \tag{6.26}$$

$$= \left(n + \frac{1}{2}\right)\hbar\omega_c + \hbar \begin{pmatrix} \frac{+\Delta}{2} & g\sqrt{n+1} \\ g\sqrt{n+1} & -\frac{\Delta}{2} \end{pmatrix}. \tag{6.27}$$

This has eigenvalues

$$E_{\pm}^{(n+1)} = \left(n + \frac{1}{2}\right)\hbar\omega_c \pm \frac{\hbar}{2}\sqrt{\Delta^2 + 4g^2(n+1)} \tag{6.28}$$

and the eigenfunctions in Eq. (6.24) given by

$$\Psi_+ = \begin{pmatrix} \alpha_+ \\ \beta_+ \end{pmatrix} = \begin{pmatrix} \cos(\theta/2) \\ \sin(\theta/2) \end{pmatrix} \tag{6.29}$$

$$\Psi_- = \begin{pmatrix} \alpha_- \\ \beta_- \end{pmatrix} = \begin{pmatrix} -\sin(\theta/2) \\ \cos(\theta/2) \end{pmatrix}, \tag{6.30}$$

where

$$\theta = \tan^{-1}\left(\frac{2g\sqrt{n+1}}{\Delta}\right). \tag{6.31}$$

In the dispersive limit ($g \ll \Delta$) we can perform a Taylor series expansion of the energy eigenvalues in Eq. (6.28) to obtain

$$E_{\pm}^{(n+1)} \approx \left(n + \frac{1}{2}\right)\hbar\omega_c \pm \hbar\Delta\left[\frac{1}{2} + \left(\frac{g}{\Delta}\right)^2(n+1) - \left(\frac{g}{\Delta}\right)^4(n+1)^2\right]. \tag{6.32}$$

This can be reexpressed as an effective Hamiltonian

$$\tilde{H} \approx \left(\hat{N}_{ex} - \frac{1}{2}\right)\hbar\omega_c + \Sigma^z\hbar\Delta\left[\frac{1}{2} + \left(\frac{g}{\Delta}\right)^2\hat{N}_{ex} - \left(\frac{g}{\Delta}\right)^4\hat{N}_{ex}^2\right], \tag{6.33}$$

where $\Sigma^z = \pm 1$ is a spin label that smoothly connects to σ^z in the limit $g \longrightarrow 0$.

The lowest order term in the expansion reproduces the result in Eq. (6.20) and the next order term shows that the cavity inherits some non-linearity (anharmonicity or self-Kerr effect) from the qubit. The advantage of the exact (within the RWA) solution is that it applies even for small Δ where the dispersive approximation fails. For $\Delta = 0$ the uncoupled levels occur in degenerate pairs and the degeneracy is lifted by an amount linear in g giving the simple result which is plotted in the left panel of Fig. (6.2)

$$E_{\pm}^{(n+1)} = \left(n + \frac{1}{2}\right)\hbar\omega_c \pm g\hbar\sqrt{n+1}. \tag{6.34}$$

The single excitation eigenstates are 'polaritons', coherent superpositions of cavity and qubit excitations. The 'vacuum Rabi splitting' (Blais *et al.*, 2004) of the upper and lower polariton states can be observed spectroscopically (Wallraff *et al.*, 2004; Fragner *et al.*, 2008; Bishop *et al.*, 2009*a*) provided the system is in the strong-coupling limit ($g \gg \gamma, \kappa$) where the splitting $2g$ exceeds the atom and cavity line widths, γ and

κ respectively. In the strong-coupling limit, the line width of each single polariton excitation is in fact (Blais *et al.*, 2004) (for $\Delta = 0$)

$$\tilde{\gamma} = \frac{\gamma + \kappa}{2}, \tag{6.35}$$

because the excitation is half qubit and half photon. Because of the peculiar $\sqrt{n+1}$ splitting of the higher excited states, the polariton spectrum is quite anharmonic so the combination of the ground state and one of the single polariton excitations can be viewed as a two-level system which (in the strong coupling limit) can be driven relatively strongly without going up the excitation ladder and therefore can be coherently Rabi flopped just like a qubit (Bishop *et al.*, 2009*a*) as shown in Fig. (6.3).

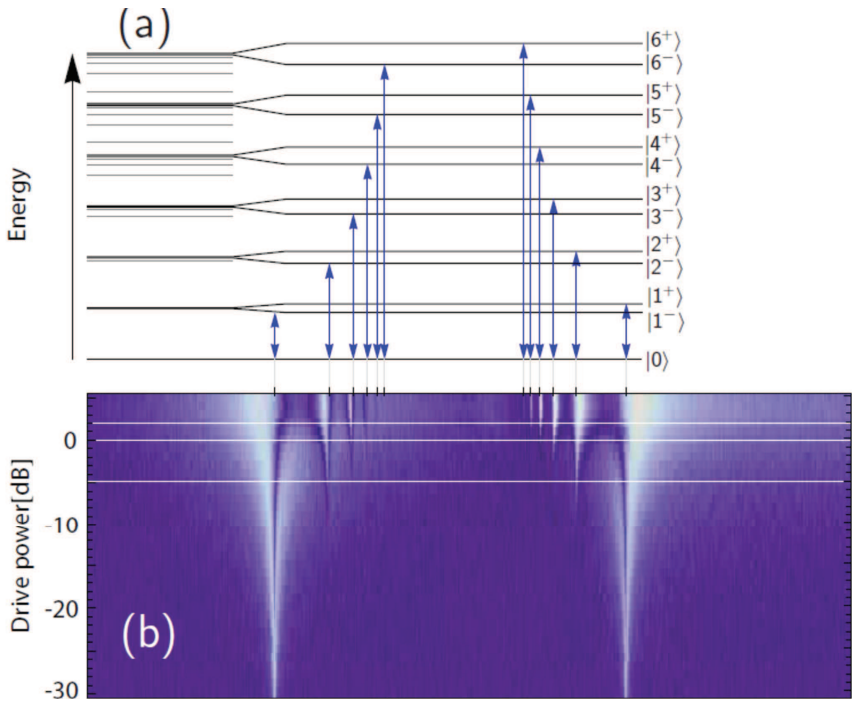

Fig. 6.3 a) Schematic illustration of n-photon non-linear transitions from ground state of qubit and cavity $|0, g\rangle$ to the n excitation manifold $\frac{1}{\sqrt{2}}[|n, g\rangle \pm |n-1, e\rangle$; b) Driven vacuum Rabi spectrum. Horizontal axis is drive frequency and vertical axis is drive intensity. At low power one sees the two widely-separated vacuum Rabi peaks corresponding to the transition from the ground state to the upper and lower polariton states. At higher powers one sees multi-photon absorption peaks in to the higher excitation manifolds. After (Bishop *et al.*, 2009*b*).

Returning now to the dispersive limit where the qubit is strongly detuned from the cavity, one polariton has primarily qubit character and the other primarily cavity

character. For the case of positive detuning, it is $\Psi_+^{(n=0)}$ which is primarily qubit. The rate of energy relaxation of this state is given by the weighted average of the bare qubit and cavity decay rates

$$\gamma_{\rm tot} = \cos^2(\theta/2)\gamma + \sin^2(\theta/2)\kappa. \tag{6.36}$$

For large detuning where $\sin^2(\theta/2)$ is small, we see that spontaneous emission of a photon via the cavity is very weak. We can say that the qubit must emit its fluorescence photon into the cavity and pay the energy denominator price of the large detuning before the photon decays out into the continuum. Equivalently the cavity filters out the vacuum noise at the qubit frequency which otherwise would have caused fairly rapid spontaneous emission.

Exercise 6.1 The Purcell effect (Purcell, 1946) is the modification of the spontaneous emission rate of an atom or qubit due to the presence of a resonator. Depending on circumstances, it can cause the rate of spontaneous fluorescence of the qubit to either be enhanced or reduced. We see from Eq. (6.36) that the fluorescence rate can be reduced by using a long-lived cavity (small κ) and detuning the qubit far from the cavity resonance ($\sin^2(\theta/2) \ll 1$). This equation was derived in the strong coupling limit $g \gg \kappa$ where it makes sense to first treat the hybridization of the qubit and the cavity and only then add the intrinsic damping of each. In the weak coupling limit $g \ll \kappa$ it makes sense to treat the density of photon states inside the cavity as a broad continuum (of width κ) and use Fermi's Golden Rule to obtain the fluorescence rate

$$\gamma_\kappa = 2\pi|g|^2\rho(\omega_{01}). \tag{6.37}$$

Show that

$$\rho(\omega_{01}) = -\frac{1}{\pi}{\rm Im}\,\frac{1}{\omega_{01} - \omega_{\rm c} + i\kappa/2}, \tag{6.38}$$

and hence that

$$\gamma_\kappa = |g|^2\frac{\kappa}{\Delta^2 + (\kappa/2)^2}. \tag{6.39}$$

Notice that for large detuning $\Delta \gg \kappa$

$$\gamma_\kappa \approx \frac{g^2}{\Delta^2}\kappa \tag{6.40}$$

in agreement with Eq. (6.36) (for $N_{\rm ex} = 1$). On the other hand, for $\Delta = 0$, the rate

$$\gamma_\kappa = \frac{4|g|^2}{\kappa} \tag{6.41}$$

is *inversely* proportional to κ rather than linearly proportional to κ as in the strong coupling case. This can be understood from the density of states in the resonator being spread out over a greater width and hence having a lower value for large κ as shown in Fig. (6.4). One can view the Purcell effect as the resonator performing an impedance transformation on the external dissipation presented by the environment to the qubit (Houck *et al.*, 2008). Neeley *et al.*(Neeley *et al.*, 2008) have used a tunable transformer coupling to quantitatively explore the role of environmental coupling in a phase qubit circuit over a wide range of coupling strengths.

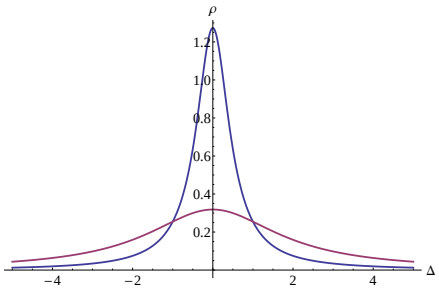

Fig. 6.4 Cavity density of states for two different cavity widths, κ. The larger value of κ yields a broader line but the height is lower at the peak corresponding to a lower density of states.

The rate of progress in observing novel strong coupling non-linear quantum optics effects in superconducting electrical circuits is quite remarkable. As noted above, Houck *et al.*used the Purcell effect (Houck *et al.*, 2008) to generate non-classical photon states in a cavity (Houck *et al.*, 2007). The states were a superposition of $n = 0$ and $n = 1$ Fock states with controlled amplitude and phase. 'Fluorescence tomography' was performed on these states using square law detection to determine the probability of having a photon. In addition, homodyne measurements were performed to determine the two quadratures of the electric field which are controlled by the off-diagonal coherence between the $n = 0$ and $n = 1$ Fock states. In particular they showed that the mean electric field of the one-photon Fock state was zero.

Higher Fock states up to $n = 6$ were synthesized by the UCSB group (Hofheinz *et al.*, 2008) who also observed that the decay rate scaled linearly with n as expected (Wang *et al.*, 2008). This same effect was seen qualitatively in the frequency domain in the experiment of Schuster *et al.*(Schuster *et al.*, 2007*a*). The qubit spectrum showed up to 6 resolved peaks displaying the distribution of photon numbers within the driven cavity and the line width of the peaks increased with n. In a 2009 tour-de-force, Hofheinz *et al.*(Hofheinz *et al.*, 2009) demonstrated a remarkable method for synthesizing arbitrary photon states (including Fock and various cat states) in a cavity and measuring their Wigner distributions. This level of control now exceeds what has been possible to date with atomic physics methods.

Because microwave photons have 10^4 to 10^5 times less energy than visible photons, they are much more difficult to detect. The work of Houck *et al.*(Houck *et al.*, 2007) and Schuster *et al.*(Schuster *et al.*, 2007*a*) showed that individual photons could be detected with low efficiency and recent work (Hofheinz *et al.*, 2009; Johnson *et al.*, 2010) demonstrated very high efficiency detection of individual photons in a cavity. However a general purpose high bandwidth 'photomultiplier' does not yet exist in the microwave regime. There have been some theoretical proposals for single photon detection (Helmer *et al.*, 2009; Romero *et al.*, 2009) but this remains an important open experimental problem.

Another novel new direction is construction of single artificial atom 'lasers' (Astafiev *et al.*, 2007; Marthaler *et al.*, 2008; Ashhab *et al.*, 2009) as well as Sisyphus cooling and amplification (Grajcar *et al.*, 2008) of an oscillator. The extreme strong coupling avail-

able should permit observation of 'photon blockade' effects (Birnbaum *et al.*, 2005), and parametric down-conversion by three-wave mixing (Moon and Girvin, 2005; Marquardt, 2007). The advances in our understanding and fabrication of Josephson junction circuits motivated by the quest for a quantum computer have led to dramatic advances in the ability to do four-wave mixing, parametric amplification near the quantum limit, as well as strong squeezing of the vacuum (Castellanos-Beltran *et al.*, 2008; Bergeal *et al.*, 2010*b*; Bergeal *et al.*, 2010*a*). These advances will not only permit much better dispersive readout of qubits, they also open up the possibility of continuous variable quantum information processing (Gottesman *et al.*, 2001; Braunstein and van Loock, 2005) since two-mode squeezed states are an entanglement resource.

6.1 Quantum Control of Qubits in Cavities

Suppose that we apply a classical drive with a smooth envelope centered on the qubit transition frequency ω_{01} to the cavity

$$V_{\rm d} = \{v_{\rm R}(t)\cos\omega_{01}t + v_{\rm I}(t)\sin\omega_{01}t\}\,(\hat{a}^\dagger + \hat{a}). \tag{6.42}$$

In the dispersive regime this drive is far removed from the cavity resonance and only weakly populates the cavity with virtual photons. The vacuum Rabi coupling term of the Jaynes-Cummings model in Eq. (6.9) can then cause coherent rotations of the qubit. This is most easily analyzed by applying the dispersive unitary transformation of Eq. (6.14). To lowest order in g/Δ we have the original drive on the cavity plus an effective drive directly on the qubit

$$\tilde{V_{\rm d}} \approx V_{\rm d} + V_{\rm dq} \tag{6.43}$$

where

$$V_{\rm dq} \equiv [\eta, V_{\rm d}] = \{\lambda_{\rm R}(t)\cos\omega_{01}t + \lambda_{\rm I}(t)\sin\omega_{01}t\}\,\sigma^x. \tag{6.44}$$

For large detuning ($\Delta \gg \kappa, \chi$) the complex qubit drive amplitude

$$\lambda_{\rm R(I)} \equiv v_{\rm R(I)}(t)\frac{g}{\Delta} \tag{6.45}$$

can be interpreted as the external drive filtered by the response function of the cavity. (It is important to note that we assume here that since $\Delta \gg \chi$ the filter factor is the same independent of the state of the qubit.) It is convenient to apply a unitary transformation to take us into a frame rotating at the qubit transition frequency

$$U_{\rm rot} = e^{\frac{i}{2}\omega_{01}t\sigma^z} \tag{6.46}$$

to remove the rapid precession of the 'spin'. Within the rotating wave approximation for the drive we are left with

$$H_{\rm rot} = U_{\rm rot}HU_{\rm rot}^\dagger \tag{6.47}$$

$$= \frac{\lambda_{\rm R}(t)}{2}\sigma^x - \frac{\lambda_{\rm I}(t)}{2}\sigma^y. \tag{6.48}$$

Thus we see that the cosine and sine drives produce rotations of the qubit around the x and y axes (in the rotating frame). Rotations about the z axis can be achieved 'in

hardware' by manipulating the qubit transition frequency to speed up or slow down the precession or 'in software' by mathematically rotating between the cosine and sine components of the drive. This gives us complete quantum control of the qubit state.

We have thus demonstrated that a single input wire to the cavity can be frequency multiplexed. A drive near the cavity frequency produces a dispersive measurement of the qubit state because the resonance frequency of the cavity and hence the reflection coefficient depends on the state of the qubit. On the other hand, a drive at the qubit frequency is so far detuned from cavity frequency that reflection coefficient is independent of the state of the qubit and so almost no measurement (and almost no measurement induced dephasing) occurs when applying coherent control pulses to rotate the qubit.

Exercise 6.2 In the derivation above we assumed a classical drive and implicitly neglected the light shift of the qubit transition frequency that occurs when the cavity contains photons. Consider the derivation above more carefully and what constraints the light shift (and the quantum fluctuations in the drive) puts on the fidelity and/or speed of the single qubit gates.

7

Quantum Measurements in Circuit QED

The theory of quantum measurements has a long history starting with the founders of quantum mechanics torturing each other with the implications of various gedanken experiments and their interpretation. Today measurements that are essentially quantum in nature are routinely achieved experimentally. Many of the relevant ideas are better known in the quantum optics community than in the condensed matter community because the idealized measurement limits were first achieved using quantum optics methods. However the development of superconducting qubits has also spurred great experimental advances in achieving quantum limited measurements in condensed matter systems. The author's introduction to the basic facts of quantum measurements came from the review article of Makhlin, Schön and Shnirman (Makhlin *et al.*, 2001). For a recent discussion that bridges the quantum optics/condensed matter domain, the reader is also directed to (Clerk *et al.*, 2010). The reader is also directed to the discussion in this volume by Korotkov (Korotkov, 2012) of conditional evolution.

Let us start by reviewing the basics. Consider a particle that lives in one dimension and is in quantum state $|\Psi\rangle$. The wave function of the particle in the position basis is

$$\psi(x) = \langle x|\Psi\rangle \tag{7.1}$$

where $|x\rangle$ is the position eigenstate with position eigenvalue x. According to the 'Copenhagen interpretation' of quantum mechanics, the probability of finding the particle at position x when the position is measured is given by the Born rule

$$P(x) = \langle\Psi|x\rangle\langle x|\Psi\rangle = |\psi(x)|^2. \tag{7.2}$$

After such a sudden and strong measurement of position, the particle state is said to 'collapse' to $|x\rangle$.

Similarly, if we choose instead to measure the particle's momentum (or wavevector k) the probability of distribution of the results is given by

$$\tilde{P}(k) = \langle\Psi|k\rangle\langle k|\Psi\rangle = |\psi[k]|^2, \tag{7.3}$$

where $|k\rangle$ is a momentum eigenstate with momentum eigenvalue $\hbar k$ and the wave function in the momentum basis is given by the Fourier transform of the position basis wave function.

$$\psi[k] = \frac{1}{\sqrt{2\pi}} \int_{-\infty}^{+\infty} dx\, e^{-ikx} \psi(x). \tag{7.4}$$

Note that because we have included a factor of $1/\sqrt{2\pi}$ in the Fourier transform, we have

$$\int_{-\infty}^{+\infty} dk\, \tilde{P}(k) = 1. \tag{7.5}$$

One important difference (for a free particle) between measuring position and momentum is that, the momentum measurement leaves the system in an eigenstate of the Hamiltonian. Hence a subsequent measurement of the momentum will yield the same answer. The first result will be a random number drawn from the probability distribution $\tilde{P}(k)$, but all subsequent repeated measurements will yield the same result. This repeatability of the results is the defining characteristic of so-called 'quantum non-demolition' (QND) measurements.

The above simple description of a 'strong projective' measurement can be physically realized in certain experimental situations. Frequently however, we need a more sophisticated description of how measurements are done in the laboratory. In practice, we often make experimental measurements on quantum systems by coupling the system to a physical measurement apparatus which itself has a quantum Hamiltonian. We then subsequently make what is effectively a strong projective measurement of some 'pointer variable' which is a degree of freedom of the measurement apparatus. Suppose that the measurement pointer variable is described by a position coordinate y. Before the measurement the wave function of the system plus measurement apparatus might be a product state

$$\Psi_0(x, y) = \psi(x)\phi(y), \tag{7.6}$$

where ψ describes the initial state of the system of interest and ϕ describes the initial state of the measurement apparatus. As a result of the coupling between the system and the measurement apparatus, they become correlated (entangled) and the wave function is no longer separable. The joint probability distribution for the two variables in terms of the subsequent state Ψ of the combined system is

$$P(x, y) = |\Psi(x, y)|^2, \tag{7.7}$$

while the probability for each separately is

$$P_X(x) = \int dy\, P(x, y) \tag{7.8}$$

$$P_Y(y) = \int dx\, P(x, y). \tag{7.9}$$

Note that these are correctly normalized to unity.

Suppose now that we measure the pointer variable and the result (drawn from the distribution P_Y) is some value y. What can we say from this about the value of x, the quantity we are really interested in? We can say that x has a random value drawn from the *conditional* probability distribution $P(x|y)$. The vertical bar indicates that this is the probability distribution for x given y. Prior to the measurement, x has probability distribution $P_X(x)$. After the measurement of a value y for the pointer variable, we learn that the variable x is drawn from a new probability distribution $P(x|y)$. If

this distribution has very narrow support in the vicinity of some value $x_0(y)$, then by measuring the pointer variable y we have effectively measured the value of x to be $x_0(y)$. This would be a 'strong measurement.' In a weak measurement, $P(x|y)$ is broadly distributed, but still slightly narrower than the prior distribution $P_X(x)$. We don't know the precise value of x but we have learned something about it because the width of its probability distribution has been reduced by conditioning upon the value of y.

From basic probability theory we know that

$$P(x, y) = P(x|y)P_Y(y). \tag{7.10}$$

That is, the joint probability for x and y to occur is the probability that x occurs given y, times the probability that y occurs. From this we readily derive

$$P(x|y) = \frac{P(x, y)}{P_Y(y)} \tag{7.11}$$

which tells us how to update our knowledge of the distribution of x given the new information we have acquired on the value of y. $P_X(x)$ is called the 'prior distribution' and $P(x|y)$ is the posterior or updated distribution.

Using Eq. (7.7) and Eq. (7.9) we can express this in terms of the wave function

$$P(x|y) = \frac{|\Psi(x, y)|^2}{\int dx\, |\Psi(x, y)|^2}. \tag{7.12}$$

This simply tells us that the conditional probability of x given y is nothing more than the joint probability evaluated at y and then multiplied by a constant to get the normalization right

$$\int dx\, P(x|y) = 1. \tag{7.13}$$

Exercise 7.1 Bayes Theorem

We can also write the inverse relation

$$P(y|x) = \frac{P(x, y)}{P_X(x)} \tag{7.14}$$

from which we can immediately derive the famous Bayes rule which relates the two conditional probabilities

$$P(x|y) = P(y|x)\frac{P_X(x)}{P_Y(y)}. \tag{7.15}$$

Consider one of the examples that Reverend Bayes presented in the 18th century. Your friend drops a marble at random somewhere in the interval $[0, L]$. The probability distribution of its position is therefore $P_X(x) = 1/L$. Now your friend drops a second marble at random in the same interval. Suppose your friend updates your knowledge by telling you that the second marble landed to the left of the first marble. How should you update your estimate of the probability distribution of the position of the first marble? Clearly the new information biases the distribution to the right, but how? The Bayes rule gives us the answer. Let y be a

discrete variable that takes values $y = \pm 1$ representing the result that the second marble is left/right of the first. Clearly

$$P(y = +1|x) = \frac{x}{L} \tag{7.16}$$

because the further the first marble is to the right, the more likely the second will be to the left. Furthermore

$$P_Y(y = \pm 1) = \frac{1}{2} \tag{7.17}$$

because a priori (that is, without prior information about the position of the first marble), the second marble is equally likely to be on the left or right of the first. Thus from Eq. (7.15)

$$P(x|y = +1) = \frac{2x}{L^2}. \tag{7.18}$$

Given that the second marble landed to the left, there is zero probability that the first marble is at the far left and the distribution rises linearly from there.

What happens to this conditional probability if we iterate the procedure and the next marble also happens to land to the left of the first one? To the right? Clearly in the limit of a large number, N, of such 'measurements' the probability distribution for x becomes very narrow and is centered on $x = fL$, where f is the fraction of the marbles that landed to the left of the first. Can you derive the asymptotic form of the probability distribution for large N?

Historical note: Bayes never actually wrote down his rule as an equation. Eqn. (7.15) was probably first derived later by Simon Laplace (McGrayne, 2011).

Exercise 7.2 Apply the Bayes rule to answer the following questions.

- A certain disease has an incidence rate of 10^{-4} in the general population. The diagnostic test for this disease is highly accurate: the probability of a false negative is only 2%, and the probability of a false positive result is only 1%. You are given the test and the result is positive. What is the probability that you have the disease?

- A magician has two unfair coins. Coin A comes up heads with probability $p > \frac{1}{2}$. Coin B comes up heads with probability $1 - p$. The magician chooses one of the coins at random and flips it randomly in N trials. It comes up heads every time. What is the probability this is coin A? What is the probability that the next flip will come up heads?

- A resonant cavity coupled to a cold bath has the property that its mean energy decays exponentially at rate κ. You have available a photomultiplier which can detect any photons emitted from the cavity. The cavity is initially prepared in a state that contains 1 photon with probability p and zero photons with probability $1 - p$. After time t, the photomultiplier has not detected a photon. Based on this information, what is the posterior probability that the cavity contains a photon?

7.1 Stern-Gerlach Measurement of a Spin

Ultimately we will be interested in interrogating the state of a qubit in a resonant cavity using a microwave drive. Before analyzing this somewhat complicated situation, it will be very useful to gain some intuition by reviewing the familiar case of measurement of a spin by using a Stern-Gerlach magnet. The key idea is that we do not directly measure the spin. Rather we use the magnet to *entangle* the spin with the position

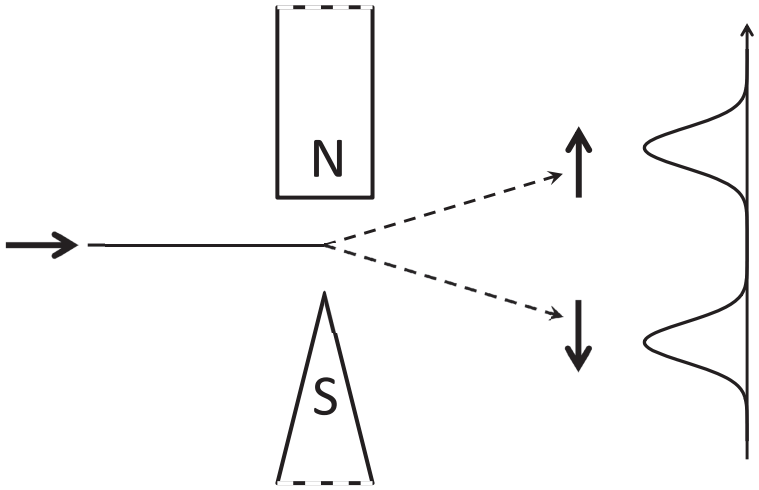

Fig. 7.1 Measurement of a spin using the Zeeman field gradient of a Stern-Gerlach magnet to entangle spin with momentum. The curves on the right show the momentum distribution of each spin component. One can either measure the momentum directly or wait for the momentum difference to evolve into position difference. In the example depicted, the measurement is strong because the momentum distributions of the two compomnents are essentially non-overlapping.

of of the particle and then use a detector that measures the position as illustrated in Fig. (7.1).

To keep matters simple let us stick to a one-dimensional description with a free-particle kinetic energy Hamiltonian H_0 and imagine that the effect of passing through the magnetic field gradient of the Stern-Gerlach magnet is to produce a spin-dependent impulsive force on the particle (assumed to be electrically neutral so that there is no Lorentz force)

$$F(x,t) = +\hbar k_0\, \delta(t)\, \sigma^z, \tag{7.19}$$

via a potential of the form

$$V(x,t) = -\hbar k_0\, \delta(t)\, \sigma^z x, \tag{7.20}$$

where $\hbar k_0$ is the impulse delivered in some brief interval of time (approximated here by the delta function). Just such spin-dependent impulsive forces are routinely implied in ion-trap quantum computers via application of laser beams with appropriate polarizations.

This coupling term commutes with σ^z, the quantity we want to measure, and hence in principle we can make a quantum non-demolition measurement (QND) of the spin. The necessary repeatability is only possible if the quantity in question is a constant of the motion[1], both respect to the unperturbed Hamiltonian $[H_0, \sigma^z] = 0$ and the perturbation coupling the system to the measurement apparatus, $[V, \sigma^z] = 0$.

[1]It is a confusing but common practice to refer to a measurement as being QND even if the quantity being measured is not quite a constant of the motion due to weak coupling of the system

Suppose that in the absence of the Stern-Gerlach coupling term, the wave function is given by a product of spin and space functions:

$$\psi_0(x) = [a|\uparrow\rangle + b|\downarrow\rangle]\Phi(x) \tag{7.21}$$

where $|a|^2 + |b|^2 = 1$ and $\langle\Phi|\Phi\rangle = 1$. Let us further suppose that the spatial wave packet Φ is made up of plane waves all of low enough energy so that for a short time interval around $t = 0$, the packet maybe treated as approximately stationary (i.e., $H_0\Phi(x,t) \approx 0$). Then in the vicinity of time $t = 0$ the solution of the Schrödinger equation will be discontinuous and approximately given by

$$\psi(x,t) \approx e^{ik_0 x\sigma^z\theta(t)}\psi_0(x), \tag{7.22}$$

where $\theta(t)$ is the Heaviside step function. This can be written for $t > 0$ as

$$|\psi\rangle = a|\uparrow\rangle|\Phi_\uparrow\rangle + b|\downarrow\rangle|\Phi_\downarrow\rangle, \tag{7.23}$$

or

$$\psi(x) \approx a|\uparrow\rangle e^{ik_0 x}\Phi(x) + b|\downarrow\rangle e^{-ik_0 x}\Phi(x), \tag{7.24}$$

or equivalently the momentum basis wave function will be

$$\psi[k] = a|\uparrow\rangle\Phi[k - k_0] + b|\downarrow\rangle\Phi[k + k_0]. \tag{7.25}$$

We no longer have a separable wave function because the measuring apparatus has entangled the spin with the momentum. The full time-dependent solution is such that this displacement in momentum space will eventually result in displacement in real space, but for the purposes of the present discussion, let us imagine we have a mechanism for measuring the momentum directly and immediately. This measurement of the momentum will, via the entanglement, tell us something about the spin.

For simplicity let us assume that the spatial wave packet is gaussian

$$\Phi(x) = (2\pi\sigma_0^2)^{-1/4}e^{-\frac{x^2}{4\sigma_0^2}} \tag{7.26}$$

with Fourier transform

$$\Phi[k] = \left(\frac{2\sigma_0^2}{\pi}\right)^{+1/4} e^{-k^2\sigma_0^2}. \tag{7.27}$$

The probability distribution at time $t = 0^+$ for the measured momentum conditioned on the spin being up or down is given by a displaced gaussian

$$P(k|\uparrow) = |\Phi_0[k - k_0]|^2 \tag{7.28}$$

$$P(k|\downarrow) = |\Phi_0[k + k_0]|^2 \tag{7.29}$$

and is shown in Fig. (7.2) for different values of the dimensionless impulse $k_0\sigma_0$. Clearly if $k_0\sigma_0 \gg 1$, there is no ambiguity in the result. If the measured value of k is positive (negative), then the spin is definitely up (down). This corresponds to a strong

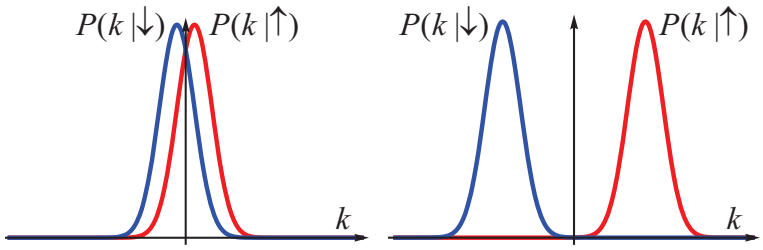

Fig. 7.2 Momentum distribution of the particle after passage through the Stern-Gerlach magnet, conditioned on the spin being up or down. Left panel: weak measurement in which the momentum difference is small relative to the momentum uncertainty. Right panel: strong measurement in which the momentum distributions do not overlap.

measurement. However if $k_0\sigma_0 \ll 1$, we have a weak measurement in which we have acquired only a small amount of information about the spin.

To quantify how much information we have gained, we can make use of the Bayes rule. Given the state of the spin, we can predict the distribution of measured values of k using Eqs. (7.28,7.29). In particular, suppose we are given the prior probability for the spin to be up, $p(\uparrow) = |a|^2$, and to be down, $p(\downarrow) = |b|^2$. The prior probability distribution for k is thus

$$P(k) = P(k|\uparrow)p(\uparrow) + P(k|\downarrow)p(\downarrow) = |a|^2|\Phi_0[k-k_0]|^2 + |b|^2|\Phi_0[k+k_0]|^2. \tag{7.30}$$

What we want however is the inverse conditional probability. Namely, given the measured value of k what can we say about the probability that the spin is up or down? This is given by Bayes rule

$$P(\uparrow|k) = P(k|\uparrow)\frac{p(\uparrow)}{P(k)} = \frac{1}{P(k)}|a|^2|\Phi_0[k-k_0]|^2 \tag{7.31}$$

$$P(\downarrow|k) = P(k|\downarrow)\frac{p(\downarrow)}{P(k)} = \frac{1}{P(k)}|b|^2|\Phi_0[k+k_0]|^2 \tag{7.32}$$

For the case of gaussian wave packets considered here, this simplifies to

$$P(\uparrow|k) = \frac{|a|^2}{Z}e^{+\lambda k} \tag{7.33}$$

$$P(\downarrow|k) = \frac{|b|^2}{Z}|e^{-\lambda k}, \tag{7.34}$$

where $\lambda \equiv 4k_0\sigma_0^2$ and the normalization simplifies to

$$Z = |a|^2e^{\lambda k} + |b|^2e^{-\lambda k}. \tag{7.35}$$

We now specialize to the particular case of $|a|^2 = |b|^2 = \frac{1}{2}$, where the prior polarization of the qubit is $m = |a|^2 - |b|^2 = 0$ and the estimate of the polarization following the measurement is

to a dissipative bath. This non-ideality is ignored as long as the damping is weak and the quantity would otherwise truly be constant even in the presence of the measurement apparatus.

$$m(k) = P(\uparrow|k) - P(\downarrow|k) = \tanh(\lambda k), \tag{7.36}$$

which shows explicitly how the new information from the measurement revises our estimate of the state of the spin. The Shannon entropy for the prior distribution of the value of the spin is

$$S = -\sum_{\sigma} p_\sigma \ln p_\sigma = -[p_\uparrow \ln p_\uparrow + p_\downarrow \ln p_\downarrow] = \ln 2. \tag{7.37}$$

(This entropy in base e familiar from statistical mechanics, corresponds to one classical bit of information which is calculated in base 2.) After the measurement yields a value of k, the Shannon entropy for the spin distribution is

$$S(k) = -\sum_{\sigma} P(\sigma|k) \ln P(\sigma|k) \tag{7.38}$$

$$= \ln 2 + \ln(\cosh \lambda k) - \lambda k \tanh \lambda k. \tag{7.39}$$

This is reduced from the prior entropy by the amount of information gained by the measurement about the state of the qubit. The information gained is

$$\mathcal{I}(k) = -\ln(\cosh \lambda k) + \lambda k \tanh \lambda k, \tag{7.40}$$

and the average information gained is

$$\bar{\mathcal{I}} = \int dk\, P(k) \mathcal{I}(k). \tag{7.41}$$

For a very weak measurement, we expect λk to be small, in which case to leading order in the expansion we have

$$\mathcal{I}(k) \approx \frac{\lambda^2 k^2}{2}, \tag{7.42}$$

and using Eq. (7.30) the average information gain for weak measurements is

$$\bar{\mathcal{I}} \approx \frac{\lambda^2}{2}\left(\frac{1}{4\sigma_0^2} + k_0^2\right) \approx 2k_0^2\sigma_0^2 = \frac{1}{2}\frac{k_0^2}{(\Delta k)^2} \tag{7.43}$$

where (for $k_0\sigma_0 \ll 1$), the momentum uncertainty is $(\Delta k)^2 = \frac{1}{4\sigma_0^2}$. It makes sense that the narrower is the momentum uncertainty of the wave packet, the more information we will gain from the measurement of the spin-dependent impulse imparted to the particle.

The above discussion was couched in the language of classical probability distributions. Let us now repeat it in the language of quantum density matrices[2]. Using the entangled state of the spin and position in Eq. (7.23) the full density matrix is

[2]Of course quantum probability amplitudes are not the same thing as classical probabilities which is why we have to be a bit careful and recall that density matrices have off-diagonal elements which represent superposition effects with no classical analog. Even the interpretation of the density matrix itself can be tricky. It might represent an ensemble of quantum systems or it might represent the observer's incomplete state of knowledge about the state of a quantum system.

$$\rho = \begin{pmatrix} |\Phi_\uparrow\rangle aa^* \langle\Phi_\uparrow| & |\Phi_\uparrow\rangle ab^* \langle\Phi_\downarrow| \\ |\Phi_\downarrow\rangle ba^* \langle\Phi_\uparrow| & |\Phi_\downarrow\rangle bb^* \langle\Phi_\downarrow| \end{pmatrix}. \tag{7.44}$$

If the measurement of the momentum yields the result k, then the reduced density matrix for the spin is given by

$$\rho_k = \frac{1}{P(k)} \langle k|\rho|k\rangle = \frac{1}{P(k)} \begin{pmatrix} \langle k|\Phi_\uparrow\rangle aa^* \langle\Phi_\uparrow|k\rangle & \langle k|\Phi_\uparrow\rangle ab^* \langle\Phi_\downarrow|k\rangle \\ \langle k|\Phi_\downarrow\rangle ba^* \langle\Phi_\uparrow|k\rangle & \langle k|\Phi_\downarrow\rangle bb^* \langle\Phi_\downarrow|k\rangle \end{pmatrix} \tag{7.45}$$

$$= \frac{1}{Z} \begin{pmatrix} |a|^2 e^{+\lambda k} & ab^* \\ a^* b & |b|^2 e^{-\lambda k} \end{pmatrix}, \tag{7.46}$$

where Z is given in Eq. (7.35) and the normalization factor $P(k)$ is

$$P(k) \equiv \mathrm{Tr}\, \langle k|\rho|k\rangle = |a\Phi_0[k - k_0]|^2 + |b\Phi_0[k + k_0]|^2, \tag{7.47}$$

is nothing but the probability that measurement of the momentum will yield k.

Notice that the diagonal elements of Eq. (7.46) match the classical probabilities in Eq. (7.33-7.34). Eq. (7.46) has a simple interpretation. Suppose for example that the measured value of the momentum turns out to be $k = 0$. Then nothing happens to the spin as a result of the measurement. For $k > 0$ the weight of the up-spin amplitude increases and the down-spin weight decreases by the corresponding factor. The reverse occurs for $k < 0$. Notice that there is no explicit reweighting of the off-diagonal elements of the density matrix because the competing exponential factors cancel. However the normalization factor indirectly changes the value of the off-diagonal term. The net effect is simply a rotation of the qubit around an axis passing through the equator of the Bloch sphere and lying perpendicular to the qubit polarization. This rotation moves the qubit along a line of constant 'longitude' on the Bloch sphere.

If the spin is up, the probability of observing a positive value of k is increased. Conversely, observation of a positive value of k means that the spin is more likely to be up. As mentioned above and as Korotkov (Korotkov, 2012) has discussed, this application of the Born Rule of quantum mechanics is consistent with the Bayes Rule from classical probability theory. Gaining information from the measured value of k allows us to update our estimate of the spin polarization. Despite the fact that σ^z is a constant of the motion, the polarization of the spin has changed, not due to any unitary evolution under the action of the Hamiltonian, but rather due to the measurement-induced collapse of the momentum state which is entangled with the spin. It is readily verified that the spin is still in a pure state because the eigenvalues of ρ are zero and one. (Hint: $\mathrm{Tr}\rho = 1$ and $\mathrm{Det}\rho = 0$.) Equivalently, the von Neuman entropy (as opposed to the Shannon entropy used above and calculated only from the diagonal elements of ρ) vanishes since the state remains pure:

$$\tilde{S} = -\mathrm{Tr}\, \rho \ln \rho = 0. \tag{7.48}$$

If we ignore the result of the measurement (or equivalently ensemble average over all measurement results) by tracing out the orbital degree of freedom in Eq. (7.44),

we obtain the following reduced density matrix for the spin as a result of carrying out (but ignoring) the measurement[3]

$$\bar{\rho} = \mathrm{Tr}_{\,\mathrm{orbital}}\,\rho = \int_{-\infty}^{+\infty} dk\, P(k)\rho_k = \begin{pmatrix} aa^* & ab^*\langle\Phi_\downarrow|\Phi_\uparrow\rangle \\ ba^*\langle\Phi_\uparrow|\Phi_\downarrow\rangle & bb^* \end{pmatrix}. \tag{7.49}$$

Because we have ignored the measurement results we see that in this case there is no change in the diagonal elements–we receive no information about the orientation of the spin. Note however that the act of measurement has *dephased* the spin because the off-diagonal elements are reduced by a factor given by the overlap of the two pointer states. The stronger the measurement the greater this reduction will be as the two pointer states become orthogonal and therefore fully distinguishable. This dephasing reduces the expectation value of the transverse components of the spin without affecting the z component. Using

$$\langle\Phi_\downarrow|\Phi_\uparrow\rangle = \int dx\, e^{2ik_0x}|\Phi(x)|^2 = e^{-2k_0^2(\Delta x)^2}, \tag{7.50}$$

where $(\Delta x)^2 = \sigma_0^2$. As we will see below, it makes sense that the dephasing should be proportional to the position uncertainty because the magnetic field acting on the spin varies linearly with position. The greater is the position uncertainty, the greater is the magnetic field uncertainty. As we will see below, if we measure the position x, then we know the magnetic field that acted on the spin and know that this rotated the spin through a definite angle $2k_0x$. The off-diagonal element of the density matrix is thus multiplied by e^{2ik_0x} but the qubit remains in a pure state. Now however we have a simple interpretation of Eq. (7.50) which tells us that we are ensemble averaging over all the different rotation angles. The average of a bunch of density matrices each of which corresponds to a pure state, leads to an impure state. More on this below.

If we assume that the measurement takes time Δt, we can define a dephasing rate Γ_φ via

$$\langle\Phi_\downarrow|\Phi_\uparrow\rangle = e^{-\Gamma_\varphi\Delta t} \tag{7.51}$$

so that

$$\Gamma_\varphi = \frac{2k_0^2(\Delta x)^2}{\Delta t}. \tag{7.52}$$

Similarly, we can define a measurement rate Γ_{meas} from the rate of acquisition of information when we monitor the pointer variable

$$\Gamma_{\mathrm{meas}} = \frac{\bar{\mathcal{I}}}{\Delta t} = \frac{1}{2}\frac{k_0^2}{(\Delta k)^2}\frac{1}{\Delta t}. \tag{7.53}$$

As expected, the measurement rate is inversely proportional to the momentum uncertainty.

[3]Notice the very important fact that the probability measure for k exactly cancels the normalization factor in the denominator of Eq. (7.45) which allows the integral to be trivially carried out.

The ratio of these two rates is given by the simple Heisenberg uncertainty expression:

$$\frac{\Gamma_\varphi}{\Gamma_{\rm meas}} = 4(\Delta k)^2(\Delta x)^2 \geq 1. \tag{7.54}$$

The best we can do is have the ensemble average dephasing rate equal the ensemble averaged measurement rate. In the present example this equality is actually achieved, meaning that the measurement is quantum limited. The equality of the measurement rate and the dephasing rate in our quantum limited detector follows from the uncertainty relation between momentum and position for a minimum uncertainty Gaussian wave packet. Quantum limited measurements are discussed in great detail in our recent review on quantum noise (Clerk *et al.*, 2010) and the Chapter by Clerk in this volume (Clerk, 2012).

Let us now consider the situation where we decide that rather than measure the particle *momentum* (which contains information about the spin through its entanglement), we decide instead to measure the particle *position* which initially is not affected by the momentum boost and hence is *not* entangled with the spin[4]. We see from Eq. (7.24) that the probability distribution for position is $|\Phi(x)|^2$ independent of the position. Nevertheless, something interesting happens when we make the measurement. Suppose that the measured value of position turns out to be x. Then the analog of Eq. (7.45) for the reduced density matrix for the spin conditioned on having measured x is

$$\rho_x = \frac{1}{P_X(x)}\langle x|\rho|x\rangle = \frac{1}{P_X(x)}\begin{pmatrix} \langle x|\Phi_\uparrow\rangle aa^*\langle\Phi_\uparrow|x\rangle & \langle x|\Phi_\uparrow\rangle ab^*\langle\Phi_\downarrow|x\rangle \\ \langle x|\Phi_\downarrow\rangle ba^*\langle\Phi_\uparrow|x\rangle & \langle x|\Phi_\downarrow\rangle bb^*\langle\Phi_\downarrow|x\rangle \end{pmatrix} \tag{7.55}$$

$$= \begin{pmatrix} |a|^2 & e^{-i\varphi}ab^* \\ e^{+i\varphi}a^*b & |b|^2 \end{pmatrix}, \tag{7.56}$$

where $\varphi \equiv 2k_0x$ and

$$P_X(x) = \mathrm{Tr}\,\langle x|\rho|x\rangle = |\Phi_0(x)|^2 \tag{7.57}$$

is the probability distribution for position. Clearly the probabilities to find the spin up and down remain $|a|^2$ and $|b|^2$ and have not been changed by the measurement. Note however the spin has been rotated by an angle φ around the z axis so that it moves along a line of constant latitude. Unlike the previous example of momentum measurement, there is no state collapse which is affecting the spin. Rather this change in the spin state is the result of the measurement back-action through the unitary time evolution generated by the coupling V. As we can see from Eq. (7.20), the size of the Zeeman field which briefly acts on the spin varies linearly with the position x. Hence the measured value X determines the rotation angle caused by the coupling V. This is not surprising, because while V commutes with σ^z, it does not commute with the transverse components of the spin and we expect them to be changed by the measurement. Because the measurement of position yields no information about σ^z, the collapse of the position has no effect on σ^z.

[4]After some time the momentum boost will affect the position of each spin component and position then *is* entangled with the spin.

The message here is that if we measure the state of the environment presented to the qubit by the measurement apparatus (in this case the pointer variable which is the particle position or momentum), then we have complete information about what happened to the qubit. What happened may be random, but we know precisely what it is. If however we ignore the results of the measurement by ensemble averaging over the measurement results, the random results will lead to *measurement induced dephasing* of the qubit. In this example, we can ensemble average over all possible results of the momentum measurement or the position measurement. Either way we should get the same answer because this corresponds to tracing out the environmental degrees of freedom by summing over a complete set of states (in some particular basis).

7.2 Dispersive Readout of a Qubit in a Cavity

Now that we understand Stern-Gerlach measurements we are ready to study dispersive readout of a qubit in a cavity. This readout works because the cavity frequency, and hence the phase of the reflection coefficient for microwaves, depends on the state of the qubit. In the Stern-Gerlach example, the state of the qubit is entangled with the momentum of the particle wave and we considered the different back-action effects of measuring the particle momentum or the conjugate variable, the position. In this example, the phase of the microwaves reflected from the cavity is entangled with the state of the qubit and will consider the different back-action effects of measuring the phase of the microwaves or its conjugate variable, the photon number.

Suppose that we have the effective Hamiltonian in the dispersive limit given by Eq. (6.20). This is the analog of the Stern-Gerlach Hamiltonian Eq. (7.20). Instead of the Zeeman splitting varying linearly with position, it now varies linearly with photon number $\hat{N} = a^\dagger a$. The analogy is not perfect because the photon number has discrete integer eigenvalues and for a coherent state obeys a Poisson distribution, while the position is continuous and (in our example) Gaussian distributed. However as we shall see, in the limit of weak measurements involving a large number of photons, the Poisson distribution effectively becomes a Gaussian.

If we send a microwave pulse at the bare cavity frequency ω_c in coherent state $|\alpha\rangle$ towards the (one-sided) cavity, then the initial state of the system (before the wave packet hits the cavity) is a product state

$$|\psi_{\rm in}\rangle = [a|\uparrow\rangle + b|\downarrow\rangle]|\alpha\rangle, \tag{7.58}$$

while the final state has the qubit and cavity entangled

$$|\psi_{\rm out}\rangle = [a|e^{-i\theta_0}\alpha\rangle|\uparrow\rangle + b|e^{+i\theta_0}\alpha\rangle|\downarrow\rangle], \tag{7.59}$$

where θ_0 is the phase of the complex reflection coefficient given in Eq. (B.22) of Appendix B. Using the expression for the dispersive cavity pull in Eq. (6.20) and noting that the drive at the bare cavity frequency is detuned from the actual cavity frequency by an amount $\chi\sigma^z$, the reflection coefficient becomes (with $j = -i$)

$$r = \frac{\chi\sigma^z - i\kappa/2}{\chi\sigma^z + i\kappa/2} = e^{-i\theta_0\sigma^z} \tag{7.60}$$

with $\tan\frac{\theta_0}{2} = \frac{\kappa}{2\chi}$. As can be seen in Fig. (7.3), for a fixed phase angle difference, the two coherent states become more and more distinguishable as the amplitude increases. Thus the more photons we use, the stronger the measurement we make.

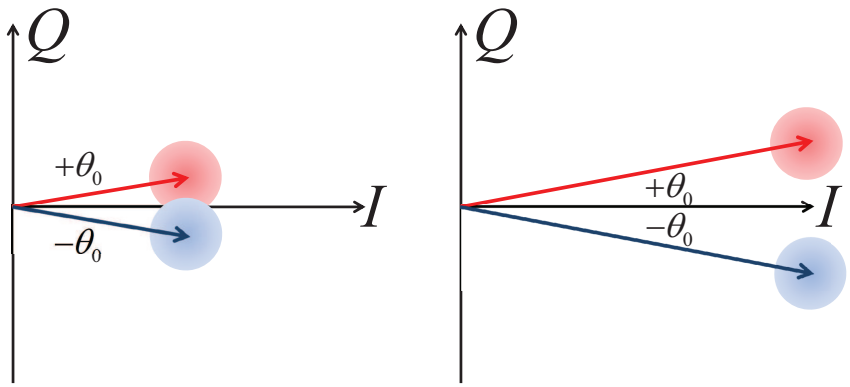

Fig. 7.3 Fresnel 'lollipops' showing that two coherent states differing by a fixed phase angle, become more and more distinguishable as the amplitude increases. For sufficiently large amplitude, the difference in the Q quadratures exceeds the uncertainty due to the vacuum noise. When fully distinguishable we have a strong quantum measurement of the spin which is entangled with the photon field.

If, as illustrated in Fig. (7.4), we make a homodyne measurement of the reflected wave we can choose to measure either of the two quadrature amplitudes defined in Eqs. (2.81-2.82). The two quadratures $\hat{X}$ and $\hat{Y}$ are precisely analogous to the position and momentum in the Stern-Gerlach example introduced above.[5] For the coherent state $|e^{-i\theta_0\sigma^z}\alpha\rangle$ with $\alpha = \sqrt{\bar{N}}$ real, we have (see Appendix E)

$$\langle\hat{Y}\rangle = -\sigma^z\alpha\sin\theta_0, \tag{7.61}$$

so that, at least for $\theta_0 \ll 1$, measuring $\hat{Y}$ is equivalent to measuring the phase of the wave.[6] and

$$\left\langle\left\{\hat{Y} - \langle\hat{Y}\rangle\right\}^2\right\rangle = \frac{1}{4}. \tag{7.62}$$

By comparison with our previous example, we see that the 'momentum kick' is

$$Y_0 = -\sqrt{\bar{N}}\sin\theta_0 \tag{7.63}$$

and (as shown in Appendix E) the momentum is gaussian distributed with variance

[5]Note however the important fact that with the normalization we have chosen, their commutator is smaller by a factor of two $[\hat{X},\hat{Y}] = \frac{i}{2}$. Hence the Heisenberg uncertainty relation for the two quadratures is $(\Delta X)^2(\Delta Y)^2 \geq \frac{1}{16}$.

[6]Strictly speaking there is no 'phase operator'. Only operators like $\sin\theta$ which are periodic in theta are well-defined.

$$(\Delta Y)^2 = \frac{1}{4}. \tag{7.64}$$

Hence by analogy to Eq. (7.53), the measurement rate is

$$\Gamma_{\rm meas} = \frac{1}{\Delta t}\frac{Y_0^2}{2(\Delta Y)^2} = 2\dot{\bar{N}}\sin^2\theta_0, \tag{7.65}$$

where $\dot{\bar{N}} = \frac{\bar{N}}{\Delta t}$ is the incident (and outgoing) photon flux. Thus we see that the measurement rate is maximized when $\theta_0 = \frac{\pi}{2}$ which is achieved when the dispersive shift is half a linewidth: $\chi = \frac{\kappa}{2}$. However the measurement is weak and continuous only for $\theta_0 \ll 1$ and in this limit we can make the approximation

$$\Gamma_{\rm meas} \approx 2\dot{\bar{N}}\theta_0^2. \tag{7.66}$$

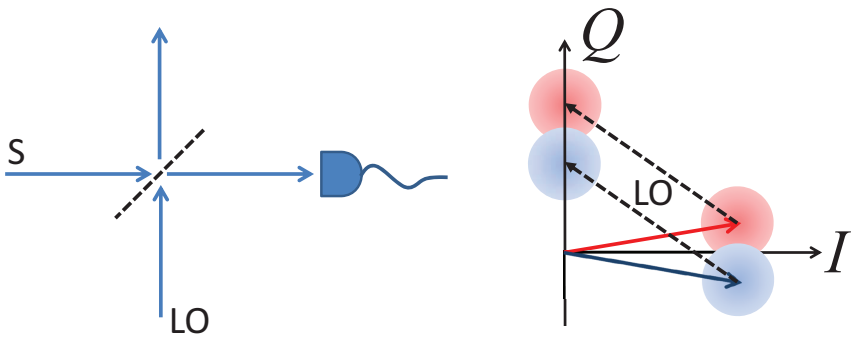

Fig. 7.4 Left panel: Homodyne measurement in which the signal is mixed with a local oscillator of the same frequency. The resulting interference allows one to determine the amplitude (rather than simply the power) of the signal. The phase of the local oscillator determines the signal quadrature which is measured by the square-law detector. The beam splitter can be made very strongly transmitting and only weakly reflecting (at the expense of needing more LO power), so that the vacuum noise added by the LO port is negligible. Right panel: Vector addition of the signal and LO phasors which converts a phase change of the signal into an amplitude (and hence intensity) change which can be detected by the square-law detector.

The corresponding dephasing is most easily determined using the overlap of the pointer coherent states (see Appendix E)

$$\langle e^{i\theta_0}\alpha|e^{-i\theta_0}\alpha\rangle = e^{|\alpha|^2(e^{-2i\theta_0}-1)} \approx e^{-i2\theta_0\bar{N}}e^{-2\bar{N}\theta_0^2}. \tag{7.67}$$

The complex exponential simply represents the average phase rotation of the qubit by an angle $2\theta_0$ for each photon which passes through the cavity. The dephasing term represents the ensemble averaging over the fluctuations in the photon number in the coherent state. From this we deduce

$$\Gamma_\varphi \Delta t = 2\bar{N}\theta_0^2, \tag{7.68}$$

so that again we have a quantum limited measurement with $\Gamma_\varphi = \Gamma_{\rm meas}$.

Continuing the Stern-Gerlach analogy, the analog of Eq. (7.46) for the reduced density matrix conditioned on measuring a value y for the $\hat{Y}$ signal quadrature can be found using the results in Appendix E

$$\rho_y = \frac{1}{P(y)}\langle y|\rho|y\rangle = \frac{1}{Z}\begin{pmatrix} |a|^2 e^{+\lambda y} & e^{i\varphi}ab^* \\ e^{-i\varphi}a^*b & |b|^2 e^{-\lambda y} \end{pmatrix}, \tag{7.69}$$

where

$$\lambda \equiv -4\sqrt{\bar{N}}\sin\theta_0, \tag{7.70}$$

and

$$P(y) = |a|^2 e^{-\lambda y} + |b|^2 e^{+\lambda y}, \tag{7.71}$$

and (unlike the Stern-Gerlach case) there is an additional deterministic phase rotation given by

$$\varphi = -\bar{N}\sin 2\theta_0. \tag{7.72}$$

Let us now consider what happens when instead of measuring the 'momentum' (the $\hat{Y}$ signal quadrature), we instead measure the 'position' (the $\hat{X}$ signal quadrature). Using the results from Appendix E) to project onto a given value x of $\hat{X}$, the analog of Eq. (7.56) is

$$\rho_x = \begin{pmatrix} |a|^2 & e^{i\lambda(x-\bar{x})}e^{i\varphi}ab^* \\ e^{-i\lambda(x-\bar{x})}e^{-i\varphi}a^*b & |b|^2 \end{pmatrix}, \tag{7.73}$$

where $\bar{x} = \sqrt{\bar{N}}\cos\theta_0$ is the mean value of x.

Suppose that instead of measuring the $\hat{X}$ quadrature amplitude via a homodyne measurement, we choose instead to use a photomultiplier to measure $\hat{N}$. Suppose that the result of this measurement is an integer n. Then the reduced density matrix of the spin is readily determined using the following property of coherent states (see Appendix E)

$$\langle n|e^{+i\theta_0}\alpha\rangle = \frac{\left[e^{i\theta_0}\alpha\right]^n}{\sqrt{n!}}. \tag{7.74}$$

From this we have

$$\rho_n = \begin{pmatrix} |a|^2 & ab^* e^{-i2\theta_0 n} \\ ba^* e^{+i2\theta_0 n} & |b|^2 \end{pmatrix}. \tag{7.75}$$

Thus the qubit is left in a pure state but rotated around the z axis by an angle $\theta_n = -2\theta_0 n$. This simply means that each photon that reflects from the cavity deterministically shifts the phase of the superposition of the two qubit states by a fixed angle $-2\theta_0$. This is the direct analog of Eq. (7.56) in the Stern-Gerlach example (except here n has a non-zero mean value rather than fluctuating around zero). For sufficiently small θ_0 we can carry out the ensemble average over the photon number fluctuations using the following approximation

$$\left\langle\left\langle e^{-i2\theta_0 n}\right\rangle\right\rangle \approx e^{-i2\theta_0\langle\langle n\rangle\rangle}e^{-\frac{1}{2}\langle\langle[2\theta_0(n-\bar{N})]^2\rangle\rangle} \approx e^{-i2\theta_0\bar{N}}e^{-2\bar{N}\theta_0^2}, \tag{7.76}$$

which correctly reproduces Eq. (7.67).

The connection between measuring the photon number and the $\hat{X}$ signal quadrature can be seen by noting that (for real α) the number of photons is related to the value of $\hat{X}$ whose fluctuations modulate the length of phasor

$$\hat{N} = \left(\alpha + \Delta\hat{X}\right)^2 + \left(\Delta\hat{Y}\right)^2 - \frac{1}{2} \tag{7.77}$$

$$= \bar{N} + 2\sqrt{\bar{N}}\Delta\hat{X} + \left(\left(\Delta\hat{X}\right)^2 + \left(\Delta\hat{Y}\right)^2 - \frac{1}{2}\right). \tag{7.78}$$

For sufficiently small θ_0 the last term in parentheses can be neglected (it vanishes exactly in the state $|\alpha\rangle$). Thus the off-diagonal phase factor in Eq. (7.75) which contains the photon number measurement result can be written in terms of the measurement result for the $\hat{X}$ quadrature signal amplitude measurement result

$$e^{-i2\theta_0 n} \approx e^{-i2\bar{N}\theta_0} e^{-i4\theta_0\sqrt{\bar{N}}(x-\bar{x})} \tag{7.79}$$

which precisely matches the phase factor of the off-diagonal element Eq. (7.73) in the limit of small θ_0. In this limit it takes many photons to make the measurement and n becomes gaussian distributed and (its discreteness is hard to see) just like the continuous measurement result for x. It is important to emphasize that Eq. (7.73) and Eq. (7.75) are exact for any value of θ_0. We have a simple physical equivalence between them only for small θ_0 however.

7.2.1 Heterodyne Detection

The above results tell us that the back-action of the homodyne measurement on the qubit depends on which quadrature of the homodyne signal is being measured. In a heterodyne measurement, the frequency of the local oscillator is detuned from that of the signal. One can view this as rotating the measurement between the two quadrature amplitudes at a rate given by the detuning. Thus we obtain information about both quadratures. This is a bit strange because the two quadratures are canonically conjugate and hence are incompatible observables–we cannot know them both simultaneously with perfect precision. Thus, just as a phase-preserving amplifier must add some noise (Clerk *et al.*, 2010), so a heterodyne measurement must be subject to some inefficiency. From the quantum noise point of view, this comes about because of additional vacuum noise mixed into the output. If the signal is at frequency f and the local oscillator is at frequency $f - \Delta$ the output will be at frequency Δ. However vacuum noise at the image frequency $f + \Delta$ will also be mixed down to the same output frequency increases the uncertainty in the measurement of the quadrature amplitudes by just the amount required by the Heisenberg uncertainty relation (Clerk *et al.*, 2010).

Alternatively one can make the equivalent of a heterodyne measurement using two simultaneous homodyne measurements as shown in Fig. (7.5). Here the additional vacuum noise is introduced by the 50-50 beam splitter needed to allow the separate homodyne measurements. Despite the additional noise introduced by the vacuum port of this beam splitter, the qubit remains in a pure state. Measurement of $\hat{X}$ quadrature yields a rotation around the z axis and measurement of the $\hat{Y}$ quadrature pushes the polarization towards $\sigma^z = \pm 1$ as before. However because only half the signal is used for the $\hat{Y}$ measurement, the measurement rate is only 50% of the previous rate.

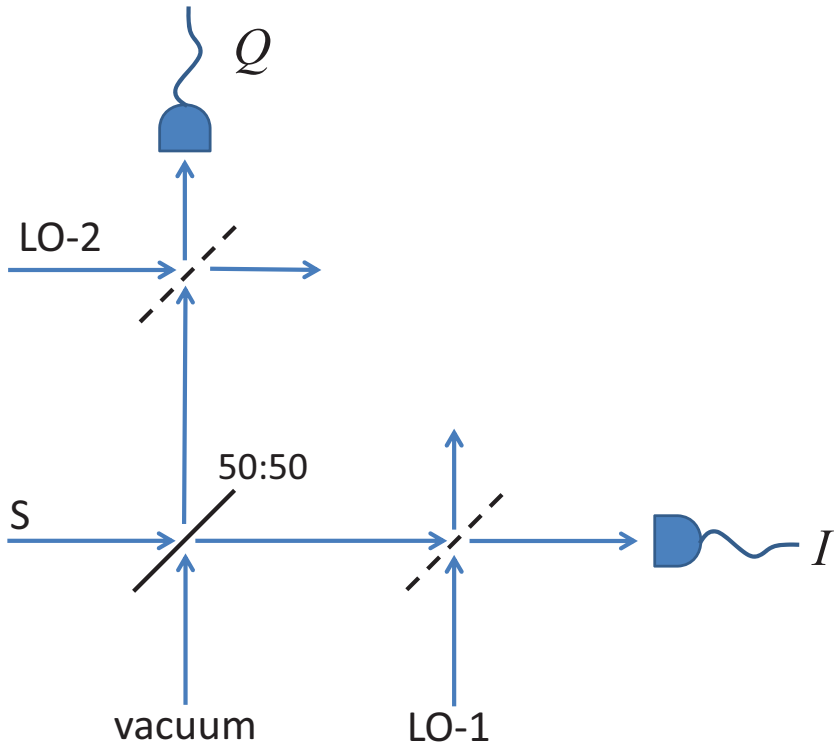

Fig. 7.5 Idealized version of a heterodyne measurement consisting of two separate homodyne measurements. The local oscillator beam splitters indicatd by the dashed lines are highly transmitting and only weakly reflecting. The 50-50 beam splitter necessarily introduces an extra vacuum port. By correctly choosing the phase of each of the two local oscillators, both quadratures (I, Q) of the input signal can be measured using the two square-law detectors. The added noise of the vacuum port reduces the measurement efficiency by 50% for a given quadrature relative to homodyne measurement of that quadrature. Nevertheless the state of the qubit remains pure if the two square-law detectors are ideal. In practice, heterodyne measurement is done with a single beam splitter and local oscillator detuned from the signal. The resulting beat note at the intermediate frequency (IF) is then amplified. The analog of the added noise from the 50:50 beam splitter is the extra vacuum noise from the 'image frequency' which is also mixed down by the local oscillator to the IF frequency.

Exercise 7.3 Show that if the phases of the two local oscillators in the pseudo-heterodyne setup in Fig. (7.5) are set to measure the same quadrature, then it is possible to recover the homodyne measurement result with no additional noise. Hint, first write down the S mstrix for the 50-50 beam splitter, making sure that it is unitary. Use this to determine whether the shot noise in the two homodyne signals is correlated. Recall that the shot noise can be viewed as resulting from the interference between the classical input and the vacuum noise that comes with it.

7.2.2 Strong-Dispersive Limit

We have seen that when the qubit transition frequency $\omega_{\rm Q}$ is strongly detuned from the cavity resonance frequency $\omega_{\rm R}$, the resulting 'dispersive' Hamiltonian takes the form in Eq. (6.20)

$$H = \omega_{\rm R} a^\dagger a + \frac{\omega_{\rm Q}}{2}\sigma^z + \frac{\chi}{2} a^\dagger a \sigma^z. \tag{7.80}$$

This Hamiltonian is diagonal and deceptively simple looking, yet we have come to realize that it provides a powerful toolbox for quantum control of the joint states of the cavity and the qubit. The coefficient χ tells us the that the frequency of the cavity shifts by χ when the qubit changes state. The same dispersive coupling term also tells us that the qubit transition frequency changes by χ each time a photon is added to the cavity. Because of the very large transition dipole of superconducting artificial atoms (several electron charges moving ~ 1 millimeter), the dispersive shift χ can be $\sim 10^3$ times larger than the line widths of both the cavity and the atom placing the system deep into what is known as the 'strong-dispersive' regime. In this regime one can easily resolve the different spectral peaks of the qubit corresponding to the different possible integer number of photons in the cavity (Schuster *et al.*, 2007*a*; Johnson *et al.*, 2010; Paik *et al.*, 2011; Sears *et al.*, 2012). That is, the light shift of the qubit is strongly quantized. This opens up new avenues for quantum control by allowing one to apply a Rabi rotation to the qubit which is effective if and only if there is some particular chosen photon number in the cavity.

Conversely the two possibly cavity frequencies (depending on the state of the qubit) are well resolved. Hence a drive tone at frequency $\omega_{\rm R} \pm \frac{\chi}{2}$ will excite (coherently displace) the cavity only if the qubit is in the particular selected state. The combination of a photon number dependent qubit rotation and a qubit state dependent cavity displacement is an extremely powerful tool set (Leghtas *et al.*, 2013; Leghtas *et al.*, 2012; Nigg and Girvin, 2013). For example, it becomes a relatively simple matter to create entangled states of the qubit and cavity

$$|\psi\rangle = \frac{1}{\sqrt{2}}\big[|g\rangle|\alpha\rangle \pm |e\rangle|-\alpha\rangle\big] \tag{7.81}$$

where $|e\rangle$ and $|g\rangle$ are the states of the qubit and $|\pm\alpha\rangle$ are coherent states of amplitude $\pm\alpha$ of the cavity.

With a few additional steps one can disentangle the qubit from the cavity to yield a photon cat state

$$|\psi\rangle = \frac{1}{\sqrt{2}}|g\rangle\big|\alpha\rangle \pm |-\alpha\rangle\big], \tag{7.82}$$

or even entangle the qubit with two different cats (one with even photon number parity and one with odd)

$$|\psi\rangle = \frac{1}{2}\big[|g\rangle[|\alpha\rangle + |-\alpha\rangle\big] + |e\rangle\big[|g\rangle[|\alpha\rangle - |-\alpha\rangle]\big]. \tag{7.83}$$

Furthermore the same tool set allows easy state tomography and direct measurement of the cavity Wigner function as well as the photon number parity (Kirchmair *et al.*,

2013). Schrödinger cats of size up to ~ 100 photons can now be produced (Vlastakis *et al.*, 2013). The ability to measure the photon number parity opens up the possibility for using Schrödinger cat states as code words in a quantum memory protocol which remarkably is robust against photon loss errors (Leghtas *et al.*, 2012).

Experimental progress in Circuit QED has now brought us into a new ultra-strong coupling regime which is well beyond what can be achieved in conventional non-linear quantum optics. This new regime is opening up new vistas of fundamental quantum physics and affords radically new possibilities for quantum information processing.

7.2.3 Multi-port Resonators

All of the results derived above assumed a single-sided cavity in which there is only one port so the reflected energy is equal to the incident energy. In this case the reflection coefficient has unit magnitude and information about the state of the qubit is encoded only in the phase of the reflection coefficient. For a two-port cavity there will be a signal reflected from the input port and another signal transmitted through the output port. Depending on the relative coupling strengths of these two ports, information on the qubit state can be contained in one or both signals. This is discussed in more detail in (Clerk *et al.*, 2010).

One interesting case is where the input port is very weakly coupled and the damping of the cavity is dominated by the output port. In this case there is no information in the signal reflected from the input port. in general, the information in the output port resides in both amplitude and phase of the signal. For example if the cavity is irradiated not at the bare cavity frequency ω_c (as in the example discussed above) but rather at $\omega_c - \chi$, then the amplitude will be large for one qubit state and small for the other. This setup is very useful in the strong dispersive limit $\chi \gg \kappa$. In this limit the power transmitted through the cavity at frequency ω_c is very small and so not useful for measurement (even though the phase difference between the two qubit states is π; that is, $\theta_0 = \frac{\pi}{2}$).

7.3 Multi-qubit Dispersive Readout

An important idea in circuit QED is the understanding that dispersive coupling to the cavity can be used to perform a simultaneous joint readout of multiple qubits (Blais *et al.*, 2004; Bishop *et al.*, 2009*b*). This joint readout was used for two-qubit state tomography by Majer *et al.*(Majer *et al.*, 2007). In its most basic form, the idea is simply that with two qubits, there are four possible quantum states and four different dispersive frequency pulls of the cavity. If one is in the strong dispersive coupling regime and all four frequency pulls can be reliably distinguished in a single shot, then one has two bits of classical information and a complete projective measurement of both qubits. Of course in the presence of qubit decay and amplifier noise, the detector tomography can be complex (Bishop *et al.*, 2009*b*). A more sophisticated understanding of the situation of imperfect resolution of the four peaks has been developed recently and (Filipp *et al.*, 2009) demonstrated that it is possible to still reliably measure two-qubit correlations even in the presence of readout noise.

A simplified version of the theory for joint readout of two qubits is the following. While the cavity pull is linear in the qubit polarizations

$$\delta\omega_{\rm c} = \chi_1\sigma_1^z + \chi_2\sigma_2^z, \tag{7.84}$$

the corresponding homodyne (transmission) amplitude is *not*

$$A(\sigma_1^z, \sigma_2^z) = {\rm Re}\left\{e^{i\varphi}\frac{\kappa/2}{\Delta - \delta\omega_{\rm c} + i\kappa/2}\right\}. \tag{7.85}$$

Here, Δ is the detuning of the readout tone from the bare cavity resonance, κ is the cavity line width, and φ is the local oscillator phase. Because this can take on only four distinct values (corresponding to two classical bits of information) this expression can always be recast in the form

$$A(\sigma_1^z, \sigma_2^z) = \beta_0 + \beta_1\sigma_1^z + \beta_2\sigma_2^z + \beta_{12}\sigma_1^z\sigma_2^z. \tag{7.86}$$

The joint coefficient β_{12} is in general non-zero (as long as $\Delta \neq 0$) and typically on the same scale as the other coefficients. By using pre-rotations (by angle zero or π) of each of the two qubits prior to making the measurement, it is straightforward to obtain any one or two-qubit correlator in the z basis. Ensemble averaging many such measurements will reduce the statistical uncertainty to arbitrarily low values. For example,

$$\langle\sigma_1^z\sigma_2^z\rangle = \frac{1}{4\beta_{12}}\left\langle A(\sigma_1^z, \sigma_2^z) - A(-\sigma_1^z, \sigma_2^z) - A(\sigma_1^z, -\sigma_2^z) + A(\sigma_1^z, \sigma_2^z)\right\rangle. \tag{7.87}$$

Any other arbitrary correlators (e.g. $\langle\sigma_1^x\sigma_2^y\rangle$) can be achieved by pre-pending rotations through appropriate arbitrary angles. The Yale group has recently used this multi-qubit readout method to measure values of the CHSH entanglement witness well above the classical bound (Chow *et al.*, 2010) and to prove three-qubit entanglement in a GHZ state (DiCarlo *et al.*, 2010).

7.4 Non-linear and latching readouts

We have focused here on dispersive readout using a simple harmonic oscillator resonator parametrically coupled to the qubit. For binary readout of the state of a two-level qubit, other readout methods based on coupling to a non-linear oscillator have been developed. The Josephson bifurcation amplifier, and its cousin the cavity bifurcation amplifier, (Siddiqi *et al.*, 2004; Metcalfe *et al.*, 2007; Mallet *et al.*, 2009) use a large Josephson junction as the non-linear element. The advantage of a non-linear cavity is that it can 'latch' into one of two stable oscillation modes depending on the state of the qubit. Because of hysteresis, the readout can remain 'latched' in its stable state even if the qubit decays, thus providing a high signal to noise ratio. A very simple readout scheme has been developed by the Yale group (Reed *et al.*, 2010*a*) in which the bare cavity is linear but one takes advantage of the anharmonicity inherited from the qubit itself so that a separate non-linear element is not needed. It is also very robust and easy to implement under a large range of circuit parameter values.

For phase qubits, the UCSB group has developed a high-fidelity readout based on the qubit modulating the macroscopic quantum tunneling rate of a large junction placed in a meta-stable current carrying state (Martinis *et al.*, 2002).

8
Summary and Future Directions

The rate of progress in the realization of quantum microwave circuits over the past decade has been truly remarkable and represents both progress towards building novel quantum machines and realizing non-linear quantum optics in a novel strong-coupling regime. Circuit QED is much more than atomic physics with wires. We have a set of modular elements which are readily connected together. Hence, we have the opportunity to assemble large scale structures from these quantum building blocks and do some real quantum engineering. Further progress will require scaling up both the number of qubits and resonators and continuing to advance coherence times and gate fidelities. As the number of qubits grows, it will be important to increase the on-off ratio of the couplings among them. Simply detuning them from each other will probably not be sufficient and interference between two coupling channels which can null out the net coupling will likely be needed. Houck et al. have developed a novel transmon structure in which the vacuum Rabi coupling can be tuned over a wide range using magnetic flux to control the interference between two internal modes of the qubit (Srinivasan *et al.*, 2011*b*; Gambetta *et al.*, 2011*b*; Hoffman *et al.*, 2011*a*).

Another exciting direction involves using multiple physical qubits to realize individual logical qubits to overcome the difficulties of maintaining stable transition frequencies. In particular, the possibility of topological protection (Kitaev, 2003; Ioffe and Feigelman, 2002; Ioffe *et al.*, 2002; Doucot *et al.*, 2003; Doucot *et al.*, 2005) is beginning to be explored in superconducting qubits (Gladchenko *et al.*, 2009). The central idea is that qubits are constructed in which the ground and excited states are degenerate and this degeneracy is robust against local variations in Hamiltonian parameters. Even if the energy levels are not exactly degenerate, it would be very useful to have a qubit with a "Lambda" energy level scheme, that is, two nearly degenerate levels that can be coupled via stimulated Raman pulses through a third level. This would be advantageous both as a robust qubit and for purposes of fundamental quantum optics studies. It seems reasonably certain that this cannot be achieved without applied magnetic flux to frustrate the Josephson couplings (as in a flux qubit or in the fluxonium qubit). Indeed the fluxonium qubit may turn out to be quite useful as a Lambda system.

The development of large resonator arrays will be interesting not only as a quantum computation architecture but also for fundamental quantum optics purposes. An array of resonators each containing a qubit that induces a Kerr nonlinearity will be a realization of the boson Hubbard model (Fisher *et al.*, 1989) which exhibits both superfluid and Mott insulator phases. There is now a burgeoning interest in seeing 'quantum phase transitions of light' (Greentree *et al.*, 2006; Illuminati, 2006; Hart-

mann and Plenio, 2007; Jarrett *et al.*, 2007; Rossini and Fazio, 2007; Angelakis *et al.*, 2007; Hartmann *et al.*, 2008; Makin *et al.*, 2008; Aichhorn *et al.*, 2008; Cho *et al.*, 2008*c*; Cho *et al.*, 2008*a*; Zhao *et al.*, 2008; Na *et al.*, 2008; Lei and Lee, 2008; Cho *et al.*, 2008*b*; Ji *et al.*, 2009; Hartmann *et al.*, 2009; Grochol, 2009; Dalidovich and Kennett, 2009; Carusotto *et al.*, 2009; Schmidt and Blatter, 2009; Koch and Le Hur, 2009; Lieb and Hartmann, 2010; Hartmann, 2010; Schmidt *et al.*, 2010; Houck *et al.*, 2012; Hayward *et al.*, 2012; Nissen *et al.*, 2012; Petrescu *et al.*, 2012; Hwang and Choi, 2013; Schmidt and Koch, 2013). Since the transmon qubit is itself an anharmonic oscillator, one might imagine it would be easier to simply use a lattice of coupled transmons to realize the boson Hubbard model (with negative Kerr coefficient). The advantage of using a lattice of resonators is that their resonance frequencies can be closely matched to a single fixed value. The Kerr coefficient induced by coupling each resonator to an off-resonant qubit will have some variation due to variations in qubit transition frequencies, but this disorder in the Hubbard U will be more tolerable than disorder in the photon 'site energies.' Just as cold atom systems are now used to simulate condensed matter models, so we may be able to use photons as interacting strongly correlated bosons, which can be probed, measured and controlled in ways that are impossible in ordinary condensed matter.

The demands placed on classical computers to design and simulate even small numbers of qubits and resonators is already enormous. As the size of our quantum machines grows, the modeling complexity will grow exponentially. Similarly the experimental measurements and process tomography needed to verify the operation of larger quantum machines will become extremely challenging. We will have to develop calibration and verification protocols that can reliably vet each segment of a quantum processor without the luxury of complete end-to-end process tomography. Today, classical computers are sufficiently complex that we cannot design the next generation by hand. We must use the current generation of computers to design the next. Eventually this might be true of quantum machines. However, one wonders if we might soon find ourselves in a situation where both existing quantum machines and classical computers are not powerful enough to be used to design and model the next generation of quantum machines. We are rapidly gathering supplies to cross that novel and exciting desert!

8.1 Acknowledgments

This work was supported by Yale University and grants NSF DMR-1004406 and ARO W911NF-05-1-0365. The author is grateful to his many colleagues at Yale and around the world with whom he has collaborated in learning to apply the ideas of quantum optics to electrical circuits.

Appendix A
Cooper Pair Box Hamiltonian

The Cooper pair box consists of a superconducting island coupled to a superconducting ground via a Josephson junction, or two islands connected by a Josephson junction. The Hamiltonian has the same form in both cases. The equivalent circuit is shown in Fig. (4.1). The bias voltage V could be an intentionally applied dc or ac voltage, or a quantum fluctuating voltage associated with a microwave photon field, or it could be a random voltage representing some local charge asymmetry in the vicinity of the island. For simplicity, we will take the voltage to be supplied by an ideal zero-impedance source. Because figuring out the Hamiltonian of a system connected to a power supply can be confusing, we will consider a physical realization of the voltage source as a very large 'buffer' capacitor C_{B} as shown in Fig. (A.1). In this configuration, the circuit has two islands with corresponding node fluxes, Φ_1 and Φ_2. The charging energy can be determined by writing the Lagrangian for the two flux variables

$$\mathcal{L} = \frac{1}{2}C_{\mathrm{B}}\dot{\Phi}_2^2 + \frac{1}{2}C_{\mathrm{g}}\left(\dot{\Phi}_2 - \dot{\Phi}_1\right)^2 + \frac{1}{2}C_{\mathrm{J}}\dot{\Phi}_1^2. \tag{A.1}$$

Defining

$$\Phi \equiv \begin{pmatrix} \Phi_1 \\ \Phi_2 \end{pmatrix}, \tag{A.2}$$

the Lagrangian can be written

$$\mathcal{L} = \frac{1}{2}\dot{\Phi}^{\mathrm{T}} C \dot{\Phi}, \tag{A.3}$$

where the capacitance matrix is given by

$$C = \begin{pmatrix} C_{\mathrm{g}} + C_{\mathrm{J}} & -C_{\mathrm{g}} \\ -C_{\mathrm{g}} & C_{\mathrm{g}} + C_{\mathrm{B}} \end{pmatrix}. \tag{A.4}$$

The electrostatic Hamiltonian is now readily expressed in terms of the charges canonically conjugate to Φ

$$H = \frac{1}{2}Q^{\mathrm{T}} C^{-1} Q, \tag{A.5}$$

where

$$Q \equiv \begin{pmatrix} Q_1 \\ Q_2 \end{pmatrix}. \tag{A.6}$$

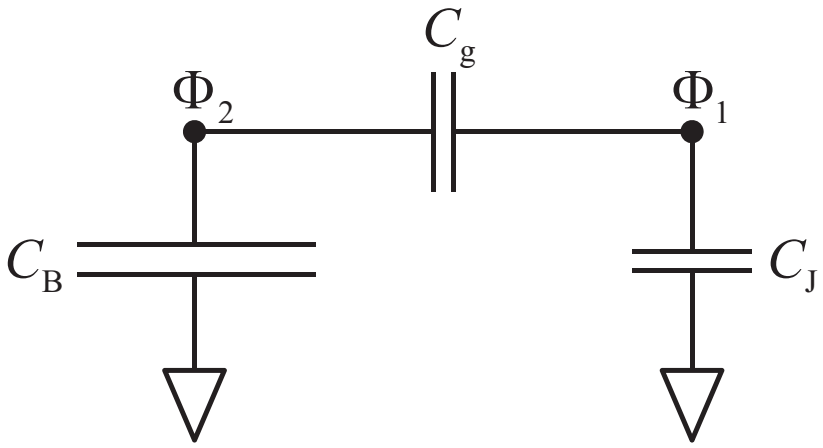

Fig. A.1 Equivalent circuit for determining the electrostatic energy of a Cooper pair box biased by a voltage source represented by a large capacitor C_B. The Josephson junction capacitance C_J is coupled to the voltage source via the capacitor C_g. There are two node fluxes Φ_1 and Φ_2.

The inverse capacitance matrix is given by

$$C^{-1} = \frac{1}{C_g C_B + C_g C_J + C_B C_J} \begin{pmatrix} C_g + C_B & C_g \\ C_g & C_g + C_J \end{pmatrix}. \tag{A.7}$$

This can be simplified by defining the total capacitance to ground for each of the two islands

$$C_{1\Sigma} \equiv C_J + C_{2s} \tag{A.8}$$

$$C_{2\Sigma} \equiv C_B + C_{1s}, \tag{A.9}$$

and the two series capacitances

$$\frac{1}{C_{1s}} \equiv \frac{1}{C_g} + \frac{1}{C_J} \tag{A.10}$$

$$\frac{1}{C_{2s}} \equiv \frac{1}{C_g} + \frac{1}{C_B}. \tag{A.11}$$

Using these definitions, the inverse capacitance matrix can be written

$$C^{-1} = \begin{pmatrix} \frac{1}{C_{1\Sigma}} & \frac{\beta}{C_{2\Sigma}} \\ \frac{\beta}{C_{2\Sigma}} & \frac{1}{C_{2\Sigma}} \end{pmatrix}, \tag{A.12}$$

where the dimensionless coupling constant is given by

$$\beta \equiv \frac{C_{\rm g}}{C_{\rm g} + C_{\rm J}}. \tag{A.13}$$

The electrostatic Hamiltonian can then be written

$$H = \frac{Q_1^2}{2C_{1\Sigma}} + \beta \frac{Q_2}{C_{2\Sigma}} Q_1 + \frac{Q_2^2}{2C_{2\Sigma}}. \tag{A.14}$$

We define the 'nominal' bias voltage as[1]

$$V_{\rm B} = \frac{Q_2}{C_{2\Sigma}}. \tag{A.16}$$

In terms of this we can write the electrostatic Hamiltonian as

$$H = \frac{Q_1^2}{2C_{1\Sigma}} + \beta V_{\rm B} Q_1 + \frac{1}{2} C_{2\Sigma} V_{\rm B}^2. \tag{A.17}$$

Including now the Josephson junction energy and quantizing we arrive at the full Cooper pair box Hamiltonian

$$H = \frac{\hat{Q}_1^2}{2C_{1\Sigma}} + \beta V_{\rm B} \hat{Q}_1 - E_{\rm J} \cos \frac{2e}{\hbar} \Phi_1 + \frac{1}{2} C_{2\Sigma} V_{\rm B}^2. \tag{A.18}$$

Note that the last term is a constant of the motion and can be ignored.

Defining the dimensionless offset (or 'gate') charge $n_{\rm g}$

$$n_{\rm g} \equiv -\beta \frac{C_{1\Sigma} V_{\rm B}}{2e} \approx -\frac{C_{\rm g} V_{\rm B}}{2e}, \tag{A.19}$$

(with the latter equality only in the limit of large $C_{\rm B}$) and defining the charging energy

$$E_{\rm C} \equiv \frac{e^2}{2C_{1\Sigma}}, \tag{A.20}$$

we can also write the Hamiltonian in terms of the integer-valued number operator

$$\hat{n} \equiv \frac{\hat{Q}_1}{2e} \tag{A.21}$$

representing the excess number of Cooper pairs on island one. Its conjugate variable is the relative phase angle for the superconducting order parameter across the junction

$$\varphi = \frac{2e}{\hbar} \Phi_1 = 2\pi \frac{\Phi_1}{\Phi_0}, \tag{A.22}$$

[1] N.B. The *actual* voltage on island two is

$$V = \frac{\partial H}{\partial Q_2} = V_{\rm B} + \beta \frac{Q_1}{C_{2\Sigma}}. \tag{A.15}$$

In the limit of of large $C_{\rm B}$ the actual voltage is fully buffered (i.e., becomes independent of Q_1) and is given by $V \approx V(Q_1 = 0) = V_{\rm B}$.

where Φ_0 is the superconducting flux quantum. In terms of this pair of dimensionless charge and phase variables, the Hamiltonian becomes

$$H = 4E_{\rm C}\left(\hat{n}^2 - 2n_{\rm g}\hat{n}\right) - E_{\rm J}\cos\varphi + \frac{1}{2}C_{2\Sigma}V_{\rm B}^2 \tag{A.23}$$

$$= 4E_{\rm C}\left(\hat{n} - n_{\rm g}\right)^2 - E_{\rm J}\cos\varphi + \frac{1}{2}\frac{C_{1\Sigma}C_{2\Sigma}}{C_{\rm g}+C_{\rm J}}V_{\rm B}^2, \tag{A.24}$$

It is sometimes convenient to work in the (angular) position basis with wave function $\Psi(\varphi)$ and $\hat{n} = -i\frac{\partial}{\partial\varphi}$ being represented by the angular momentum conjugate to the angle φ. In other cases, it is more convenient to work in the angular momentum (charge) eigenbasis and recognize that the operator $\cos\varphi$ term is a 'torque' that changes the angular momentum by ± 1 unit.

Dropping the last constant term in Eq. (A.24) and assuming the voltage bias is fully buffered (large $C_{\rm B}$), we arrive at Eq. (4.2). We again emphasize that $n_{\rm g}$ is a continuous variable (and often subject to $1/f$ noise), while $\hat{n}$ is integer-valued (i.e., is the angular momentum conjugate to the angular variable φ) and changes by ± 1 each time a Cooper pair tunnels through the Josephson junction connected across $C_{\rm J}$.

A.1 Cooper Pair Box Coupled to an LC Resonator

Consider the circuit in Fig. (A.2) which shows a Cooper pair box coupled to an LC resonator. For simplicity we will ignore the possibility of a dc bias voltage on the qubit. The Hamiltonian can be immediately written down by analogy with Eq. (A.14)

$$H = H_1 + H_2 + H_{12} \tag{A.25}$$

$$H_1 = \frac{\hat{Q}_1^2}{2C_{1\Sigma}} - E_{\rm J}\cos\frac{2e}{\hbar}\hat{\Phi}_1 \tag{A.26}$$

$$H_2 = \frac{\hat{Q}_2^2}{2C_{2\Sigma}} + \frac{1}{2L_{\rm B}}\hat{\Phi}_2^2 \tag{A.27}$$

$$H_{12} = \frac{\beta}{C_{2\Sigma}}\hat{Q}_1\hat{Q}_2. \tag{A.28}$$

Let the eigenfunctions of H_1 obey

$$H_1|j\rangle = \epsilon_j|j\rangle, \tag{A.29}$$

and let us denote the matrix elements of the charge operator in this basis by

$$Q_{jk} = \langle j|\hat{Q}_1|k\rangle. \tag{A.30}$$

This is the analog of the dipole matrix elements of an atom. The LC resonator hamiltonian can be written

$$H_2 = \hbar\omega_{\rm c}\hat{a}^\dagger\hat{a}, \tag{A.31}$$

where $\omega_{\rm c} = \frac{1}{\sqrt{L_{\rm B}C_{2\Sigma}}}$, and the second charge operator can be written following Eq. (2.42)

$$\hat{Q}_2 = -iQ_{\rm 2ZPF}\left(\hat{a} - \hat{a}^\dagger\right), \tag{A.32}$$

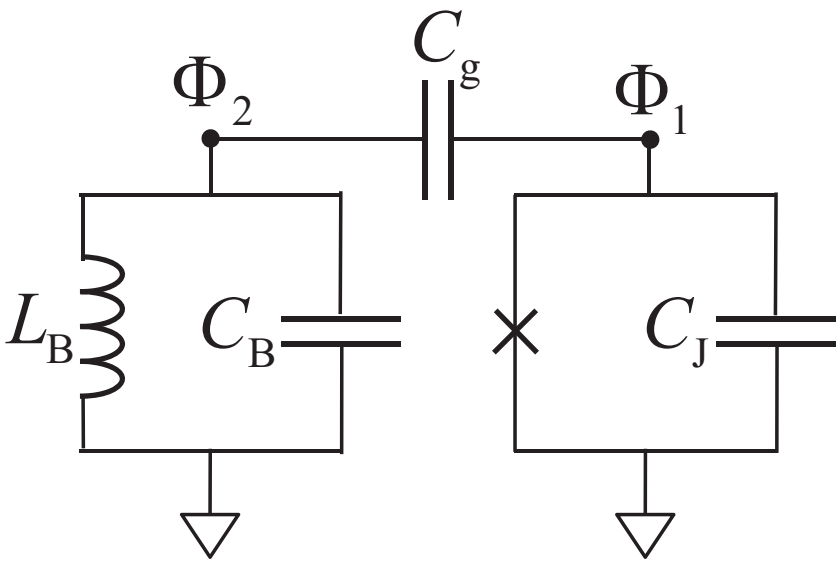

Fig. A.2 Equivalent circuit for a Cooper pair box (without dc voltage bias) capacitively coupled to an LC resonator.

where following Eq. (2.43) we have

$$Q_{2\mathrm{ZPF}} = \sqrt{\frac{C_{\mathrm{B}}\hbar\omega_{\mathrm{c}}}{2}}. \tag{A.33}$$

We now have the full Hamiltonian

$$H = \hbar\omega_{\mathrm{c}}\hat{a}^{\dagger}\hat{a} + \sum_{k=0}^{\infty}\epsilon_k|k\rangle\langle k| - i\frac{\beta Q_{2\mathrm{ZPF}}Q_{jk}}{2C_{2\Sigma}}|j\rangle(\hat{a}-\hat{a}^{\dagger})\langle k|, \tag{A.34}$$

in a form which is convenient for numerical diagonalization.

If the spectrum of the qubit is sufficiently anharmonic, we may be able to restrict our attention to its two lowest states. Projecting our Hamiltonian onto these two states allows us to represent the qubit operators in terms of Pauli spin matrices. Taking the ground state $|0\rangle$ to be represented by spin down $|\downarrow\rangle$ and the excited state $|1\rangle$ to be represented by spin up $|\uparrow\rangle$ we can represent all possible qubit operators within the 2×2 Hilbert space:

$$|0\rangle\langle 0| = \frac{1-\sigma^z}{2} \tag{A.35}$$

$$|1\rangle\langle 1| = \frac{1+\sigma^z}{2} \tag{A.36}$$

$$|1\rangle\langle 0| = \sigma^{+} \tag{A.37}$$

$$|0\rangle\langle 1| = \sigma^{-}. \tag{A.38}$$

The Hamiltonian then becomes (dropping an irrelevant constant)

$$H = \hbar\omega_c \hat{a}^\dagger \hat{a} + \frac{\hbar\omega_{01}}{2}\sigma^z - i(\hat{a} - \hat{a}^\dagger)\hbar \left\{ g_{11}\frac{1+\sigma^z}{2} + g_{00}\frac{1-\sigma^z}{2} + g_{10}\sigma^+ + g_{01}\sigma^- \right\} \quad \text{(A.39)}$$

where

$$\hbar\omega_{01} \equiv \epsilon_1 - \epsilon_0 \quad \text{(A.40)}$$

and

$$\hbar g_{jk} \equiv \frac{\beta Q_{2\text{ZPF}} Q_{jk}}{2C_{2\Sigma}}. \quad \text{(A.41)}$$

If the eigenstates of H_1 have a static dipole moment, then the diagonal matrix elements of the charge operator Q_1 will be non-zero. Here we are, for simplicity, ignoring the possibility of a dc bias which produces an offset charge. In this case H_1 has a charge-parity symmetry which guarantees that the diagonal matrix elements of the charge operator Q_1 vanish. We are free to choose a gauge (i.e., choose the arbitrary phases of the eigenstates of H_1) so that $g_{01} = g_{10} = g$ is real. We then arrive at the celebrated Jaynes-Cummings Hamiltonian

$$H = \hbar\omega_c \hat{a}^\dagger \hat{a} + \frac{\hbar\omega_{01}}{2}\sigma^z - i\hbar g(\hat{a} - \hat{a}^\dagger)(\sigma^+ + \sigma^-), \quad \text{(A.42)}$$

which, when the rotating wave approximation is justified, further simplifies to

$$H = \hbar\omega_c \hat{a}^\dagger \hat{a} + \frac{\hbar\omega_{01}}{2}\sigma^z - i\hbar g(\hat{a}\sigma^+ - \hat{a}^\dagger\sigma^-). \quad \text{(A.43)}$$

We can reduce this to the more familiar expression given in Eq. (6.7) by making a rotation of the spin axes via the unitary transformation

$$\hat{U} = e^{i\frac{\pi}{4}\sigma^z}, \quad \text{(A.44)}$$

which yields

$$U\sigma^+ U^\dagger = +i\sigma^+ \quad \text{(A.45)}$$

$$U\sigma^- U^\dagger = -i\sigma^+. \quad \text{(A.46)}$$

and thus finally

$$H = \hbar\omega_c \hat{a}^\dagger \hat{a} + \frac{\hbar\omega_{01}}{2}\sigma^z + \hbar g(\hat{a}\sigma^+ + \hat{a}^\dagger\sigma^-). \quad \text{(A.47)}$$

Appendix B
Semi-Infinite Transmission Lines, Dissipation and Input/Output Theory

This appendix is based on material presented in (Clerk *et al.*, 2010).

So far we have studied transmission line resonators which contain discrete standing wave resonance. We turn now to the case of infinite and semi-infinite transmission lines where we will deal with traveling waves rather than standing waves. In order to control the state of quantum bits we will want to send control pulses down a transmission line to the qubit. However opening up a port into the qubit to allow control signals in can also allow quantum and thermal noise to also enter. Such noises can dephase the coherent superpositions of qubits and also permit the qubits to decay by spontaneously emitting energy out the port and into the transmission line.

Another reason for studying the case of traveling waves in semi-infinite transmission lines is the following. In addition to controlling qubits by sending pulses down transmission lines, we may also wish to *m*easure the state of a qubit by sending microwave pulses down a transmission line and seeing out the reflected pulse is modified according to the state of the qubit. Thus we also need to understand continuum scattering theory for microwaves and how to relate the properties of the reflected wave to those of the incident wave and of the system from which they are reflecting.

You might think that since a transmission line is made of purely reactive elements, it cannot dissipate energy. If however it is semi-infinite in length, then a wave launched at one end carries away energy and never returns. As usual in studying irreversible behavior, there is a subtle order of limits here. If time goes to infinity before the transmission line length goes to infinity then there is no dissipation. In the opposite order of limits, there is dissipation because the waves travel away and never have time to reach the end of the transmission line and reflect back. We will in fact see that a semi-infinite transmission line acts just like a resistor with resistance equal to its characteristic impedance $R = Z_{\rm c} = \sqrt{\ell/c}$. Remarkably however because the transmission line is made of purely reactive elements we know, as we have already seen, how to treat it quantum mechanically. Hence we will be able to develop a fully quantum theory of a dissipative resistor (Caldeira and Leggett, 1983).

It is useful to start with a classical model considering as before a coaxial transmission line modeled as a perfectly conducting wire with inductance per unit length of ℓ and capacitance to ground per unit length c as shown in Fig. B.1. If the voltage

at position x at time t is $V(x,t)$, then the charge density is $q(x,t) = cV(x,t)$. By charge conservation the current I and the charge density are related by the continuity equation

$$\partial_t q + \partial_x I = 0. \tag{B.1}$$

The constitutive relation (essentially Newton's law) gives the acceleration of the charges

$$\ell \partial_t I = -\partial_x V. \tag{B.2}$$

We can decouple Eqs. (B.1) and (B.2) by introducing left and right propagating modes

$$V(x,t) = [V^{\rightarrow} + V^{\leftarrow}] \tag{B.3}$$

$$I(x,t) = \frac{1}{Z_{\rm c}}[V^{\rightarrow} - V^{\leftarrow}]. \tag{B.4}$$

In terms of the left and right propagating modes, Eqs. (B.1) and B.2 become

$$v_{\rm p}\partial_x V^{\rightarrow} + \partial_t V^{\rightarrow} = 0 \tag{B.5}$$

$$v_{\rm p}\partial_x V^{\leftarrow} - \partial_t V^{\leftarrow} = 0 \tag{B.6}$$

where $v_{\rm p} \equiv 1/\sqrt{\ell c}$ is the wave phase velocity. These equations have solutions which propagate by uniform translation without changing shape since the line is (in the present model) dispersionless

$$V^{\rightarrow}(x,t) = V_{\rm out}(t - \frac{x}{v_{\rm p}}) \tag{B.7}$$

$$V^{\leftarrow}(x,t) = V_{\rm in}(t + \frac{x}{v_{\rm p}}), \tag{B.8}$$

where $V_{\rm in}$ and $V_{\rm out}$ are *arbitrary* functions of their arguments. For an infinite transmission line, $V_{\rm out}$ and $V_{\rm in}$ are completely independent. However for the case of a semi-infinite line terminated at $x = 0$ (say) by some system S, these two solutions are not independent, but rather related by the boundary condition imposed by the system. We have

$$V(x=0,t) = [V_{\rm out}(t) + V_{\rm in}(t)] \tag{B.9}$$

$$I(x=0,t) = \frac{1}{Z_{\rm c}}[V_{\rm out}(t) - V_{\rm in}(t)], \tag{B.10}$$

from which we may eliminate $V(x=0,t)$ to derive the crucially important 'input-output' relation

$$V_{\rm out}(t) = V_{\rm in}(t) + Z_{\rm c} I(x=0,t). \tag{B.11}$$

The first term on the RHS is simply the direct reflection of the input wave, while the second term represents waves radiated into the transmission line by current injected by the system S.

If the system under study is just an open circuit so that $I(x=0,t) = 0$, then $V_{\rm out} = V_{\rm in}$, meaning that the outgoing wave is simply the result of the incoming wave

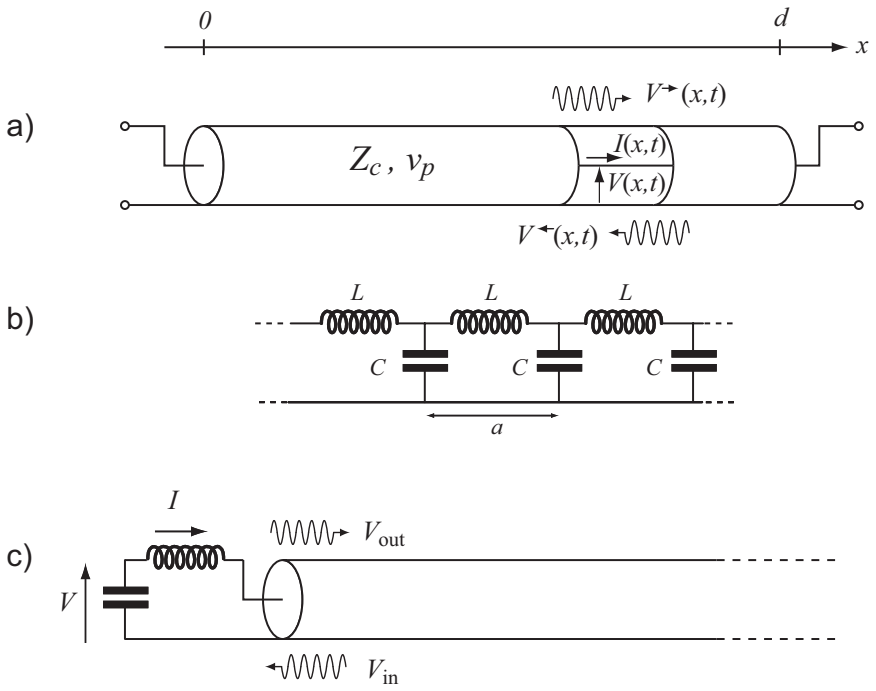

Fig. B.1 a) Coaxial transmission line, indicating voltages and currents as defined in the main text. b) Lumped element representation of a transmission line with capacitance per unit length $c = C/a$ and inductance per unit length $\ell = L/a$. c) Discrete LC resonator terminating a transmission line.

reflecting from the open circuit termination. In general however, there is an additional outgoing wave radiated by the current I that is injected by the system dynamics into the line. In the absence of an incoming wave we have

$$V(x = 0, t) = Z_{\text{c}} I(x = 0, t), \tag{B.12}$$

indicating that the transmission line acts as a simple resistor which, instead of dissipating energy by Joule heating, carries the energy away from the system as propagating waves. As noted above, the fact that the line can dissipate energy despite containing only purely reactive elements is a consequence of its infinite extent. One must be careful with the order of limits, taking the length to infinity *before* allowing time to go to infinity. In this way the outgoing waves never reach the far end of the transmission line and reflect back. Since this is a conservative Hamiltonian system, we will be able to quantize these waves and make a quantum theory of resistors (Caldeira and Leggett, 1983). The net power flow carried to the right by the line is

$$P = \frac{1}{Z_{\text{c}}}[V_{\text{out}}^2(t) - V_{\text{in}}^2(t)]. \tag{B.13}$$

The fact that the transmission line presents a dissipative impedance to the system means that it causes damping of the system. It also however opens up the possibility of controlling the system via the input field which partially determines the voltage driving the system. From this point of view it is convenient to eliminate the output field by writing the voltage as

$$V(x=0,t) = 2V_{\rm in}(t) + Z_{\rm c} I(x=0,t). \tag{B.14}$$

As we will discuss in more detail below, the first term drives the system and the second damps it. From Eq. (B.11) we see that measurement of the outgoing field can be used to determine the current $I(x=0,t)$ injected by the system into the line and hence to infer the system dynamics that results from the input drive field.

The great benefit of Eq. (B.14) is the following. If the system S is coupled to the transmission line through a capacitor, then the coupling Hamiltonian can be expressed in terms of the voltage at the end $V(x=0,t)$. By eliminating $V_{\rm out}$ we can see how the system is driven by $V_{\rm in}$ and damped by $Z_{\rm c} I(x=0,t)$. This classical result will be helpful in understanding the closely analogous quantum expressions which will be derived further below in a rather different manner.

As a simple classical example, consider the system consisting of an LC resonator shown in Fig. (B.1 c). This can be viewed as a simple harmonic oscillator whose coordinate Q is the charge on the capacitor plate (on the side connected to L_0). The current $I(x=0,t) = \dot{Q}$ plays the role of the velocity of the oscillator. The equation of motion for the oscillator is readily obtained from

$$Q = C_0[-V(x=0^+,t) - L_0 \dot{I}(x=0^+,t)]. \tag{B.15}$$

Using Eq. (B.14) we obtain a harmonic oscillator damped by the transmission line and driven by the incoming waves

$$\ddot{Q} = -\Omega_0^2 Q - \kappa \dot{Q} - \frac{2}{L_0} V_{\rm in}(t), \tag{B.16}$$

where the resonant frequency is $\Omega_0^2 \equiv 1/\sqrt{L_0 C_0}$. Note that the term $Z_{\rm c} I(x=0,t)$ in Eq. (B.14) results in the linear viscous damping rate $\kappa \equiv Z_{\rm c}/L_0$.

If we solve the equation of motion of the oscillator, we can predict the outgoing field. In the present instance of a simple oscillator we have a particular example of the general case where the system responds linearly to the input field. We can characterize any such system by a complex, frequency dependent impedance $Z[\omega]$ defined by

$$Z[\omega] = -\frac{V(x=0,\omega)}{I(x=0,\omega)}. \tag{B.17}$$

Note the peculiar minus sign which results from our definition of positive current flowing to the right (out of the system and into the transmission line). Using Eqs. (B.9, B.10) and Eq. (B.17) we have

$$V_{\rm out}[\omega] = r[\omega] V_{\rm in}[\omega], \tag{B.18}$$

where the reflection coefficient r is determined by the impedance mismatch between the system and the line and is given by the well known result

$$r[\omega] = \frac{Z[\omega] - Z_c}{Z[\omega] + Z_c}. \tag{B.19}$$

If the system is constructed from purely reactive (i.e. lossless) components, then $Z[\omega]$ is purely imaginary and the reflection coefficient obeys $|r| = 1$ which is consistent with Eq. (B.13) and the energy conservation requirement of no net power flow into the lossless system. For example, for the series LC oscillator we have been considering, we have

$$Z[\omega] = \frac{1}{j\omega C_0} + j\omega L_0, \tag{B.20}$$

where, to make contact with the usual electrical engineering sign conventions, we have used $j = -i$. If the damping κ of the oscillator induced by coupling it to the transmission line is small, the quality factor of the resonance will be high and we need only consider frequencies near the resonance frequency $\Omega_0 \equiv 1/\sqrt{L_0 C_0}$ where the impedance has a zero. In this case we may approximate

$$Z[\omega] \approx \frac{2}{jC_0\Omega_0^2}[\Omega_0 - \omega] = 2jL_0(\omega - \Omega_0) \tag{B.21}$$

which yields for the reflection coefficient

$$r[\omega] = \frac{\omega - \Omega_0 + j\kappa/2}{\omega - \Omega_0 - j\kappa/2} \tag{B.22}$$

showing that indeed $|r| = 1$ and that the phase of the reflected signal winds by 2π upon passing through the resonance. [1]

Turning to the more general case where the system also contains lossy elements, one finds that $Z[\omega]$ is no longer purely imaginary, but has a real part satisfying $\mathrm{Re}\, Z[\omega] > 0$. This in turn implies via Eq. (B.19) that $|r| < 1$. In the special case of impedance matching $Z[\omega] = Z_c$, all the incident power is dissipated in the system and none is reflected. The other two limits of interest are open circuit termination with $Z = \infty$ for which $r = +1$ and short circuit termination $Z = 0$ for which $r = -1$.

Finally, if the system also contains an active device which has energy being pumped into it from a separate external source, it may under the right conditions be described by an effective *negative* resistance $\mathrm{Re}\, Z[\omega] < 0$ over a certain frequency range. Eq. (B.19) then gives $|r| \geq 1$, implying $|V_{\mathrm{out}}| > |V_{\mathrm{in}}|$. Our system will thus act like the one-port reflection amplifier discussed in great detail in Ref. (Clerk *et al.*, 2010).

B.0.1 Quantum Input-output theory for a driven cavity

The results from the previous section can be more formally derived in a full quantum theory of a cavity driven by an external coherent source. The theory relating the drive,

[1] For the case of resonant *transmission* through a symmetric cavity, the phase shift only winds by π.

the cavity and the outgoing waves radiated by the cavity is known as input-output theory and the classical description was presented in Appendix B. The present quantum discussion closely follows standard references on the subject (Walls and Milburn, 1994; Yurke, 1984; Yurke and Denker, 1984). The crucial feature that distinguishes such an approach from many other treatments of quantum-dissipative systems is the goal of keeping the bath modes instead of tracing them out. This is obviously necessary for the situations we have in mind, where the output field emanating from the cavity contains the information acquired during a measurement of the system coupled to the cavity. As we learned from the classical treatment, we can eliminate the outgoing waves in favor of a damping term for the system. However we can recover the solution for the outgoing modes completely from the solution of the equation of motion of the damped system being driven by the incoming waves.

In order to drive the cavity we must partially open one of its ports which exposes the cavity both to the external drive and to the vacuum noise outside which permits energy in the cavity to leak out into the surrounding bath. We will formally separate the degrees of freedom into internal cavity modes and external bath modes. Strictly speaking, once the port is open, these modes are not distinct and we only have 'the modes of the universe' (Lang *et al.*, 1973; Gea-Banacloche *et al.*, 1990*a*; Gea-Banacloche *et al.*, 1990*b*). However for high Q cavities, the distinction is well-defined and we can model the decay of the cavity in terms of a spontaneous emission process in which an internal boson is destroyed and an external bath boson is created. We assume a single-sided cavity. For a high Q cavity, this physics is accurately captured in the following Hamiltonian

$$\hat{H} = \hat{H}_{\rm sys} + \hat{H}_{\rm bath} + \hat{H}_{\rm int}. \tag{B.23}$$

The bath Hamiltonian is

$$\hat{H}_{\rm bath} = \sum_q \hbar\omega_q \hat{b}_q^\dagger \hat{b}_q \tag{B.24}$$

where q labels the quantum numbers of the independent harmonic oscillator bath modes obeying

$$[\hat{b}_q, \hat{b}_{q'}^\dagger] = \delta_{q,q'}. \tag{B.25}$$

Note that since the bath terminates at the system, there is no translational invariance, the normal modes are standing not running waves, and the quantum numbers q are not necessarily wave vectors.

The coupling Hamiltonian is (within the rotating wave approximation)

$$\hat{H}_{\rm int} = -i\hbar \sum_q \left[f_q \hat{a}^\dagger \hat{b}_q - f_q^* \hat{b}_q^\dagger \hat{a} \right]. \tag{B.26}$$

For the moment we will leave the system (cavity) Hamiltonian to be completely general, specifying only that it consists of a single degree of freedom (i.e. we concentrate on only a single resonance of the cavity with frequency $\omega_{\rm c}$) obeying the usual bosonic commutation relation

$$[\hat{a}, \hat{a}^\dagger] = 1. \tag{B.27}$$

(N.B. this does not imply that it is a harmonic oscillator. We will consider both linear and non-linear cavities.) Note that the most general linear coupling to the bath modes

would include terms of the form $\hat{b}_q^\dagger \hat{a}^\dagger$ and $\hat{b}_q a$ but these are neglected within the rotating wave approximation because in the interaction representation they oscillate at high frequencies and have little effect on the dynamics.

The Heisenberg equation of motion (EOM) for the bath variables is

$$\dot{\hat{b}}_q = \frac{i}{\hbar}[\hat{H}, \hat{b}_q] = -i\omega_{\rm q}\hat{b}_q + f_q^* \hat{a} \tag{B.28}$$

We see that this is simply the EOM of a harmonic oscillator driven by a forcing term due to the motion of the cavity degree of freedom. Since this is a linear system, the EOM can be solved exactly. Let $t_0 < t$ be a time in the distant past before any wave packet launched at the cavity has reached it. The solution of Eq. (B.28) is

$$\hat{b}_q(t) = e^{-i\omega_{\rm q}(t-t_0)}\hat{b}_q(t_0) + \int_{t_0}^{t} d\tau\, e^{-i\omega_{\rm q}(t-\tau)} f_q^*\, \hat{a}(\tau). \tag{B.29}$$

The first term is simply the free evolution of the bath while the second represents the waves radiated by the cavity into the bath.

The EOM for the cavity mode is

$$\dot{\hat{a}} = \frac{i}{\hbar}[\hat{H}_{\rm sys}, \hat{a}] - \sum_q f_q \hat{b}_q. \tag{B.30}$$

Substituting Eq. (B.29) into the last term above yields

$$\sum_q f_q \hat{b}_q = \sum_q f_q e^{-i\omega_{\rm q}(t-t_0)}\hat{b}_q(t_0)$$
$$+ \sum_q |f_q|^2 \int_{t_0}^{t} d\tau\, e^{-i(\omega_{\rm q}-\omega_{\rm c})(t-\tau)}[e^{+i\omega_{\rm c}(\tau-t)}\hat{a}(\tau)], \tag{B.31}$$

where the last term in square brackets is a slowly varying function of τ. To simplify our result, we note that if the cavity system were a simple harmonic oscillator of frequency $\omega_{\rm c}$ then the decay rate from the $n = 1$ single photon excited state to the $n = 0$ ground state would be given by the following Fermi Golden Rule expression

$$\kappa(\omega_{\rm c}) = 2\pi \sum_q |f_q|^2 \delta(\omega_{\rm c} - \omega_{\rm q}). \tag{B.32}$$

From this it follows that

$$\int_{-\infty}^{+\infty} \frac{d\nu}{2\pi} \kappa(\omega_{\rm c} + \nu) e^{-i\nu(t-\tau)} = \sum_q |f_q|^2 e^{-i(\omega_{\rm q}-\omega_{\rm c})(t-\tau)}. \tag{B.33}$$

We now make the Markov approximation which assumes that $\kappa(\nu) = \kappa$ is a constant over the range of frequencies relevant to the cavity so that Eq. (B.33) may be represented as

$$\sum_q |f_q|^2 e^{-i(\omega_{\rm q}-\omega_{\rm c})(t-\tau)} = \kappa\delta(t-\tau). \tag{B.34}$$

Using

$$\int_{-\infty}^{x_0} dx\, \delta(x - x_0) = \frac{1}{2} \tag{B.35}$$

we obtain for the cavity EOM

$$\dot{\hat{a}} = \frac{i}{\hbar}[\hat{H}_{\rm sys}, \hat{a}] - \frac{\kappa}{2}\hat{a} - \sum_q f_q e^{-i\omega_{\rm q}(t-t_0)}\hat{b}_q(t_0). \tag{B.36}$$

The second term came from the part of the bath motion representing the wave radiated by the cavity and, within the Markov approximation, has become a simple linear damping term for the cavity mode. Note the important factor of 2. The amplitude decays at half the rate of the intensity (the energy decay rate κ).

Within the spirit of the Markov approximation it is further convenient to treat $f \equiv \sqrt{|f_q|^2}$ as a constant and define the density of states (also taken to be a constant) by

$$\rho = \sum_q \delta(\omega_{\rm c} - \omega_{\rm q}) \tag{B.37}$$

so that the Golden Rule rate becomes

$$\kappa = 2\pi f^2 \rho. \tag{B.38}$$

We can now define the so-called 'input mode'

$$\hat{b}_{\rm in}(t) \equiv \frac{1}{\sqrt{2\pi\rho}} \sum_q e^{-i\omega_{\rm q}(t-t_0)}\hat{b}_q(t_0)\,. \tag{B.39}$$

corresponding to the initial pulse propagating towards the cavity. We finally have for the cavity EOM

$$\dot{\hat{a}} = \frac{i}{\hbar}[\hat{H}_{\rm sys}, \hat{a}] - \frac{\kappa}{2}\hat{a} - \sqrt{\kappa}\,\hat{b}_{\rm in}(t). \tag{B.40}$$

Note that when a wave packet is launched from the bath towards the cavity, causality prevents it from knowing about the cavity's presence until it reaches the cavity. Hence the input mode evolves freely as if the cavity were not present until the time of the collision at which point it begins to drive the cavity. Since $\hat{b}_{\rm in}$(t) evolves under the free bath Hamiltonian and acts as the driving term in the cavity EOM, we interpret it physically as the input mode. Eq. (B.40) is the quantum analog of the classical equation (B.16), for our previous example of an LC-oscillator driven by a transmission line. The latter would also have been first order in time if we had worked with the complex amplitude A instead of the coordinate Q.

Eq. (B.39) for the input mode contains a time label just as in the interaction representation. However it is best interpreted as simply labeling the particular linear combination of the bath modes which is coupled to the system at time t. Some authors even like to think of the bath modes as non-propagating while the cavity flies along the bath (taken to be 1D) at a velocity v. The system then only interacts briefly with the local mode positioned at $x = vt$ before moving on and interacting with the next local bath mode. We will elaborate on this view further at the end of this subsection.

The expression for the power $P_{\rm in}$ (energy per time) impinging on the cavity depends on the normalization chosen in our definition of $\hat{b}_{\rm in}$. It can be obtained, for example, by imagining the bath modes $\hat{b}_q$ to live on a one-dimensional waveguide with propagation velocity v and length L (using periodic boundary conditions). In that case we have to sum over all photons to get the average power flowing through a cross-section of the waveguide, $P_{\rm in} = \sum_q \hbar\omega_q (v_p/L) \left\langle \hat{b}_q^\dagger \hat{b}_q \right\rangle$. Inserting the definition for $\hat{b}_{\rm in}$, Eq. (B.39), the expression for the input power carried by a monochromatic beam at frequency ω is

$$P_{\rm in}(t) = \hbar\omega \left\langle \hat{b}_{\rm in}^\dagger(t) \hat{b}_{\rm in}(t) \right\rangle \tag{B.41}$$

Note that this has the correct dimensions due to our choice of normalization for $\hat{b}_{\rm in}$ (with dimensions $\sqrt{\omega}$). In the general case, an integration over frequencies is needed (as will be discussed further below). An analogous formula holds for the power radiated by the cavity, to be discussed now.

The output mode $\hat{b}_{\rm out}(t)$ is radiated into the bath and evolves freely after the system interacts with $\hat{b}_{\rm in}(t)$. If the cavity did not respond at all, then the output mode would simply be the input mode reflected off the cavity mirror. If the mirror is partially transparent then the output mode will also contain waves radiated by the cavity (which is itself being driven by the input mode partially transmitted into the cavity through the mirror) and hence contains information about the internal dynamics of the cavity. To analyze this output field, let $t_1 > t$ be a time in the distant future after the input field has interacted with the cavity. Then we can write an alternative solution to Eq. (B.28) in terms of the final rather than the initial condition of the bath

$$\hat{b}_q(t) = e^{-i\omega_q(t-t_1)} \hat{b}_q(t_1) - \int_t^{t_1} d\tau\, e^{-i\omega_{\rm q}(t-\tau)} f_q^* \hat{a}(\tau). \tag{B.42}$$

Note the important minus sign in the second term associated with the fact that the time t is now the lower limit of integration rather than the upper as it was in Eq. (B.29).

Defining

$$\hat{b}_{\rm out}(t) \equiv \frac{1}{\sqrt{2\pi\rho}} \sum_q e^{-i\omega_{\rm q}(t-t_1)} \hat{b}_q(t_1), \tag{B.43}$$

we see that this is simply the free evolution of the bath modes from the distant future (after they have interacted with the cavity) back to the present, indicating that it is indeed appropriate to interpret this as the outgoing field. Proceeding as before we obtain

$$\dot{\hat{a}} = \frac{i}{\hbar}[\hat{H}_{\rm sys}, \hat{a}] + \frac{\kappa}{2}\hat{a} - \sqrt{\kappa}\, \hat{b}_{\rm out}(t). \tag{B.44}$$

Subtracting Eq. (B.44) from Eq. (B.40) yields

$$\hat{b}_{\rm out}(t) = \hat{b}_{\rm in}(t) + \sqrt{\kappa}\, \hat{a}(t) \tag{B.45}$$

which is consistent with our interpretation of the outgoing field as the reflected incoming field plus the field radiated by the cavity out through the partially reflecting mirror.

The above results are valid for any general cavity Hamiltonian. The general procedure is to solve Eq. (B.40) for $\hat{a}(t)$ for a given input field, and then solve Eq. (B.45) to obtain the output field. For the case of an empty cavity we can make further progress because the cavity mode is a harmonic oscillator

$$\hat{H}_{\rm sys} = \hbar\omega_{\rm c}\hat{a}^\dagger\hat{a}. \tag{B.46}$$

In this simple case, the cavity EOM becomes

$$\dot{\hat{a}} = -i\omega_{\rm c}\hat{a} - \frac{\kappa}{2}\hat{a} - \sqrt{\kappa}\,\hat{b}_{\rm in}(t). \tag{B.47}$$

Eq. (B.47) can be solved by Fourier transformation, yielding

$$\hat{a}[\omega] = -\frac{\sqrt{\kappa}}{i(\omega_{\rm c}-\omega)+\kappa/2}\,\hat{b}_{\rm in}[\omega] \tag{B.48}$$

$$= -\sqrt{\kappa}\chi_{\rm c}[\omega-\omega_{\rm c}]\hat{b}_{\rm in}[\omega] \tag{B.49}$$

and

$$\hat{b}_{\rm out}[\omega] = \frac{\omega-\omega_{\rm c}-i\kappa/2}{\omega-\omega_{\rm c}+i\kappa/2}\,\hat{b}_{\rm in}[\omega] \tag{B.50}$$

which is the result for the reflection coefficient quoted in Eq. (B.22). For brevity, here and in the following, we will sometimes use the susceptibility of the cavity, defined as

$$\chi_{\rm c}[\omega-\omega_{\rm c}] \equiv \frac{1}{-i(\omega-\omega_{\rm c})+\kappa/2} \tag{B.51}$$

For the case of steady driving on resonance where $\omega = \omega_{\rm c}$, the above equations yield

$$\hat{b}_{\rm out}[\omega] = \frac{\sqrt{\kappa}}{2}\hat{a}[\omega]. \tag{B.52}$$

In steady state, the incoming power equals the outgoing power, and both are related to the photon number inside the single-sided cavity by

$$P = \hbar\omega\left\langle \hat{b}^\dagger_{\rm out}(t)\hat{b}_{\rm out}(t)\right\rangle = \hbar\omega\frac{\kappa}{4}\left\langle \hat{a}^\dagger(t)\hat{a}(t)\right\rangle \tag{B.53}$$

Note that this does not coincide with the naive expectation, which would be $P = \hbar\omega\kappa\left\langle\hat{a}^\dagger\hat{a}\right\rangle$. The reason for this discrepancy is the the interference between the part of the incoming wave which is promptly reflected from the cavity and the field radiated by the cavity. The naive expression becomes correct after the drive has been switched off (where ignoring the effect of the incoming vacuum noise, we would have $\hat{b}_{\rm out} = \sqrt{\kappa}\hat{a}$). We note in passing that for a driven two-sided cavity with coupling constants κ_L and κ_R (where $\kappa = \kappa_L + \kappa_R$), the incoming power sent into the left port is related to the photon number by

$$P = \hbar\omega\kappa^2/(4\kappa_L)\left\langle\hat{a}^\dagger\hat{a}\right\rangle. \tag{B.54}$$

Here for $\kappa_L = \kappa_R$ the interference effect completely eliminates the reflected beam and we have in contrast to Eq. (B.53)

$$P = \hbar\omega \frac{\kappa}{2} \left\langle \hat{a}^\dagger \hat{a} \right\rangle . \tag{B.55}$$

Eq. (B.47) can also be solved in the time domain to obtain

$$\begin{aligned} \hat{a}(t) &= e^{-(i\omega_c + \kappa/2)(t-t_0)} \hat{a}(t_0) \\ &\quad - \sqrt{\kappa} \int_{t_0}^{t} d\tau \, e^{-(i\omega_c + \kappa/2)(t-\tau)} \hat{b}_{\rm in}(\tau). \end{aligned} \tag{B.56}$$

If we take the input field to be a coherent drive at frequency $\omega_L = \omega_c + \Delta$ so that its amplitude has a classical and a quantum part

$$\hat{b}_{\rm in}(t) = e^{-i\omega_L t} [\bar{b}_{\rm in} + \hat{\xi}(t)] \tag{B.57}$$

and if we take the limit $t_0 \to \infty$ so that the initial transient in the cavity amplitude has damped out, then the solution of Eq. (B.56) has the form with

$$\bar{a} = -\frac{\sqrt{\kappa}}{-i\Delta + \kappa/2} \bar{b}_{\rm in} \tag{B.58}$$

and (in the frame rotating at the drive frequency)

$$\hat{d}(t) = -\sqrt{\kappa} \int_{-\infty}^{t} d\tau \, e^{+(i\Delta - \kappa/2)(t-\tau)} \hat{\xi}(\tau). \tag{B.59}$$

Even in the absence of any classical drive, the input field delivers vacuum fluctuation noise to the cavity. Notice that from Eqs. (B.39, B.57)

$$\begin{aligned} [\hat{b}_{\rm in}(t), \hat{b}_{\rm in}^\dagger(t')] &= [\hat{\xi}(t), \hat{\xi}^\dagger(t')] \\ &= \frac{1}{2\pi\rho} \sum_q e^{-i(\omega_q - \omega_L)(t-t')} \\ &= \delta(t-t'). \end{aligned} \tag{B.60}$$

This is the operator equivalent of white noise. Using Eq. (B.56) in the limit $t_0 \to -\infty$ in Eq. (B.59) yields

$$\begin{aligned} [\hat{a}(t), \hat{a}^\dagger(t)] &= [\hat{d}(t), \hat{d}^\dagger(t)] \\ &= \kappa \int_{-\infty}^{t} d\tau \int_{-\infty}^{t} d\tau' \, e^{-(-i\Delta + \kappa/2)(t-\tau)} \\ &\quad e^{-(+i\Delta + \kappa/2)(t-\tau')} \delta(\tau - \tau') \\ &= 1 \end{aligned} \tag{B.61}$$

as is required for the cavity bosonic quantum degree of freedom. We can interpret this as saying that the cavity zero-point fluctuations arise from the vacuum noise that enters through the open port. We also now have a simple physical interpretation of the quantum noise in the number of photons in a driven cavity. It is due to the vacuum

noise which enters the cavity through the same ports that bring in the classical drive. The interference between the vacuum noise and the classical drive leads to the photon number fluctuations in the cavity.

In thermal equilibrium, $\hat{\xi}$ also contains thermal radiation. If the bath is being probed only over a narrow range of frequencies centered on ω_c (which we have assumed in making the Markov approximation) then we have to a good approximation (consistent with the above commutation relation)

$$\langle \hat{\xi}^\dagger(t)\hat{\xi}(t')\rangle = N\delta(t-t') \tag{B.62}$$

$$\langle \hat{\xi}(t)\hat{\xi}^\dagger(t')\rangle = (N+1)\delta(t-t') \tag{B.63}$$

where $N = n_B(\hbar\omega_c)$ is the thermal equilibrium occupation number of the mode at the frequency of interest. We can gain a better understanding of Eq. (B.62) by Fourier transforming it to obtain the spectral density

$$S[\omega] = \int_{-\infty}^{+\infty} dt\, \langle \hat{\xi}^\dagger(t)\hat{\xi}(t')\rangle e^{i\omega(t-t')} = N. \tag{B.64}$$

As mentioned previously, this dimensionless quantity is the spectral density that would be measured by a photomultiplier: it represents the number of thermal photons passing a given point per unit time per unit bandwidth. Equivalently the thermally radiated power in a narrow bandwidth B is

$$P = \hbar\omega NB. \tag{B.65}$$

One often hears the confusing statement that the noise added by an amplifier is a certain number N of photons ($N = 20$, say for a good cryogenic HEMT amplifier operating at 5 GHz). This means that the excess output noise (referred back to the input by dividing by the power gain) produces a flux of N photons per second in a 1 Hz bandwidth, or $10^6 N$ photons per second in 1 MHz of bandwidth.

We can gain further insight into input-output theory by using the following picture. The operator $\hat{b}_{in}(t)$ represents the classical drive plus vacuum fluctuations which are just about to arrive at the cavity. We will be able to show that the output field is simply the input field a short while later after it has interacted with the cavity. Let us consider the time evolution over a short time period Δt which is very long compared to the inverse bandwidth of the vacuum noise (i.e., the frequency scale beyond which the vacuum noise cannot be treated as constant due to some property of the environment) but very short compared to the cavity system's slow dynamics. In this circumstance it is useful to introduce the quantum Wiener increment

$$d\widehat{W} \equiv \int_t^{t+\Delta t} d\tau\, \hat{\xi}(\tau) \tag{B.66}$$

which obeys

$$[d\widehat{W}, d\widehat{W}^\dagger] = \Delta t. \tag{B.67}$$

In the interaction picture (in a displaced frame in which the classical drive has been removed) the Hamiltonian term that couples the cavity to the quantum noise of the environment is from Eq. (B.26)

$$\hat{V} = -i\hbar\sqrt{\kappa}(\hat{a}^\dagger\hat{\xi} - \hat{a}\hat{\xi}^\dagger). \tag{B.68}$$

Thus the time evolution operator (in the interaction picture) on the jth short time interval $[t_j, t_j + \Delta t]$ is

$$\hat{U}_j = e^{\sqrt{\kappa}(\hat{a}\, d\widehat{W}^\dagger - \hat{a}^\dagger\, d\widehat{W})} \tag{B.69}$$

Using this we can readily evolve the incoming temporal mode forward in time by a small step Δt

$$d\widehat{W}' = \hat{U}^\dagger d\widehat{W}\hat{U} \approx d\widehat{W} + \sqrt{\kappa}\Delta t\, \hat{a}. \tag{B.70}$$

Recall that in input-output theory we formally defined the outgoing field as the bath field far in the future propagated back (using the free field time evolution) to the present, which yielded

$$\hat{b}_{\rm out} = \hat{b}_{\rm in} + \sqrt{\kappa}\hat{a}. \tag{B.71}$$

Eq. (B.70) is completely equivalent to this. Thus we confirm our understanding that the incoming field is the bath temporal mode just before it interacts with the cavity and the outgoing field is the bath temporal mode just after it interacts with the cavity.

This leads to the following picture which is especially useful in the quantum trajectory approach to conditional quantum evolution of a system subject to weak continuous measurement (Gardiner *et al.*, 1992; Walls and Milburn, 1994). On top of the classical drive $\bar{b}_{\rm in}(t)$, the bath supplies to the system a continuous stream of "fresh" harmonic oscillators, each in their ground state (if $T = 0$). Each oscillator with its quantum fluctuation $d\widehat{W}$ interacts briefly for a period Δt with the system and then is disconnected to propagate freely thereafter, never interacting with the system again. Within this picture it is useful to think of the oscillators arrayed in an infinite stationary line and the cavity flying over them at speed $v_{\rm p}$ and touching each one for a time Δt.

Appendix C
Coupling a qubit to a linear black box

As we learned in Chapter 4, the transmon qubit is essentially a weakly anharmonic oscillator. In the limit of large Josephson energy and small charging energy ($E_J/E_C \gg 1$), the quantum fluctuations in the phase φ across the Josephson junction are small and we can ignore the fact that φ is a periodic variable. It is important to understand that this is a good approximation only in the limit that the charge dispersion enforced by the periodic boundary conditions on φ can be neglected. One way to make the charging energy small is to make the transmon islands large which makes the coupling of the transmon to the electromagnetic modes of the cavity large. We therefore do not want to treat this coupling as a perturbation since the presence of the transmon can significantly alter the cavity modes due to this strong coupling. It is very useful therefore to treat the harmonic part of the cavity plus qubit Hamiltonian exactly (Manucharyan *et al.*, 2007; Nigg *et al.*, 2012). We then simply have coupled harmonic oscillators whose spectrum is straightforward to understand. In the strong-coupling case, this harmonic oscillator basis can be very efficient for expressing the full Hamiltonian including the anharmonic part of the Hamiltonian. In certain situations if the anharmonicity is weak, we may be able to treat it analytically in low-order perturbation theory. Even if this is not the case, we have an efficient basis in which to numerically diagonalize the full Hamiltonian. This is particularly true when the cavity has many resonant modes. The mixing and renormalization of these modes by the qubit is largely taken care of by the exact treatment of the harmonic part of H and so we obtain faster convergence of the numerics in terms of the number of modes we need to keep and the number of quanta in each mode.

The simple harmonic oscillator approximation to the transmon Hamiltonian is given in Eq. (4.10). Let us imagine that we have included this effective LC oscillator in our 'black box' whose equivalent circuit is shown in Fig. (2.9a). The normal modes of the box include a qubit-like mode and many cavity-like modes coupled capacitively via the transmon 'antenna.' Note that the equivalent circuit describing the input admittance across the terminals of the Josephson junction is still precisely of the form shown in Fig. (2.9a). The coupling capacitor C_g and the junction capacitance C_J and inductance L_J do *not* appear explicitly in the circuit. Their values help control the resonance frequencies and characteristic impedances of the resonances (i.e. the values of the equivalent circuit elements), but these individual elements from the real circuit do not themselves explicitly appear in the equivalent circuit.

We now turn to the treatment of the anharmonicity. Using Eq. (2.180) the phase across the Josephson junction can be expressed in terms of the normal modes

$$\varphi = \frac{2e}{\hbar}\Phi = \sum_m \varphi_{\mathrm{ZPF}}^{(m)}(\hat{a}_m + \hat{a}_m^\dagger). \tag{C.1}$$

The Josephson energy is

$$U = -E_\mathrm{J}\cos\varphi = -E_\mathrm{J}\left\{1 - \frac{1}{2}\varphi^2 + \frac{1}{24}\varphi^4 + \dots\right\}. \tag{C.2}$$

The leading constant is irrelevant and we have already included the quadratic term in the harmonic part of the Hamiltonian. Hence the anharmonic part of the Hamiltonian analogous to Eq. (4.34) which we need to keep is

$$V = -E_\mathrm{J}\cos\varphi + E_\mathrm{J}\left\{1 - \frac{1}{2}\varphi^2\right\} \approx -E_\mathrm{J}\frac{1}{24}\varphi^4 + \dots \tag{C.3}$$

We will make the approximation (valid for large $E_\mathrm{J}/E_\mathrm{C}$, i.e. small φ_{ZPF}) of keeping only the quartic term[1]

$$V \approx -E_\mathrm{J}\frac{1}{24}\left\{\sum_m \varphi_{\mathrm{ZPF}}^{(m)}(\hat{a}_m + \hat{a}_m^\dagger)\right\}^4. \tag{C.4}$$

Recall from examination of the transmon anharmonicity that the small parameter in this expansion is E_C, not E_J, because the quantum fluctuations φ_{ZPF} are inversely proportional to E_J.

In general we will have to treat this expression numerically, but we can immediately make some general remarks about the effect of V by normal ordering the terms and making the rotating wave approximation. We see that there will be quadratic terms of the form $\hat{b}_m^\dagger\hat{b}_m$ generated which shift the frequencies of the 'bare' modes and other quadratic terms of the form $\hat{b}_j^\dagger\hat{b}_k$ which will mix modes that are close in frequency relative to E_C. More significantly there will be 'self-Kerr' terms of the form $\hat{b}_j^\dagger\hat{b}_j^\dagger\hat{b}_j\hat{b}_j$ which make the modes anharmonic and 'cross-Kerr' terms of the form $\hat{b}_j^\dagger\hat{b}_j\hat{b}_k^\dagger\hat{b}_k$. The qubit state-dependent shift of the cavity frequency appears here as a cross-Kerr term between the qubit and the cavity mode(s). This gives us a nice physical picture of how to think about the modes even if we need to numerics to obtain quantitative accuracy.

[1] It is important to note however that even if we kept all the terms in the expansion of V we would still not have the exact result because we are still neglecting the charge dispersion associated with the periodic boundary conditions on φ.

Appendix D
Feynman Disentangling Theorem

The Feynman 'disentangling theorem' states that the exponential of the sum of two operators A and B can be simplified in the following manner

$$e^{(A+B)} = e^A e^B e^{\frac{1}{2}[B,A]}, \tag{D.1}$$

provided that the commutator $[B, A]$ itself commutes with both A and B.

Here is a simple proof that begins with the following lemma. Let us define

$$\tilde{B}(\lambda) = e^{\lambda A} B e^{-\lambda A}, \tag{D.2}$$

where λ is a variable parameter. This object obeys the differential equation

$$\frac{d\tilde{B}}{d\lambda} = e^{\lambda A}[A, B]e^{-\lambda A} = [A, B]. \tag{D.3}$$

This has solution

$$\tilde{B}(\lambda) = B + \lambda[A, B]. \tag{D.4}$$

With this lemma in hand, consider now

$$V(\lambda) \equiv e^{\lambda(A+B)} - e^{\lambda A} e^{\lambda B} e^{\frac{1}{2}\lambda^2[B,A]}. \tag{D.5}$$

Clearly $V(0) = 0$. If we can prove $V(1)$ also vanishes, then the theorem is proved. Consider the differential equation

$$\frac{dV}{d\lambda} = (A + B)V - AV - e^{\lambda A} B e^{\lambda B} e^{\frac{1}{2}\lambda^2[B,A]} + \lambda[B, A]V \tag{D.6}$$

$$= BV - \tilde{B}(\lambda)V + \lambda[B, A]V = 0, \tag{D.7}$$

where the last equality follows from our first lemma. The solution of this equation is of course

$$V(\lambda) = V(0) = 0, \tag{D.8}$$

which proves our theorem.

Appendix E
Coherent States

A coherent state with complex amplitude α has the defining property of being an eigenstate of the lowering operator

$$\hat{a}|\alpha\rangle = \alpha|\alpha\rangle, \tag{E.1}$$

from which it follows that

$$\langle\alpha|\hat{a}^\dagger\hat{a}|\alpha\rangle = |\alpha|^2 = \bar{N}, \tag{E.2}$$

where $\bar{N}$ is the mean photon number in the coherent state. It is important to note that a coherent state is *not* an eigenstate of the raising operator. We have

$$\langle\alpha|\hat{a}^\dagger = \langle\alpha|\alpha^*, \tag{E.3}$$

but

$$\hat{a}^\dagger|\alpha\rangle \neq \alpha^*|\alpha\rangle. \tag{E.4}$$

Exercise E.1 A common source of confusion is to fail to understand the distinction between $e^{i\varphi}|\alpha\rangle$ and $|e^{i\varphi}\alpha\rangle$. If you compute $\langle\hat{a}\rangle$ for the two cases you will see the difference.

It is readily verified that Eq. (E.1) is solved by the unitary displacement of the vacuum state

$$|\alpha\rangle = e^{(\alpha\hat{a}^\dagger - \alpha^*\hat{a})}|0\rangle. \tag{E.5}$$

To see this consider

$$\hat{a}|\alpha\rangle = e^{(\alpha\hat{a}^\dagger - \alpha^*\hat{a})}\left\{e^{-(\alpha\hat{a}^\dagger - \alpha^*\hat{a})}\hat{a}e^{(\alpha\hat{a}^\dagger - \alpha^*\hat{a})}\right\}|0\rangle. \tag{E.6}$$

Using Eq. (D.4) the term in curly brackets becomes

$$\tilde{a} \equiv \hat{a} + \alpha, \tag{E.7}$$

which from which Eq. (E.1) readily follows.

Using the Feynman disentangling theorem D Eq. (E.5) can be written in normal-ordered form with the annhilation operators to the right of the creation operators

$$|\alpha\rangle = e^{+\alpha\hat{a}^\dagger}e^{-\alpha^*\hat{a}}e^{\frac{1}{2}[-\alpha^*\hat{a},+\alpha\hat{a}^\dagger]}|0\rangle \tag{E.8}$$

$$= e^{-\frac{1}{2}|\alpha|^2}e^{+\alpha\hat{a}^\dagger}|0\rangle \tag{E.9}$$

$$= e^{-\frac{1}{2}|\alpha|^2}\sum_{n=0}\frac{\alpha^n}{\sqrt{n!}}|n\rangle. \tag{E.10}$$

From this result it is straightforward to derive the overlap of two coherent states

$$\langle\beta|\alpha\rangle = e^{-\frac{1}{2}\left(|\alpha|^2+|\beta|^2-2\alpha\beta^*\right)}. \tag{E.11}$$

The following special case appears in the theory of decoherence in the dispersive readout of a qubit

$$\langle e^{+i\theta_0}\alpha|e^{-i\theta_0}\alpha\rangle = e^{-\bar{N}(1-e^{-2i\theta_0})} = e^{-i\bar{N}\sin 2\theta_0}e^{-\bar{N}(1-\cos 2\theta_0)}. \tag{E.12}$$

Let us now examine the properties of the quadrature amplitudes

$$\hat{X} \equiv \frac{\hat{a}+\hat{a}^\dagger}{2} \tag{E.13}$$

$$\hat{Y} \equiv -i\frac{\hat{a}-\hat{a}^\dagger}{2} \tag{E.14}$$

which obey the commutation relation

$$\left[\hat{X},\hat{Y}\right] = \frac{i}{2}. \tag{E.15}$$

Let us define the projector onto the state with definite quadrature amplitude

$$P_X(x) = \delta(x-\hat{X}) \tag{E.16}$$

$$P_Y(y) = \delta(y-\hat{Y}). \tag{E.17}$$

Using the integral representation of the Dirac delta function we have

$$P_X(x) = \int_{-\infty}^{\infty}\frac{d\xi}{2\pi}\,e^{i\xi x}e^{-i\xi\hat{X}} \tag{E.18}$$

$$P_Y(y) = \int_{-\infty}^{\infty}\frac{d\xi}{2\pi}\,e^{i\xi y}e^{-i\xi\hat{Y}}. \tag{E.19}$$

Normal ordering the operators using the disentangling theorem yields

$$P_X(x) = \int_{-\infty}^{\infty}\frac{d\xi}{2\pi}\,e^{-\frac{\xi^2}{8}}e^{i\xi x}e^{-\frac{i}{2}\xi\hat{a}^\dagger}e^{-\frac{i}{2}\xi\hat{a}} \tag{E.20}$$

$$P_Y(y) = \int_{-\infty}^{\infty}\frac{d\xi}{2\pi}\,e^{-\frac{\xi^2}{8}}e^{i\xi y}e^{+\frac{1}{2}\xi\hat{a}^\dagger}e^{-\frac{1}{2}\xi\hat{a}}, \tag{E.21}$$

which allows us to readily compute the matrix elements of these projectors between two coherent states

$$\langle\beta|P_X(x)|\alpha\rangle = \int_{-\infty}^{\infty}\frac{d\xi}{2\pi}\,e^{-\frac{\xi^2}{8}}e^{i\xi x}e^{-\frac{i}{2}\xi\beta^*}e^{-\frac{i}{2}\xi\alpha}\langle\beta|\alpha\rangle \tag{E.22}$$

$$= \sqrt{\frac{2}{\pi}}e^{-2\left[x-\frac{\beta^*+\alpha}{2}\right]^2}e^{-\frac{1}{2}\left(|\alpha|^2+|\beta|^2-2\alpha\beta^*\right)} \tag{E.23}$$

$$\langle\beta|P_Y(y)|\alpha\rangle = \int_{-\infty}^{\infty}\frac{d\xi}{2\pi}\,e^{-\frac{\xi^2}{8}}e^{i\xi y}e^{+\frac{1}{2}\xi\beta^*}e^{-\frac{1}{2}\xi\alpha}\langle\beta|\alpha\rangle \tag{E.24}$$

$$= \sqrt{\frac{2}{\pi}}e^{-2\left[y-i\frac{\beta^*-\alpha}{2}\right]^2}e^{-\frac{1}{2}\left(|\alpha|^2+|\beta|^2-2\alpha\beta^*\right)}. \tag{E.25}$$

For the case $\beta = \alpha$, we recognize here the (displaced version of the) gaussian distribution of position and momentum in the ground state of the harmonic oscillator. For the particular case associated with the dispersive readout of a qubit we have (for α real)

$$\langle e^{-i\theta_0\sigma^z}\alpha|P_X(x)|e^{-i\theta_0\sigma^z}\alpha\rangle = \sqrt{\frac{2}{\pi}}e^{-2\left[x-\sqrt{\bar{N}}\cos\theta_0\right]^2} \tag{E.26}$$

$$\langle e^{-i\theta_0\sigma^z}\alpha|P_Y(y)|e^{-i\theta_0\sigma^z}\alpha\rangle = \sqrt{\frac{2}{\pi}}e^{-2\left[y+\sqrt{\bar{N}}\sin\theta_0\sigma^z\right]^2} \tag{E.27}$$

$$\langle e^{i\theta_0}\alpha|P_X(x)|e^{-i\theta_0}\alpha\rangle = \sqrt{\frac{2}{\pi}}e^{-2\left[x-\sqrt{\bar{N}}\cos\theta_0+i\sqrt{\bar{N}}\sin\theta_0\right]^2}e^{\bar{N}\left(e^{-2i\theta_0}-1\right)} \tag{E.28}$$

$$\langle e^{i\theta_0}\alpha|P_Y(y)|e^{-i\theta_0}\alpha\rangle = \sqrt{\frac{2}{\pi}}e^{-2[y]^2}e^{\bar{N}\left(e^{-2i\theta_0}-1\right)}. \tag{E.29}$$

References

Aassime, A., Johansson, G., Wendin, G., Schoelkopf, R. J., and Delsing, P. (2001). Radio-frequency single-electron transistor as readout device for qubits: Charge sensitivity and backaction. *Phys. Rev. Lett.*, **86**, 3376–3379.

Aichhorn, Markus, Hohenadler, Martin, Tahan, Charles, and Littlewood, Peter B. (2008). Quantum fluctuations, temperature, and detuning effects in solid-light systems. *Phys. Rev. Lett.*, **100**, 216401.

Al-Saidi, W. A. and Stroud, D. (2001). Eigenstates of a small Josephson junction coupled to a resonant cavity. *Phys. Rev. B*, **65**, 014512.

Ambegaokar, V. and Baratoff, A. (1963). Tunneling between superconductors. *Phys. Rev. Lett.*, **10**, 486. Erratum: *Phys. Rev. Lett.* **11**, 104 (1963).

Angelakis, Dimitris G., Santos, Marcelo Franca, and Bose, Sougato (2007, Sep). Photon-blockade-induced mott transitions and xy spin models in coupled cavity arrays. *Phys. Rev. A*, **76**, 031805.

Ansmann, Markus, Wang, H., Bialczak, Radoslaw C., Hofheinz, Max, Lucero, Erik, Neeley, M., O'Connell, A. D., Sank, D., Weides, M., Wenner, J., Cleland, A. N., and Martinis, John M. (2009). Violation of bell's inequality in Josephson phase qubits. *Nature*, **461**, 504–506.

Ashhab, S., Johansson, J. R., Zagoskin, A. M., and Nori, Franco (2009). Single-artificial-atom lasing using a voltage-biased superconducting charge qubit. *NJP*, **11**, 023030.

Astafiev, O., Inomata, K., Niskanen, A. O., Yamamoto, T., Pashkin, Yu. A., Nakamura, Y., and Tsai, J. S. (2007). Single artificial-atom lasing. *Nature*, **449**, 588–590.

Astafiev, O., Zagoskin, A.M., A.A. Abdumalikov, Jr., Pashkin, Yu. A., Yamamoto, T., Inomata, K., Nakamura, Y., and Tsai, J.S. (2010). Resonance fluorescence of a single artificial atom. *Science*, **327**, 840–843.

Averin, D.V., Zorin, A.B., and Likharev, K.K. (1985). Bloch oscillations in small Josephson junctions. *Sov. Phys. JETP*, **61**, 407.

Averin, D. V. and Bruder, C. (2003). Variable electrostatic transformer: Controllable coupling of two charge qubits. *Phys. Rev. Lett.*, **91**, 057003.

Barends, R., Kelly, J., Megrant, A., Sank, D., Jeffrey, E., Chen, Y., Yin, Y., annd J. Mutus, B. Chiaro, Neill, C., O'Malley, P., Roushan, P., Wenner, J., White, T. C., Cleland, A. N., and Martinis, John M. Coherent Josephson qubit suitable for scalable quantum integrated circuits. arXiv:1304.2322.

Baur, M., Fedorov, A., Steffen, L., Filipp, S., da Silva, M. P., and Wallraff, A. (2012, Jan). Benchmarking a quantum teleportation protocol in superconducting circuits using tomography and an entanglement witness. *Phys. Rev. Lett.*, **108**, 040502.

Baur, M., Filipp, S., Bianchetti, R., Fink, J.M., Göppl, M., Steffen, L., Leek, P.J., Blais, A., and Wallraff, A. (2009). Measurement of autler-townes and mollow tran-

sitions in a strongly driven superconducting qubit. *Phys. Rev. Lett.*, **102**, 243602.
Bergeal, N., Schackert, F., Metcalfe, M., Vijay, R., Manucharyan, V. E., Frunzio, L., Prober, D.E., Schoelkopf, R. J., Girvin, S. M., and Devoret, M. H. (2010*a*). Analog information processing at the quantum limit with a Josephson ring modulator. *Nature Physics*, **6**, 296–302.
Bergeal, N., Vijay, R., Manucharyan, V. E., Siddiqi, I., Schoelkopf, R. J., Girvin, S. M., and Devoret, M. H. (2010*b*). Phase-preserving amplification near the quantum limit with a Josephson ring modulator. *Nature*, **465**, 64–68.
Berkley, A. J., Xu, H., Ramos, R. C., Gubrud, M. A., Strauch, F. W., Johnson, P. R., Anderson, J. R., Dragt, A. J., Lobb, C. J., and Wellstood, F. C. (2003). Entangled Macroscopic Quantum States in Two Superconducting Qubits. *Science*, **300**, 1548–1550.
Bertet, P., Chiorescu, I., Burkard, G., Semba, K., Harmans, C. J. P. M., DiVincenzo, D. P., and Mooij, J. E. (2005). Dephasing of a superconducting qubit induced by photon noise. *Phys. Rev. Lett.*, **95**, 257002.
Bianchetti, R., Filipp, S., Baur, M., Fink, J. M., Lang, C., Steffen, L., Boissonneault, M., Blais, A., , and Wallraff, A. (2010). Control and tomography of a three level superconducting artificial atom. *Phys. Rev. Lett.*, **105**, 223601.
Birnbaum, K. M., Boca, A., Miller, R., Boozer, A. D., Northup, T. E., and Kimble, H. J. (2005). Photon blockade in an optical cavity with one trapped atom. *Nature*, **436**, 87–90.
Bishop, Lev S., Chow, J. M., Koch, Jens, Houck, A. A., Devoret, M. H., Thuneberg, E., Girvin, S. M., and Schoelkopf, R. J. (2009*a*). Nonlinear response of the vacuum Rabi resonance. *Nature Physics*, **5**, 105–109.
Bishop, Lev S, Tornberg, L, Price, D, Ginossar, E, Nunnenkamp, A, Houck, A A, Gambetta, J M, Koch, Jens, Johansson, G, Girvin, S M, and Schoelkopf, R J (2009*b*). Proposal for generating and detecting multi-qubit ghz states in circuit qed. *NJP*, **11**, 073040.
Blais, Alexandre, Huang, Ren-Shou, Wallraff, Andreas, Girvin, S. M., and Schoelkopf, R. J. (2004). Cavity quantum electrodynamics for superconducting electrical circuits: an architecture for quantum computation. *Phys. Rev. A*, **69**, 062320.
Blais, A., Maassen van den Brink, A., and Zagoskin, A. (2003). Tunable coupling of superconducting qubits. *Phys. Rev. Lett.*, **90**, 127901.
Boca, A, Miller, R, Birnbaum, KM, Boozer, AD, McKeever, J, and Kimble, HJ (2004). Observation of the vacuum Rabi spectrum for one trapped atom. *Phys. Rev. Lett.*, **93**, 233603.
Boissonneault, Maxime, Gambetta, J. M., and Blais, Alexandre (2008). Nonlinear dispersive regime of cavity QED: The dressed dephasing model. *Phys. Rev. A*, **77**, 060305.
Boissonneault, Maxime, Gambetta, J. M., and Blais, Alexandre (2009). Dispersive regime of circuit QED: Photon-dependent qubit dephasing and relaxation rates. *Phys. Rev. A*, **79**, 013819.
Bouchiat, V., Vion, D., Joyez, P., Esteve, D., and Devoret, M. H. (1998). Quantum coherence with a single cooper pair. *Phys. Scr.*, **T76**, 165.
Boulant, N., Ithier, G., Meeson, P., Nguyen, F., Vion, D., Esteve, D., Siddiqi, I.,

Vijay, R., Rigetti, C., Pierre, F., and Devoret, M. (2007). Quantum nondemolition readout using a Josephson bifurcation amplifier. *Phys. Rev. B*, **76**, 014525.

Bourassa, Jérôme, Gambetta, Jay M., Jr, Abdufarrukh A. Abdumalikov, Astafiev, Oleg, and Yasunobu Nakamura, Alexandre Blais (2009). Ultra-strong coupling regime of cavity qed with phase-biased flux qubits. *Phys. Rev. A*, **80**, 032109.

Bozyigit, D., Lang, C., Steffen, L., Fink, J.M., Eichler, C., Baur, M., Bianchetti, R., Leek, P.J., Filipp, S., da Silva, M.P., Blais, A., and Wallraff, A. (2011). Antibunching of microwave-frequency photons observed in correlation measurements using linear detectors. *Nature Physics*, **7**, 154–158.

Braak, D. (2011). Integrability of the rabi model. *Phys. Rev. Lett.*, **107**, 100401.

Braunstein, Samuel L. and van Loock, Peter (2005). Quantum information with continuous variables. *Rev. Mod. Phys.*, **77**, 513–577.

Buisson, O. and Hekking, F. (2001). *Macroscopic Quantum Coherence and Quantum Computing*, Chapter 'Entangled states in a Josephson charge qubit coupled to a superconducting resonator', p. 137. Kluwer, New York.

Büttiker, M. (1987). Zero-current persistent potential drop across small-capacitance Josephson junctions. *Phys. Rev. B*, **36**, 3548–3555.

Bylander, Jonas, Gustavsson, Simon, Yan, Fei, Yoshihara, Fumiki, Harrabi, Khalil, Fitch, George, Cory, David G., Nakamura, Yasunobu, Tsai, Jaw-Shen, and Oliver, William D. (2011). Noise spectroscopy through dynamical decoupling with a superconducting flux qubit. *Nature Physics*, **7**, 565–570.

Caldeira, AO and Leggett, AJ (1983). Quantum tunneling in a dissipative system. *Annals of Physics*, **149**, 374–456.

Carmichael, HJ (1993). *An Open Systems Approach to Quantum Optics*. Springer-Verlag.

Carusotto, I., Gerace, D., Tureci, H. E., Liberato, S. De, Ciuti, C., and Imamoglu, A. (2009). Fermionized photons in an array of driven dissipative nonlinear cavities. *Phys. Rev. Lett.*, **103**, 033601.

Castellanos-Beltran, M. A., Irwin, K. D., Hilton, G. C., Vale, L. R., and Lehnert, K. W. (2008). Amplification and squeezing of quantum noise with a tunable Josephson metamaterial. *Nature Physics*, **4**, 929–931.

Chang, Josephine B., Vissers, Michael R., Corcoles, Antonio D., Sandberg, Martin, Gao, Jiansong, Abraham, David W., Chow, Jerry M., Gambetta, Jay M., Rothwell, Mary Beth, Keefe, George A., Steffen, Matthias, and Pappas, David P. (2013). Improved superconducting qubit coherence using titanium nitride. *Applied Physics Letters*, **103**(1), 012602.

Chiorescu, I., Bertet, P., Semba, K., Nakamura, Y., Harmans, C. J. P. M., and Mooij, J. E. (2004). Coherent dynamics of a flux qubit coupled to a harmonic oscillator. *Nature*, **431**, 159–162.

Chiorescu, I., Nakamura, Y., Harmans, C. J. P. M., and Mooij, J. E. (2003). Coherent Quantum Dynamics of a Superconducting Flux Qubit. *Science*, **299**, 1869–1871.

Cho, Jaeyoon, Angelakis, Dimitris G., and Bose, Sougato (2008*a*). Fractional quantum hall state in coupled cavities. *Phys. Rev. Lett.*, **101**, 246809.

Cho, Jaeyoon, Angelakis, Dimitris G., and Bose, Sougato (2008*b*, Dec). Fractional quantum hall state in coupled cavities. *Phys. Rev. Lett.*, **101**, 246809.

Cho, Jaeyoon, Angelakis, Dimitris G., and Bose, Sougato (2008*c*). Simulation of high-spin heisenberg models in coupled cavities. *Phys. Rev. A*, **78**, 062338.

Chow, J. M., DiCarlo, L., Gambetta, J. M., Nunnenkamp, A., Bishop, Lev S., Frunzio, L., Devoret, M. H., Girvin, S. M., and Schoelkopf, R. J. (2010). Detecting highly entangled states with a joint qubit readout. *Phys. Rev. A*, **81**, 062325.

Chow, J. M., Gambetta, J. M., Tornberg, L., Koch, Jens, Bishop, Lev S., Houck, A. A., Johnson, B. R., Frunzio, L., Girvin, S. M., and Schoelkopf, R. J. (2009). Randomized Benchmarking and Process Tomography for Gate Errors in a Solid-State Qubit. *Phys. Rev. Lett.*, **102**, 090502.

Ciuti, C. and Nataf, P. (2011). Comment on "superradiant phase transitions and the standard description of circuit qed". arXiv:1112.0986v1 (unpublished).

Clarke, John, Cleland, Andrew N., Devoret, Michel H., Esteve, Daniel, and Martinis, John M. (1988). Quantum Mechanics of a Macroscopic Variable: The Phase Difference of a Josephson Junction. *Science*, **239**, 992–997.

Clarke, John and Wilhelm, Frank K. (2008). Superconducting quantum bits. *Nature*, **453**, 1031–1042.

Clerk, Aashish A. (2012). *Proceedings of the 2011 Les Houches Summer School on Quantum Machines*, Chapter Quantum noise and quantum measurement. Oxford University Press.

Clerk, A. A., Devoret, M. H., Girvin, S. M., Marquardt, F., and Schoelkopf, R. J. (2010). Introduction to quantum noise, measurement and amplification. *Rev. Mod. Phys.*, **82**, 1155–1208. (Longer version with pedagogical appendices available at: arXiv.org:0810.4729).

Córcoles, A. D., Gambetta, Jay M., Chow, Jerry M., Smolin, John A., Ware, Matthew, Strand, Joel, Plourde, B. L. T., and Steffen, M. (2013, Mar). Process verification of two-qubit quantum gates by randomized benchmarking. *Phys. Rev. A*, **87**, 030301.

da Silva, Marcus P., Bozyigit, Deniz, Wallraff, Andreas, and Blais, Alexandre (2010). Schemes for the observation of photon correlation functions in circuit qed with linear detectors. *Phys. Rev. A*, **82**, 043804.

Dalidovich, Denis and Kennett, Malcolm P. (2009). Bose-hubbard model in the presence of ohmic dissipation. *Phys. Rev. A*, **79**, 053611.

Deleglise, Samuel, Dotsenko, Igor, Sayrin, Clement, Bernu, Julien, Brune, Michel, Raimond, Jean-Michel, and Haroche, Serge (2008). Reconstruction of non-classical cavity field states with snapshots of their decoherence. *Nature*, **455**, 510–514.

Deppe, Frank, Mariantoni, Matteo, Menzel, E. P., Marx, A., Saito, S., Kakuyanagi, K., Tanaka, H., Meno, T., Semba, K., Takayanagi, H., Solano, E., and Gross, R. (2008). Two-photon probe of the Jaynes-Cummings model and controlled symmetry breaking in circuit QED. *Nature Physics*, **4**, 686–691.

Devoret, M. (1997). *Quantum Fluctuations*, Chapter , pp. 351–385. Elsevier, Amsterdam.

Devoret, Michel, Girvin, Steven, and Schoelkopf, Robert (2007). Circuit-qed: How strong can the coupling between a Josephson junction atom and a transmission line resonator be? *Annalen der Physik*, **16**, 767–779.

Devoret, MH and Martinis, JM (2004). Superconducting qubits. In *Quantum Entan-*

glement and Information Processing (ed. Esteve, D and Raimond, JM and Dalibard, J), Volume 79, pp. 443–485. Les Houches Session 79th on Quantum Entanglement and Information Processing, Les Houches, France, June 30-July 25, 2003.

Devoret, M. H., Esteve, D., Grabert, H., Ingold, G.-L., Pothier, H., and Urbina, C. (1990). Effect of the electromagnetic environment on the coulomb blockade in ultrasmall tunnel junctions. *Phys. Rev. Lett.*, **64**, 1824–1827.

Devoret, Michel H. and Martinis, John M. (2005). *Experimental Aspects of Quantum Computing*, Volume 3, Chapter Implementing Qubits with Superconducting Integrated Circuits, pp. 163–203. Springer.

Devoret, M. H. and Schoelkopf, R. J. (2013). Superconducting circuits for quantum information: An outlook. *Science*, **339**(6124), 1169–1174.

Dewes, Andreas, Lauro, Romain, Ong, Florian R., Schmitt, Vivient, Milman, Perola, Bertet, Patrice, Vion, Denis, and Esteve, Daniel (2012, Apr). Quantum speeding-up of computation demonstrated in a superconducting two-qubit processor. *Phys. Rev. B*, **85**, 140503.

DiCarlo, L., Chow, J. M., Gambetta, J. M., Bishop, Lev S., Johnson, B. R., Schuster, D. I., Majer, J., Blais, A., Frunzio, L., Girvin, S. M., and Schoelkopf, R. J. (2009). Demonstration of two-qubit algorithms with a superconducting quantum processor. *Nature*, **460**, 240–244.

DiCarlo, L., Reed, M.D., Sun, L., Johnson, B.R., Chow, J.M., Gambetta, J.M., Frunzio, L., Girvin, S.M., Devoret, M.H., and Schoelkopf, R.J. (2010). Preparation and measurement of three-qubit entanglement in a superconducting circuit. *Nature*, **467**, 574–578.

Doucot, B., Feigelman, M. V., and Ioffe, L. B. (2003). Topological order in the insulating Josephson junction arrays. *Phys. Rev. Lett.*, **90**, 107003.

Doucot, B., Feigelman, M. V., Ioffe, L. B., and Ioselevich, A. S. (2005). Protected qubits and chern-simons theories in Josephson junction arrays. *Phys. Rev. B*, **71**, 024505.

Duty, T, Johansson, G, Bladh, K, Gunnarsson, D, Wilson, C, and Delsing, P (2005). Observation of quantum capacitance in the cooper-pair transistor. *Phys. Rev. Lett.*, **95**, 206807.

Eichler, C., Bozyigit, D., Lang, C., Baur, M., Steffen, L., Fink, J.M., Filipp, S., and Wallraff, A. (2011*a*). Observation of two-mode squeezing in the microwave frequency domain. *Phys. Rev. Lett.*, **107**, 113601.

Eichler, C., Bozyigit, D., Lang, C., Steffen, L., Fink, J., and Wallraff, A. (2011*b*). Experimental state tomography of itinerant single microwave photons. *Phys. Rev. Lett.*, **106**, 220503.

Eichler, C., Lang, C., Fink, J. M., Govenius, J., Filipp, S., and Wallraff, A. (2012, Dec). Observation of entanglement between itinerant microwave photons and a superconducting qubit. *Phys. Rev. Lett.*, **109**, 240501.

Esteve, D and Vion, D (2005). Solid state quantum bit circuits. In *Nanophysics: Coherence and Transport* (ed. Bouchiat, H and Gefen, Y and Gueron, S and Montambaux, G and Dalibard, J), Volume 81, pp. 537+. Les Houches Session 81st on Nanophysics - Coherence and Transport, Les Houches, France, June 28 - July 30, 2004.

Filipp, S., Maurer, P., Leek, P. J., Baur, M., Bianchetti, R., Fink, J. M., Göppl, M., Steffen, L., Gambetta, J. M., Blais, A., and Wallraff, A. (2009). Two-qubit state tomography using a joint dispersive readout. *Physical Review Letters*, **102**, 200402.

Fink, J.M., Bianchetti, R., Baur, M., Göppl, M., Steffen, L., Filipp, S., Leek, P. J., Blais, A., and Wallraff, A. (2009). Dressed collective qubit states and the tavis-cummings model in circuit qed. *Phys. Rev. Lett.*, **103**, 083601.

Fink, J. M., Goeppl, M., Baur, M., Bianchetti, R., Leek, P. J., Blais, A., and Wallraff, A. (2008). Climbing the Jaynes-Cummings ladder and observing its root n nonlinearity in a cavity QED system. *Nature*, **454**, 315–318.

Fink, J. M., Steffen, L., Studer, P., Bishop, Lev S., Baur, M., Bianchetti, R., Bozyigit, D., Lang, C., Filipp, S., Leek, P. J., and Wallraff, A. (2010). Quantum-to-classical transition in cavity quantum electrodynamics. *Phys. Rev. Lett.*, **105**, 163601.

Fisher, Matthew P. A., Weichman, Peter B., Grinstein, G., and Fisher, Daniel S. (1989). Boson localization and the superfluid-insulator transition. *Phys. Rev. B*, **40**, 546–570.

Foster, Ronald M. (1924). A reactance theorem. *Bell System Technical Journal*, **3**, 259–267.

Fragner, A., Goeppl, M., Fink, J. M., Baur, M., Bianchetti, R., Leek, P. J., Blais, A., and Wallraff, A. (2008). Resolving Vacuum Fluctuations in an Electrical Circuit by Measuring the Lamb Shift. *Science*, **322**, 1357–1360.

Gambetta, Jay, Blais, Alexandre, Schuster, D. I., Wallraff, A., Frunzio, L., Majer, J., Devoret, M. H., Girvin, S. M., and Schoelkopf, R. J. (2006). Qubit-photon interactions in a cavity: Measurement-induced dephasing and number splitting. *Phys. Rev. A*, **74**, 042318.

Gambetta, J. M., Houck, A. A., and Blais, Alexandre (2011*a*, Jan). Superconducting qubit with purcell protection and tunable coupling. *Phys. Rev. Lett.*, **106**, 030502.

Gambetta, J. M., Houck, A. A., and Blais, Alexandre (2011*b*). Superconducting qubit with purcell protection and tunable coupling. *Phys. Rev. Lett.*, **106**, 030502.

Gardiner, C. W., Parkins, A. S., and Zoller, P. (1992). Wave-function quantum stochastic differential equations and quantum simulation methods. *Phys. Rev. A*, **46**, 4363.

Gea-Banacloche, Julio, Lu, Ning, Pedrotti, Leno M., Prasad, Sudhakar, Scully, Marlan O., and Wodkiewicz, Krzysztof (1990*a*). Treatment of the spectrum of squeezing based on the modes of the universe. i. theory and a physical picture. *Phys. Rev. A*, **41**, 369.

Gea-Banacloche, Julio, Lu, Ning, Pedrotti, Leno M., Prasad, Sudhakar, Scully, Marlan O., and Wodkiewicz, Krzysztof (1990*b*). Treatment of the spectrum of squeezing based on the modes of the universe. ii. applications. *Phys. Rev. A*, **41**, 381.

Geerlings, K., Pop, I.M., Masluk, N., Kamal, A., Catelani, G., Glazman, L., and Devoret, M.H. (2013). Fluxonium qubit in a 3d cavity: Measurement and analysis. Bull. Am. Phys. Soc. 2013.MAR.C25.9; Abstract: C25.00009.

Girvin, S. M., Glazman, L. I., Jonson, M., Penn, D. R., and Stiles, M. D. (1990, Jun). Quantum fluctuations and the single-junction coulomb blockade. *Phys. Rev. Lett.*, **64**, 3183–3186.

Gladchenko, Sergey, Olaya, David, Dupont-Ferrier, Eva, Doucot, Benoit, Ioffe, Lev B.,

and Gershenson, Michael E. (2009). Superconducting nanocircuits for topologically protected qubits. *Nature Physics*, **5**, 48–53.

Gleyzes, Sebastien, Kuhr, Stefan, Guerlin, Christine, Bernu, Julien, Deleglise, Samuel, Busk Hoff, Ulrich, Brune, Michel, Raimond, Jean-Michel, and Haroche, Serge (2007). Quantum jumps of light recording the birth and death of a photon in a cavity. *Nature*, **446**, 297–300.

Gottesman, Daniel, Kitaev, Alexei, and Preskill, John (2001). Encoding a qubit in an oscillator. *Phys. Rev. A*, **64**, 012310.

Grajcar, M., van der Ploeg, S. H. W., Izmalkov, A., Il'ichev, E., Meyer, H.-G., Fedorov, A., Shnirman, A., and Schon, Gerd (2008). Sisyphus cooling and amplification by a superconducting qubit. *Nature Physics*, **4**, 612–616.

Greentree, Andrew D., Tahan, Charles, Cole, Jared H., and Hollenberg, Lloyd C. L. (2006). Quantum phase transitions of light. *Nature Physics*, **2**, 856–861.

Grochol, Michal (2009). Quantum phase transitions in an array of coupled nanocavity quantum dots. *Phys. Rev. B*, **79**, 205306.

Guerlin, Christine, Bernu, Julien, Deleglise, Samuel, Sayrin, Clement, Gleyzes, Sebastien, Kuhr, Stefan, Brune, Michel, Raimond, Jean-Michel, and Haroche, Serge (2007). Progressive field-state collapse and quantum non-demolition photon counting. *Nature*, **448**, 889–893.

Haroche, Serge and Raimond, Jean-Michel (2006). *Exploring the Quantum: Atoms, Cavities and Photons*. Oxford University Press.

Hartmann, J., Brandao, F.G.S.L., and Plenio, M.B. (2009). Quantum many-body phenomena in coupled cavity arrays. *Laser & Photonics Review*, **2**, 527–556.

Hartmann, Michael J. (2010, Mar). Polariton crystallization in driven arrays of lossy nonlinear resonators. *Phys. Rev. Lett.*, **104**, 113601.

Hartmann, M J, Brandao, F G S L, and Plenio, M B (2008). A polaritonic two-component bose-hubbard model. *NJP*, **10**, 033011.

Hartmann, Michael J. and Plenio, Martin B. (2007). Strong photon nonlinearities and photonic mott insulators. *Phys. Rev. Lett.*, **99**, 103601.

Hatridge, M., Shankar, S., Mirrahimi, M., Schackert, F., Geerlings, K., Brecht, T., Sliwa, K. M., Abdo, B., Frunzio, L., Girvin, S. M., Schoelkopf, R. J., and Devoret, M. H. (2013). Quantum back-action of an individual variable-strength measurement. *Science*, **339**(6116), 178–181.

Hayward, Andrew L. C., Martin, Andrew M., and Greentree, Andrew D. (2012, Jun). Fractional quantum hall physics in jaynes-cummings-hubbard lattices. *Phys. Rev. Lett.*, **108**, 223602.

Helmer, Ferdinand, Mariantoni, Matteo, Solano, Enrique, and Marquardt, Florian (2009). Quantum nondemolition photon detection in circuit qed and the quantum zeno effect. *Phys. Rev. A*, **79**, 052115.

Hoffman, A. J., Srinivasan, S. J., Gambetta, J. M., and Houck, A. A. (2011*a*). Coherent control of a superconducting qubit with dynamically tunable qubit-cavity coupling. *Phys. Rev. B*, **84**, 184515.

Hoffman, A. J., Srinivasan, S. J., Schmidt, S., Spietz, L., Aumentado, J., Türeci, H. E., and Houck, A. A. (2011*b*, Jul). Dispersive photon blockade in a superconducting circuit. *Phys. Rev. Lett.*, **107**, 053602.

Hofheinz, Max, Wang, H., Ansmann, M., Bialczak, Radoslaw C., Lucero, Erik, Neeley, M., O'Connell, A. D., Sank, D., Wenner, J., Martinis, John M., and Cleland, A. N. (2009). Synthesizing arbitrary quantum states in a superconducting resonator. *Nature*, **459**, 546–549.

Hofheinz, Max, Weig, E. M., Ansmann, M., Bialczak, Radoslaw C., Lucero, Erik, Neeley, M., O'Connell, A. D., Wang, H., Martinis, John M., and Cleland, A. N. (2008). Generation of Fock states in a superconducting quantum circuit. *Nature*, **454**, 310–314.

Hoi, Io-Chun, Kockum, Anton F., Palomaki, Tauno, Stace, Thomas M., Fan, Bixuan, Tornberg, Lars, Sathyamoorthy, Sankar R., Johansson, Göran, Delsing, Per, and Wilson, C. M. (2013, Aug). Giant cross˘kerr effect for propagating microwaves induced by an artificial atom. *Phys. Rev. Lett.*, **111**, 053601.

Hoi, Io-Chun, Palomaki, Tauno, Lindkvist, Joel, Johansson, Göran, Delsing, Per, and Wilson, C. M. (2012, Jun). Generation of nonclassical microwave states using an artificial atom in 1d open space. *Phys. Rev. Lett.*, **108**, 263601.

Hoi, Io-Chun, Wilson, C. M., Johansson, Göran, Palomaki, Tauno, Peropadre, Borja, and Delsing, Per (2011, Aug). Demonstration of a single-photon router in the microwave regime. *Phys. Rev. Lett.*, **107**, 073601.

Houck, A.A., Koch, Jens, Devoret, M.H., Girvin, S.M., and Schoelkopf, R.J. (2009). Life after charge noise: recent results with transmon qubits. *Quantum Information Processing*, **8**, 105.

Houck, A. A., Schreier, J. A., Johnson, B. R., Chow, J. M., Koch, Jens, Gambetta, J. M., Schuster, D. I., Frunzio, L., Devoret, M. H., Girvin, S. M., and Schoelkopf, R. J. (2008). Controlling the spontaneous emission of a superconducting transmon qubit. *Phys. Rev. Lett.*, **101**, 080502.

Houck, A. A., Schuster, D. I., Gambetta, J. M., Schreier, J. A., Johnson, B. R., Chow, J. M., Frunzio, L., Majer, J., Devoret, M. H., Girvin, S. M., and Schoelkopf, R. J. (2007). Generating single microwave photons in a circuit. *Nature*, **449**, 328–331.

Houck, Andrew A., Tureci, Hakan, and Koch, Jens (2012). On-chip quantum simulation with superconducting circuits. *Nature Physics*, **8**, 292–299.

Hwang, Myung-Joong and Choi, Mahn-Soo (2013, Mar). Large-scale maximal entanglement and majorana bound states in coupled circuit quantum electrodynamic systems. *Phys. Rev. B*, **87**, 125404.

Il'ichev, E., van der Ploeg, S. H. W., Grajcar, M., and Meyer, H. G. (2009). Weak continuous measurements of multiqubits systems. *Quantum Information Processing*, **8**, 133–153.

Illuminati, Fabrizio (2006). Quantum optics: Light does matter. *Nature Physics*, **2**, 803–804.

Ioffe, L. B. and Feigelman, M. V. (2002). Possible realization of an ideal quantum computer in Josephson junction array. *Phys. Rev. B*, **66**, 224503.

Ioffe, L. B., Feigel'man, M. V., Ioselevich, A., Ivanov, D., Troyer, M., and Blatter, G. (2002). Topologically protected quantum bits using Josephson junction arrays. *Nature*, **415**, 503–506.

Ithier, G, Collin, E, Joyez, P, Meeson, PJ, Vion, D, Esteve, D, Chiarello, F, Shnirman, A, Makhlin, Y, Schriefl, J, and Schon, G (2005). Decoherence in a superconducting

quantum bit circuit. *Phys. Rev. B*, **72**, 134519.
Jackson, John David (1999). *Electrodynamics* (3rd edn). Wiley.
Jarrett, T. C., Olaya-Castro, A., and Johnson, N. F. (2007). Optical signatures of quantum phase transitions in a light-matter system. *EPL*, **77**, 34001.
Ji, An-Chun, Sun, Qing, Xie, X. C., and Liu, W. M. (2009). Josephson effect for photons in two weakly linked microcavities. *Phys. Rev. Lett.*, **102**, 023602.
Johansson, J., Saito, S., Meno, T., Nakano, H., Ueda, M., Semba, K., and Takayanagi, H. (2006). Vacuum rabi oscillations in a macroscopic superconducting qubit lc oscillator system. *Phys. Rev. Lett.*, **96**, 127006.
Johnson, B. R., Reed, M. D., Houck, A. A., Schuster, D. I., Bishop, Lev S., Ginossar, E., Gambetta, J. M., DiCarlo, L., Frunzio, L., Girvin, S.M., and Schoelkopf, R.J. (2010). Quantum non-demolition detection of single microwave photons in a circuit. *Nature Physics*, **6**, 663–667.
Johnson, J. E., Macklin, C., Slichter, D. H., Vijay, R., Weingarten, E. B., Clarke, John, and Siddiqi, I. (2012, Aug). Heralded state preparation in a superconducting qubit. *Phys. Rev. Lett.*, **109**, 050506.
Kane, C. L. and Fisher, Matthew P. A. (1992*a*). Transmission through barriers and resonant tunneling in an interacting one-dimensional electron gas. *Phys. Rev. B*, **46**, 15233–15262.
Kane, C. L. and Fisher, Matthew P. A. (1992*b*). Transport in a one-channel luttinger liquid. *Phys. Rev. Lett.*, **68**, 1220–1223.
Kim, Z., Suri, B., Zaretskey, V., Novikov, S., Osborn, K. D., Mizel, A., Wellstood, F. C., and Palmer, B. S. (2011). Decoupling a cooper-pair box to enhance the lifetime to 0.2 ms. *Phys. Rev. Lett.*, **106**, 120501.
Kirchmair, Gerhard, Vlastakis, Brian, Leghtas, Zaki, Nigg, Simon E, Paik, Hanhee, Ginossar, Eran, Mirrahimi, Mazyar, Frunzio, Luigi, Girvin, S M, and Schoelkopf, R J (2013, March). Observation of quantum state collapse and revival due to the single-photon kerr effect. *Nature*, **495**(7440), 205–209.
Kitaev, A.Yu. (2003). Fault-tolerant quantum computation by anyons. *Ann. Phys.*, **303**, 2–30.
Koch, Jens, Houck, Andrew A., Hur, Karyn Le, and Girvin, S. M. (2010). Time-reversal symmetry breaking in circuit-qed based photon lattices. *Phys. Rev. A*, **82**, 043811.
Koch, Jens and Le Hur, Karyn (2009). Superfluid–mott insulator transition of light in the jaynes-cummings lattice. *Phys. Rev. A*, **80**, 023811.
Koch, Jens, Yu, Terri M., Gambetta, Jay, Houck, A. A., Schuster, D. I., Majer, J., Blais, Alexandre, Devoret, M. H., Girvin, S. M., and Schoelkopf, R. J. (2007). Charge-insensitive qubit design derived from the Cooper pair box. *Phys. Rev. A*, **76**, 042319.
Korotkov, Alexander N. (2009). Special issue on quantum computing with superconducting qubits. *Quantum Information Processing*, **8**, 51–54.
Korotkov, Alexander N. (2012). *Proceedings of the 2011 Les Houches Summer School on Quantum Machines*, Chapter Quantum Bayesian approach to circuit QED measurement, p. (arXiv:1111.4016). Oxford University Press.

Lafarge, P., Joyez, P., Esteve, D., Urbina, C., and Devoret, M. H. (1993). Two-electron quantization of the charge on a superconductor. *Nature*, **365**, 422–424.

Lang, C., Bozyigit, D., Eichler, C., Steffen, L., Fink, J. M., A.A. Abdumalikov, Jr., Baur, M., Filipp, S., da Silva, M. P., Blais, A., and Wallraff, A. (2011). Observation of resonant photon blockade at microwave frequencies using correlation function measurements. *Phys. Rev. Lett.*, **106**, 243601.

Lang, Roy, Scully, Marlan O., and Willis E. Lamb, Jr. (1973). Why is the laser line so narrow? a theory of single-quasimode laser operation. *Phys. Rev. A*, **7**, 1788.

Leek, P.J., Baur, M., Fink, J.M., Bianchetti, R., Steffen, L., Filipp, S., and Wallraff, A. (2010). Cavity quantum electrodynamics with separate photon storage and qubit readout modes. *Phys. Rev. Lett. 104*, **104**, 100504.

Leek, P. J., Filipp, S., Maurer, P., Baur, M., Bianchetti, R., Fink, J. M., Göppl, M., Steffen, L., and Wallraff, A. (2009). Using sideband transitions for two-qubit operations in superconducting circuits. *Phys. Rev. B*, **79**, 180511(R).

Leek, P. J., Fink, J. M., Blais, A., Bianchetti, R., Goeppl, M., Gambetta, J. M., Schuster, D. I., Frunzio, L., Schoelkopf, R. J., and Wallraff, A. (2007). Observation of Berry's phase in a solid-state qubit. *Science*, **318**, 1889–1892.

Leggett, AJ (1980). Macroscopic quantum systems and the quantum theory of measurement. *Progress of Theoretical Physics Suppl.*, **69**, 80–100.

Leghtas, Zaki, Kirchmair, Gerhard, Vlastakis, Brian, Devoret, Michel H., Schoelkopf, Robert J., and Mirrahimi, Mazyar (2013, Apr). Deterministic protocol for mapping a qubit to coherent state superpositions in a cavity. *Phys. Rev. A*, **87**, 042315.

Leghtas, Zaki, Kirchmair, Gerhard, Vlastakis, Brian, Schoelkopf, Robert, Devoret, Michel, and Mirrahimi, Mazyar (2012). Hardware-efficient autonomous quantum error correction. arXiv:1207.0679.

Lehnert, K. W., Bladh, K., Spietz, L. F., Gunnarsson, D., Schuster, D. I., Delsing, P., and Schoelkopf, R. J. (2003). Measurement of the excited-state lifetime of a microelectronic circuit. *Phys. Rev. Lett.*, **90**, 027002.

Lei, Soi-Chan and Lee, Ray-Kuang (2008). Quantum phase transitions of light in the dicke-bose-hubbard model. *Phys. Rev. A*, **77**, 033827.

Lieb, M. and Hartmann, M.J. (2010). Bose-hubbard dynamics of polaritons in a chain of circuit quantum electrodynamics cavities. *New J. Phys.*, **12**, 093031.

Likharev, K.K. and Zorin, A.B. (1985). Theory of the bloch-wave oscillations in small Josephson junctions. *J. Low Temp. Phys.*, **59**, 347.

Lupascu, A, Harmans, CJPM, and Mooij, JE (2005). Quantum state detection of a superconducting flux qubit using a dc-SQUID in the inductive mode. *Phys. Rev. B*, **71**, 184506.

Mabuchi, H. and Doherty, A. (2002). Cavity quantum electrodynamics: Coherence in context. *Science*, **298**, 1372.

Mahan, Gerald D. (2000). *Many-Particle Physics* (3rd edn). Springer.

Majer, J., Chow, J. M., Gambetta, J. M., Koch, Jens, Johnson, B. R., Schreier, J. A., Frunzio, L., Schuster, D. I., Houck, A. A., Wallraff, A., Blais, A., Devoret, M. H., Girvin, S. M., and Schoelkopf, R. J. (2007). Coupling superconducting qubits via a cavity bus. *Nature*, **449**, 443–447.

Makhlin, Y., Schön, G., and Shnirman, A. (2001). Quantum-state engineering with

Josephson-junction devices. *Rev. Mod. Phys.*, **73**, 357.

Makin, M. I., Cole, Jared H., Tahan, Charles, Hollenberg, Lloyd C. L., and Greentree, Andrew D. (2008). Quantum phase transitions in photonic cavities with two-level systems. *Phys. Rev. A*, **77**, 053819.

Mallet, Franois, Ong, Florian R., Palacios-Laloy, Agustin, Nguyen, François, Bertet, Patrice, Vion, Denis, and Esteve, Daniel (2009). Single-shot qubit readout in circuit quantum electrodynamics. *Nature Phys.*, **5**, 791.

Manucharyan, V. E., Boaknin, E., Metcalfe, M., Vijay, R., Siddiqi, I., , and Devoret, M. (2007). Microwave bifurcation of a Josephson junction: Embedding-circuit requirements. *Phys. Rev. B*, **76**, 014524.

Manucharyan, Vladimir E., Koch, Jens, Brink, Markus, Glazman, Leonid I., and Devoret, Michel H. (2009*a*). Coherent oscillations between classically separable quantum states of a superconducting loop. *arXiv:0910.3039*.

Manucharyan, Vladimir E., Koch, Jens, Glazman, Leonid, and Devoret, Michel (2009*b*). Fluxonium: Single cooper-pair circuit free of charge offsets. *Science*, **326**, 113–116.

Mariantoni, Matteo, Wang, H., Bialczak, Radoslaw C., Lucero, Erik, Neeley, M., OConnell, A.D., Sank, D., Weides, M., Wenner, J., Yamamoto, T., Yin, Y., Zhao, J., Martinis, John M., and Cleland, A.N. (2011*a*). Photon shell game in three-resonator circuit quantum electrodynamics. *Nature Physics*, **7**, 287–293.

Mariantoni, Matteo, Wang, H., Yamamoto, T., Neeley, M., Bialczak, Radoslaw C., Chen, Y., Lenander, M., Lucero, Erik, OConnell, A. D., Sank, D., Weides, M., Wenner, J., Yin, Y., Zhao, J., Korotkov, A. N., Cleland, A. N., and Martinis, John M. (2011*b*). Implementing the quantum von neumann architecture with superconducting circuits. *Science*, **334**, 61.

Marquardt, Florian (2007). Efficient on-chip source of microwave photon pairs in superconducting circuit qed. *Phys. Rev. B*, **76**, 205416.

Marquardt, F. and Bruder, C. (2001). Superposition of two mesoscopically distinct quantum states: Coupling a cooper pair box to a large superconducting island. *Phys. Rev. B*, **63**, 054514.

Marthaler, M., Schön, Gerd, and Shnirman, Alexander (2008). Photon-number squeezing in circuit quantum electrodynamics. *Phys. Rev. Lett.*, **101**, 147001.

Martinis, JM, Devoret, MH, and Clarke, J (1985). Energy level quantization in the zero-voltage state of a current-biased Josephson junction. *Phys. Rev. Lett.*, **55**, 1543 – 1546.

Martinis, JM, Nam, S, Aumentado, J, Lang, KM, and Urbina, C (2003). Decoherence of a superconducting qubit due to bias noise. *Phys. Rev. B*, **67**, 094510.

Martinis, JM, Nam, S, Aumentado, J, and Urbina, C (2002). Rabi oscillations in a large Josephson-junction qubit. *Phys. Rev. Lett.*, **89**, 117901.

McGrayne, Sharon Bertsch (2011). *The Theory That Would Not Die: How Bayes Rule Cracked the Enigma Code, Hunted Down Russian Submarines, and Emerged Triumphant from Two Centuries of Controversy*. Yale University Press.

Menzel, E. P., Deppe, F., Mariantoni, M., Caballero, M.A. Araque, Baust, A., Niemczyk, T., Hoffmann, E., Marx, A., Solano, E., and Gross, R. (2010). Dual-path state reconstruction scheme for propagating quantum microwaves and detector noise to-

mography. *Phys. Rev. Lett.*, **105**, 100401.
Metcalfe, M., Boaknin, E., Manucharyan, V., Vijay, R., Siddiqi, I., Rigetti, C., Frunzio, L., Schoelkopf, R. J., and Devoret, M. H. (2007). Measuring the decoherence of a quantronium qubit with the cavity bifurcation amplifier. *Phys. Rev. B*, **76**, 174516.
Meystre, P. and III, M. Sargent (1998). *Elements of Quantum Optics*. Spinger-Verlag.
Mooij, J. E., Orlando, T. P., Levitov, L., Tian, Lin, van der Wal, Caspar H., and Lloyd, Seth (1999). Josephson Persistent-Current Qubit. *Science*, **285**, 1036–1039.
Moon, K and Girvin, SM (2005). Theory of microwave parametric down-conversion and squeezing using circuit QED. *Phys. Rev. Lett.*, **95**, 140504.
Murch, K. W., Vool, U., Zhou, D., Weber, S. J., Girvin, S. M., and Siddiqi, I. (2012, Oct). Cavity-assisted quantum bath engineering. *Phys. Rev. Lett.*, **109**, 183602.
Murch, K. W., Weber, S. J., Beck, K. M., Ginossar, E., and Siddiqi, I. (2013). Reduction of the radiative decay of atomic coherence in squeezed vacuum. *Nature*, **499**, 62–65.
Na, Neil, Utsunomiya, Shoko, Tian, Lin, and Yamamoto, Yoshihisa (2008). Strongly correlated polaritons in a two-dimensional array of photonic crystal microcavities. *Phys. Rev. A*, **77**, 031803.
Nakamura, Y., Pashkin, Yu. A., and Tsai, J. S. (1999). Coherent control of macroscopic quantum states in a single-cooper-pair box. *Nature*, **398**, 786–788.
Nataf, Pierre and Ciuti, Cristiano (2010). No-go theorem for superradiant quantum phase transitions in cavity qed and counter-example in circuit qed. *Nature Communications*, **1**, 72.
Neeley, Matthew, Ansmann, M., Bialczak, Radoslaw C., Hofheinz, M., Katz, N., Lucero, Erik, O'Connell, A., Wang, H., Cleland, A. N., and Martinis, John M. (2008). Transformed dissipation in superconducting quantum circuits. *Phys. Rev. B*, **77**, 180508.
Neeley, Matthew, Bialczak, Radoslaw C., Lenander, M., Lucero, E., Mariantoni, Matteo, O'Connell, A. D., Sank, D., Wang, H., Weides, M., Wenner, J., Yin, Y., Yamamoto, T., Cleland, A. N., and Martinis, John M. (2010). Generation of three-qubit entangled states using superconducting phase qubits. *Nature*, **467**, 570.
Niemczyk, T., Deppe, F., Huebl, H., Menzel, E.P., Hocke, F., Schwarz, M. J., Garcia-Ripoll, J.J., Zueco, D., Hümmer, T., Solano, E., Marx, A., and Gross, R. (2010). Circuit quantum electrodynamics in the ultrastrong-coupling regime. *Nature Physics*, **6**, 772–776.
Nigg, Simon E. and Girvin, S. M. (2013, Jun). Stabilizer quantum error correction toolbox for superconducting qubits. *Phys. Rev. Lett.*, **110**, 243604.
Nigg, Simon E., Paik, Hanhee, Vlastakis, Brian, Kirchmair, Gerhard, Shankar, S., Frunzio, Luigi, Devoret, M. H., Schoelkopf, R. J., and Girvin, S. M. (2012, Jun). Black-box superconducting circuit quantization. *Phys. Rev. Lett.*, **108**, 240502.
Nissen, Felix, Schmidt, Sebastian, Biondi, Matteo, Blatter, Gianni, Türeci, Hakan E., and Keeling, Jonathan (2012, Jun). Nonequilibrium dynamics of coupled qubit-cavity arrays. *Phys. Rev. Lett.*, **108**, 233603.
Nogues, G., Rauschenbeutel, A., Osnaghi, S., Brune, M., Raimond, J. M., and Haroche, S. (1999). Seeing a single photon without destroying it. *Nature*, **400**,

239–242.

Nori, Franco (2008). Superconducting qubits: Atomic physics with a circuit. *Nature Physics*, **4**, 589–590.

Nunnenkamp, A., Koch, Jens, and Girvin, S. M. (2011). Synthetic gauge fields and homodyne transmission in jaynes-cummings lattices. *New J. Phys.*, **13**, 095008.

Ong, F. R., Boissonneault, M., Mallet, F., Palacios-Laloy, A., Dewes, A., Doherty, A. C., Blais, A., Bertet, P., Vion, D., and Esteve, D. (2011, Apr). Circuit qed with a nonlinear resonator: ac-stark shift and dephasing. *Phys. Rev. Lett.*, **106**, 167002.

Paik, Hanhee, Schuster, D. I., Bishop, Lev S., Kirchmair, G., Catelani, G., Sears, A. P., Johnson, B. R., Reagor, M. J., Frunzio, L., Glazman, L. I., Girvin, S. M., Devoret, M. H., and Schoelkopf, R. J. (2011). Observation of high coherence in Josephson junction qubits measured in a three-dimensional circuit qed architecture. *Phys. Rev. Lett.*, **107**, 240501.

Pechal, M., Eichler, C., Zeytinoglu, S., Berger, S., Wallraff, A., and Filipp, S. (2013). Microwave-controlled generation of shaped single photons in circuit quantum electrodynamics. arXiv:1308.4094.

Petrescu, Alexandru, Houck, Andrew A., and Le Hur, Karyn (2012, Nov). Anomalous hall effects of light and chiral edge modes on the kagomé lattice. *Phys. Rev. A*, **86**, 053804.

Pierre, F., Pothier, H., Joyez, P., Birge, Norman O., Esteve, D., and Devoret, M. H. (2001, Feb). Electrodynamic dip in the local density of states of a metallic wire. *Phys. Rev. Lett.*, **86**, 1590–1593.

Pines, David (1963). *Elementary Excitations in Solids*. W.A. Benjamin.

Plastina, F. and Falci, G. (2003). Communicating Josephson qubits. *Phys. Rev. B*, **67**, 224514.

Purcell, E. M. (1946). Spontaneous emission probabilities at radio frequencies. *Phys. Rev.*, **69**, 681.

Raimond, J., Brune, M., and Haroche, S. (2001). Manipulating quantum entanglement with atoms and photons in a cavity. *Rev. Mod. Phys.*, **73**, 565.

Reed, M. D., DiCarlo, L., Johnson, B. R., Sun, L., Schuster, D. I., Frunzio, L., and Schoelkopf, R. J. (2010*a*). High-fidelity readout in circuit quantum electrodynamics using the jaynes-cummings nonlinearity. *Phys. Rev. Lett.*, **105**, 173601.

Reed, M. D., DiCarlo, L., Nigg, S. E., Sun, L., Frunzio, L., Girvin, S. M., and Schoelkopf, R. J. (2012). Realization of three-qubit quantum error correction with superconducting circuits. *Nature*, **482**, 382–385.

Reed, M. D., Johnson, B.R., Houck, A.A., DiCarlo, L., Chow, J.M., Schuster, D.I., Frunzio, L., and Schoelkopf, R.J. (2010*b*). Fast reset and suppressing spontaneous emission of a superconducting qubit. *Applied Physics Letters*, **96**(20), 203110–203110–3.

Rigetti, Chad, Gambetta, Jay M., Poletto, Stefano, Plourde, B. L. T., Chow, Jerry M., Córcoles, A. D., Smolin, John A., Merkel, Seth T., Rozen, J. R., Keefe, George A., Rothwell, Mary B., Ketchen, Mark B., and Steffen, M. (2012, Sep). Superconducting qubit in a waveguide cavity with a coherence time approaching 0.1 ms. *Phys. Rev. B*, **86**, 100506.

Romero, G., Garcia-Ripoll, J. J., and Solano, E. (2009). Microwave Photon Detector

in Circuit QED. *Phys. Rev. Lett.*, **102**, 173602.

Rossini, Davide and Fazio, Rosario (2007). Mott-insulating and glassy phases of polaritons in 1d arrays of coupled cavities. *Phys. Rev. Lett.*, **99**, 186401.

Sandberg, M., Wilson, C. M., Persson, F., Johansson, G., Shumeiko, V., Bauch, T., Duty, T., and Delsing, P. (2008). Fast tuning of superconducting microwave cavities. In *Solid-state Quantum Computing, Proceedings* (ed. Goan, HS and Chen, YN), Volume 1074, AIP Conference Proceedings, pp. 12–21. 2nd International Workshop on Solid-State Quantum Computing/Mini-School on Quantum Information Science, Taipei, Taiwan, June 23-27, 2008.

Schmidt, S. and Blatter, G. (2009). Strong coupling theory for the jaynes-cummings-hubbard model. *Phys. Rev. Lett.*, **103**, 086403.

Schmidt, S., Gerace, D., Houck, A. A., Blatter, G., and Türeci, H. E. (2010). Nonequilibrium delocalization-localization transition of photons in circuit quantum electrodynamics. *Phys. Rev. B*, **82**, 100508.

Schmidt, S. and Koch, J. (2013). Circuit qed lattices: Towards quantum simulation with superconducting circuits. *Annalen der Physik*, **525**, 395412.

Schoelkopf, RJ and Girvin, SM (2008). Wiring up quantum systems. *Nature*, **451**, 664.

Schreier, J. A., Houck, A. A., Koch, Jens, Schuster, D. I., Johnson, B. R., Chow, J. M., Gambetta, J. M., Majer, J., Frunzio, L., Devoret, M. H., Girvin, S. M., and Schoelkopf, R. J. (2008). Suppressing charge noise decoherence in superconducting charge qubits. *Phys. Rev. B*, **77**, 180502.

Schuster, D.I., Houck, A.A., Schreier, J.A., Wallraff, A., Gambetta, J., Blais, A., Frunzio, L., Johnson, B., Devoret, M.H., Girvin, S.M., and Schoelkopf, R.J. (2007*a*). Resolving photon number states in a superconducting circuit. *Nature*, **445**, 515–518.

Schuster, DI, Wallraff, A, Blais, A, Frunzio, L, Huang, RS, Majer, J, Girvin, SM, and Schoelkopf, RJ (2005). ac Stark shift and dephasing of a superconducting qubit strongly coupled to a cavity field. *Phys. Rev. Lett.*, **94**, 123602.

Schuster, D. I., Wallraff, A., Blais, A., Frunzio, L., Huang, R.-S., Majer, J., Girvin, S. M., and Schoelkopf, R. J. (2007*b*). Erratum: ac stark shift and dephasing of a superconducting qubit strongly coupled to a cavity field [*Phys. Rev. Lett.* **94**, 123602 (2005)]. *Phys. Rev. Lett.*, **98**, 049902.

Schuster, I., Kubanek, A., Fuhrmanek, A., Puppe, T., Pinkse, P. W. H., Murr, K., and Rempe, G. (2008). Nonlinear spectroscopy of photons bound to one atom. *Nature Physics*, **4**, 382–385.

Sears, A. P., Petrenko, A., Catelani, G., Sun, L., Paik, Hanhee, Kirchmair, G., Frunzio, L., Glazman, L. I., Girvin, S. M., and Schoelkopf, R. J. (2012, Nov). Photon shot noise dephasing in the strong-dispersive limit of circuit qed. *Phys. Rev. B*, **86**, 180504.

Sete, Eyob A., Galiautdinov, Andrei, Mlinar, Eric, Martinis, John M., and Korotkov, Alexander N. (2013, May). Catch-disperse-release readout for superconducting qubits. *Phys. Rev. Lett.*, **110**, 210501.

Shanks, W. E., Underwood, D. L., and Houck, A. A. (2013). A scanning transmon qubit for strong coupling circuit quantum electrodynamics. *Nature Communications*, **4**, 1991.

Shnirman, A., Schön, G., and Hermon, Z. (1997). Quantum manipulations of small Josephson junctions. *Phys. Rev. Lett.*, **79**, 2371.

Siddiqi, I, Vijay, R, Metcalfe, M, Boaknin, E, Frunzio, L, Schoelkopf, RJ, and Devoret, MH (2006). Dispersive measurements of superconducting qubit coherence with a fast latching readout. *Phys. Rev. B*, **73**, 054510.

Siddiqi, I., Vijay, R., Pierre, F., Wilson, C. M., Metcalfe, M., Rigetti, C., Frunzio, L., and Devoret, M. H. (2004). Rf-driven Josephson bifurcation amplifier for quantum measurement. *Phys. Rev. Lett.*, **93**, 207002.

Sillanpää, MA, Lehtinen, T, Paila, A, Makhlin, Y, Roschier, L, and Hakonen, PJ (2005). Direct observation of Josephson capacitance. *Phys. Rev. Lett.*, **95**, 206806.

Sillanpää, Mika A., Park, Jae I., and Simmonds, Raymond W. (2007). Coherent quantum state storage and transfer between two phase qubits via a resonant cavity. *Nature*, **449**, 438–442.

Srinivasan, S. J., Hoffman, A. J., Gambetta, J. M., and Houck, A. A. (2011*a*, Feb). Tunable coupling in circuit quantum electrodynamics using a superconducting charge qubit with a *v*-shaped energy level diagram. *Phys. Rev. Lett.*, **106**, 083601.

Srinivasan, S. J., Hoffman, A. J., Gambetta, J. M., and Houck, A. A. (2011*b*). Tunable coupling in circuit quantum electrodynamics using a superconducting charge qubit with a V-shaped energy level diagram. *Phys. Rev. Lett.*, **106**, 083601.

Srinivasan, Srikanth J., Sundaresan, Neereja M., Sadri, Darius, Liu, Yanbing, Gambetta, Jay M., Yu, Terri, Girvin, S. M., and Houck, Andrew A. (2013). Time-reversal symmetrization of spontaneous emission for high fidelity quantum state transfer. arXiv:1308.3471.

Tavis, Michael and Cummings, Frederick W. (1968). Exact solution for an n-molecule radiation-field hamiltonian. *Phys. Rev.*, **170**, 379–384.

Thompson, R. J., Rempe, G., and Kimble, H. J. (1992). Observation of normal-mode splitting for an atom in an optical cavity. *Phys. Rev. Lett.*, **68**, 1132–1135.

Tinkham, M. (1996). *Introduction to Superconductivity.* McGraw-Hill.

Turlot, Emmanuel, Esteve, Daniel, Urbina, Cristian, Martinis, John M., Devoret, Michel H., Linkwitz, Sebastian, and Grabert, Hermann (1989). Escape oscillations of a Josephson junction switching out of the zero-voltage state. *Phys. Rev. Lett.*, **62**, 1788–1791.

Underwood, D. L., Shanks, W. E., Koch, Jens, and Houck, A. A. (2012, Aug). Low-disorder microwave cavity lattices for quantum simulation with photons. *Phys. Rev. A*, **86**, 023837.

van der Wal, Caspar H., ter Haar, A. C. J., Wilhelm, F. K., Schouten, R. N., Harmans, C. J. P. M., Orlando, T. P., Lloyd, Seth, and Mooij, J. E. (2000). Quantum superposition of macroscopic persistent-current states. *Science*, **290**, 773–777.

Viehmann, Oliver, von Delft, Jan, and Marquardt, Florian (2011). Superradiant phase transitions and the standard description of circuit qed. *Phys. Rev. Lett.*, **107**, 113602.

Viehmann, Oliver, von Delft, Jan, and Marquardt, Florian (2012). Reply to comment on "superradiant phase transitions and the standard description of circuit qed". arXiv:1202.2916.

Vijay, R., Slichter, D. H., and Siddiqi, I. (2011, Mar). Observation of quantum jumps

in a superconducting artificial atom. *Phys. Rev. Lett.*, **106**, 110502.

Vion, D., Aassime, A., Cottet, A., Joyez, P., Pothier, H., Urbina, C., Esteve, D., and Devoret, M. H. (2002). Manipulating the Quantum State of an Electrical Circuit. *Science*, **296**, 886–889.

Vlastakis, Brian, Kirchmair, Gerhard, Leghtas, Zaki, Simon E. Nigg, and Luigi Frunzio, Girvin, S. M., Mirrahimi, Mazyar, Devoret, M. H., and Schoelkopf, R. J. (2013). Deterministically encoding quantum information in 100-photon schrodinger cat states. *Science*. (in press).

Wallraff, A, Schuster, DI, Blais, A, Frunzio, L, Majer, J, Devoret, MH, Girvin, SM, and Schoelkopf, RJ (2005). Approaching unit visibility for control of a superconducting qubit with dispersive readout. *Phys. Rev. Lett.*, **95**, 060501.

Wallraff, A., Schuster, D. I., Blais, A., Frunzio, L., Huang, R.-S., Majer, J., Kumar, S., Girvin, S. M., and Schoelkopf, R. J. (2004). Circuit quantum electrodynamics: Coherent coupling of a single photon to a cooper pair box. *Nature*, **431**, 162–167.

Wallraff, A., Schuster, D. I., Blais, A., Gambetta, J. M., Schreier, J., Frunzio, L., Devoret, M. H., Girvin, S. M., and Schoelkopf, R. J. (2007). Sideband transitions and two-tone spectroscopy of a superconducting qubit strongly coupled to an on-chip cavity. *Phys. Rev. Lett.*, **99**, 050501.

Walls, D. and Milburn, G. (1994). *Quantum optics*. Spinger-Verlag, Berlin.

Wang, H., Hofheinz, M., Ansmann, M., Bialczak, R. C., Lucero, E., Neeley, M., O'Connell, A. D., Sank, D., Wenner, J., Cleland, A. N., and Martinis, John M. (2008). Measurement of the Decay of Fock States in a Superconducting Quantum Circuit. *Phys. Rev. Lett.*, **101**, 240401.

Wang, H., Mariantoni, Matteo, Bialczak, Radoslaw C., Lenander, M., Lucero, Erik, Neeley, M., O'Connell, A., Sank, D., Weides, M., Wenner, J., Yamamoto, T., Yin, Y., Zhao, J., Martinis, John M., and Cleland, A. N. (2011). Deterministic entanglement of photons in two superconducting microwave resonators. *Phys. Rev. Lett.*, **106**, 060401.

Wendin, G. and Shumeiko, V.S. (2006). *Handbook of Theoretical and Computational Nanotechnology, Vol. 3*, Chapter 'Superconducting circuits, qubits and computing', pp. 223–309. American Scientific Publishers, Los Angeles.

Wendin, G. and Shumeiko, V. S. (2007). Quantum bits with Josephson junctions. *J. Low Temperature Physics*, **33**, 724.

Widom, A., Megaloudis, G., Clark, T.D., Mutton, J.E., Prance, R.J., and Prance, H. (1984). The Josephson pendulum as a nonlinear capacitor. *J. Low Temp. Phys.*, **57**, 651.

Wilson, C. M., Johansson, G., Pourkabirian, A., Simoen, M., Johansson, J. R., Duty, T., Nori, F., and Delsing, P. (2011). Observation of the dynamical casimir effect in a superconducting circuit. *Nature*, **479**, 376379.

Woolley, M. J., Lang, C., Eichler, C., Wallraff, A., and Blais, A. (2013). Signatures of hong-ou-mandel interference at microwave frequencies. arXiv:1304.6068.

Yang, C.-P., Chu, S.-I., and Han, S. (2003). Possible realization of entanglement, logical gates, and quantum-information transfer with superconducting-quantum-interference device qubits in cavity qed. *Phys. Rev. A*, **67**, 042311.

Yin, Yi, Chen, Yu, Sank, Daniel, O'Malley, P. J. J., White, T. C., Barends, R.,

Kelly, J., Lucero, Erik, Mariantoni, Matteo, Megrant, A., Neill, C., Vainsencher, A., Wenner, J., Korotkov, Alexander N., Cleland, A. N., and Martinis, John M. (2013, Mar). Catch and release of microwave photon states. *Phys. Rev. Lett.*, **110**, 107001.

You, JQ and Nori, F (2005). Superconducting circuits and quantum information. *Physics Today*, **58**, 42–47.

You, J. Q. and Nori, F. (2003). Quantum information processing with superconducting qubits in a microwave field. *Phys. Rev. B*, **68**, 064509.

Yurke, B. (1984). Use of cavities in squeezed state generation. *Phys. Rev. A*, **29**, 408.

Yurke, B. and Denker, J. S. (1984). Quantum network theory. *Phys. Rev. A*, **29**, 1419.

Zhao, J., Sandvik, A. W., and Ueda, K. (2008). Insulator to superfluid transition in coupled photonic cavities in two dimensions. arXiv:0806.3603.